NOTICE

The quality of this microform is heavily dependent upon the quality of the original thesis submitted for microfilming. Every effort has been made to ensure the highest quality of reproduction possible.

If pages are missing, contact the university which granted the degree.

Some pages may have indistinct print especially if the original pages were typed with a poor typewriter ribbon or if the university sent us an inferior photocopy.

Reproduction in full or in part of this microform is governed by the Canadian Copyright Act, R.S.C. 1970, c. C-30, and subsequent amendments.

AVIS

La qualité de cette microforme dépend grandement de la qualité de la thèse soumise au microfilmage. Nous avons tout fait pour assurer une qualité supérieure de reproduction.

S'il manque des pages, veuillez communiquer avec l'université qui a conféré le grade.

La qualité d'impression de certaines pages peut laisser à désirer, surtout si les pages originales ont été dactylographiées à l'aide d'un ruban usé ou si l'université nous a fait parvenir une photocopie de qualité inférieure.

La reproduction, même partielle, de cette microforme est soumise à la Loi canadienne sur le droit d'auteur, SRC 1970, c. C-30, et ses amendements subséquents.

STABLE ISOTOPE RATIOS OF CARBONATE AND SULFIDE MINERALS FROM THE GUNFLINT FORMATION: EVIDENCE FOR THE ORIGIN OF IRON-FORMATIONS.

By

William J. Carrigan

Ottawa-Carleton Geoscience Center and
Department of Geology
University of Ottawa
Ottawa, Canada, 1990

A thesis submitted to the School of Graduate Studies and Research
in partial fulfillment of the requirements for the degree
of Doctor of Philosophy at the University of Ottawa

NOTICE

The quality of this microform is heavily dependent upon the quality of the original thesis submitted for microfilming. Every effort has been made to ensure the highest quality of reproduction possible.

If pages are missing, contact the university which granted the degree.

Some pages may have indistinct print especially if the original pages were typed with a poor typewriter ribbon or if the university sent us an inferior photocopy.

Reproduction in full or in part of this microform is governed by the Canadian Copyright Act, R.S.C. 1970, c. C-30, and subsequent amendments.

AVIS

La qualité de cette microforme dépend grandement de la qualité de la thèse soumise au microfilmage. Nous avons tout fait pour assurer une qualité supérieure de reproduction.

S'il manque des pages, veuillez communiquer avec l'université qui a conféré le grade.

La qualité d'impression de certaines pages peut laisser à désirer, surtout si les pages originales ont été dactylographiées à l'aide d'un ruban usé ou si l'université nous a fait parvenir une photocopie de qualité inférieure.

La reproduction, même partielle, de cette microforme est soumise à la Loi canadienne sur le droit d'auteur, SRC 1970, c. C-30, et ses amendements subséquents.

ISBN 0-315-60593-6

UNIVERSITÉ D'OTTAWA
UNIVERSITY OF OTTAWA

To my daughter,

Megan

ABSTRACT

The ~1.9 Ga Gunflint Formation is a Lake Superior type iron-formation, located in the Thunder Bay district of northwestern Ontario, that was deposited on a shallow shelf analogous to modern carbonate environments. The base of the Gunflint Formation is composed of a thin conglomerate facies, which unconformably overlies Archean basement, and is overlain by iron-rich, complexly interlayered arenitic (arenite and stromatolite facies) and lutitic (banded chert-carbonate, laminated carbonate, and black shale facies) lithofacies. The top of the formation is an iron-poor limestone facies, which is conformably overlain by shale, siltstone and greywacke of the Rove Formation. The Gunflint and Rove Formations comprise the Animikie Group; a transgressive sequence that was deposited within a basin with restricted communication with the open ocean, such as a foredeep or backarc basin. These sediments are essentially unmetamorphosed and undeformed, except within the contact zones of late Proterozoic gabbroic sills.

Carbonate minerals in the iron-rich lithofacies of the Gunflint Formation include siderite, ankerite, and calcite. Petrographic evidence indicates that siderite precipitation initiated either within the water column or at the sediment/water interface and continued during very early diagenesis. Ankerite and calcite formed during early to late diagenesis as pore-filling cements and as replacements of other minerals. The iron-poor limestone facies contains very early diagenetic dolomite and early to late diagenetic calcite.

$\delta^{13}C$ values of carbonate minerals from unmetamorphosed rocks range between 0 and -6 ‰ (PDB). The values near 0 ‰, which are considered to be representative of the basin water composition, indicate that the primary source of carbon was marine bicarbonate. The lighter values indicate that a minor component of oxidized organic carbon was added during early diagenesis. $\delta^{13}C$ values in

metamorphosed rocks range between -6 and -20 °/oo and were the result of isotopic exchange or decarbonation reactions during metamorphism.

The heaviest $\delta^{18}O$ values for unmetamorphosed carbonate minerals range between -5 and -7 °/oo (PDB), which is the same range of values observed for many early Proterozoic marine carbonates. These values are interpreted to reflect original seawater conditions. This suggests that either the water temperature was about 45 °C or else that the $\delta^{18}O$ of the seawater was about -5.5 °/oo (SMOW). $\delta^{18}O$ values of carbonate minerals in unmetamorphosed rocks range between -5 and -16 °/oo (PDB), and are the result of isotopic exchange with pore waters, originally of marine composition, at increasing temperatures and/or are the result of isotopic exchange with ^{18}O-depleted meteoric water during early diagenesis. Metamorphosed rocks have a narrower range of values between -10 and -18 °/oo (PDB) indicating isotopic exchange at elevated temperatures.

Disseminated fine-grained, very early diagenetic pyrite is widespread throughout the formation, usually in amounts less than about 2 %. However, pyrite is locally observed as laminae or thin layers, suggesting that some pyrite may have formed at or above the sediment/water interface. Low S/C ratios indicate that dissolved sulphate was the limiting factor in pyrite formation. $\delta^{34}S$ values between +5 and +12 °/oo (CDT) imply that sulfide formed by bacterial sulphate reduction under closed system conditions. The shift to heavier values (+13 to +21 °/oo) in the overlying Rove Formation indicates that the basin was partially closed to the oceanic reservoir of sulphate, which is consistent with the interpretation that the Animikie Group was deposited in a partially closed basin.

In the lower part of the Gunflint Formation coarse-grained pyrite and pyrite concretions are associated with syndepositional faults. High S/C ratios and highly variable $\delta^{34}S$ values (-33 to +35 °/oo) suggest an external source of sulphate was introduced by fluids moving upward along these faults.

The Gunflint basin is best characterized by a stratified water column with high concentrations of dissolved ferrous iron below the redox boundary. Volcanic activity or rifting within this basin contributed a high flux of reducing hydrothermal solutions to the seawater, which would have kept dissolved sulphate and oxygen levels within the basin to low values. This allowed dissolved ferrous iron to accumulate below the redox boundary. Hydrothermal activity was probably the dominant source of iron, although reduction of detrital ferric iron may have contributed significant amounts of dissolved iron. During periods of increased tectonic activity, the expansion of the redox boundary to shallower water allowed the transport of iron to the shallow shelf. Ferric iron-bearing minerals (i.e. ferric hydroxide) would have been precipitated on the shelf by oxidation in surface waters whereas ferrous iron-bearing minerals (i.e. siderite, greenalite, and pyrite) would have been precipitated under more reducing conditions either in deeper water or in sheltered environments. The transition to the iron-poor limestone member resulted from a lowering of the redox boundary.

ACKNOWLEDGEMENTS

I would like to thank E.M. Cameron (Geological Survey of Canada and the University of Ottawa) for originally suggesting this thesis and for financial and academic support throughout this study. I would also like to acknowledge P. Fralick (Lakehead University), for helpful discussions in the field, and R.J. Shegelski (Esso) for sharing much of his data on the Gunflint Formation. I would especially like thank B.R. Rust (U of O) for reviewing parts of this thesis and for offering many improvements. I would also like to express my gratitude to all of the graduate students at both the University of Ottawa and Carleton for the many friendships, social functions, and geological discussions.

I am also grateful to B.E. Taylor (GSC and U of O) for helpful suggestions concerning the analysis and interpretation of the isotope data, and also to P. Middlestead, G. St. Jean, and J. Loop (U of O) for technical and analytical assistance during the course of my research. G. Mrazek and J.F. Tardif (U of O) made normal and polished thin sections and E. Hearn (U of O) provided photographic assistance. G. Pringle and M. Bonardi are thanked for their patient instruction on the use of the electron microprobe at the GSC.

Funding for this research was provided by a Natural Sciences and Engineering Research Council (NSERC) grant to E.M. Cameron. Additional financial support was provided to me by an NSERC scholarship and a University of Ottawa Entrance Scholarship.

TABLE OF CONTENTS

LIST OF FIGURES

LIST OF PLATES

LIST OF TABLES

1. INTRODUCTION

Iron-formations are widespread during the Archean, become enormous in size during the early Proterozoic, and abruptly decline in abundance at about 1.8 Ga. This time restriction has provoked many researchers to speculate that iron-formations represent a period of fundamental change in the biological and chemical evolution of the oceans and atmosphere. Therefore, in addition to their economic importance, iron-formations may provide valuable information on an important period in the evolution of the Earth's lithosphere, hydrosphere, atmosphere and biosphere. However, despite the vast amount of research conducted on these enigmatic deposits (or perhaps because of it), their origin still remains a controversial topic.

The term iron-formation was defined by James (1954) as a chemical sediment, typically either thin-bedded or laminated, containing 15% or more iron of sedimentary origin and commonly, but not necessarily, containing layers of chert. James (1966) made a distinction between the abundant Precambrian iron-formations and the Phanerozoic ironstones, which are typically oolitic and non-cherty. The term banded iron-formation (BIF) is used in a more restricted sense to refer to iron-formations that are composed of alternating laminae of chert and iron minerals (James, 1983).

James (1954) also sub-divided iron-formations into oxide, silicate, carbonate, and sulfide facies based on the predominant mineralogy. Gross (1965) defined two general classes of iron-formation: Algoma type, which is closely associated with volcanism, and Lake Superior type, which lacks obvious volcanic relations. The Lake Superior type is mostly restricted to the early Proterozoic, whereas the Algoma type, although most common in Archean rocks, is also found in late Proterozoic and Paleozoic rocks. Several other definitions and classifications also exist and are

discussed by Trendall (1983).

The Early Proterozoic Gunflint Formation is a Lake Superior type iron-formation located in the Thunder Bay district of Ontario. It has undergone only very low grade metamorphism and contains well preserved primary textures. For this reason the stable isotope ratios of carbon and oxygen in carbonate minerals and of sulphur in sulfide minerals are expected to retain important information concerning the origin of this iron-formation. Because gabbroic sills intrude the Gunflint Formation, the effects of thermal metamorphism on the primary isotope ratios can also be evaluated.

Most minerals form in or near stable isotopic equilibrium with their environment. Variations in isotope ratios are primarily dependant on temperature, although important kinetic effects are associated with biological activity. Because elements such as carbon, oxygen and sulphur are major components of many sedimentary minerals and form the basis for most forms of life, the stable isotope ratios of these elements provide significant information on depositional environments and on the isotopic composition of the water from which they precipitated. Post-depositional processes can result in exchange reactions with earlier formed minerals or the addition of newly formed minerals, which can provide information on diagenetic and metamorphic conditions.

Compared to other sedimentary rocks, such as limestones, relatively few stable isotope studies have been carried out on iron-formations. Previous isotopic studies include: oxygen isotope ratios, mostly in quartz, magnetite and carbonate minerals, (James and Clayton, 1962; Becker and Clayton, 1976; Knauth and Epstein, 1976; Knauth and Lowe, 1979; Perry et al, 1973, 1978; Perry and Ahmad, 1980, 1981) carbon isotope ratios in carbonate minerals and organic matter (Becker and Clayton, 1972; Perry and Tan, 1973; Thode and Goodwin, 1983; Baur et al, 1985; Hayes et al, 1983; Schidlowski et al 1979; Barghoorn et al, 1977) and sulphur isotope ratios in

sulfides (Goodwin et al, 1976; 1985; Thode and Goodwin, 1983; Monster et al, 1979; Fripp et al, 1979; Cameron and Garrels, 1980; Cameron, 1983; Lavigne and Crocket, 1980; Crocket et al, 1983).

Siderite and ankerite in iron-formations are either primary (Floran and Papike, 1975) or diagenetic (Drever, 1974) in origin. Studies of the Hammersley iron-formations show that carbonates are typically ^{13}C depleted. It has been proposed that these iron-formations formed in a basin that had intermittent restricted circulation with the open ocean (Becker and Clayton, 1972). Isotopically light carbonate was precipitated during a period of basin closure during which the oxidation of organic matter caused a shift of seawater $\delta^{13}C$ to lighter values. Alternatively, carbonate formed as a result of the oxidation of organic matter during diagenesis (Baur et al, 1985). However, both of these studies were from the oxide-facies BIF macrobands of Trendall and Blockley (1970) and did not include the siderite-rich S macrobands. Perry and Tan (1973) analysed all lithologies of the Biwabik Iron Formation and found that magnetite-rich rocks contained ^{13}C depleted carbonates, whereas magnetite-poor rocks contained carbonates having near-normal marine $\delta^{13}C$ values. They proposed that the light values were the result of isotopic exchange reactions during diagenesis and metamorphism.

The stable isotope ratios of sulphur have been used to distinguish between sulfide of hydrothermal origin and sulfide produced by the bacterial reduction of seawater sulphate. A wide range of $\delta^{34}S$ values has been taken as evidence for the presence of sulphur-reducing bacteria in some Archean iron-formations (Goodwin et al, 1976, 1985; Thode and Goodwin, 1983). However, Skyring and Donnelly (1982) and Cameron and Hattori (1987) note that this range of values could also have resulted from isotopic fractionation in a hydrothermal system. Most iron-formations have a narrow range of $\delta^{34}S$ values, which has been interpreted to indicate a hydrothermal origin for the sulfide (i.e. Cameron, 1983), but under certain

conditions bacterial sulphate reduction can also produce sulfides with a narrow range of values (Ashendorf, 1980; Ohmoto and Felder, 1987). Therefore, $\delta^{34}S$ data alone are not sufficient to establish the origin of sulfide. Other evidence, such as petrography and the elemental ratios of pyrite-sulphur and organic carbon, must be used in conjunction with isotope ratios. Sulphur isotopes have also been used to recognize periods of sulphate limitation associated with basin restriction (Goodfellow and Jonasson, 1984).

Oxygen isotope ratios, which are fractionated during evaporation and precipitation cycles, can be used to distinguish meteoric waters from seawater (Craig and Gordon, 1965). However, the $\delta^{18}O$ value of Precambrian seawater is uncertain. Many researchers have analysed oxygen-bearing minerals in iron-formations, as well as other chemical sediments, in an attempt to determine the temperature and $\delta^{18}O$ of the Precambrian oceans (i.e. Knauth and Lowe, 1979; Perry et al, 1978) but the influx of diagenetic fluids can alter the primary ratios. Oxygen isotope ratios have also been used in defining metamorphic conditions (i.e. Becker and Clayton, 1976).

The interpretation of isotopic data can be ambiguous without other supporting lines of evidence. For this reason the depositional setting and petrography of the Gunflint Formation, as well as the stratigraphy and tectonic history of the basin, must first be established. The stratigraphy and tectonic history of the early Proterozoic rocks in the Lake Superior region has been compiled from the literature and is presented in Chapter 2. Lithofacies types in the Gunflint Formation were determined by examination of representative stratigraphic sections in the field. Descriptions of these lithofacies and the interpretation of the depositional setting of the Gunflint Formation is presented in Chapter 2. Approximately 250 samples from the various lithofacies were obtained; from these polished slabs ($\sim$50), standard thin sections ($\sim$150) and polished thin sections ($\sim$100) were examined in order to determine the petrographic relations, which are shown in Chapter 3.

In this study, sulphur isotope analyses were obtained from 117 samples from the Gunflint Formation and 8 samples from the overlying Rove Formation. In some cases detailed sampling within single hand samples was carried out, for a total of 171 analyses of sulphur isotope ratios. In addition, 91 samples from the Gunflint Formation were analysed for carbon and oxygen isotope ratios in carbonate minerals. In most cases, these samples contained 2 or 3 different carbonate phases, for a total of 167 analyses. All of these analyses are presented in Chapter 4. In Chapter 5 the isotopic data are interpreted in light of the geological and petrographic evidence. The significance of these results for the origin of the Gunflint Formation, and to iron-formations in general, is discussed in Chapter 6. The analytical methods used in this study are described in Appendix A, $\delta^{13}C$ and $\delta^{18}O$ results are listed in Appendix B, and $\delta^{34}S$ results are listed in Appendix C.

2. GEOLOGICAL SETTING

2.1. REGIONAL GEOLOGY

In the western Lake Superior region, Early Proterozoic rocks lie along the southern margin of the Late Archean Superior Province of the Canadian Shield (Figures 1 & 2). Two distinct lithologic domains are present (Figure 1): a northern deformed continental margin prism composed mostly of sedimentary rocks and a southern assemblage consisting mostly of volcanic and intrusive rocks called the Wisconsin magmatic terranes (Sims et al, 1989). The south-facing continental margin prism, which contains the Gunflint Formation, overlies Archean basement and consists of a lower rifted passive margin sequence overstepped northward by a synorogenic foredeep sequence (Hoffman, 1987; Barovich et al, 1989; Southwick et al, 1988). The Wisconsin magmatic terranes consist of island arcs and/or closed back-arc basins that were accreted to the continental margin during the Penokean Orogeny (Sims et al, 1989).

2.1.1. ARCHEAN BASEMENT

Archean rocks of two contrasting types form the basement to the continental margin sequence: a volcano-plutonic terrane and a gneiss terrane (Figure 2). The boundary between these two terranes, which formed as a result of their juxtaposition at about 2.70 Ga, has been termed the Great Lakes tectonic zone (GLTZ) by Sims et al (1980). The volcano-plutonic terrane is the southwestern extension of the Wawa Subprovince of the Superior Province (Card and Ciesielski, 1986). Ages for these rocks lie between 2.75 and 2.65 Ga. High grade gneisses, exposed in the cores of mantled gneiss domes and fault-bounded blocks, underlie Proterozoic sediments to the south of the volcano-plutonic terrane. Ages for the gneisses range from 3.55 Ga

Figure 1. Early Proterozoic terranes in the Lake Superior region.

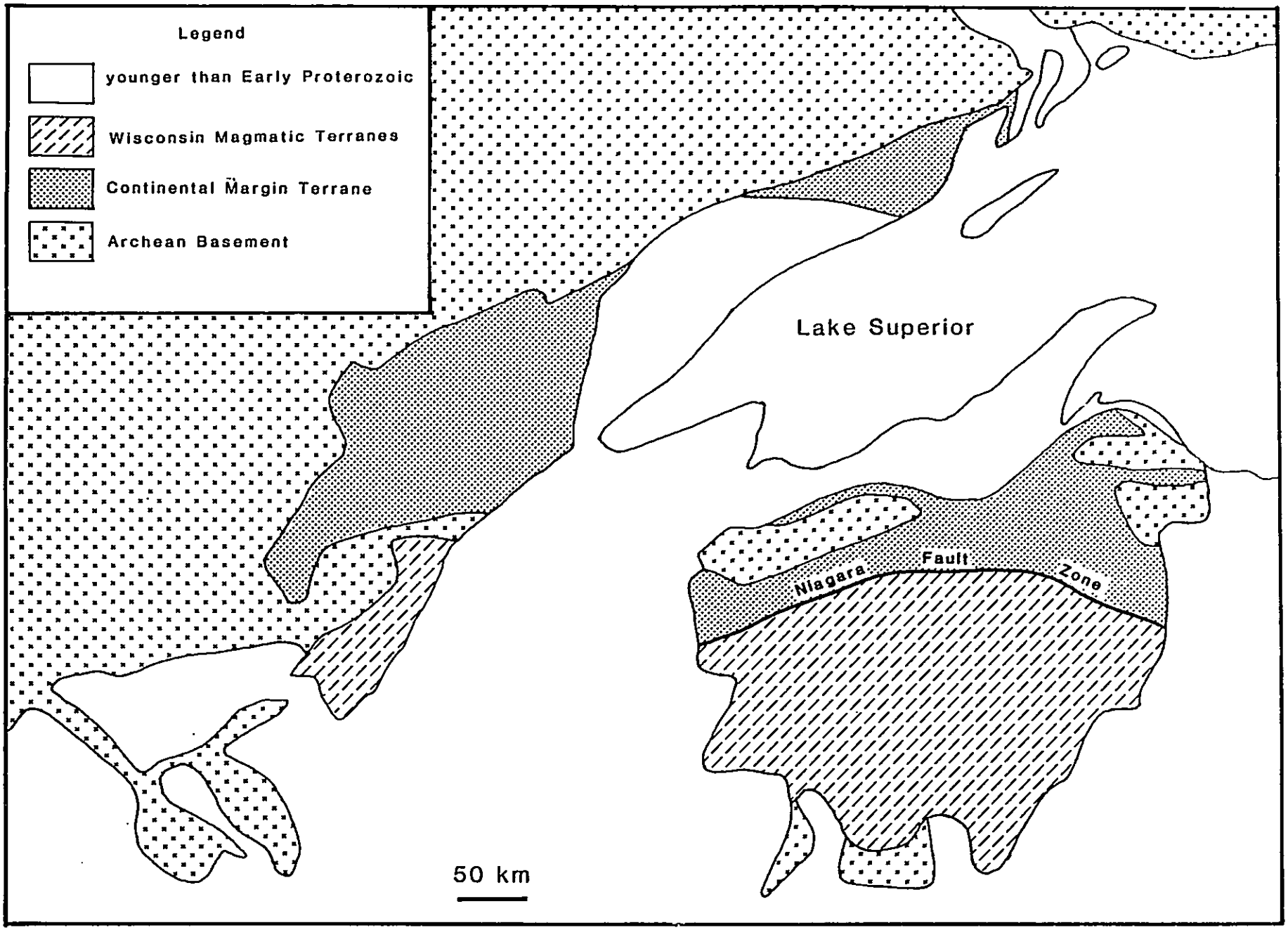
Legend
younger than Early Proterozoic
Wisconsin Magmatic Terranes
Continental Margin Terrane
Archean Basement
Lake Superior
Niagara Fault Zone
50 km

Figure 2. Generalized geologic map of the Lake Superior region (modified from Morey et al, 1982).

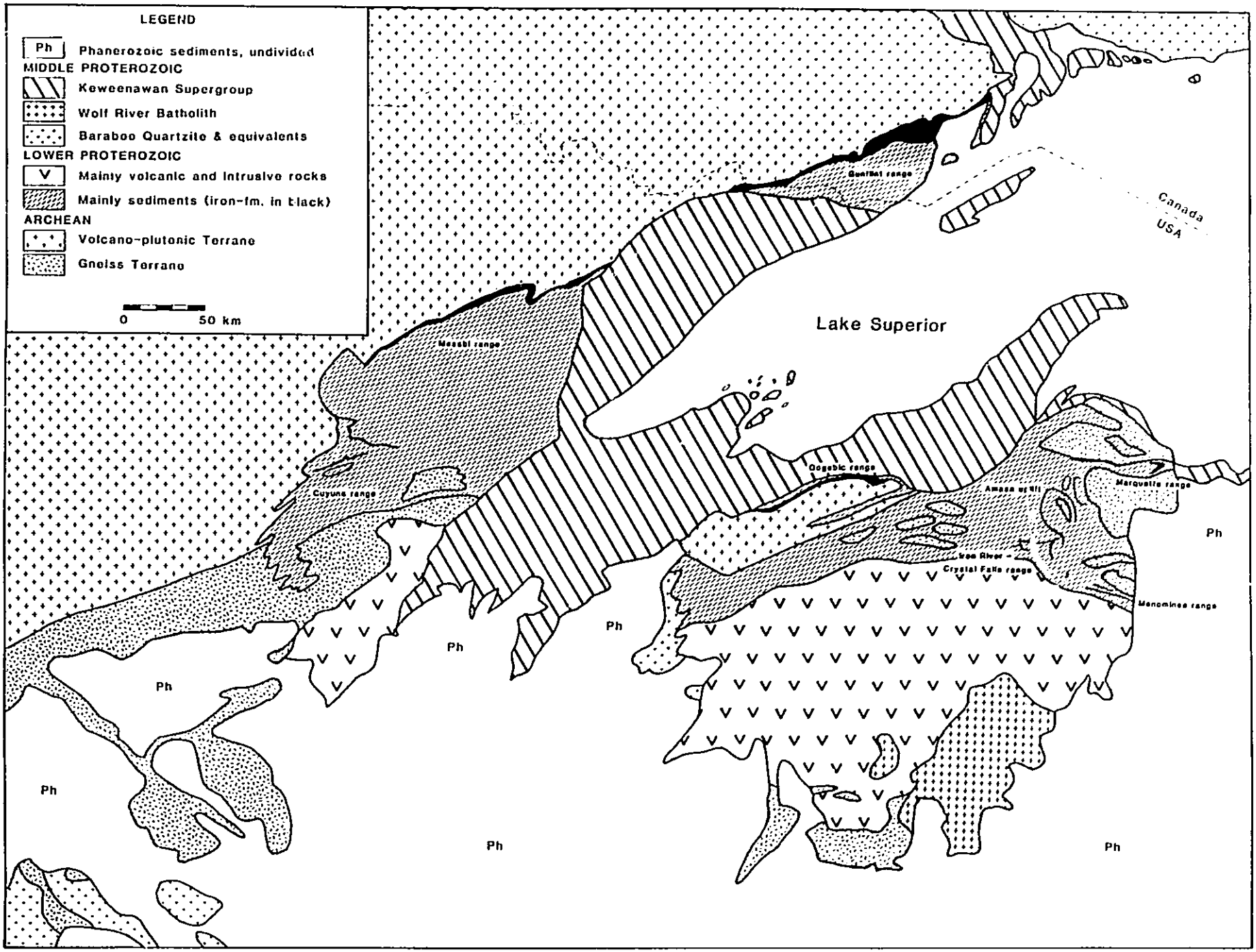
LEGEND
Ph
Phanerozoic sediments, undivided
MIDDLE PROTEROZOIC
Keweenawan Supergroup
Wolf River Batholith
Baraboo Quartzite & equivalents
LOWER PROTEROZOIC
V
Mainly volcanic and intrusive rocks
Mainly sediments (iron-fm. in black)
ARCHEAN
Volcano-plutonic Terrane
Gneiss Terrane
0
50 km
Lake Superior
Canada
USA
Gunflint range
Mesabi range
Cuyuna range
Ogogbic range
Marquette range
Menominee range
Ph

to about 2.60 Ga (Peterman et al, 1980). No basement is known to underlie the Wisconsin magmatic terranes, except for isolated blocks found within and to the south of its southern margin.

2.1.2. THE CONTINENTAL MARGIN

The continental margin rocks have been separated into two physically isolated segments by the Midcontinent Rift System (Morey 1983a), which is represented by the rocks of the Keweenawan Supergroup (Figure 2). Rocks of the northwest segment, in Minnesota and Ontario, are assigned to the Mille Lacs Group and the overlying Animikie Group. Rocks in the southeastern segment, in Michigan and Wisconsin, are assigned to the Marquette Range Supergroup (MRS) (Figure 3).

A maximum age for the continental margin rocks is obtained from metabasalts within the Mille Lacs Group (Figure 4), which have an estimated age greater than 2150 Ma (Beck cited in Southwick et al, 1988). The Animikie Group sediments in Minnesota (Figure 4) erosionally truncate diabase dikes with a Rb-Sr age of 2120 +/-67 Ma (Beck and Murthy, 1982) that intrude Archean basement. A zircon age of 1910 Ma has been obtained from the Hemlock Formation of the Menominee Group by Banks and Van Schmus (1972) and a lead-lead age of 1929 Ma from apatite in iron-formation beneath the Michigamme Formation of the Baraga Group (Zartman cited in Klasner et al, 1989). A minimum age is defined by a zircon age of 1824 Ma from an undeformed granite that intrudes the Badwater Greenstone (Peterman cited in Klasner et al, 1989) and by the 1870 +/-25 Ma age of the Penokean Orogeny (Sims et al, 1989).

The oldest rocks of the northwest segment occur in the Cuyuna range (Figure 2) and are assigned to the Mille Lacs Group (Figure 3). Morey (1978) has divided this sequence into five formations (Figure 4). However, these rocks are complexly

Figure 3. Correlation chart for Early Proterozoic strata in the Lake Superior region (from Morey and Van Schmus, 1988).

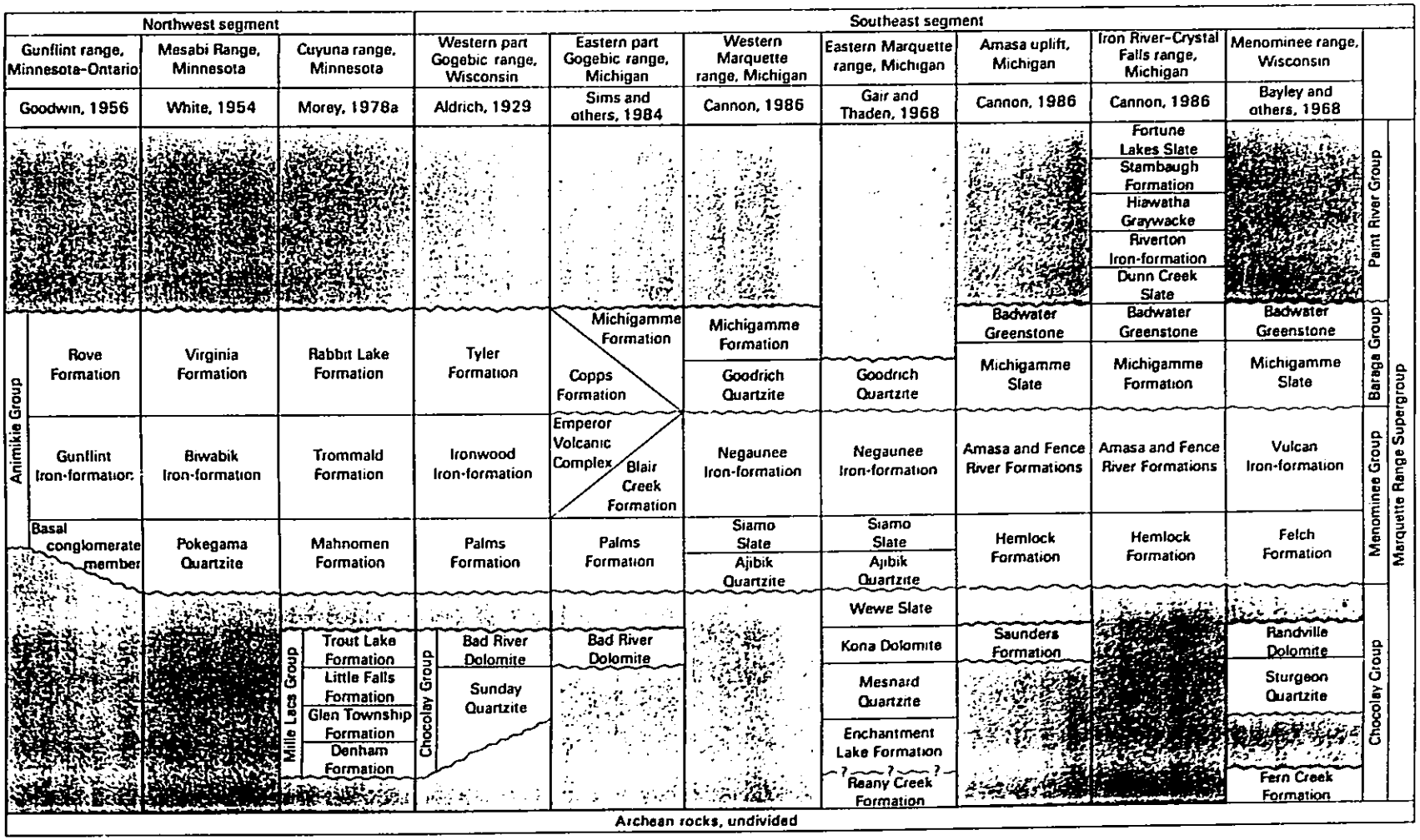
Northwest segment
Southeast segment
Gunflint range, Minnesota-Ontario
Goodwin, 1956
Mesabi Range, Minnesota
White, 1954
Cuyuna range, Minnesota
Morey, 1978a
Western part Gogebic range, Wisconsin
Aldrich, 1929
Eastern part Gogebic range, Michigan
Sims and others, 1984
Western Marquette range, Michigan
Cannon, 1986
Eastern Marquette range, Michigan
Gair and Thaden, 1968
Amasa uplift, Michigan
Cannon, 1986
Iron River-Crystal Falls range, Michigan
Cannon, 1986
Menominee range, Wisconsin
Bayley and others, 1968
Animikie Group
Rove Formation
Virginia Formation
Rabbit Lake Formation
Tyler Formation
Michigamme Formation
Copps Formation
Michigamme Formation
Goodrich Quartzite
Goodrich Quartzite
Michigamme Slate
Michigamme Formation
Michigamme Slate
Gunflint Iron-formation
Biwabik Iron-formation
Trommald Formation
Ironwood Iron-formation
Emperor Volcanic Complex
Blair Creek Formation
Negaunee Iron-formation
Negaunee Iron-formation
Amasa and Fence River Formations
Amasa and Fence River Formations
Vulcan Iron-formation
Basal conglomerate member
Pokegama Quartzite
Mahnomen Formation
Palms Formation
Palms Formation
Siamo Slate
Ajibik Quartzite
Siamo Slate
Ajibik Quartzite
Hemlock Formation
Hemlock Formation
Felch Formation
Wewe Slate
Kona Dolomite
Saunders Formation
Randville Dolomite
Mesnard Quartzite
Sturgeon Quartzite
Enchantment Lake Formation
Reany Creek Formation
Fern Creek Formation
Mille Lacs Group
Trout Lake Formation
Little Falls Formation
Glen Township Formation
Denham Formation
Chocolay Group
Bad River Dolomite
Sunday Quartzite
Bad River Dolomite
Fortune Lakes Slate
Stambaugh Formation
Hiawatha Graywacke
Riverton Iron-formation
Dunn Creek Slate
Badwater Greenstone
Badwater Greenstone
Badwater Greenstone
Paint River Group
Baraga Group
Menominee Group
Chocolay Group
Marquette Range Supergroup
Archean rocks, undivided

deformed and poorly exposed, prompting Southwick et al (1988) to propose that the formal stratigraphy be de-emphasized. They have shown that this area is a fold and thrust belt, consisting of four tectonically bounded slices or structural panels, that probably represent a deformed rifted passive margin. The southernmost slice is made up mostly of gneiss, metasedimentary schist and granitoid plutons of early Proterozoic age. The central two slices consist of mafic to intermediate volcanic rocks and subvolcanic sills, graphitic ar 1 sulfidic schist, and iron-formation. These three slices are assigned to the Mille Lacs Group by Southwick et al (1988). The northernmost slice contains folded and weakly metamorphosed sediments that have previously been assigned to the Mahnomen, Trommald, and Rabbit Lake Formations (Morey, 1978). They unconformably overlie rocks of the Mille Lacs Group and are lithologically similar to the Animikie Group and so have been considered by Morey (1978, 1983b) to be correlative with Animikie Group sediments to the northeast (Figure 4). However, Southwick et al (1988) have proposed that an unconformity separates these sediments from the overlying Animikie Group, suggesting that they occupy a position between the Mille Lacs Group and the Animikie Group. They have informally designated this sequence as the North Range group (not shown on Figure 3 or 4).

The sediments of the Animikie Group unconformably overlie either Archean basement or rocks of the fold and thrust belt, i.e. the Mille Lacs Group, (Figure 4). They form a gently, south-dipping homocline along the northern margin of the basin and become progressively more deformed toward the south. A basal clastic sequence consists of a thin conglomerate overlain by interbedded quartzite, siltstone and shale (the Pokegama Quartzite), which thickens to the west. Only a thin discontinuous conglomerate layer was deposited in Ontario, the basal conglomerate member of the Gunflint Formation. About 100 to 200 m of iron-formation conformably overlies the clastic sediments (the Gunflint and Biwabik Formations) and is, in turn, conformably

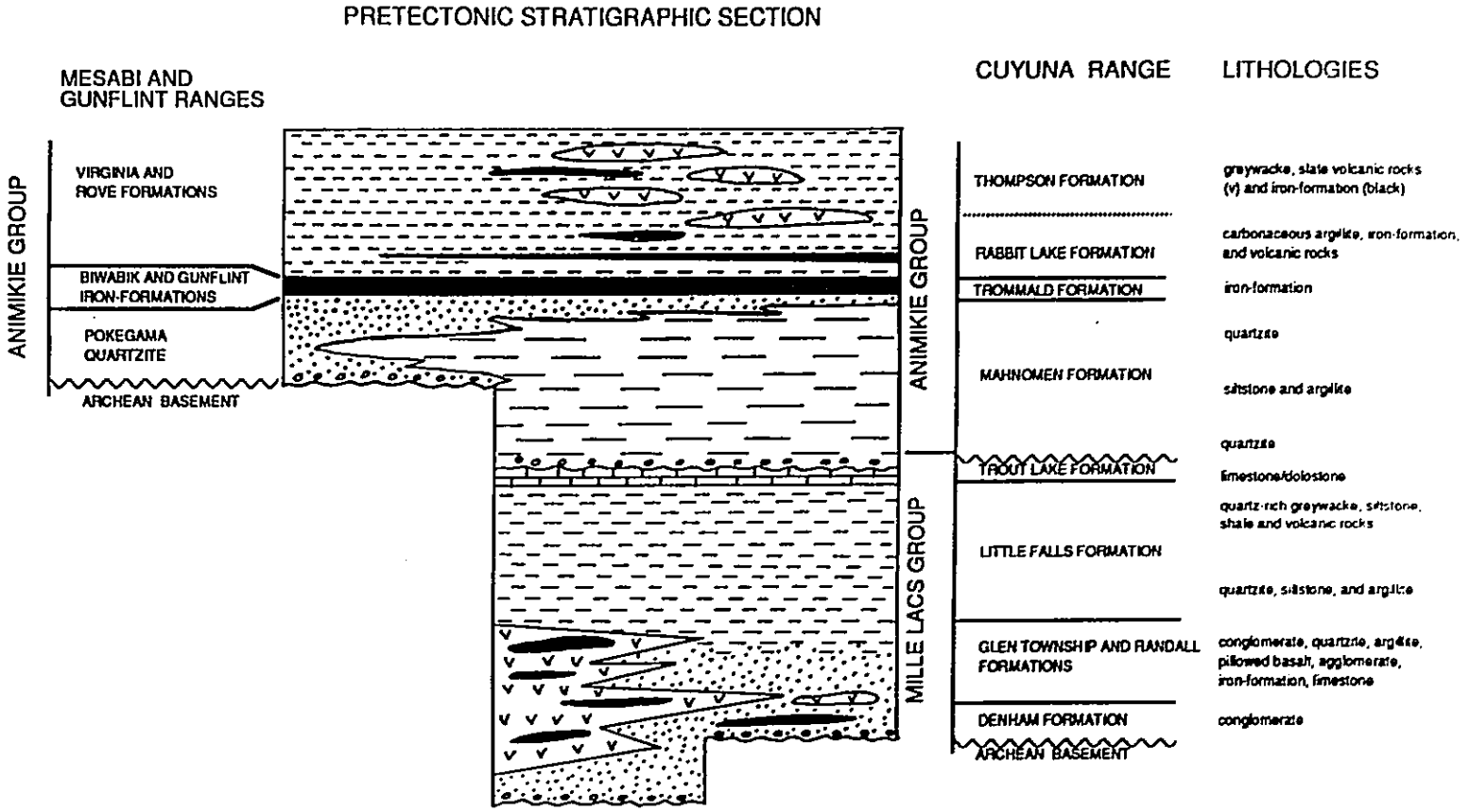

Figure 4. Lithostratigraphic summary and schematic pretectonic section for the Penokean Orogen (modified from Morey, 1983). This interpretation depends on the equivalence of the Biwabik and Trommald Iron Formations, which has been questioned by Southwick et al (1988), who interpret the Pokegama Quartzite as resting unconformably on rocks of the Mahomen Formation.

overlain by up to 2000 m of interbedded sandstone, siltstone and greywacke, which contains minor iron-formation and volcanic rocks (the Rove and Virginia Formations).

It is proposed that the early Proterozoic rocks in Minnesota and Ontario consist of a foredeep and its associated fold and thrust belt (Hoffman, 1987; Southwick et al, 1988), and that the cratonic side of the orogen lay to the north. However, the processes leading to plate convergence are uncertain. According to Hoffman (1987), the earliest sediments of the Mille Lacs Group represent initial rift deposits laid down on the newly rifted Archean Superior craton. These are overlain by passive margin deposits, represented by quartzose units of the Mille Lacs Group (stage 1 of Figure 5a). Subduction of the continental margin beneath a tectonic collage of arcs, accretionary prisms and continental fragments, as the ocean basin was consumed, resulted in the loading of the crust by the fold and thrust belt and the development of an actively migrating foredeep (stage 2 of Figure 5a) in which the sediments of the Animikie Group were deposited. The marginal deposits, as well as early deposits laid down in the rear of the foredeep, may also be incorporated into the fold and thrust belt. Alternatively, Southwick et al (1988) have proposed that a back-arc basin developed to the south of the Superior craton, which was subsequently destroyed by arc to craton convergence and the development of the foredeep as the ocean floor was subducted beneath the arc (Figure 5b). This scenario implies a northwest-dipping subduction zone and the development of an Andes-style continental arc somewhere to the southeast of the fold and thrust belt, possibly the Wisconsin magmatic terranes. The fold and thrust belt represents the remnants of the deformed back-arc basin.

In the southeast segment, the Marquette Range Supergroup is interrupted by unconformities that serve to divide it into the Chocolay, Menominee, Baraga, and Paint River Groups (Figure 3). The Chocolay Group, which is probably correlative

Figure 5. Evolution of the tectonic foredeep. In 5a (from Hoffman, 1987), the initial rift deposits and the overlying passive margin sediments, which are represented by the Mille Lacs Group (A), were deposited on the rifted Superior craton during stage 1. During stage 2, the continental margin was partially subducted beneath a tectonic collage of arcs, accretionary prisms and continental fragments (the fold and thrust belt), as the ocean basin was consumed, leading to the formation of an actively migrating foredeep in which the Animikie Group sediments were deposited. In 5b (from Southwick et al, 1988), the Mille Lacs Group were deposited in a back-arc basin along the southern margin of the Superior craton. Ocean floor subduction in front of the arc led to the compression of the back-arc basin and the development of a foredeep on the cratonic side of the resulting fold and thrust belt.

5a

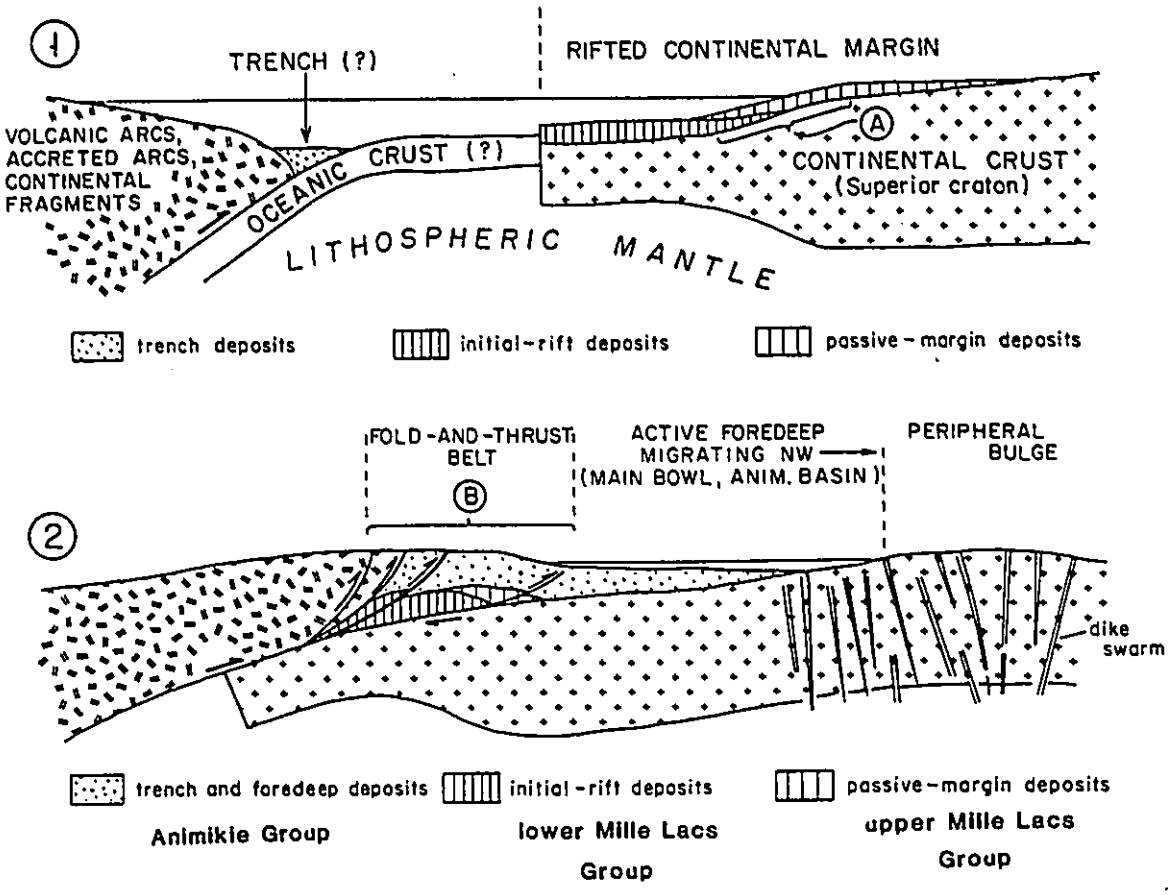
1
TRENCH (?)
RIFTED CONTINENTAL MARGIN
VOLCANIC ARCS, ACCRETED ARCS, CONTINENTAL FRAGMENTS
OCEANIC CRUST (?)
A
CONTINENTAL CRUST (Superior craton)
LITHOSPHERIC MANTLE
trench deposits
initial-rift deposits
passive-margin deposits
FOLD-AND-THRUST BELT
B
ACTIVE FOREDEEP MIGRATING NW (MAIN BOWL, ANIM. BASIN)
PERIPHERAL BULGE
2
dike swarm
trench and foredeep deposits
initial-rift deposits
passive-margin deposits
Animikie Group
lower Mille Lacs Group
upper Mille Lacs Group

5b

A. Before collapse of back-arc basin

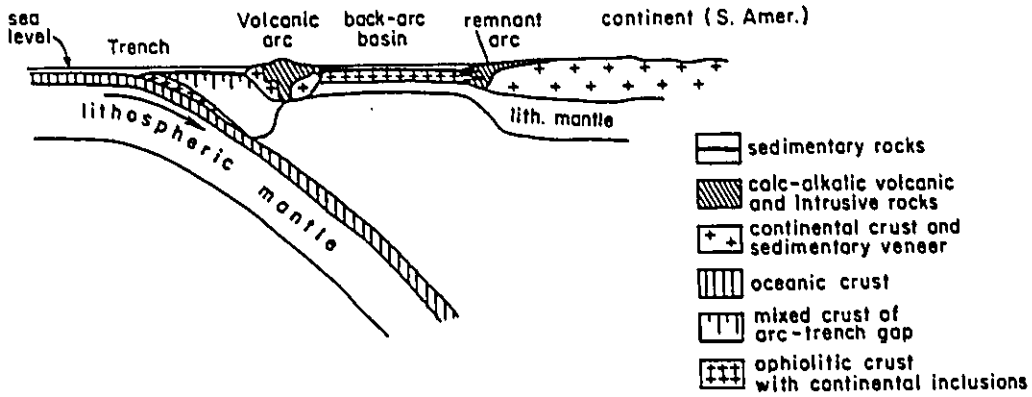

B. Following uplift, compression of back-arc basin

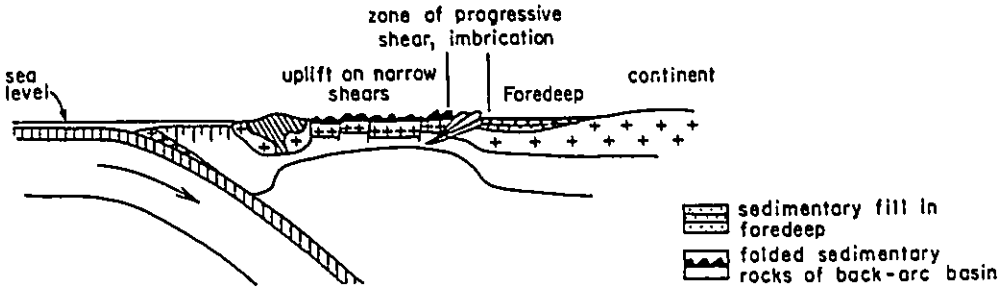

with the Mille Lacs Group of the northwest segment, is only exposed in parts of the Gogebic, Marquette, Amasa, and Menominee regions (Figure 3). It unconformably overlies Archean basement and consists of a basal coarse clastic unit (the Enchantment Lake, Reany Creek and Fern Creek Formations) overlain by several hundred meters of quartz arenite (the Sunday, Mesnard and Sturgeon Quartzites) and is capped by dolomite, which is in part stromatolitic (the Bad River, Kona, and Randville Dolomites). In the Marquette district about 500 m of muddy terrigenous material, the Wewe Slate, was deposited in the Marquette structural trough. Larue and Sloss (1980) suggest that extensional troughs, such as the Marquette trough, started to form at about the onset of sedimentation. The rocks of the Chocolay Group were mildly deformed and uplifted, leading to their erosional removal in most areas prior to deposition of the Menominee Group.

In the Gogebic Range (Figure 2) the Menominee Group is conformably overlain by the Baraga Group. Together they comprise a sequence of rocks which is similar to the Animikie Group in the northwest segment. Sedimentation of the Menominee Group starts with clastic sediments of the Palms Formation and is conformably overlain by the Ironwood Iron Formation. The Emperor Volcanic Complex, which underlies and is interbedded with the Ironwood Iron Formation, contains both a series of tholeiitic sills intruding a basalt sequence and a sequence of calc-alkaline volcanic rocks (Greenberg and Brown, 1983). The conformably overlying Tyler Formation of the Baraga Group consists of a thick sequence of interbedded sandstone, siltstone and greywacke.

Elsewhere in northern Michigan, an unconformity separates the Menominee and Baraga Groups and the stratigraphy of the MRS is more complex. The Menominee Group unconformably overlies either erosional remnants of the Chocolay Group or Archean basement (Figure 3). Sedimentation began with the accumulation of as much as 750 m of quartzite (the Felch Formation and the Ajibik

Quartzite). In the Marquette trough the quartzite is overlain by the Siamo Slate, at least 600 m of interbedded argillite, quartzite and detritus-rich iron-formation. The clastic units are overlain by up to 300 m of iron-formation (the Vulcan Iron Formation), except in the Marquette trough where as much as 1000 m of iron-formation was deposited (the Negaunee Iron Formation). Substantial stratigraphic differences between the sedimentary units from place to place suggest that sedimentation occurred in isolated fault-bounded, second-order troughs and on intervening platforms within the larger basin (Larue and Sloss, 1980). Volcanic rocks of the Hemlock Formation are considered by Prinz (1976) to correlate with the Negaunee Iron Formation of the Menominee Group and to be overlain by iron-formation of the Amasa and Fence River Formations (Morey and Van Schmus, 1988) (Figure 3). Alternatively, it has been placed at the base of the Baraga Group (James, 1958). It contains a thick sequence of pillow basalt, pyroclastic rocks, tuffaceous and terrigenous turbidites, and chert and is intruded by coeval ultramafic and gabbroic sills (Ueng et al, 1988). Ueng et al (1988) have shown that the source magma was probably a high-Ti tholeiitic basalt similar to present-day MORB.

Baraga Group sedimentation was an interval of pronounced crustal disturbance characterized by differential uplift and erosion which led to nearly total removal of Menominee Group strata and sedimentation in several graben-like depositional basins. Sedimentation began with up to 450 m of quartzite, the Goodrich Quartzite, which is overlain by the Michigamme Formation, containing up to 3000 m of interbedded greywacke and slate, thick sequences of mafic volcanic rocks and minor iron-formation. The Badwater Greenstone, a unit of pillow basalt that is lithologically similar to the Hemlock Formation (Ueng et al, 1988), either stratigraphically overlies the Michigamme Formation (James et al, 1968) or else has been tectonically emplaced (Larue and Ueng, 1985).

The Paint River Group consists of slate, greywacke, and iron-formation and is

found exclusively in the Crystal Falls area above the Badwater Greenstone. Because of the uncertainty of the stratigraphic position of the Badwater Greenstone, the Paint River Group has been interpreted to be either the youngest sequence in the region (James et al, 1968), the lithostratigraphic equivalent to the Menominee Group (Cambray, 1978), or a parautochthonous fault-bounded package that was transported here from its original site of deposition (Larue, 1983).

Sedimentation of the MRS records a progressive change in tectonic conditions from a stable craton (Chocolay Group) through a sedimentary basin with mild tectonism (Menominee Group), to a highly active tectonic basin (Baraga Group) during accretion of the Wisconsin magmatic terranes to the continental margin, now represented by a fold and thrust belt (Figure 6) (Klasner et al, 1989). Barovich et al (1989) have shown, using Nd isotope model ages, that the sediments in the lower part of the Baraga Group were derived from an Archean provenance whereas the upper part of the Baraga Group were derived from an early Proterozoic provenance, most likely the Wisconsin magmatic terranes. This implies that these sediments were deposited in a foredeep and were subsequently incorporated into the fold and thrust belt as the foredeep migrated northward (i.e. Hoffman, 1987). The boundary between the continental margin prism and the Wisconsin magmatic terranes is the east-trending Niagara fault zone (Figure 1), a broadly arcuate, convex system of ductile shears as much as 10 km wide. This zone has been interpreted as a suture between the northern passive margin assemblage and a southern island-arc terrane (Larue, 1983).

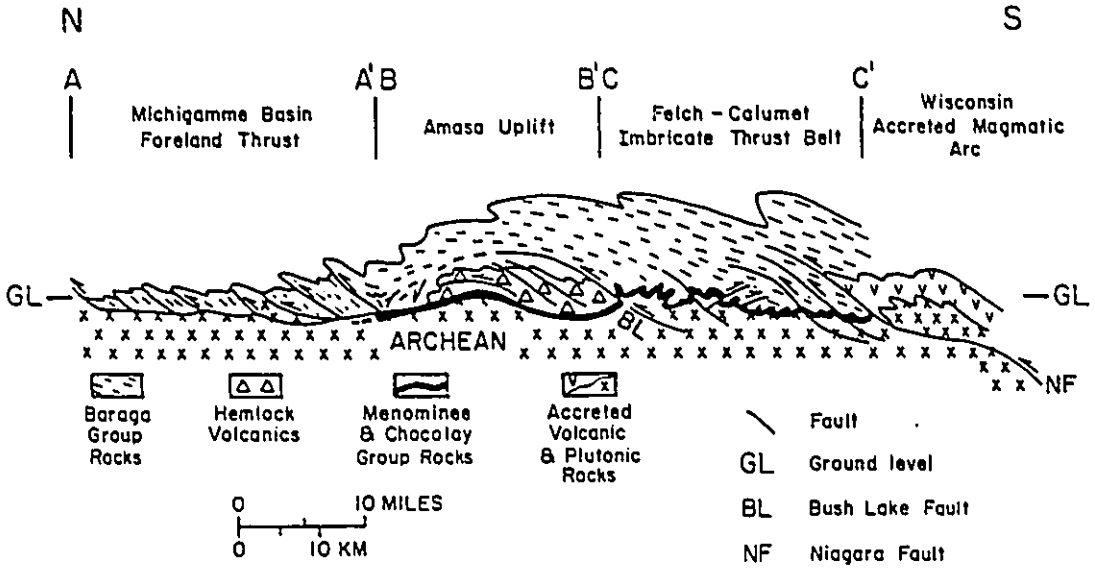

Figure 6. Composite structural profile through the early Proterozoic rocks of northern Michigan (from Klasner et al, 1989). Profile extends from just south of the Niagara Fault zone, northward through the Menominee range and Amasa Uplift (Figure 2).

2.1.3. THE WISCONSIN MAGMATIC TERRANES

Volcanic and plutonic rocks occur as a series of east-trending belts in northeastern and central Wisconsin (Figure 1). They are in fault-contact with rocks of the Marquette Range Supergroup to the north and with Archean rocks to the south. These rocks represent a complex volcanic arc formed on oceanic crust. Sims et al (1989) have divided the magmatic terranes into two subterranes: a northern terrane named the Pembine-Wausau terrane and a southern terrane called the Marshfield terrane. They are separated by the Eau Pleine shear zone.

The Pembine-Wausau terrane is the larger of the two and is composed mostly of volcanic rocks and derived sediments deposited between 1889 Ma and 1860 Ma. The oldest rocks are tholeiitic basalts and basaltic andesites overlain locally by a calc-alkaline suite ranging in composition from andesite to rhyolite. The association of sheeted dikes, serpentinite and plagiorhyolite, found in the northern part of this terrane, with tholeiitic basalt suggests that these rocks are a dismembered ophiolite (Schulz, 1987). The calc-alkaline rocks are geochemically similar to oceanic island arcs (Sims et al, 1989). In the central part of the terrane a bimodal association of high-Al basalt and dacite-rhyolite suites with Cu-Zn massive sulfide deposits and iron-formations resembles an intra-arc rift. The arc complex, which formed above a south-dipping subduction zone, collided with the northern continental margin at about 1860 Ma. Following collision a more restricted calc-alkaline volcanic succession with abundant rhyolite was deposited on top of the older succession between about 1835 and 1845 Ma. This period of renewed magmatism may have accompanied northward subduction during the closure of an ocean basin between the accreted arc terrane and a minicontinent on the south represented by the Marshfield terrane. Syn- to post-tectonic plutons, ranging in composition from gabbro and diorite through quartz monzonite and granite, intruded the volcanic

rocks from about 1870 to 1760 Ma (Sims et al, 1989).

The Marshfield terrane consists of remnants of an approximately 1860 Ma succession of mafic to felsic volcanic rocks and quartzitic sedimentary rocks that overlies a possibly continuous Archean basement (Sims et al, 1989). The layered rocks are intruded by 1890 to 1840 Ma tonalite and granite bodies. The Marshfield terrane collided with the Pembine-Wausau terrane along the Eau Pleine shear zone. The suturing marks the termination of the Penokean Orogeny and was completed by 1835 Ma, which is the age of alkali-feldspar granites that intrude the shear zone.

2.1.4. POST-PENOKEAN ROCKS

Following the Penokean Orogeny a thick sequence of platform quartzites, the Baraboo Quartzite and its equivalents (Figure 2), were deposited during the interval 1760 to 1630 Ma (Van Schmus, 1980). At about 1470 Ma (Van Schmus et al, 1975) the Wolf River Batholith, a large anorthositic and granitic intrusive complex, was emplaced in central Wisconsin. A major period of continental rifting between about 1200 and 1000 Ma (Morey and Van Schmus, 1988) resulted in thick successions of flood basalts, cogenetic gabbroic intrusions and associated sedimentary rocks that are collectively referred to as the Keweenawan Supergroup. Finally, the region was covered by generally flat-lying sedimentary rocks of Phanerozoic age.

2.2. GEOLOGY OF THE GUNFLINT FORMATION

The Gunflint Formation extends northeast from the Minnesota border to Thunder Bay, with isolated erosional remnants found as far east as Schreiber (Figure 7). It unconformably overlies a peneplained Archean basement (Goodwin, 1956), and is conformably overlain by the Rove Formation. Together they comprise

Figure 7. Geologic map of the Thunder Bay region (modified from Ontario Department of Mines, Maps 2065 and 2232).

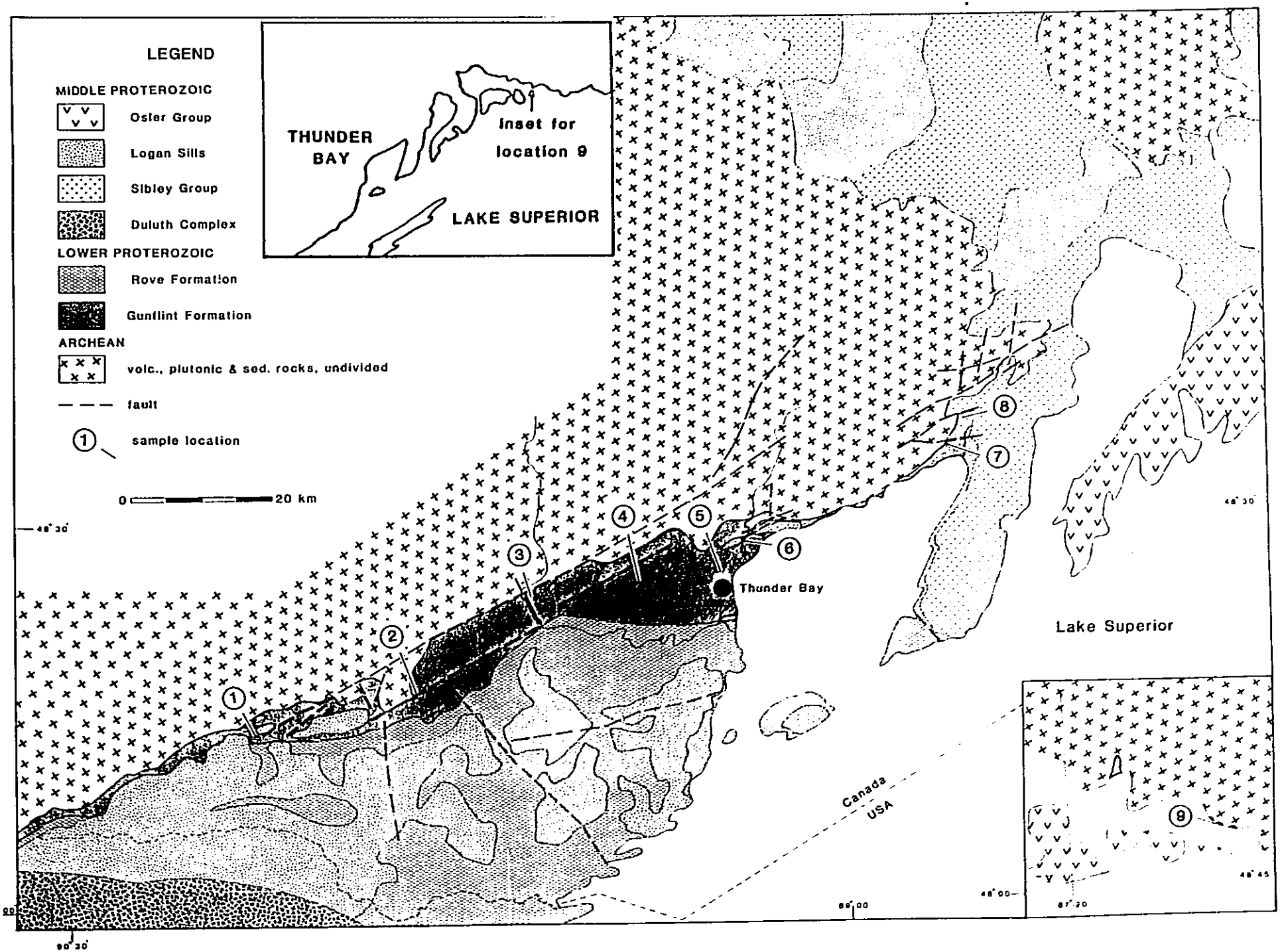
LEGEND
MIDDLE PROTEROZOIC
Osler Group
Logan Sills
Sibley Group
Duluth Complex
LOWER PROTEROZOIC
Rove Formation
Gunflint Formation
ARCHEAN
volc., plutonic & sed. rocks, undivided
fault
sample location
0
20 km
THUNDER BAY
Inset for location 9
LAKE SUPERIOR
Thunder Bay
Lake Superior
Canada
USA
48° 30'
48° 00'
88° 00'
90° 30'
87° 30'
48° 45'

the Animikie Group in Ontario (Figure 3). The Animikie strata are generally flat lying or dip gently to the southeast. Normal faults are common and are often accompanied by local folding and brecciation. Gabbroic dikes and sills, up to 30 m in thickness, are found throughout the region. The thickness of the Gunflint ranges from 100 m to 160 m.

Much of the Gunflint Formation is probably the least metamorphosed Precambrian iron-formation in the world (Floran and Papike, 1978). Near the Minnesota-Ontario border a portion lies within the contact aureole of the Duluth Complex. Within this aureole Floran and Papike (1978) have documented a progressive increase in metamorphic grade from essentially unmetamorphosed iron-formation to the pyroxene hornfels facies. Elsewhere, metamorphism is restricted to the contact zones of the gabbroic sills. Floran and Papike (1975, 1978) estimated a temperature between 100 and 150 ^{o}C for burial metamorphism. More recently Miyano (1987) estimated a temperature of 100 to 130 ^{o}C for the regionally metamorphosed rocks. For the remainder of this thesis, only those rocks that have undergone contact metamorphism will be referred as metamorphosed. The regional low grade rocks will be referred to as unmetamorphosed.

The stratigraphy of the Gunflint Formation is complex because of abrupt facies variations, which are evident at all scales. Lack of lateral continuity makes correlation of individual units within areas of sparse exposure difficult. Wolff (1917), divided the correlative Biwabik Iron Formation into "cherty" (granular textured) and "slaty" (nongranular textured) units, which were subsequently redefined as informal members (White, 1954). These terms are misleading though, because many of the "slaty" units also contain chert. Dimroth and Chauvel (1973) and Mengel (1973) showed that the granular textured iron-formation were reworked chemical sediments. Simonson (1985) preferred to classify iron-formation into two groups: those that are granular textured are referred to as iron-formation arenite and those

that are nongranular are referred to as iron-formation lutite. Goodwin (1956) was the first to attempt to work out the sedimentary facies relations in the Gunflint Formation. He divided the "cherty" (or arenitic) rocks into the algal chert and taconite facies and the "slaty" (or lutitic) rocks into the banded chert-carbonate and tuffaceous shale facies. The term taconite has commonly been used as an informal name for the iron-bearing rocks of the Lake Superior region (Morey, 1973), but is no longer in common usage. Goodwin (1956) also defined a conglomerate facies at the base and a limestone facies at the top of the Gunflint Formation. He further divided the Gunflint Formation into four members: the Basal Conglomerate member, the Lower and Upper Gunflint Members, and the Upper Limestone member.

The six sedimentary facies as defined by Goodwin (1956) have been retained but in modified form, and a seventh facies has been included. The algal chert facies, which is characterized by stromatolites, is renamed the stromatolite facies. The taconite facies, which consists mostly of beds of sand-sized intraclasts composed of chert and a variety of iron-minerals with some interbedded shale, is renamed the arenite facies. The tuffaceous shale, which contains variable quantities of pyroclastic detritus, is here referred to as the black shale facies. The new facies, called the laminated carbonate facies, was previously included with the banded chert-carbonate facies, but is relatively chert-poor. The sequences comprise five facies (Figure 8) that resemble the shallowing-upward sequences of James (1984). Goodwin (1956) defined two such cycles, the Lower and Upper Gunflint Members. However, Shegelski (1982) uncovered additional cycles indicating that at least three sequences are present. The conglomerate and limestone facies make up the Basal Conglomerate and Upper Limestone Members respectively.

LEGEND FOR FIGURE 8.

Rove Formation


shale

Gunflint Formation


Limestone facies


Arenite facies


Stromatolite facies


Black shale facies


Banded chert-carbonate facies


Laminated carbonate facies


Conglomerate facies


Archean Basement

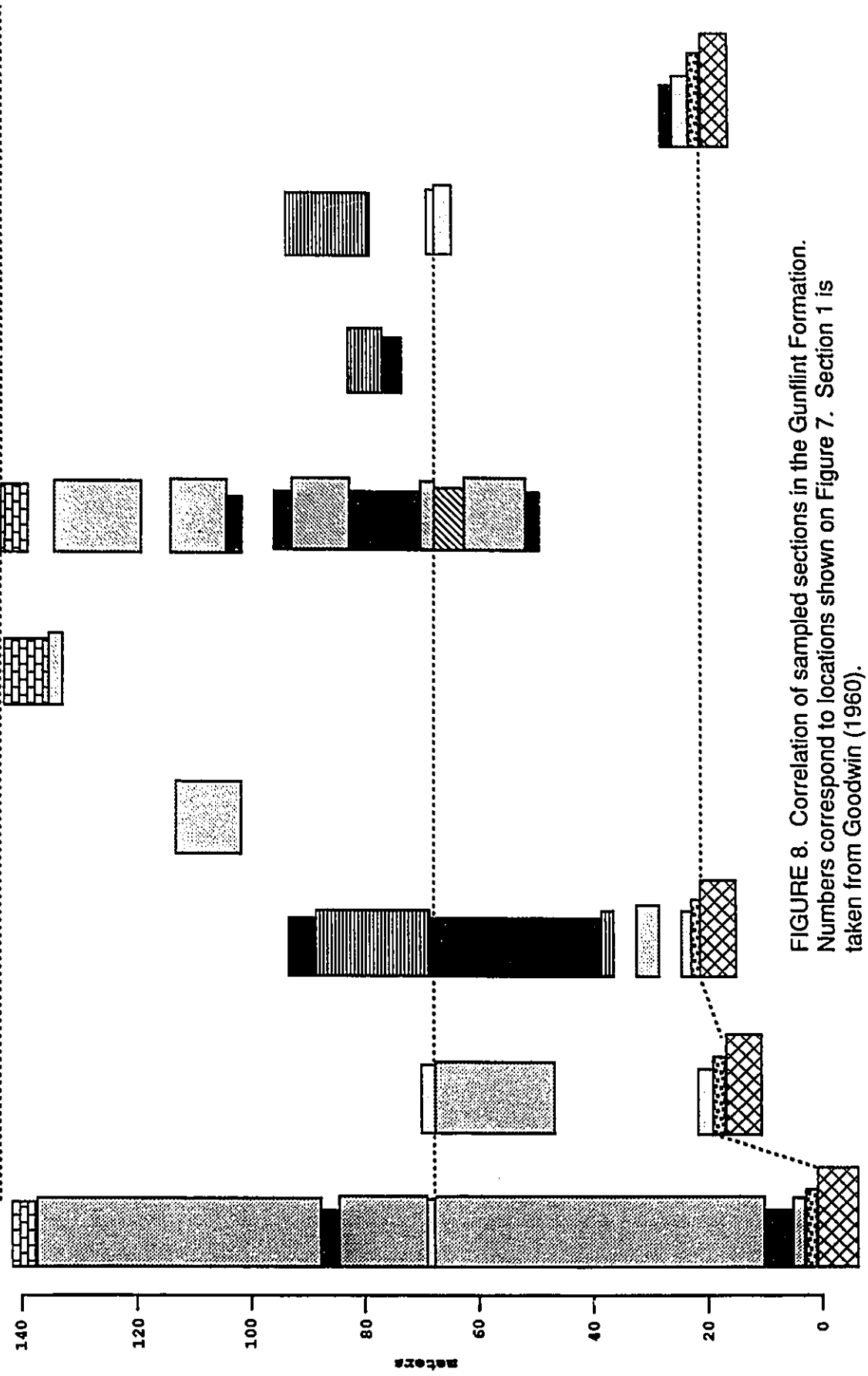

FIGURE 8. Correlation of sampled sections in the Gunflint Formation. Numbers correspond to locations shown on Figure 7. Section 1 is taken from Goodwin (1960).

2.2.1. THE CONGLOMERATE FACIES

The conglomerate facies is a thin, discontinuous unit unconformably overlying the Archean basement. The thickness is generally less than 1 m but locally may be up to 3 m. The clasts are well rounded, predominantly pebble-size and are made up mostly of white vein quartz, with some chert, jasper and Archean iron-formation, in a matrix of sand-sized quartz grains with variable chloritic matrix. Locally-derived boulders are occasionally present that are the same composition as the immediately underlying granite-greenstone basement. The conglomerate is overlain by the stromatolite and arenite facies. The conglomerate is considered to have formed during initial transgression of the sea over a peneplained Archean basement (Goodwin, 1956, 1960; Moorhouse, 1960). A basal conglomerate facies is typical for marine transgressive sequences (i.e. Bourgeois, 1980).

2.2.2. THE STROMATOLITE FACIES

The stromatolite facies is characterized by biohermal mounds, up to 1.5 m in height, containing millimeter to centimeter-sized planar, columnar and domal structures (Hofmann, 1969). At the base of the Gunflint Formation the bioherms encrust boulders of the conglomerate facies or basement rocks. Arenite forms the substrate for mounds higher in the stratigraphy. According to Goodwin (1956) this facies occurs at two stratigraphic intervals, and define the base of his Lower and the base of his Upper Gunflint Members. The stromatolites consist dominantly of chert, but have laminae that are rich in iron-silicates, hematite, magnetite or organic matter.

Arenite is present within stromatolitic laminae, between individual columns, and surrounding bioherms. The arenite consists mostly of medium to coarse

sand-size, well-sorted and well-rounded oolitic grains with lesser quantities of pisoliths, oncolites and nonoolitic grains. Arenite grains are composed dominantly of chert with variable proportions of iron-minerals, such as hematite, magnetite, greenalite and minnesotaite, and are cemented mostly by chert, but patches of ankerite and calcite commonly replace both cement and clasts.

At the base of the Gunflint near Schreiber (location 9, Figure 8) organic carbon commonly gives the chert a grey to black color (Plate 1A). Micro-fossils are well preserved in the laminae of many of these samples (see Hofmann and Schopf, 1983 for a review of Gunflint microfossils) and only minor quantities of iron-minerals are present. Iron-silicates, mainly greenalite, become more abundant towards the west and higher in the succession. Hematite is most abundant in the western end of the Gunflint (Plate 1B), where beds are locally rich in magnetite. Pyrite is locally abundant as individual euhedral grains and occasionally as irregular masses, laminae or layers. Along the Current River in Thunder Bay (location 6, Figure 8) pyrite and pyrrhotite form lenses and laminae within algal mounds. A massive layer of sulfide, a few centimeters thick, drapes some of these mounds at the contact with the overlying black shale (Plate 1C).

Many researchers (i.e. Hofmann, 1969; Gross, 1972, Simonson, 1987; Simonson and Lanier, 1987;) consider that the stromatolites formed originally as a silica gel. This interpretation is based on: 1) the presence of mega-quartz and chert-filled cracks and fractures, which contain internal sediment and micro-fossils indicating they formed near the sediment/water interface, 2) intergranular pore spaces between arenite grains are filled by similar chert and mega-quartz, 3) silica-cemented intraclastic pebbles of arenite indicate cementation near the sediment/water interface, and 4) excellent preservation of micro-fossils in chert indicate that silica precipitation must have been very early (Simonson, 1987; Simonson and Lanier, 1987). This implies that near-surface pore waters were

Plate 1.

A. Columnar stromatolites composed of black chert from base of Gunflint Formation near Schrieber, Ont. (Location 9, Figure 8). Siliceous oolites, which occupy spaces between columns, are cemented by chert. Organic carbon gives chert the black color. Iron minerals are very sparse in this area. Scale in inches.

B. Columnar stromatolites, from base of Gunflint Formation near Mink Mountain (Location 1, Figure 8), contain abundant hematite and chert, in contrast to Plate A. Scale in inches.

C. Massive layer of sulfide (below hammer), a few centimeters thick, drapes stromatolite mounds and is overlain by pyritic, cherty black shale. From along the Current River (Location 6, Figure 8).

D. Arenite with interbedded carbonate. Grain outlines are still visible in arenite layer (white layers) but have been extensively replaced by coarse grained ankerite (see plates 6C & D). Dark laminae and brown layer at top are composed of very fine-grained, laminated ankerite which are interpreted as primary (discussed in text). Note truncation of clastic layers by laminae of ankerite (arrow). Scale in inches.

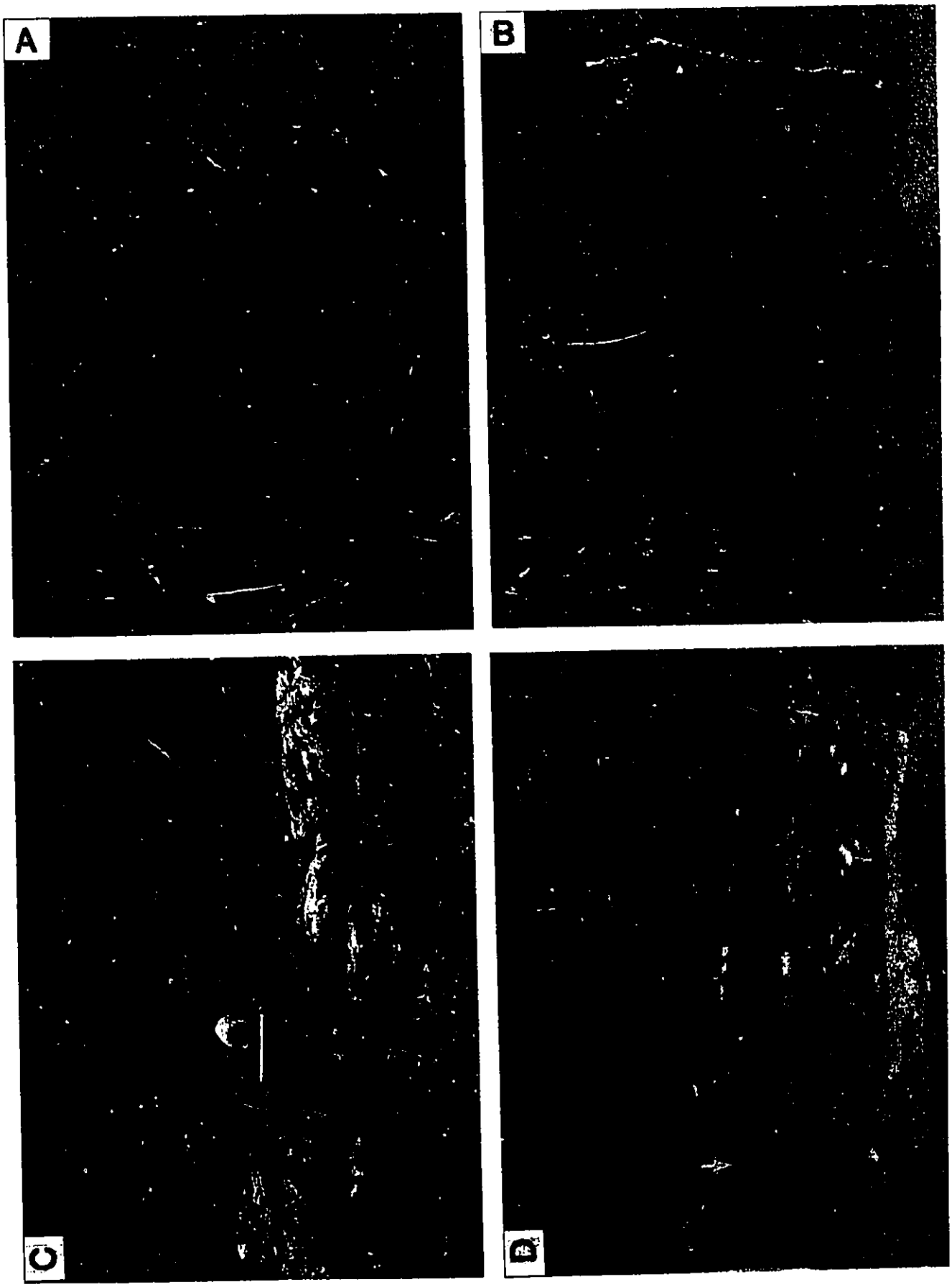

Plate 1

supersaturated with respect to silica. Others (i.e. Dimroth, 1976; Markun and Randazzo, 1980; Lougheed, 1983) propose that the stromatolite facies was originally a carbonate deposit but was replaced by silica.

Goodwin (1956) and Shegelski (1982) consider the stromatolites to have formed in shallow water, possibly in the intertidal-supratidal zone. At the base of the Gunflint Formation this facies represents the initial strandline and a reconstruction of this facies is illustrated by Shegelski (1982, fig. 4). Bioherms in the upper part of the Gunflint mark the top of a shallowing upward sequence (Goodwin, 1956; Shegelski, 1982) and formed on a silicified arenite substrate. Fralick (1989) offered an alternative interpretation to the shallowing upward sequence. He suggested that the stromatolites along the Current River (location 6, Figure 8) in the upper part of the succession formed below storm wave-base on a silicified carbonate substrate. This is based on his interpretation of hummocky cross-stratification (HCS) in arenite beds below stromatolites.

2.2.3. THE BLACK SHALE FACIES

This facies consists of carbonaceous and pyritic black shale. The term shale is used because it has been entrenched in the literature, however these rocks are primarily chemical sediments (mainly carbonate, with lesser quantities of pyrite, organic matter and chert) with variable amounts pyroclastic detritus; terrigenous detritus is minor or absent. Locally, pyroclastic beds are interlayered with shale. The fissile nature of this unit and its susceptibility to weathering often obliterate primary structures, but where they are observed they include lamination (> 0.5 mm) and very thin (< 2cm) cross-stratified or graded beds. Shegelski (1982) reported ripple marks and mudcracks preserved locally on bedding planes but these were not observed during this study. Also present are more resistant, massive-textured, thin

(up to 5 cm) carbonate-rich beds.

In most areas fine-grained pyrite is sparsely disseminated throughout the rock, but in some locations it may become very abundant. In the hydro spillway at Kakabeka Falls (Figure 8, Location 3) undeformed beds of black shale overlie folded and brecciated beds of banded chert-carbonate that contain abundant pyrite. Massive layers of pyrite within a shaly matrix are concentrated along this contact. Above this layer, an interval of black shale contains both pyrite and carbonate concretions over a vertical distance of about 5 m, at which point beds of ash and tuff appear. Concretions are not present above the first ash bed. Within the concretion-bearing shale, pyrite is abundant as fine disseminated grains, as coarse-grained aggregates and lenses, and as ellipsoidal concretions up to about 3 cm in diameter (Plate 2C). Sedimentary layering is wrapped around these concretions indicating growth before and during compaction. Carbonate concretions, up to about 1 m in diameter (Plate 3B), are also present in this section.

As indicated earlier, stromatolite mounds along the Current River (Figure 4, Location 6) are draped by a layer, about 6 cm thick, of pyrite and pyrrhotite at the contact with overlying black shale. The shale above the contact contains thin laminae of pyrite and pyrrhotite, which suggests that sulfide formed at or above the sediment/water interface. The pyrrhotite at this location, which underlies a gabbro sill, is the result of metamorphism of pyrite. Irregular-shaped pyrite concretions (Plate 2D) are found within a section of black shale in the Current River gorge, north of Highway 11-17. However, unlike the spillway section these concretions display textures suggestive of displacive growth after the sediments had undergone significant amounts of compaction.

Pyroclastic interbeds, composed of ash to lapilli-size detritus of basaltic to rhyolitic composition, are locally abundant. Variable proportions of pyroclastic material is also widespread within the shale. Sedimentary structures are widespread

Plate 2.

A. Arenite interbedded with shale. Arenite forms lenses and beds that pinch out laterally and are separated by thin-bedded shale partings.

B. Fine-grained, laminated ankerite (c) interlayered with arenite. Arenite is composed of a loosely packed framework of medium to coarse sand-size, iron-silicate (dark) and hematite-rich (red) intraclasts with abundant interstitial chert cement. Ankerite layers and rip-up clasts (arrows) of ankerite in arenite layer, do not contain any relic outlines of intraclasts indicating that ankerite did not replace intraclasts but are primary. Scale in inches.

C. Ellipsoidal pyrite concretion in black shale. Pyrite concretions occur along coarser layers (lighter colored) within black shale. Inner core of concretion contains coarse grained pyrite (black arrow) within a matrix of shale, which is texturally similar to coarse grained pyrite in shale outside of concretion (white arrow). The outer shell of the concretion consists of bladed crystals of pyrite that radiate outward from and surround the inner core. Bedding laminae are deformed around concretion except for terminations of radiating crystals of pyrite, which cut across layering which indicates they are early diagenetic. Scale in inches.

D. Irregular pyrite concretion in black shale. Coarse grained pyrite contains abundant inclusions of shale and displays textures indicating displacive growth during formation indicating that they formed during late diagenesis. Scale in inches.

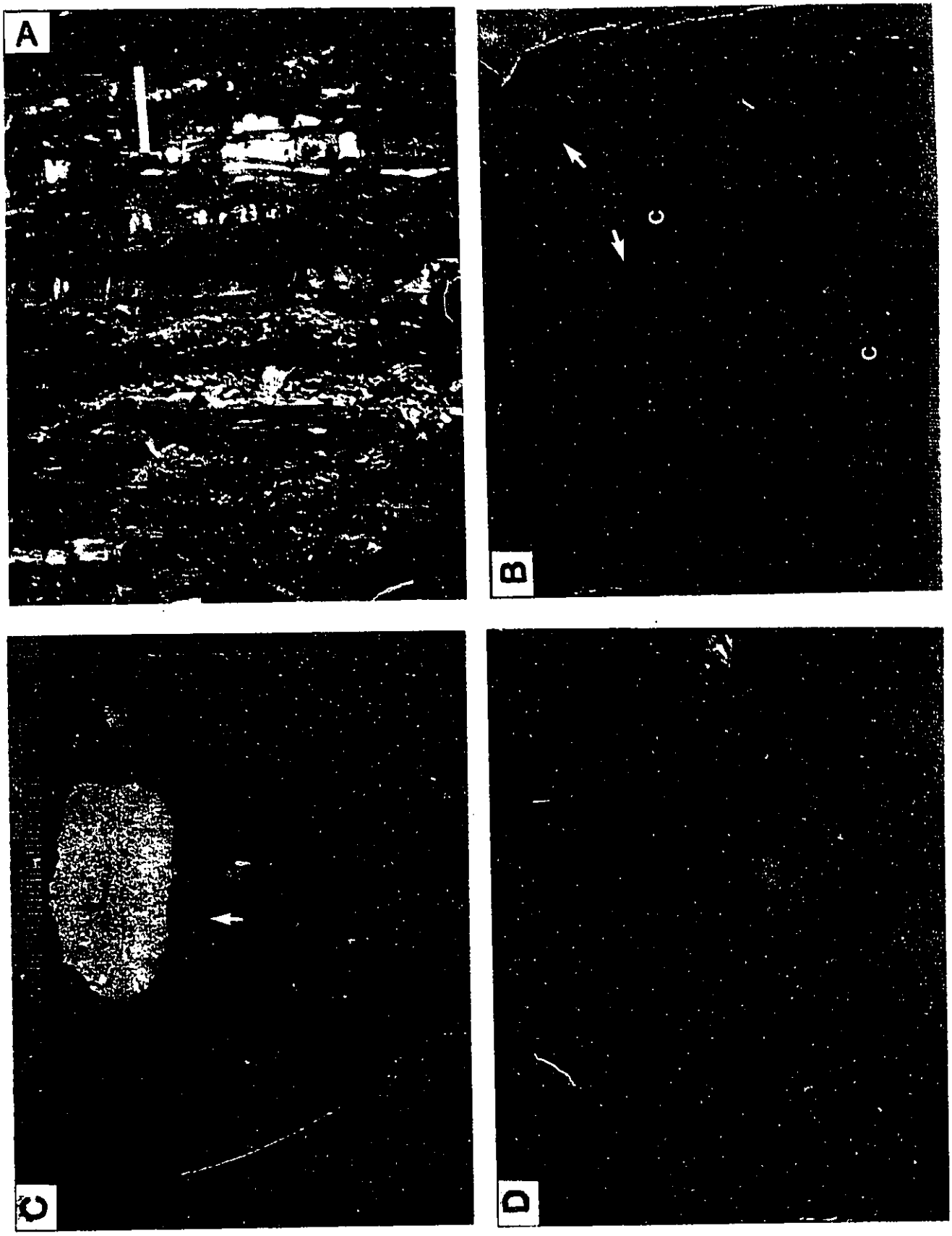

Plate 2

and well preserved in these beds, which range from a few cm to 1m in thickness, and include parallel lamination, cross-stratification and both normal and reverse graded bedding (Plate 3A).

The thickness of the black shale facies is highly variable, ranging from about 1 m to over 30 m. Black shale overlies the stromatolite, arenite and banded chert-carbonate facies, generally with a sharp contact. It is overlain gradationally by either arenite, banded chert-carbonate, or laminated carbonate facies. Shale is also interbedded with arenite, banded chert-carbonate and laminated carbonate.

Goodwin (1956) suggested that the black shale facies indicates a period of explosive volcanism that interrupted normal sedimentation. Shegelski (1982) considered the black shale to be lithologically equivalent to the overlying Rove Formation, which was deposited during drowning of the shelf. Thus the black shale facies would represent incipient drowning of the shallow platform or shelf. The presence of graded bedding, cross-stratification, parallel lamination and mud cracks in this facies and its association with other facies suggest that the black shale facies could have been deposited in a variety of water depths. The relative abundance of carbonate, organic matter and pyrite and the lateral association with the arenite facies, which is interpreted as a sand shoal, are consistent with deposition on a low energy, shallow shelf.

2.2.4. THE ARENITE FACIES

This facies is principally composed of lenticular to wavy beds of arenite interbedded with shale or carbonate. Arenite consists of medium to coarse sand-sized, well rounded, spherical to elliptical grains, which contain variable proportions of chert, greenalite, minnesotaite, hematite, magnetite and carbonate. These grains were derived from within the formation; no terrigenous detritus

Plate 3.

A. Graded beds of accretionary lapilli (towards top of photo). Clasts are relatively uncompacted and contain abundant interstitial ankerite and calcite cement, which probably formed during early diagenesis (also see Plate 9G). Large disk-shaped clast (black) at bottom of photo is shale. Scale in inches.

B. Carbonate concretion in black shale. Bedding is wrapped around concretion indicating growth during early diagenesis.

C and D. Upper Limestone member. Light colored areas are carbonate-rich (also see Plates 10B & C), dark areas are mostly chert and clastic grains (see Plates 10A & D). Chert-filled cavities, some of which resemble fenestrae (10D), contain laminated internal sediment (arrow) (see Plates 10G & H). Scale in inches.

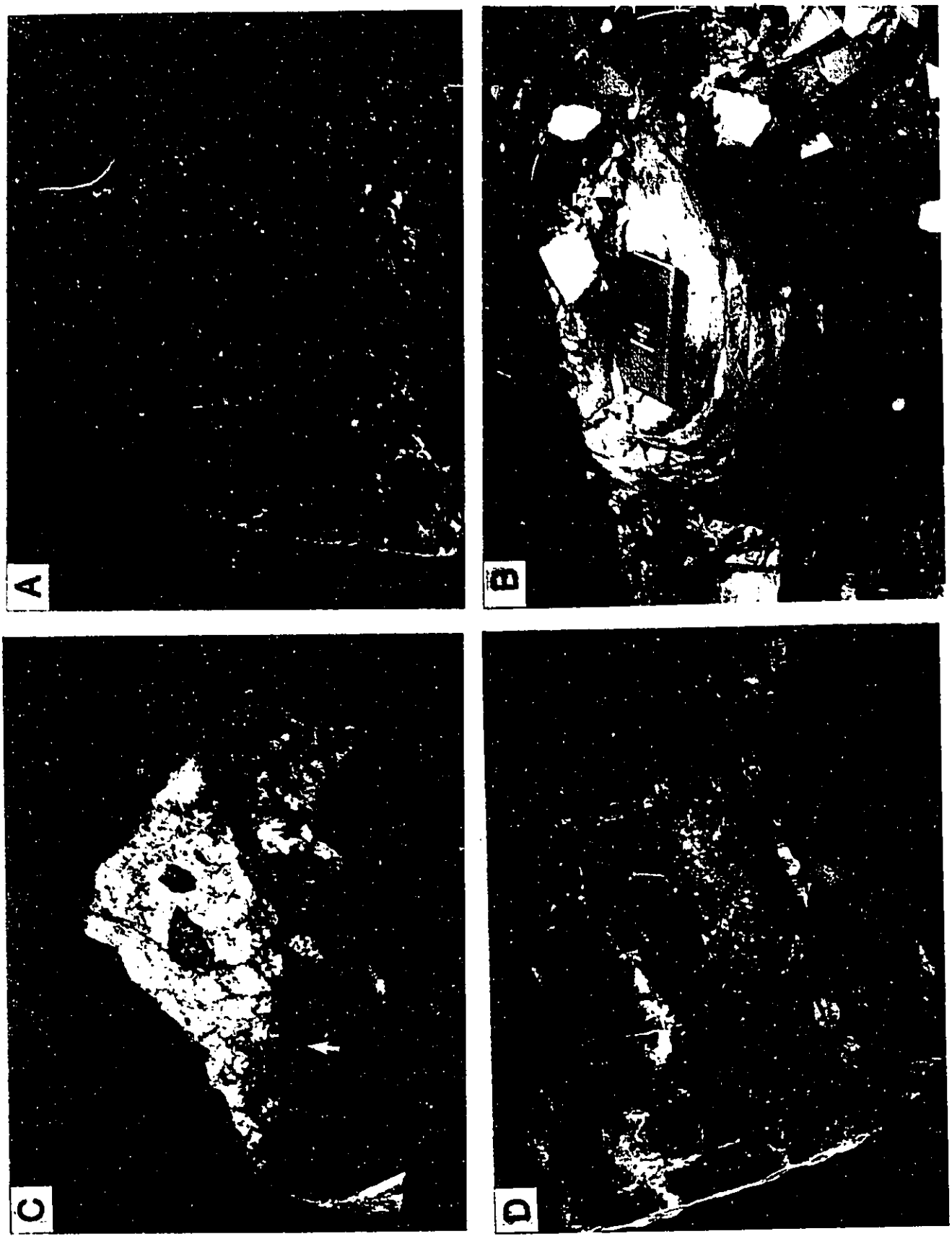

Plate 3

has been observed. Some of these grains are oolitic, especially in beds adjacent to stromatolites; however most are non-oolitic. Grains are commonly cemented by chert or carbonate. Shale beds are composed of fine-grained material that is optically similar in composition to arenite. Carbonate beds are composed of very fine-grained siderite or ankerite.

The proportion of arenite to shale is variable. Where arenite is the dominant lithology, bed thicknesses vary between a few centimeters to 50 cm and are separated by thin, shaly partings. Individual arenite beds may be uniform in thickness or may pinch and swell noticeably. Primary structures include tabular and planar cross-stratification. Locally, isolated rip-up clasts and beds of intraformational conglomerate contain rounded to angular clasts that are similar in composition to the enclosing rock. Irregular to rounded nodules, which consist of a loosely-packed framework of intraclasts with abundant interstitial chert cement, are common in arenite; areas adjacent to mottles are more tightly packed and contain less interstitial chert. Mottles often have primary stratification deformed around them indicating that they are early diagenetic features. Where shale is the dominant lithology, arenite occurs in lenses that resemble starved ripples or megaripples (Plate 2A). The shale here is finely laminated or cross-stratified.

Thin layers of finely laminated ankerite or siderite, which range from about a millimeter to a few centimeters in thickness, are commonly interbedded with arenite (Plate 1D and 2B). It has been proposed that the carbonate is diagenetic and formed as a result of the reduction of a primary ferric hydroxide by organic carbon (Drever, 1974; LaBerge et al, 1987). However, others have proposed that siderite is a primary mineral (i.e. Floran and Papike, 1975). Clastic textures are clearly visible in arenite layers (Plates 1D and 2B); adjacent carbonate layers are composed of very fine-grained, laminated siderite or ankerite that is similar to siderite layers in the banded chert-carbonate facies. This favours a primary origin for the carbonate

layers, which is supported by the presence of rip-up clasts of carbonate (Plate 2B).

The thickness of the arenite facies varies from 6 to 50 m. The contacts are gradational with underlying black shale facies, with overlying stromatolite facies and Upper Limestone member, and with laterally adjacent banded chert-carbonate and laminated carbonate facies. Layers of arenite are commonly interbedded with other lithologies. The lack of detrital quartz indicates remoteness from terrestrial relief.

The arenite facies is considered by Goodwin (1956) to have been deposited in the subtidal zone and the overlying stromatolites represent the top of a shallowing-upward sequence. Shegelski (1982) suggested that arenite interbedded with shale formed by alternating deposition of shale on tidal flats and sand on barrier bars. Interbedded carbonate layers would have formed along sites that escaped clastic dilution. Fralick (1989) interpreted primary structures in arenite along the Current River as hummocky cross-stratification and suggested that these rocks were deposited below wavebase. Variable and irregular bed thicknesses of sandy units with interbedded shale is typical of shelf carbonate sedimentation (Wilson and Jordan, 1983). Thicker, massive beds with tabular cross-stratification may represent sand shoals.

2.2.5. THE BANDED CHERT-CARBONATE FACIES

The banded chert-carbonate facies is made up of alternating layers of brown siderite and dark grey chert (Plates 4A, B & C). Thicknesses of layers vary from about a millimeter to a few centimeters and average about 1 cm. Locally, banding may be laterally continuous over the width of the outcrop (several 10's of meters) but more commonly the strata pinch out or are erosionally truncated by overlying layers (Plate 4A). Soft sediment deformation structures are common, and include intraformational breccias (Plate 4B) and slumped and folded beds sandwiched

Plate 4.

A. Banded Chert-carbonate composed of finely laminated chert (dark layers) and interlayered siderite (brown layers). Note synsedimentary erosional truncation of some bands by overlying bands (arrow), indicating that banding is primary.

B. Intraformational breccia in banded chert-carbonate indicate that deformation occurred before deposition of overlying layers. Angular clasts of chert (arrow) in matrix of siderite suggest that chert was already relatively brittle.

C. Polished slab of banded chert-carbonate showing fine grained siderite (brown layers) (also see Plates 7A to D) and laminated chert (dark layers) (see Plate 7E). Scale in inches.

D. Brecciated banded chert-carbonate from near Kakabeka Falls (Location 3, Figure 8). Pyrite is texturally complex and includes: very early diagenetic, fine-grained pyrite (not visible); early diagenetic small rounded concretion-like pyrite (arrow), and later coarse-grained pyrite which cross-cuts primary layering and contains abundant angular inclusions of host rock. Carbonate, which was originally siderite, has been recrystallized to ankerite (see Plate 7H). Scale in inches.

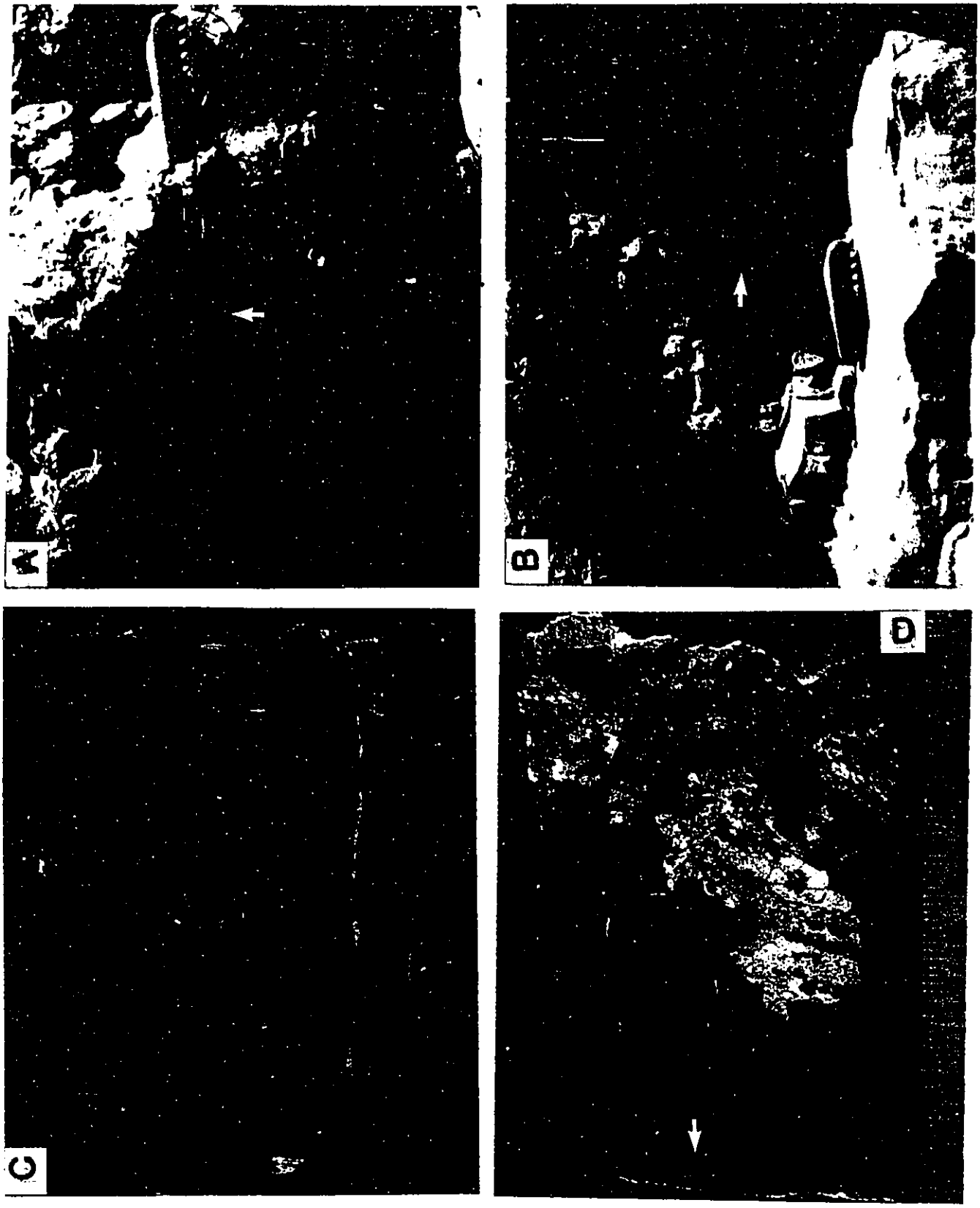

Plate 4

between undeformed beds. Shegelski (personal comm. 1987) observed desiccation cracks on bedding planes of carbonate layers. The thickness of this facies varies from a few meters up to 65 m. Banded chert-carbonate gradationally overlies black shale and grades laterally and upward into either black shale, arenite, laminated carbonate or the limestone facies.

Several faults are present in the Kakabeka Falls area (location 3, Figure 7) some of which are considered to be synsedimentary (Goodwin, 1956), while others post-date the formation. Within the Ontario Hydro spillway section, downstream from Kakabeka Falls, banded chert-carbonate beds in the lower 10 to 15 m of the Gunflint Formation have been intensely folded and brecciated along a fault. However, black shale overlying these beds is essentially undeformed, suggesting that this fault is synsedimentary. The banded chert-carbonate here is composed of coarse-grained (up to 0.5 mm) ankerite with abundant pyrite as coarse-grained aggregates and nodules, as veins, and as a cement to brecciated fragments (Plate 4D). The contact with the overlying pyritic black shale is marked by layers of undeformed massive pyrite in a black shaly matrix. Deformation of banded chert-carbonate beds and precipitation of pyrite appear to be related to synsedimentary faulting.

The banded chert-carbonate facies is thought by Moorhouse (1960) to have been deposited in deep, sheltered water. On the other hand, Goodwin (1956) suggested that this facies was deposited in broad, shallow lagoons. The presence of desiccation cracks and erosional surfaces support a shallow water environment, which may have been protected from wave action by barrier bars. Soft sediment deformation features and possible synsedimentary faults indicate a tectonically unstable environment or deposition on a slope.

2.2.6. THE LAMINATED CARBONATE FACIES

The rocks of this facies have previously been mapped as chert-carbonate (Moorhouse, 1960) and banded chert-carbonate (Goodwin, 1956). However, the distinctive chert layers typical of the banded chert-carbonate facies are not present here. This facies contains millimeter-scale parallel (Plates 5A & D) and low angle cross-lamination. Lamination consists of alternating dark, clastic rich and lighter, siderite-rich laminae (Plate 5D). Clasts consist of quartz, feldspar, chert and iron-rich intraclasts, and pyroclastic grains. Laminated carbonate has only been observed as one separate unit, about 12 m thick, along the Current River at Trowbridge Falls (Location 6, Figure 7), but is more commonly interbedded with arenite. This facies gradationally overlies and is overlain by black shale and is laterally gradational to the arenite and banded chert-carbonate facies.

Flat pebble conglomerate layers are present at several horizons throughout this section (Plate 5C). The clasts consist of shale, chert, pyroclastic grains, and quartz and are cemented by ankerite. Thicknesses are on the scale of a few centimeters. Small (less than 1cm), round ankerite nodules or concretions were observed below one conglomerate layer (Plate 5B) in a siderite-rich bed.

The fine-scale alternating clastic and carbonate laminae, the presence of flat pebble conglomerate, and its position shoreward of the laterally adjacent arenite facies suggests that this facies was deposited in a low energy, shallow environment which received periodic clastic input.

2.2.7. THE LIMESTONE FACIES

The limestone facies marks the top of the Gunflint Formation. It consists mostly of coarse-grained (up to 0.5 mm) calcite and/or dolomite with variable

Plate 5.

A. Typical example of parallel laminated carbonate containing thin clastic-rich and carbonate-rich laminae (see Plate 5D). Scale bar is in centimeters.

B. Round ankerite nodules (white) (also see Plate 8F) in layer composed mostly of siderite (dark). These nodules occur below an ankerite-cemented conglomeratic layer (see Plate 5C), partially visible at top (brown clasts). Scale in inches.

C. Thin conglomerate layer in laminated carbonate contains disk shaped clasts of chert, shale and volcaniclastic material with abundant ankerite cement (see Plates 8G & H). Scale in cm.

D. Polished slab of laminated carbonate showing parallel layering of siderite-rich (light colored) and clastic-rich (dark colored) laminae (see Plates 8A to D). Scale in inches.

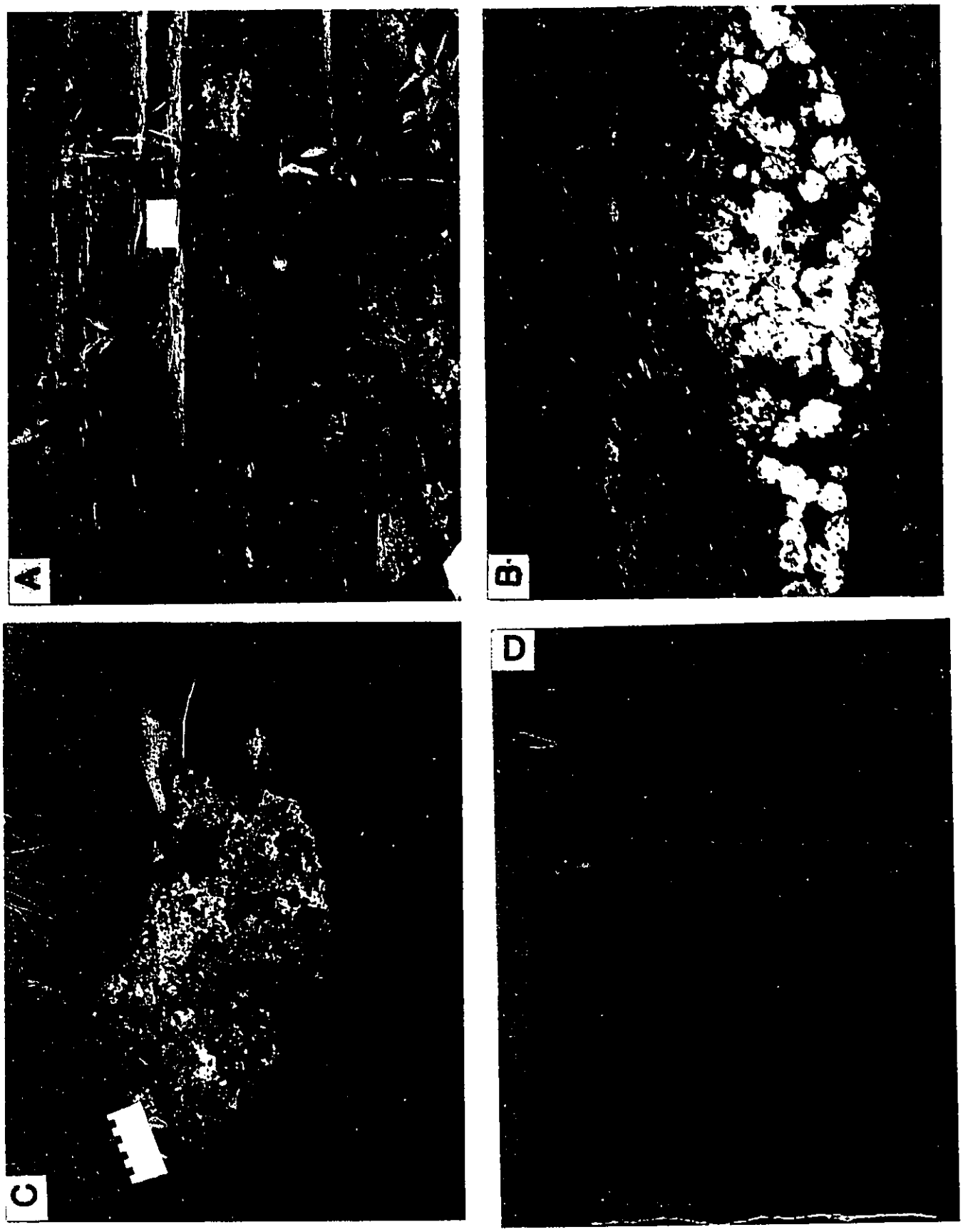

Plate 5

quantities of clastic material. A variety of chert filled cracks and irregular cavities, some of which resemble fenestrae (Simonson, 1987), are common in the limestone facies (Plates 3C & D). The relative proportion of calcite and dolomite varies considerably both on a regional scale and between adjacent beds. Near the top of this facies, thin layers of disk-shaped mudchips were observed interbedded with limestone. The limestone member varies in thickness from 1.5 m to about 12 m. It gradationally overlies arenite and is gradationally overlain by shale of the Rove Formation (Morey, 1967).

A rare exposure of calcareous stromatolites outcrop in Thunder Bay south of Hillcrest Park. This stromatolitic horizon is only a few 10's of centimeters thick; it overlies cherty arenite and is overlain by clastic textured limestone. These stromatolites differ from cherty stromatolites in the rest of the formation in that their laminae average about 1 to 2 mm in thickness compared to about 0.1 mm for cherty stromatolites, are composed of coarse-grained (up to 0.5 mm) sparry calcite, and contain chalcedony-filled voids that resemble fenestrae. The stratigraphic position of this unit is uncertain. It is lithologically similar to the limestone facies but its present elevation suggests that it occurs stratigraphically lower than the limestone member. However, this may be a result of block faulting.

Goodwin (1956) and Shegelski (1982) consider the limestone to have been deposited on a shallow carbonate shelf or platform. The presence of mudchips, fenestrae and stromatolites support this interpretation. The overlying shale of the Rove Formation was formed during drowning of the shelf.

2.2.8. DEPOSITIONAL SETTING

Goodwin (1956) proposed that the Gunflint Formation was deposited in a broad, relatively shallow basin that had limited access to the open ocean near a

region of active volcanism. Larue and Sloss (1980) suggest that the Gunflint Formation, and correlative iron-formations in Minnesota, were deposited in a broad shallow basin on a rifted passive margin, which acted as a separate depocenter from the iron-formations in Michigan. More recently, it has been proposed that the sediments of the Animikie Group were deposited within a foredeep during the Penokean Orogeny (Southwick et al, 1988; Hoffman, 1987). Volcanic activity during deposition of the iron-formations is indicated by pyroclastic beds throughout the area, which range from basaltic to rhyolitic in composition, and by mafic volcanic rocks of the Emperor Volcanic Complex, which are interbedded with the correlative Ironwood Iron Formation of the Gogebec Range (Figure 3). Goodwin (1956) suggested that volcanism was the source of the iron and silica in this iron-formation.

Shegelski (1982) proposed that the Gunflint Formation was deposited on a shallow shelf, similar to modern shelf carbonate environments, and compared the sedimentary facies to shallowing upward sequences (i.e. James, 1984). Although it may not be appropriate to compare Precambrian iron-formation settings to modern carbonate analogues, there are many similarities with the modern Persian Gulf. The Persian Gulf, which is also classified as a foredeep, is a large, shallow inland sea that has restricted communication with the Indian Ocean (Wilson and Jordan, 1983). The more or less random distribu..on of lithofacies of the carbonate shelf (Figure 9) is similar to that of the Gunflint Formation. The near-shore carbonate shelf is characterized by deposition of fine-grained carbonate muds in minor depressions and carbonate sand shoals (bioclastic and oolitic sands) and reefs on higher areas. Finer grained argillaceous carbonate sands and muds are deposited further offshore. The shelf is rimmed landward by tidal flats. Only minor amounts of fine-grained terrigenous detritus are brought into the basin by the Tigris, Euphrates, and Karun Rivers, which flow only part of the year. It must be emphasized that although physical conditions of the Gunflint Formation may have been similar to the Persian

Legend for Figure 9.

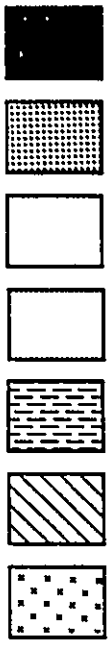

Reef limestone

Bioclastic sand

Bioclastic mud

Oolite sand

Lime mud

Tidal flat

Land

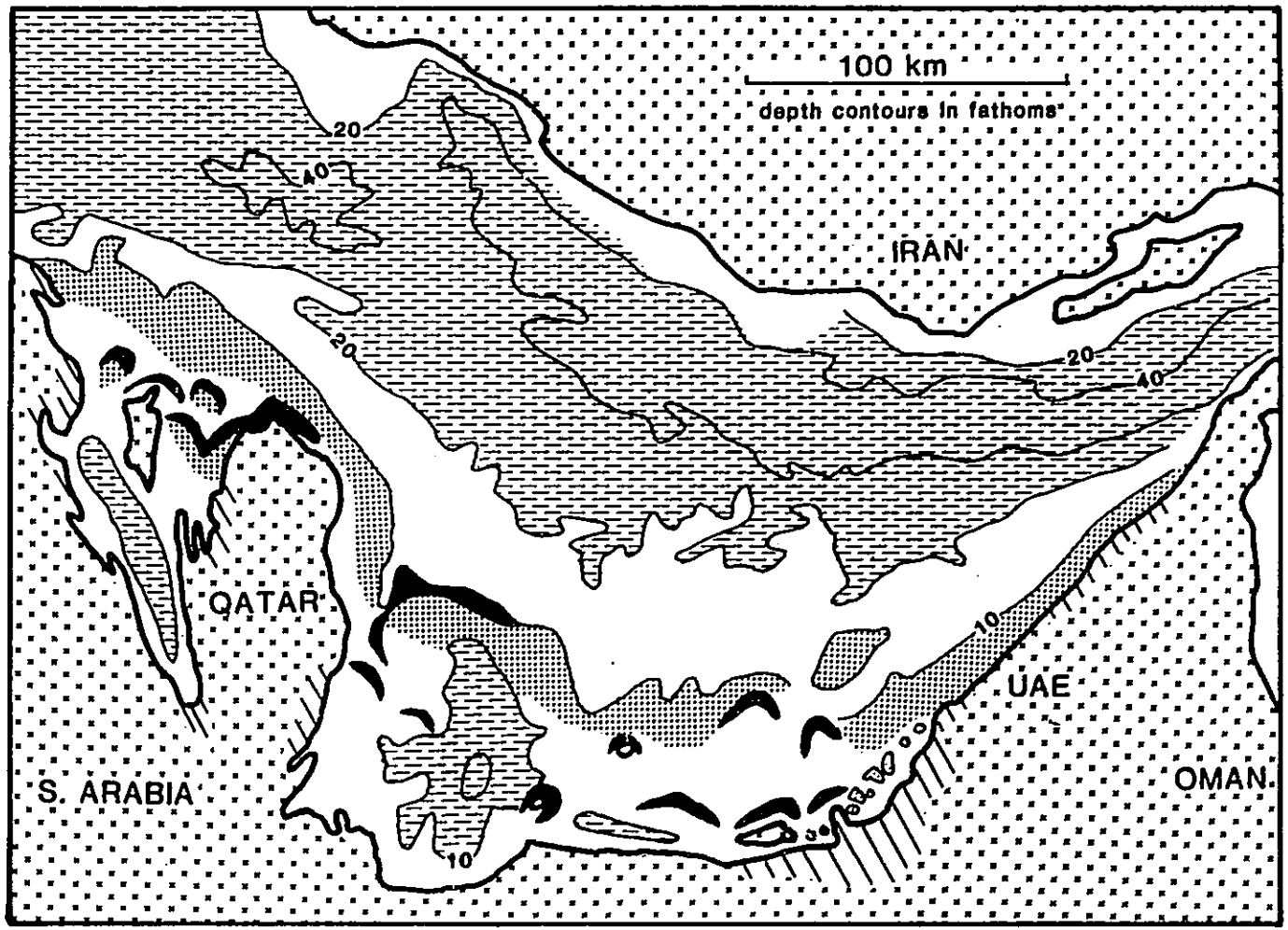

Figure 9. Carbonate facies of the Persian Gulf Great Pearl Bank.
(from Wilson & Jordan, 1983)

Gulf, chemical and biological factors would have differed substantially.

The depositional setting of the Gunflint Formation is interpreted in this thesis as follows. The basal conglomerate of the Gunflint Formation represents a transgressive lag deposit. The cherty stromatolites formed on boulders and basement rocks, which provided a firm substrate, along the shoreline and possibly on the shallow shelf where early cementation of sand shoals provided a suitable substrate. The arenite facies was deposited as intraclasts on the shallow shelf and on shoals. Fine-grained laminated chemical muds (banded chert-carbonate, laminated carbonate and black shale) precipitated in depressions on the shallow shelf and in lagoons behind sand shoals. The overlying Rove Formation was deposited further offshore in deeper water. Transitions between different lithofacies are generated readily in shallow water where minor changes in sea level or depositional topography can cause significant changes in both the physical and chemical environment. Thus relatively oxidized minerals, such as hematite (or a ferric hydroxide precursor), may be stable in wave swept sand shoals but reduced minerals, i.e. siderite or pyrite, could be the stable iron minerals in more restricted environments such as lagoons. Therefore, mineralogical facies (i.e. James, 1954) may not reliable indicators of water depth.

2.3. OTHER IRON-FORMATIONS IN THE LAKE SUPERIOR REGION

The iron-formations of the Animikie Basin (the Gunflint, Biwabik and Ironwood Iron Formations) were deposited within the shallow sub-tidal and possibly intertidal zones of a marine shelf or platform. The sediments of the Ironwood Iron Formation grade eastward into a dominantly argillaceous and mafic volcanic sequence, which is probably the source of the pyroclastic material found within these iron-formations.

Individual iron-formations in eastern Upper Michigan were deposited under differing conditions and do not appear to be continuous, although they may be synchronous. The Negaunee Iron Formation, as well as several smaller iron-formations, was deposited in a fault-controlled rift basin (Larue, 1981). Other thinner iron-formation (i.e. the Vulcan, Amasa and Fence River iron-formations) were deposited on intervening platforms. The Riverton Iron Formation is associated with deep water slates, greywackes and debris-flow deposits (James et al, 1968). Numerous thin, lenticular iron-formations are interbedded with the deep water shales, greywackes and volcanic rocks that overlie the major iron-formations of the region.

Small, lenticular iron-formations are present in the Wisconsin magmatic terranes and are associated with massive sulfide deposits found in bimodal volcanic rocks, which are considered to have formed within an intra-arc rift (Sims et al, 1989). These iron-formations are very similar to those found in Archean greenstone belts. Small lenticular iron-formations are also intercalated with volcanic rocks and black carbonaceous slate within the Mille Lacs Group in Minnesota, which represent the initial rift phase during the early stages of basin development (Southwick et al, 1988).

In summary, iron-formations were deposited in a wide variety of depositional settings indicating that depositional environment was not a controlling factor in their formation. However, all appear to have been deposited during a period of rifting and/or volcanic activity.

3. PETROGRAPHY

The purpose of the petrographic studies was to establish the mineralogy and the paragenetic sequence of the carbonate and sulfide minerals and their relation to other components. The carbonate minerals found within the Gunflint Formation include siderite, ankerite, dolomite and calcite; however all four phases are never found together. The assemblages siderite-ankerite-calcite, siderite-ankerite, and ankerite-calcite are commonly found in all facies except the Upper Limestone Member, which only has dolomite and calcite. In metamorphosed sediments, siderite may be destroyed and replaced by the assemblage ankerite-calcite or dolomite-calcite. Microprobe analyses of representative carbonate phases are shown in Figure 10. Siderite and calcite form distinct fields, whereas ankerite and dolomite form a series from almost pure dolomite to ankerite containing about 30 mole % Fe. Pyrite is the dominant sulfide mineral, although pyrrhotite is locally abundant in metamorphosed sediments.

3.1. ARENITE FACIES

This facies consists of massive to lenticular beds of arenite and interbedded shale or carbonate. Arenite is also intimately associated with stromatolites. Dimroth and Chauvel (1973) and Mengel (1973) noted the detrital nature of granular-textured or arenitic iron-formation. The framework is composed mostly of medium to coarse sand-size oolitic and nonoolitic intraclasts, but pebble-size intraclasts are common, either isolated or in conglomerate layers. Oolitic grains, which are commonly associated with stromatolites, are much less abundant than nonoolitic grains. Arenite beds tend to be dominated by either one type of grain or the other. Interstitial material is composed of chert cement and fine-grained matrix

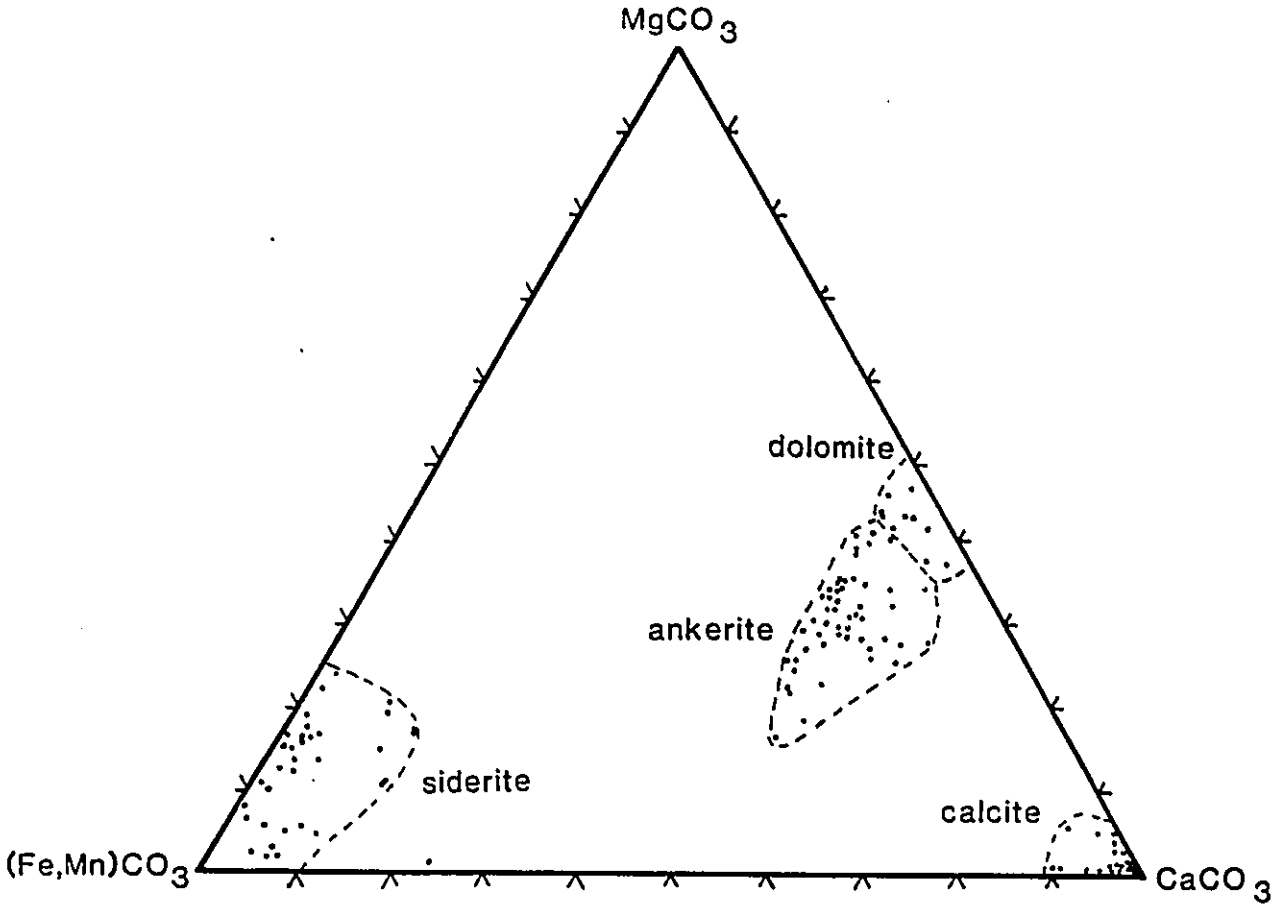

Figure 10. Ternary plot of carbonate minerals from the Gunflint Formation.

that is optically similar to intraclasts.

Nonoolitic arenite grains are mostly well-rounded and well-sorted although angular and poorly sorted varieties are not uncommon. Frameworks may be open with abundant interstitial cement, be tightly packed with little interstitial material, or be matrix supported. Matrix is usually only abundant in arenite that is interbedded with shale.

The mineralogy of these grains commonly consist of chert with variable proportions of one or more of greenalite, minnesotaite, hematite, magnetite and carbonate. The petrology and internal textures of grains from the Gunflint Formation have been described by Goodwin (1956), Floran and Papike (1975), Lougheed (1983) and Simonson (1987). Clasts in arenite that contain abundant interstitial chert or chalcedony cement tend to be chert-rich, whereas clasts in tightly packed arenite generally consist of magnetite and/or iron-silicates (Simonson, 1987). Clasts associated with shale layers are usually rich in iron-silicates.

Oolitic grains are usually well-rounded and well-sorted. The nuclei of oolitic grains is similar in composition and texture to nonoolitic grains (Simonson, 1987) and have a thinly and concentrically laminated coating of silica. The morphology of these grains from the Gunflint Formation are described by Markun and Randazzo (1980) who interpret them as silicified carbonate oolitic grains. However, this is disputed by Simonson (1987) (see below). The interstitial material is mostly chert cement with minor amounts of fine-grained intraclasts. Composite particles were often observed that consist of chert-cemented grains that resemble carbonate grapestone.

Cement consists mostly of chert, chalcedony and/or megaquartz (quartz crystals $> 35\ \mu m$ in diameter) displaying a variety of textures that have been described by Simonson (1987) from the Gunflint Formation and other Lake Superior type iron-formations. Loosely packed frameworks with abundant chert

PLATE 6. Arenite. Plane light except where noted.

A. Sample GF-6. Thin laminae composed of siderite (black arrows) in arenite appear to be primary. Intraclasts and interstitial areas are composed mostly of chert but are partially replaced by ankerite (A) adjacent to siderite laminae. Bar = 0.2 mm.

B. Sample 3B. Uncompacted oolitic grains contain abundant early chert cement except inside dotted line where coarse-grained ankerite (A) has replaced both oolitic grains and chert cement, indicating ankerite is late. Oolitic grains were originally siliceous or were replaced by silica during very early diagenesis, before cementation by chert. Bar = 2.0 mm.

C. Sample 6A. Iron-rich intraclasts adjacent to fine-grained, laminated ankerite layer (center of photo) have been replaced by coarse-grained ankerite (light colored) but still retain grain outlines (see plate 6D). Thin laminae of fine grained ankerite (dark laminae in top of photo) are often deformed around clast outlines suggesting carbonate was primary precipitate. Bar = 2.0 mm.

D. Sample 6A. Close-up ankerite replaced intraclast, is composed of inward growing coarse-grained ankerite with interior of iron-silicates and chert. Bar = 0.5 mm.

E. Sample 40B. Arenite in right half of photo has been partially replaced by coarse-grained ankerite (a). Note bleached zone (b), consisting mainly of chert, between ankerite and unaltered arenite (top left). Bar = 2.0 mm.

F. Sample 10J. Calcite (c) partially overgrows, and thus post-dates, chert cement interstitial to arenite grains (black). Bar = 0.2 mm.

G. Sample 11D. Patches of coarse-grained ankerite (A) overgrow several intraclasts and interstitial chert cement. (crossed polars) Bar = 2.0 mm.

H. Sample 10K. Matrix supported arenite. Clasts consist mostly of iron-silicates which are similar in composition to shale matrix. Bar = 0.5 mm.

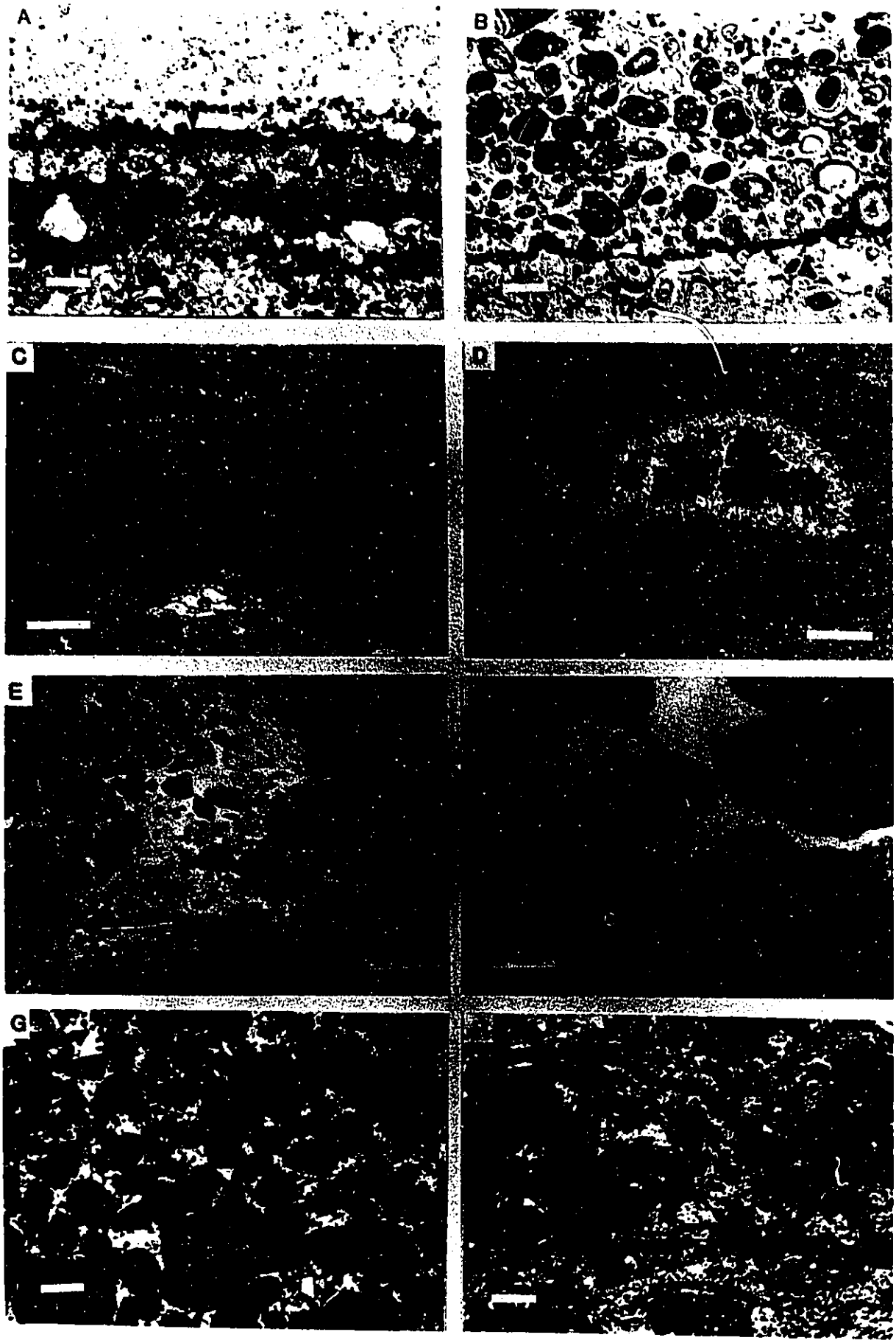

Plate 6

cement and chert-cemented intraclasts indicate that much of this cement formed during very early diagenesis. Matrix is only abundant where arenite is interbedded with shale and is similar in composition to the shale.

Carbonate occurs as primary laminae and thin layers and as replacements of earlier formed minerals. The laminae (Plates 1D & 6A) and layers (Plates 1D,2B, 6C & D) are composed of very fine-grained siderite or ankerite. The fine-grained, laminated texture of this carbonate, the bending of carbonate laminae around clastic grains, and the occurrence of isolated clastic grains (now replaced by ankerite) floating in fine-grained ankerite indicate the carbonate is primary and probably precipitated at the sediment/water interface as laminated crusts during intervals of reduced clastic supply. Where siderite is present, siderite grains and adjacent clastic grains are either cemented by or replaced by ankerite (Plate 6A), indicating ankerite formed during diagenesis. In some cases, adjacent clastic beds have been almost completely replaced by ankerite, although clastic textures have been preserved (Plate 1D & 6C).

Within arenite beds that do not contain carbonate layers, crystals of ankerite and calcite partially or completely replace both framework clasts and interstitial cement (Plates 6B, F & G), whereas adjacent clasts preserve primary textures. Coarse-grained ankerite may form small aggregates or may extensively replace entire beds (Plate E). These textures indicate that ankerite and calcite formed during late diagenesis. In metamorphosed samples, dolomite (or iron-poor ankerite) and calcite are the common carbonate minerals and are intergrown with metamorphic minerals.

Pyrite is not common in arenite but where present it is usually associated with carbonate layers and commonly shows textures, i.e. cross-cutting grain boundaries, suggesting that it post-dates framework grains and chert cement. However, in adjacent carbonate layers, pyrite occurs as very fine, disseminated grains indicating it

formed during early diagenesis and so was probably the source of the pyrite in clastic layers and formed during recrystallization.

3.2. BANDED CHERT-CARBONATE

The banded chert-carbonate facies is made up of layers of microspherical siderite grains (Plates 4C, 7A & B) interlayered with almost pure chert (Plate 7E). Previous work (Goodwin, 1956; LaBerge, 1973; Kazmierczak, 1979) has shown that individual siderite spheres have diameters mostly between 25 to 45 μm, and typically have a 10 to 20 μm thick outer wall around a central core. The outer walls are composed of aggregates of microscopic siderite crystals and have closed irregular spaces within them, which may be filled by chert, giving the walls a double layered appearance (see figs. 11-14, LaBerge, 1973; figs. 2 & 3, Kazmierczak, 1979). The inner core is filled by fine crystalline silica and may contain siderite aggregates and rare pyrite inclusions. These spheres are often observed to have rhombic overgrowths of siderite (Plate 7C).

LaBerge (1973) interpreted these microspheres as relics of the microfossil Eosphaera tyleri (Barghoorn and Tyler, 1965), which was interpreted by Kazmierczak (1976) as a eukaryotic organism. Kazmierczak (1979) compared the siderite microspheres with volvocacean-associated calcispheres common in Devonian shallow water limestones. Others suggest that the microspheres are of inorganic origin and are either siliceous or sideritic spherulitic structures that were modified by diagenesis or metamorphism (e.g. Oehler, 1976).

The density of siderite spheres within layers ranges from tightly packed with very little interstitial chert (Plate 7A) to loosely packed spheres supported by the chert matrix (Plate 7C). In the first case the contact between chert and siderite layers is sharp and often accentuated by the presence of stylolites (Plate 7F). In the latter

Plate 7. Banded Chert-carbonate.

A. Sample 5B. Siderite microspheres (dark), from siderite layer, with minor amounts of interstitial chert (light patches). Most siderite occurs as individual spheres, however some spheres have coalesced (in water column ?) to form clumps. Bar = 0.2 mm.

B. Close-up view of above showing dark inner core and lighter colored rim (arrow) of siderite microsphere. Bar = 0.1 mm.

C. Sample 35L. Loosely packed siderite microspheres in chert matrix (c). Fine-grained rhombs of ankerite partially overgrow some siderite microspheres. Bar = 0.1 mm.

D. Sample 35B. Ring-like structure composed of chain of siderite microspheres (black arrow) in chert (light area). Rest of photo contains mostly individual siderite microspheres (dark area). Bar = 0.2 mm.

E. Sample 35L. Finely laminated chert layer contains elongated inclusions of organic matter and dispersed siderite microspheres. Large rhombs of ankerite (A) overgrow chert and siderite indicating it is late formed. (crossed polars) Bar = 0.5 mm.

F. Sample 5B. Stylolite (white arrows) is developed between siderite (S) and chert (C) layers. Coarse-grained ankerite (a) partially replaces chert layer above stylolite, indicating ankerite formed by dissolution of siderite. Chert layer above stylolite contains abundant inclusions of ankerite and/or siderite. Stylolite contains abundant fine-grained pyrite (not visible). Bar = 0.5 mm.

G. Sample 35L. Cubic pyrite grains (P) overgrow both siderite microspheres (S) and chert matrix (light areas). Siderite has been slightly recrystallized. Bar = 0.2 mm.

H. Sample 4A. Siderite from brecciated bed near Kakabeka Falls (Location 3, Figure 8) has been recrystallized to coarse-grained ankerite and is overgrown by coarse-grained pyrite (P). Bar = 2.0 mm.

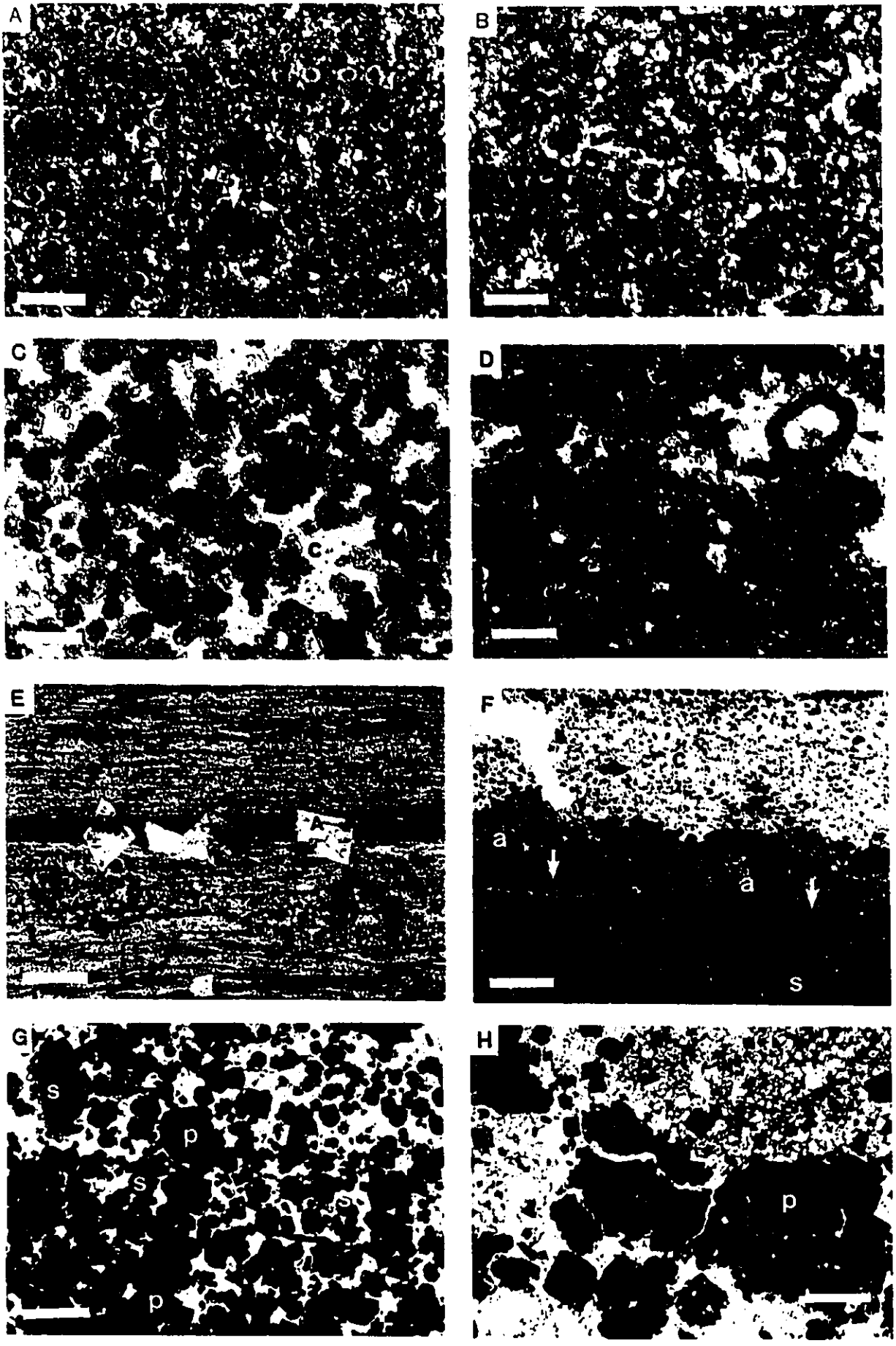

Plate 7

case the boundary between chert and siderite layers is diffuse or gradational. Siderite microspheres are dispersed within layers as individual spheres and less commonly as clusters of tightly adhering spheres. Within some of these clusters the walls between adjacent spheres are not developed and the interiors of spheres are loosely connected. In the later case they may be covered by a common sideritic coating which makes a chevron-like pattern between adjacent grains (Figures 1A, B and D of Kazmierczak, 1979). These textures are here interpreted to indicate that siderite was precipitated initially as microspheres (the inner spheres) that were sedimented on the sediment/water interface as individual grains or clumps of grains. Coatings of siderite (the outer walls) formed at or just below the sediment surface.

The interstitial spaces between siderite spheres is usually filled by chert. Fine-grained rhombs of ankerite are often observed surrounding siderite spheres. Less commonly, calcite was observed to form poikiloblasts that enclose several siderite spheres. These textures indicate that ankerite and calcite formed later than siderite. Thin layers of cryptocrystalline siderite containing black laminae of organic material were also seen. As noted earlier stylolites are common along the margins of siderite layers and are also found within layers. It is not certain whether the laminated siderite is a primary texture or is the result of recrystallization of siderite spheres, although the former seems more likely.

The chert bands consist of microgranular quartz that is characterized by abundant inclusions and by very thin black laminae and lenses of organic carbon parallel to layering (Plate 7E). Isolated siderite spheres are often present within chert layers. Fine to coarse-grained ankerite rhombehedra commonly overgrow chert and are especially abundant adjacent to stylolites (Plate 7F), indicating ankerite formed during late diagenesis, probably by recrystallization of siderite. Calcite may form anhedral patches or poikiloblasts containing ankerite inclusions, implying that calcite formed later than ankerite. Tiny veins and tension gashes are

filled by radial fibrous chalcedony and/or blocky quartz and is often partially replaced by ankerite or calcite.

Pyrite is usually a minor phase in banded chert-carbonate. As mentioned above, pyrite is found as inclusions within the cores of spherical siderite grains. More commonly, tiny ($\sim 5\mu m$) cubes of pyrite are very sparsely disseminated throughout both siderite and chert layers but become more abundant along stylolites. Locally, aggregates or small lenses, up to about 1 cm long, of coarse euhedral grains of pyrite are concentrated along the contacts between siderite and chert layers. In beds that have been significantly recrystallized or metamorphosed, pyrite occurs as euhedral grains up to about 0.5 mm across that clearly overgrow siderite, ankerite and chert (Plates 7G & H). These textures indicate that pyrite formed as disseminated fine grains during very early diagenesis and were recrystallized by pressure solution (i.e. along stylolites at contacts between siderite and chert layers) during late diagenesis.

As described in the previous chapter, beds of banded chert-carbonate near the base of the formation in the Kakabeka Falls area have been folded and brecciated and contain abundant pyrite. Siderite has been almost completely recrystallized to coarse-grained ankerite (Plate 7H). Pyrite is texturally complex and occurs as coarse-grained aggregates that overgrow ankerite, as nodular masses, and as a general cement to brecciated fragments of chert and carbonate (Plate 4D. Chert clasts in breccia are angular suggesting that sediments were lithified, but angular clasts are also observed in intraformational breccias (Plate 4B) indicating that lithification and brecciation of chert was an early feature. The cross-cutting nature of pyrite indicates that most of the pyrite either accompanied or post-dated brecciation, which may be related to syndepositional faulting.

3.3. LAMINATED CARBONATE

This facies is composed of parallel laminated to low angle cross-stratified, argillaceous carbonate. Lamination is defined by alternating clastic-rich and carbonate-rich layering (Plates 5D & 8A to D). Thin layers of flat pebble conglomerate were also observed. Clastic-rich laminae consist of angular silt to sand-size quartz and feldspar and well-rounded, sand-size intraclasts similar in composition to those in arenite (Plate 8B). These clasts are cemented by coarse-grained ankerite. Thicker layers of well-sorted sand grains may contain interstitial chert but these have often been extensively replaced by coarse-grained ankerite. In some cases fine-grained rhombs of siderite may preserve the outlines of former grains. Some thicker clastic layers contain elongated sand to pebble-size clasts (Plate 8E), which appear to be composed either of shale or altered volcanic ash. In this case the ash may be of epiclastic rather than pyroclastic origin. The interstitial areas contain fine-grained matrix, which is similar in composition to the larger clasts of shale or ash, and fine-grained siderite. Siderite mostly forms rhombs but some microspherical grains, similar to those in the banded chert-carbonate, are present. The siderite grains tend to be concentrated around clast margins (Plate 8E) suggesting that most of this siderite formed during very early diagenesis. Both clastic grains and siderite are cemented by coarse-grained ankerite. Thin layers of flat pebble conglomerate contain fine sand to pebble-size clasts of chert, shale, iron-rich intraclasts and volcaniclastic material (Plates 8G & H). The conglomerate forms an open framework that is cemented by coarse-grained ankerite and calcite. The abundant ankerite cement and lack of compaction indicate that ankerite formed during early diagenesis but later than siderite.

The carbonate-rich laminae contain siderite, ankerite, chert and very fine-grained matrix. Matrix is similar in composition to volcaniclastic grains. Layers

Plate 8. Laminate Carbonate

A to D. Sample 16D. A. Carbonate-rich layer (bottom half of photo) contains siderite microspheres (black arrow) and rhombs in a fine-grained matrix. Both siderite and matrix material is cemented by ankerite (see close-up in 8C). Clastic-rich layer (top half) contains iron-silicates (white arrow) and quartz and feldspar clasts (light colored) cemented by ankerite (close-up in 8B). Bar = 0.5 mm.

B. Close-up of clastic layer. Iron-silicate clast (is), and quartz and feldspar silt which are cemented by coarse-grained ankerite (black arrow). (X-polars) Bar = 0.2 mm.

C and D. Close-up of carbonate layer. Siderite microspheres (black arrows in Plate D) contain abundant interstitial ankerite cement (A in Plate D) and fine-grained matrix. Matrix, which is isotropic under crossed polars (P in Plate C), is probably made up of volcanic ash. (Plate C under crossed polars) Bar = 0.2 mm.

E. Sample 16B. Elongate pyroclastic grains (P) are fringed by siderite grains (white arrows). Ankerite (A) forms a general cement to siderite and pyroclastic material. Bar = 0.2 mm.

F. Sample 16J. Interior of ankerite concretion (from Plate 5B). Outlines of intraclasts, which have been replaced by coarse-grained ankerite, is preserved by fine-grained siderite (black arrows). Bar = 2.0 mm.

G. Sample 16F. Flat pebble conglomerate layer contains disk-shaped, chert pebble (c), and sand-size clasts of quartz, iron-silicates, and pyroclastic material. The lack of compaction and abundant ankerite cement (black arrow) indicates cementation was early. Very fine-grained pyrite is concentrated around margin of chert clast, in pyroclastic material and disseminated through ankerite (not visible). Bar = 2.0 mm.

H. Sample 16F. Flat pebble conglomerate, similar to above, containing disk-shaped pyroclastic and shale pebbles (dark grains), and silt to sand-size grains of quartz and feldspar in ankerite cement (black arrows). Bar = 2.0 mm.

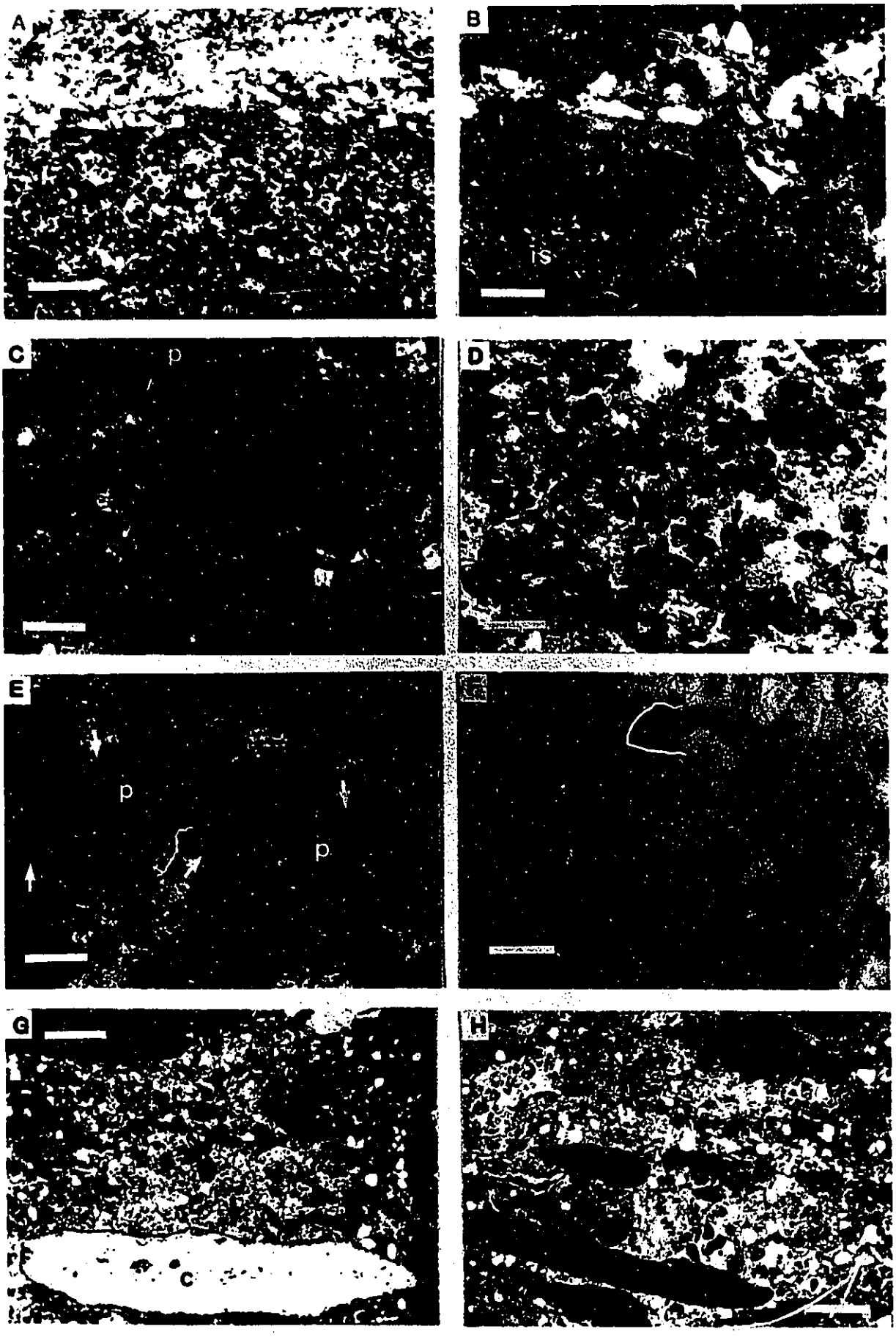

Plate 8

that have abundant matrix also contain abundant fine-grained rhombs and microspheres of siderite that are similar to those observed in the banded chert-carbonate facies. Tiny voids filled by fans of chalcedony are common in these layers. Ankerite forms a general cement to siderite and matrix. Layers that have little or no matrix lack appreciable siderite and consist mostly of fine to coarse-grained ankerite. Round nodular masses or concretions of ankerite were observed below a conglomerate layer (Plate 5B). These contain inclusion of siderite that outline the margins of former grains (Plate 8F). The siderite microspheres in carbonate-rich laminae probably have a similar origin to those in the banded chert-carbonate facies. Rhombic siderite, which outline volcanic clasts, most likely formed during very early diagenesis. Ankerite cements formed after siderite but during early diagenesis.

Within the contact zone of gabbroic sills, the carbonate minerals become coarser grained and are intergrown with metamorphic minerals. The iron content of carbonates decreases, resulting in the assemblage calcite-dolomite, and the abundance of magnetite increases with increasing proximity to these sills.

Pyrite is a very minor component of the laminated carbonate facies, generally making up less than a few tenths of a percent of the rock. It exists mainly as very fine-grained, disseminated euhedra and subhedra. In ankerite-rich layers, pyrite grain sizes increase slightly and often overgrow grain boundaries. However, pyrite is abundant in conglomerate layers, up to a few percent. It is found both within clasts and cement but is especially abundant in iron-rich volcanic clasts. Pyrite formed during early diagenesis before and possibly overlapping ankerite precipitation.

3.4. BLACK SHALE

This facies consists of finely laminated beds of black shale with thin carbonate-rich beds and local pyroclastic interbeds. The mineralogy and textures of

black shale are often difficult to determine optically because the very fine-grained nature of the rock and because the abundance of dark colored matrix make thin sections almost opaque. Components within the matrix that are identifiable include pyroclastic grains, iron-rich intraclasts, and authigenic minerals, such as carbonate, chert, chlorite (or illite) and pyrite, which occur as cements or euhdral crystals.

Laminated shale is composed of thin layers of angular, silt size grains of quartz and feldspar and sporadic sand-size iron-rich intraclasts, which are similar in composition to those in arenite, in a very fine-grained dark brown matrix (Plate 9F). Some of these layers are graded. Coarse-grained aggregates and lenses of pyrite are common and have bedding laminae wrapped around them (Plate 9E) indicating pyrite formed during early diagenesis before compaction was complete. Siderite microspheres are abundant within some layers (Plates 9A to C). These siderite microspheres average about 100 μm in diameter, contain an inner dark brown siderite core, and a concentrically laminated coating of light brown siderite. In some cases two or more dark brown cores share a common light brown coating of siderite (Plate 9C). Clumps or rip-ups clasts containing several dark siderite spheres are present in which none of the inner spheres are coated. Instead the whole clump has a discontinuous, concentrically laminated coating of lighter colored siderite. This suggests that the dark inner cores formed in the water column, or in the sediment close enough to the surface to be ripped up and redeposited. The lighter siderite coating formed at or just below the sediment surface. These microspheres are often overgrown by coarse-grained pyrite.

Carbonate-rich beds are almost featureless and virtually opaque in thin section. It is composed of up to 50% very fine to medium-grained rhombs of siderite and ankerite in a black organic-rich matrix (Plate 9D) and contains up to 2 % disseminated, very fine-grained pyrite. Coarser grained pyrite often replace carbonate rhombs, preserving rhombic cleavage. The rhombic textures indicate that

PLATE 9. Black Shale

A. Sample 26J. Laminated black shale. Coarse grained layer (light layer in center of photo) contains iron-silicates, carbonate lithoclasts (white arrow, close-up shown in Plate B), siderite microspheres and chert. Fine-grained laminated shale (above and below coarse-grained layer) contains siderite microspheres in a fine-grained matrix (close-up in Plate C). Pyrite grains (black) partially overgrow siderite and matrix. Bar = 2.0 mm.

B. Close-up of carbonate lithoclast from above. Interior consists of aggregate of dark siderite microspheres, which are similar to interiors of microspheres in matrix (Plate 9C), that had probably formed at or near the sediment/water interface and then was ripped up and redeposited. Aggregate is partially coated by concentrically laminated, light colored siderite (black arrows), probably after resedimentation. Bar = 0.2 mm.

C. Close-up of siderite microspheres from laminated shale matrix. Microspheres consist of a dark inner core of siderite and a concentrically laminated coating of light colored siderite. One grain consists of a double inner core surrounded by a single coating (white arrow). Siderite coatings probably formed after sedimentation of dark siderite (inner cores). Pyrite (P) partially replaces some grains. Bar = 0.2 mm.

D. Sample 13G. Massive textured shale is composed of fine-grained rhombs of siderite and ankerite in fine-grained black matrix. Small poikiloblasts of calcite enclose some rhombs of siderite and ankerite indicating calcite is latest carbonate phase. Bar = 0.1 mm.

E. Sample 26J. Fine-grained laminated shale wrapped around small lense of pyrite (P), suggesting pyrite formation during early diagenesis. Bar = 0.5 mm.

F. Sample 26J. Fine-grained laminated shale consists of silt-size clasts in very fine-grained matrix. Bar = 1.0 mm.

G. Sample 27F. Relatively uncompacted pyroclastic grains, which consist of rock

fragments, accretionary lapilli and crystals, are cemented by coarse-grained ankerite, indicating early cementation. Bar = 1.0 mm.

H. Sample 13R. Pyroclastic rock fragments and crystals are cemented by ankerite and calcite and are slighter more compacted and contain less cement that above photo. Note thin rim of chlorite cement (light grey) around margins of clasts. Bar = 0.5 mm.

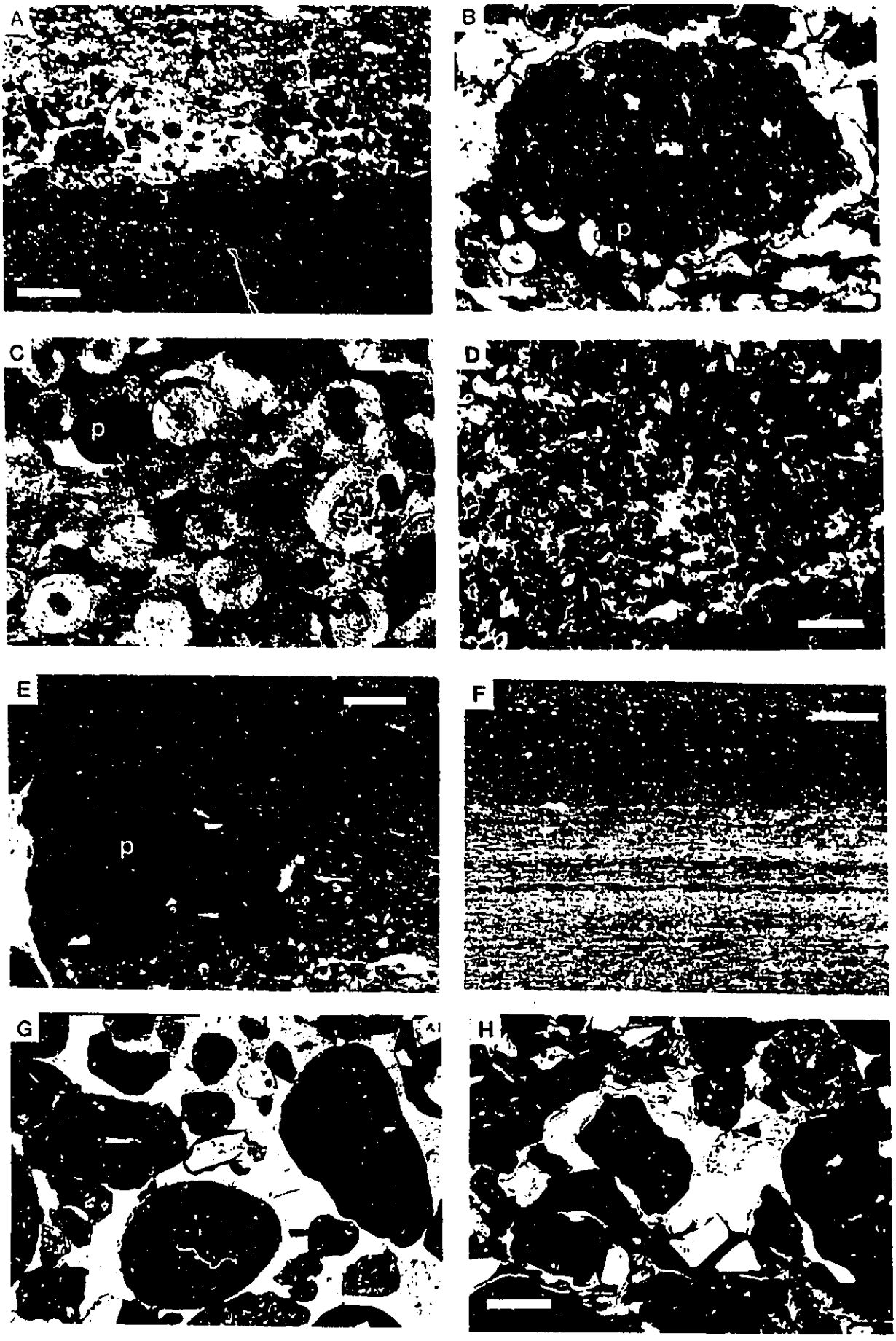

Plate 9

siderite and ankerite in these beds formed during very early diagenesis. Minor amounts of calcite occur as poikiloblasts enclosing several siderite rhombs. Siderite-rich clasts within an intraformational breccia layer are cemented by coarse-grained ankerite and calcite, which contain inclusions of siderite and ankerite rhombs, siderite microspheres, and fine to coarse-grained pyrite.

Pyroclastic interbeds in the Gunflint Formation contain, in order of abundance, vitric grains, detrital crystals, phaneritic rock fragments that range from basalt to rhyolite in composition, accretionary lapilli, armored lapilli, and ash peloids as well as iron-formation clasts (Hassler and Simonson, 1989). Pyroclastic beds that contain subordinate amounts of cement are often well-compacted with grains flattened parallel to bedding (Plate 9H), whereas beds that contain abundant cement are relatively uncompacted (Plate 9G), indicating cementation started during early diagenesis. Cement types include chlorite, carbonate and chert. Carbonate cement is mostly coarse-grained ankerite but patches of calcite are common. Pyroclastic grains are often partially replaced by adularia, quartz, chlorite, and calcite. Very fine-grained, euhedral pyrite is scattered throughout pyroclastic grains and, to a lesser extent, in carbonate cement. The source of volcanism is presumably the Emperor Volcanic Complex, which is interbedded with the Ironwood Iron Formation of the Gogebic Range (Figure 2).

In most areas pyrite is present only as very fine, disseminated grains, from trace amounts up to about 2 % of the rock, which formed during early diagenesis. Within the Kakabeka Falls area, pyrite becomes much more abundant and displays textures suggesting that more than one generation is present. In the Ontario Hydro spillway section (location 6, Figure 8), described in the previous chapter, undeformed black shale overlies beds of folded and brecciated banded chert-carbonate. Layers of massive pyrite within a shaly matrix mark the contact between these two lithologies. Above this contact the shale contains three textural types of pyrite. Very

fine-grained pyrite, similar to that found in other locations, is disseminated throughout the matrix. Coarse, euhedral pyrite grains, which overgrow fine-grained pyrite, siderite and ankerite, occur as isolated grains or coalesce to form small aggregates or lenses elongated to bedding and have bedding laminae wrapped around them (Figure 9E) indicating they formed prior to compaction. This type formed during early diagenesis but later than the fine-grained pyrite. The third type of pyrite comprises ellipsoidal concretions, which grow up to 3 or 4 cm in diameter. These pyrite concretions often show an internal zonation. Some concretions contain an inner core containing coarse-grained pyrite in a matrix of shale that is texturally similar to that described above. This core is surrounded by a shell composed almost entirely of euhedral, bladed crystals of pyrite, which shows a radial outward growth. Bedding laminae are usually bent around pyrite concretions, although outer terminations of radial pyrite crystals displace sediment layers. Other concretions do not show the same zonation but instead have cores consisting entirely of pyrite with mutually interfering grain boundaries from which euhedral pyrite radiates outward. These textures suggest that the concretions formed during the early stages of compaction.

3.5. Upper Limestone Member:

The Upper Limestone Member marks an abrupt decrease in the amount of chemically precipitated iron. It consists of impure beds of limestone/dolostone that contain variable quantities of clastic material and layers and lenses of chert. Calcite and dolomite are the only carbonate minerals present. The abundance of clastics range from minor amounts disseminated within a carbonate matrix to a dispersed or open framework that is cemented either by chert or carbonate. Shale is interbedded

with carbonate-rich beds near the top of the Limestone Member where it grades upward into shales of the Rove Formation. The clastic component consists of pyroclastic grains, intraclasts, and occasional silt to sand size quartz grains. Pyroclastic fragments vary widely in size and shape and have been extensively altered and replaced by carbonate or chlorite. Intraclasts are similar in composition to those found in the arenite facies.

Dolomite is the earliest formed carbonate mineral and ranges in abundance from scattered rhombs within interstitial areas of the clastic framework (Plate 10A) to beds displaying a coarse-grained mosaic texture surrounding and partially overgrowing isolated clastic grains (Plate 10C). Within rocks that do not contain much calcite both clastic grains and dolomite are cemented by several generations of early formed chert (Plate 10A). Isopachous layers of parallel fibrous chalcedony mantle dolomite and clastic grains. The remaining pore space is filled with radial fibrous chalcedony with larger pores containing blocky quartz in their centers. Parallel fibrous chalcedony is separated from radial chalcedony by a thin zone of black inclusions (Plate 10A). Fine-grained pyrite is disseminated within pyroclastic grains and chert cement and is often abundant within the black inclusions in chert, but is rare in dolomite. The above textures indicate that dolomite formed during very early diagenesis before any significant amount of compaction. The lack of compaction where chert cement is abundant indicates that chert was also early diagenetic. Pyrite formed in pyroclastic grains during cementation.

Calcite may either form small isolated anhedral crystals, which partially replace pyroclastic grains (Plate 10D) and chert cement (Plate 10E) or, at the other extreme, coarse-grained calcite replaces whole beds and contains inclusions of dolomite and clastic grains (Plate 10B). In calcite-rich beds much of the clastic grains are partially altered to calcite and only minor quantities of chert are found, either as small isolated vugs filled by fans of radial fibrous chalcedony or as tiny patches of

PLATE 10. Upper Limestone Member

A. Sample 8F. Loose framework of pyroclastic material (dark grey) contains rhombs of dolomite (D), which are both mantled by early formed parallel fibrous chalcedony. Remaining pore spaces are filled by radial fibrous chalcedony. Thin film of black inclusions (black arrow) separates rim and pore-filling cement. Bar = 0.2 mm.

B. Sample 8F. Coarse-grained calcite contains inclusions of dolomite (D) and abundant inclusions of fine-grained pyroclastic material (black), suggesting calcite formed late. Bar = 0.5 mm.

C. Sample 8E. Coarse-grained dolomite with deformed interstitial pyroclastic grains (v) and minor amounts of calcite and chert. Bar = 0.5 mm.

D. Sample 8F. Vesicular pyroclastic grain (large round grain in center of photo) is filled with calcite poikiloblast (c). Rest of photo contains fine-grained pyroclastic material and dolomite (D) with abundant chalcedony cement, similar to Plate A. (crossed polars) Bar = 0.5 mm.

E. Sample 8C. Pore filling chalcedony cement partially overgrown by later calcite crystals (c). Remainder of photo is mostly dark colored pyroclastic material. (crossed polars) Bar = 0.2mm.

F. Sample 8F. Chalcedony filled vug (ch1) is floored by internal sediment (i) and is cross-cut by chalcedony filled vein (ch2) also floored by internal sediment (i), indicating silica was formed early. Remainder of photo is mostly pyroclastic material and calcite. Bar = 0.5 mm.

G. Sample 8B. Layer or vein of chalcedony is floored by finely laminated, internal sediment (i). Note cubic-shaped casts of unknown precursor mineral (halite ?) filled with coarse chalcedony. (crossed polars) Bar = 2.0 mm.

H. Close-up of internal sediment layer from above photo. Very fine-grained pyrite is

disseminated throughout sediment layers but is especially abundant along black laminae (arrow), indicating pyrite formed during early diagenesis. Bar = 0.5 mm.

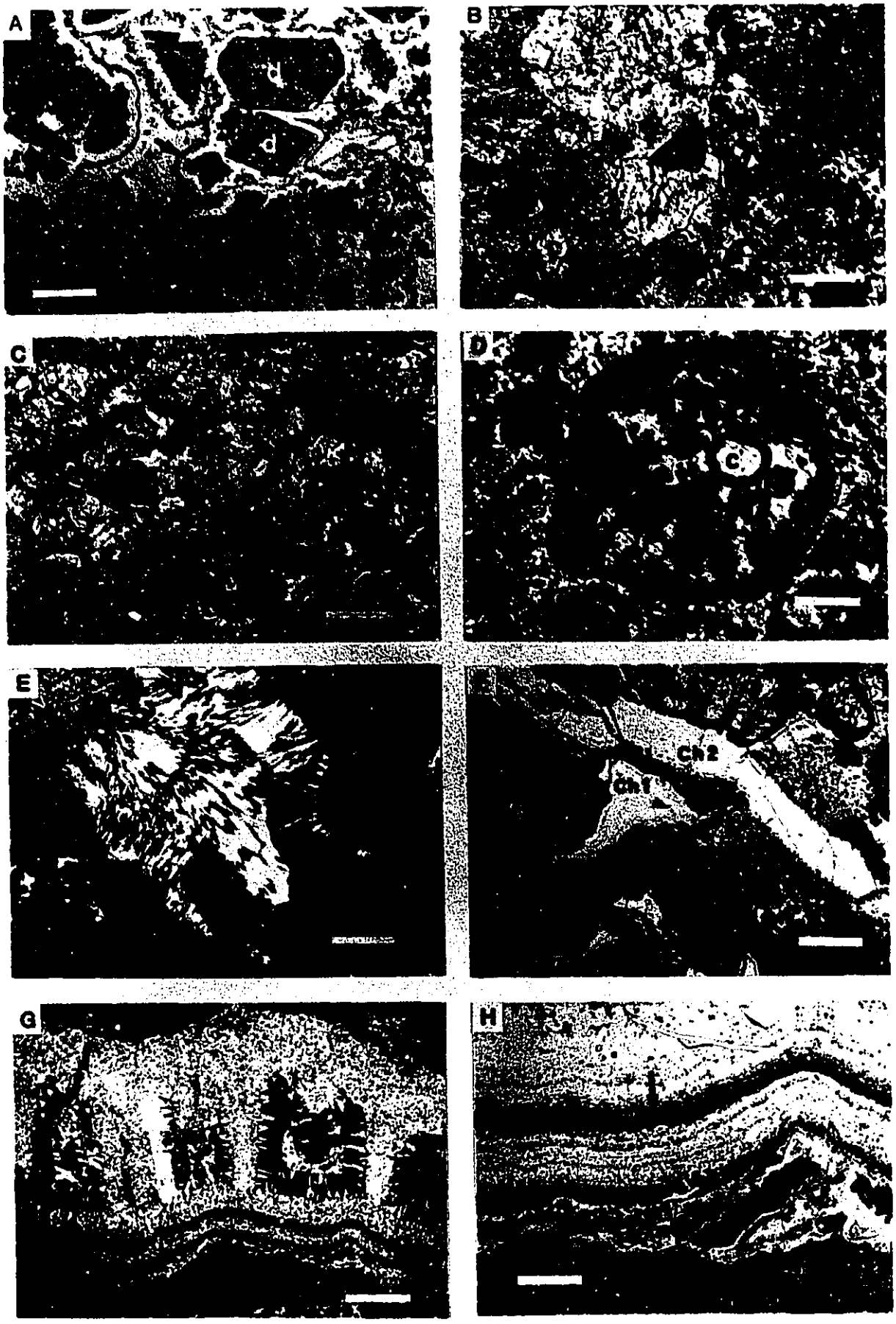

Plate 10

microgranular chert. Some vugs contain a lining of internal sediment along their bottoms that are overlain by radially fibrous chalcedony (Plate 10F). Pyrite is present as fine to coarse anhedral grains that overgrow calcite and pyroclastic material. Calcite textures indicated that it formed later than dolomite and, at least in some cases, chert.

Domal stromatolites, 10 to 20 cm in height, are found at one location within the limestone facies. The stromatolitic laminae are defined by a crude layering of altered pyroclastic grains within a matrix of coarse-grained sparry calcite. Laminae are thicker than those in cherty stromatolites. Radial fibrous chalcedony fill thin fenestrae parallel to stromatolitic laminae. Tiny pyrite cubes are scattered throughout both the stromatolitic layers and the surrounding clastic textured limestone. No dolomite was observed within stromatolitic limestone or in adjacent clastic textured limestone. Because calcite has been recrystallized it is not possible to tell if it is primary or replaced earlier dolomite.

A significant component of this facies are veins and layers of chert, some of which resemble fenestral porosity. All of these contain textures suggesting open space filling. They are generally floored by thin laminae of internal sediment and are overlain by clear radial fibrous chalcedony that coarsens inward (Plate G & H). Cross-cutting relationships are common. In one example a vug floored with internal sediment and filled by chalcedony is cross-cut by a thin folded vein which is also floored by internal sediment and filled by chalcedony (Plate 10F). Both veins are truncated by a 1 cm thick flat layer of chalcedony that is also floored by internal sediment (Plate 10G). The internal sediment often contain tiny pyrite cubes concentrated along individual organic-rich laminae. Within the chert layer, blocky quartz appear to have pseudomorphed a cubic mineral (Plate 10G), possibly halite.

3.6. MINERAL PARAGENESIS

3.6.1. CARBONATES

In all facies of the Gunflint Formation, except the Upper Limestone Member, siderite was the first carbonate phase to precipitate (Figure 11). Primary textures are well preserved and indicate that precipitation may have initiated within the water column or else at the sediment/water interface. The presence of intraclasts of siderite indicate that precipitation must have been close enough to the sediment/water interface to be ripped up and redeposited. Continued siderite precipitation after burial is indicated by discontinuous coatings of siderite around intraclasts and by disseminated siderite rhombs within the shale matrix. Chert precipitation synchronous with siderite is suggested by the ubiquitous presence of chert in siderite layers, and vice versa, in banded chert-carbonate and by early chert cements in arenite that also contain siderite layers. Within the Upper Limestone member, dolomite is the initial carbonate phase. It precipitated during very early diagenesis and is enclosed by early formed chalcedony cement.

Ankerite probably formed during early to late diagenesis and during metamorphism (Figure 11). The actual timing of ankerite is difficult to establish and is probably complex. It often forms a cement to clastic and siderite grains that have undergone little or no compaction, suggesting that it formed during early diagenesis. Layers and laminae of ankerite in arenite appear to be primary but textures are often recrystallized and may be the result of dissolution of siderite and reprecipitation as ankerite. In some cases ankerite clearly replaces earlier formed chert cement and pseudomorphs intraclasts indicating that it formed during late diagenesis. Ankerite also formed during the metamorphic breakdown of siderite. With increasing metamorphic grade, dolomite and calcite formed by the breakdown of ankerite, coupled with the formation of magnetite, as well as other metamorphic minerals.

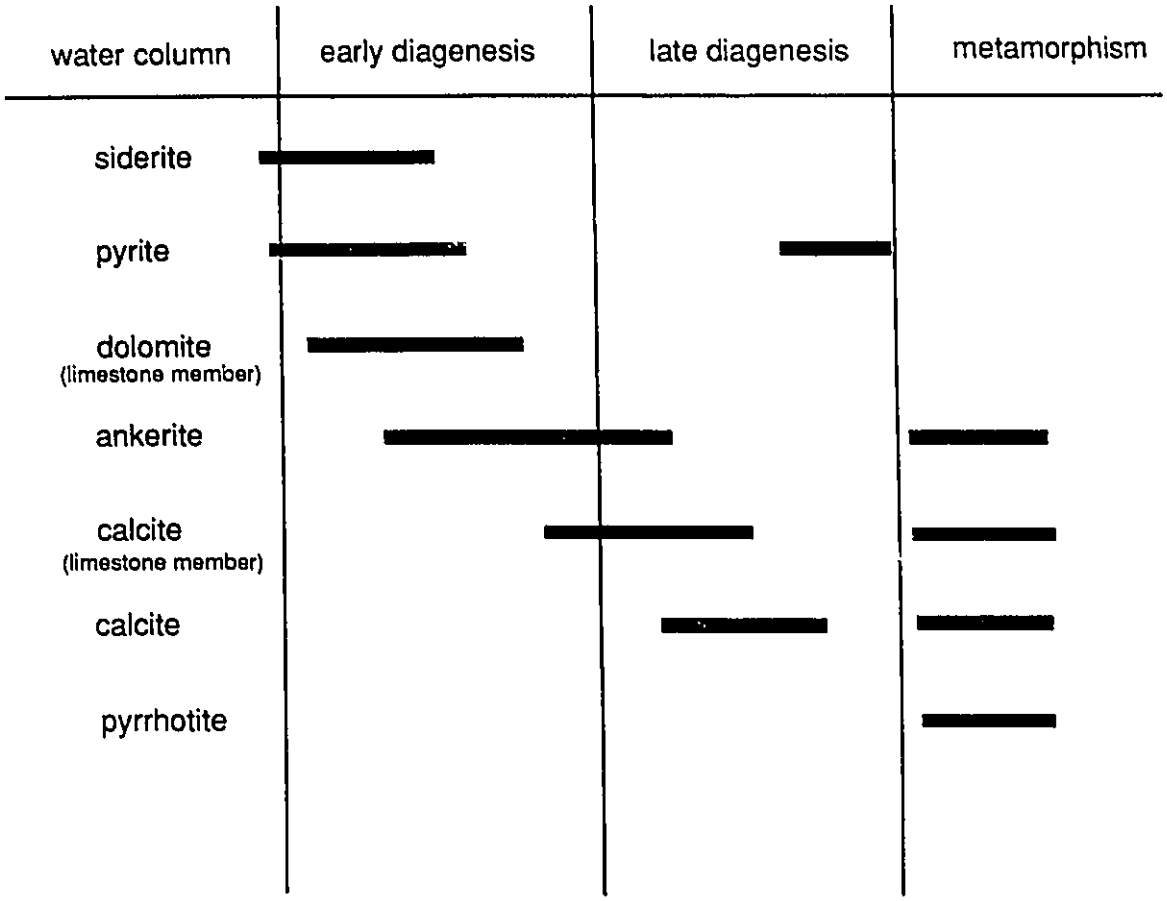

FIGUR E 11. Paragenetic sequence of carbonate and sulfide minerals from the Gunflint Formation.

In the Upper Limestone Member, calcite formed later than dolomite, because coarse-grained calcite overgrows rhombs of dolomite. Where coarse-grained calcite is not present dolomite rhombs are enclosed by chalcedony rim and pore filling cements. The calcite is either contemporaneous with chalcedony or else has replaced earlier formed chalcedony. Evidence for the latter interpretation is suggested by the presence of anhedral calcite partially overgrowing porefilling chalcedony cement. Most calcite in the rest of the formation appears to be late diagenetic or metamorphic in origin. Evidence for this includes the occurrence of calcite poikiloblasts enclosing siderite, ankerite and arenite grains. Calcite is also common in late fractures and veins and partially replaces arenite grains and interstitial cement.

3.6.2. PYRITE

Layers and laminae of pyrite suggest that precipitation may have started above the sediment/water interface, but these cases are exceptions and pyrite most often occurs as disseminated, very fine grains. The presence of very fine-grained pyrite disseminated throughout black shale and siderite layers and the presence of pyrite inclusions in siderite microspheres indicate that pyrite precipitation overlapped that of siderite (Figure 11). In many cases pyrite textures have been recrystallized and give the appearance that they formed later. For example pyrite textures in arenite often show cross-cutting relations with grains and cements suggesting that it formed late. However, $\delta^{34}S$ values are identical to fine-grained pyrite in adjacent black shale (see Chapter 4) suggesting a common source of sulphur. In other cases, such as within the black shales of the Ontario Hydro spillway section, coarse-grained pyrite pseudomorphs rhombic outlines of siderite or overgrows siderite spheres indicating that it post-dates siderite formation. This coarse-grained pyrite is in turn overgrown

by ellipsoidal pyrite concretions (Plate 2C), which formed during early diagenesis indicating that even coarse-grained pyrite is early diagenetic. Irregular pyrite concretions (Plate 2D) found within shales along the Current River formed during late diagenesis after the sediments had been compacted. Pyrite, marcasite and minor amounts of galena are found in fractures that clearly post-date lithification. During metamorphism, pyrite is often broken down to form pyrrhotite.

4. ISOTOPIC RESULTS

4.1. $\delta^{13}C$ OF CARBONATE MINERALS

The isotopic ratios of the various carbonate phases from the Gunflint Formation have a wide range of values, between +0.5 and -20.0 °/oo (PDB). However, analyses of unmetamorphosed rocks have a more restricted range, having values heavier than about -6 °/oo. Metamorphosed rocks have values that are generally lighter than -6 °/oo.

Siderite in unmetamorphosed rocks have a range of $\delta^{13}C$ values between +0.5 and -5.2 °/oo (Figure 12). There are no significant differences between different facies. Black shale has the widest range of values, from +0.5 to -4.9 °/oo. The other facies have narrower ranges with laminated carbonate between -3.5 and -5.2 °/oo, banded chert-carbonate between -1.8 and -4.6 °/oo, and two analyses of arenite at -1.5 and -2.1 °/oo. Siderite in metamorphosed rocks have values between -6.9 and -9.9 °/oo, although only three analyses were performed.

Ankerite in unmetamorphosed rocks has a range of values between -0.4 and -6.6 °/oo (Figure 13). Arenite have the widest range of values between -0.9 and -6.0 °/oo, followed by banded chert-carbonate between -2.0 and -6.6 °/oo, laminated carbonate between -0.4 and -4.6 °/oo and black shale between -0.8 and -4.4 °/oo. Ankerite values from metamorphosed rocks are between -6.8 and -15.4 °/oo. Samples collected in proximity to gabbroic sills show a progression to lighter values toward intrusive contacts.

The only unmetamorphosed rocks that contain dolomite are those belonging to the Upper Limestone Member. $\delta^{13}C$ values are between +0.5 and -2.7 °/oo (Figure 15). No iron carbonates are present in this unit. Dolomite in metamorphosed rocks from this member have values between -2.0 and -8.7 °/oo.

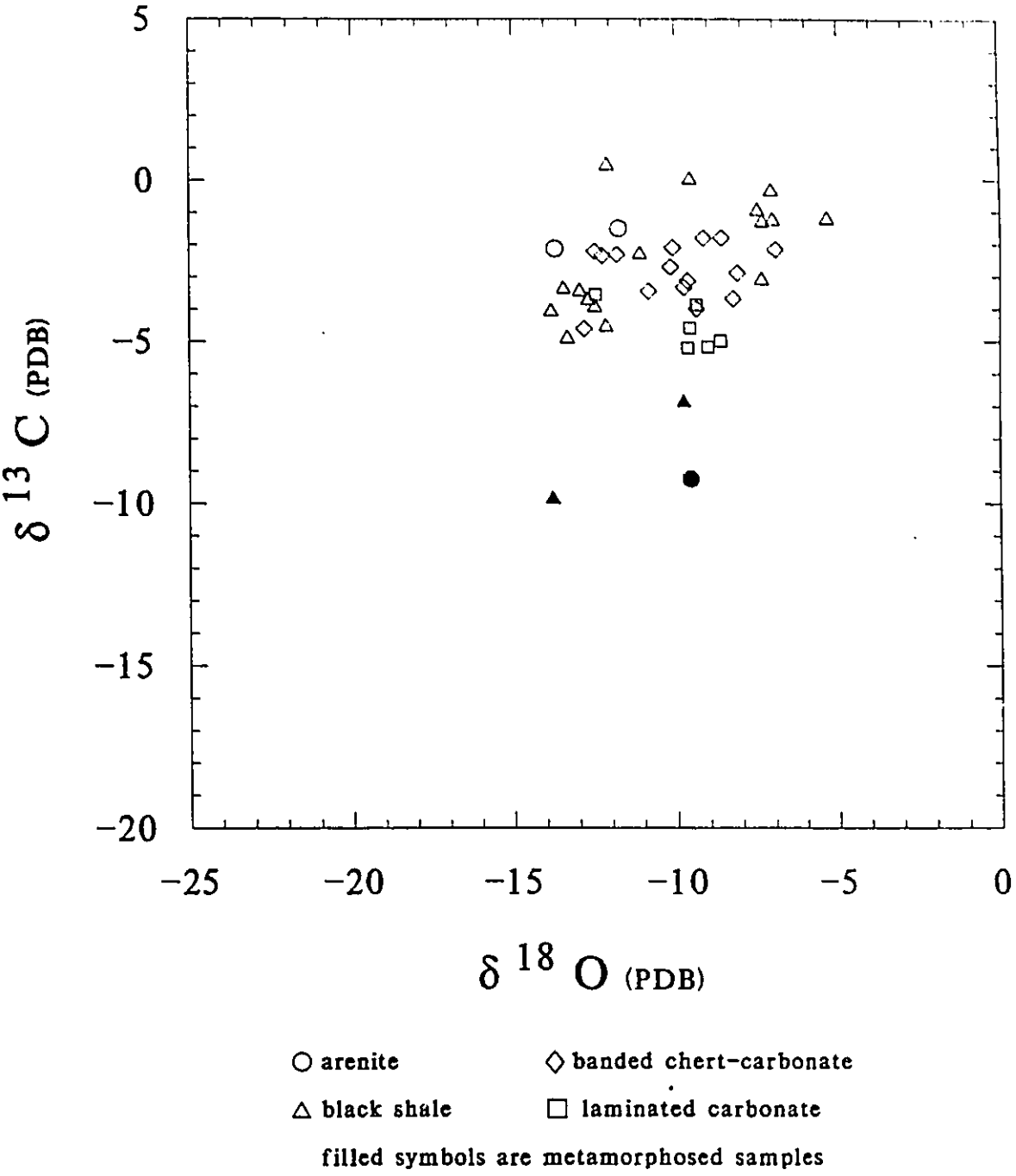

Figure 12. $\delta^{13}C$ versus $\delta^{18}O$ of siderite in the Gunflint Formation.

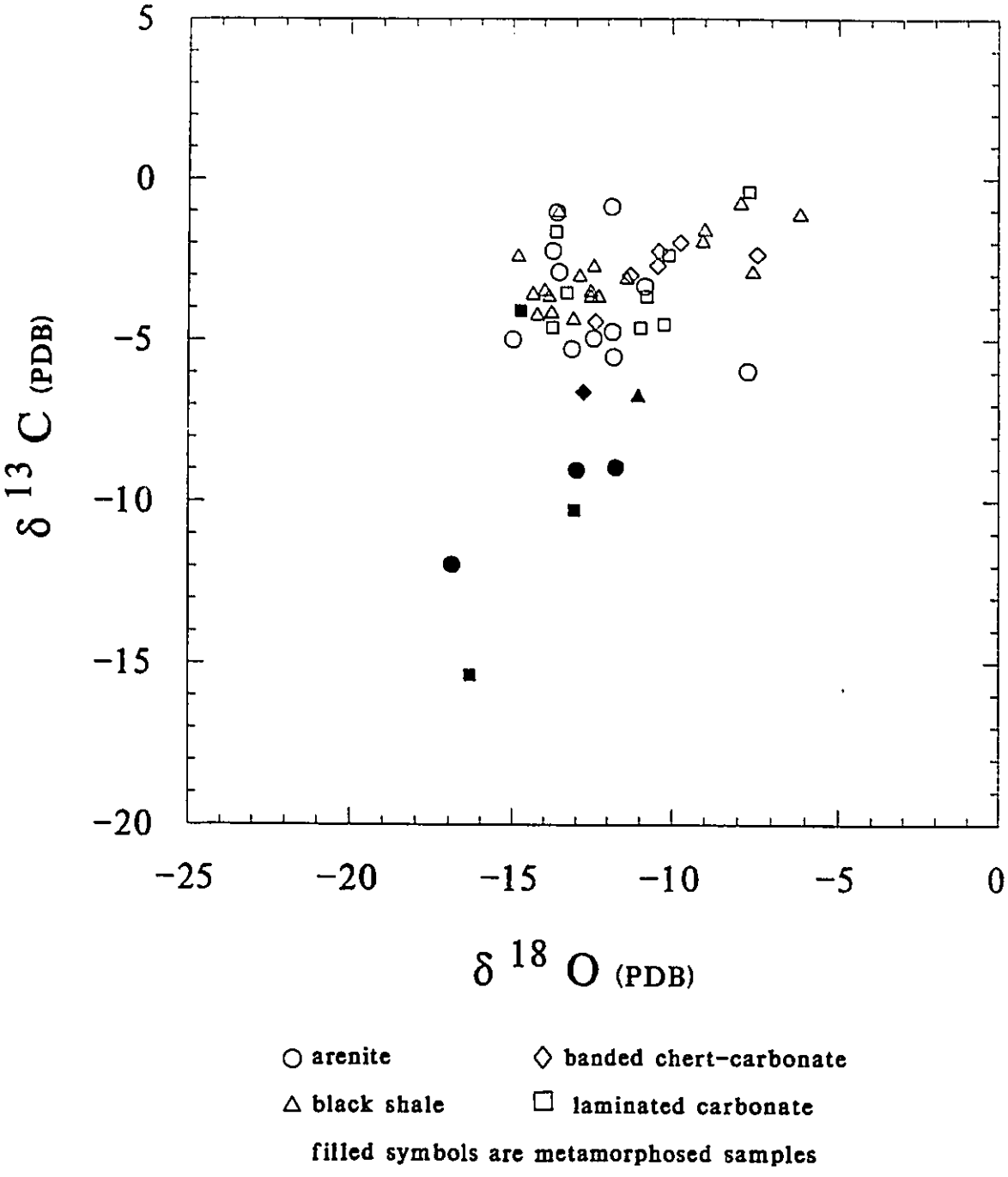

Figure 13. $\delta^{13}C$ versus $\delta^{18}O$ of ankerite in the Gunflint Formation.

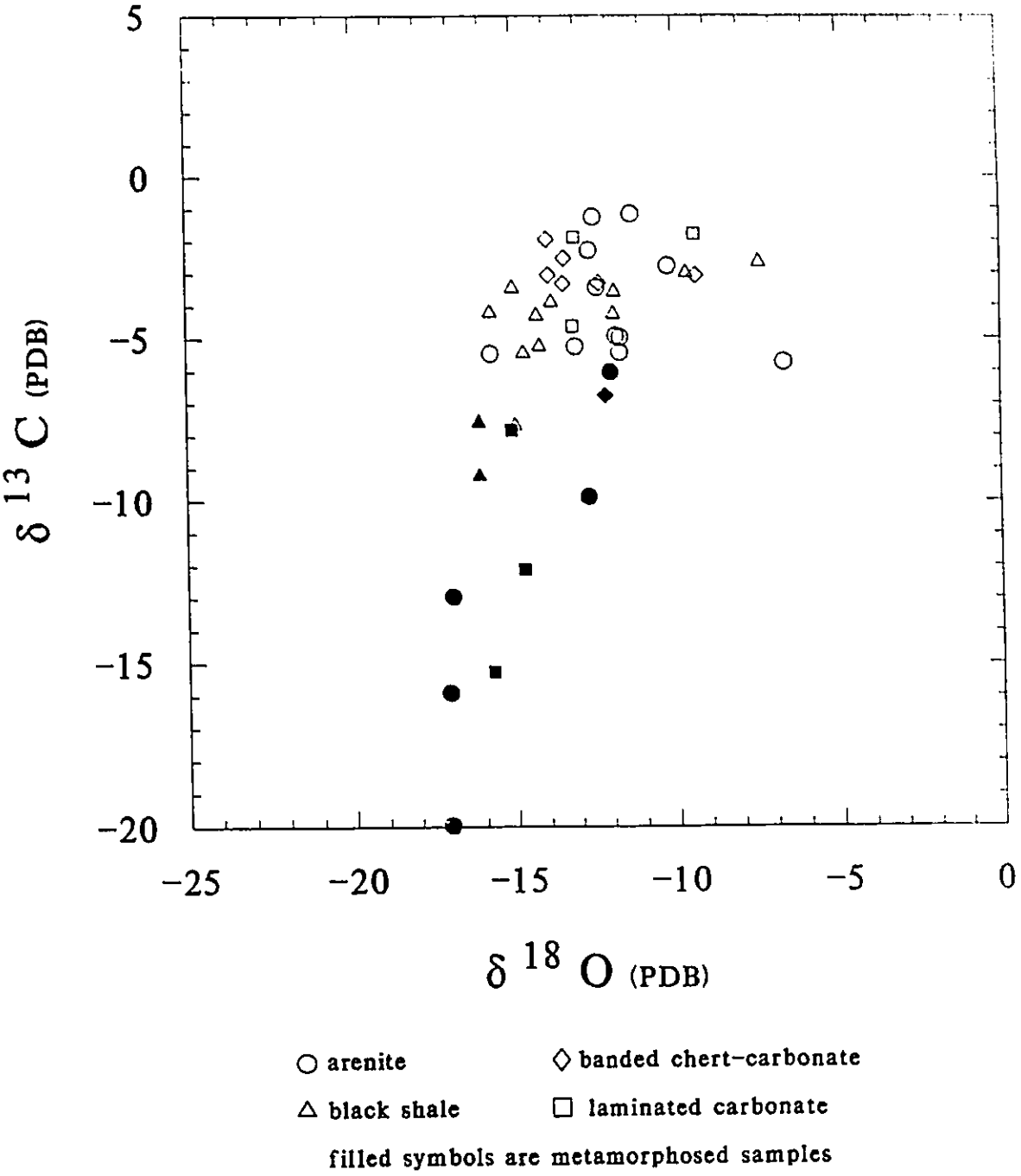

Figure 14. $\delta^{13}C$ versus $\delta^{18}O$ of calcite in the Gunflint Formation, calcite from the Upper Limestone Member not included.

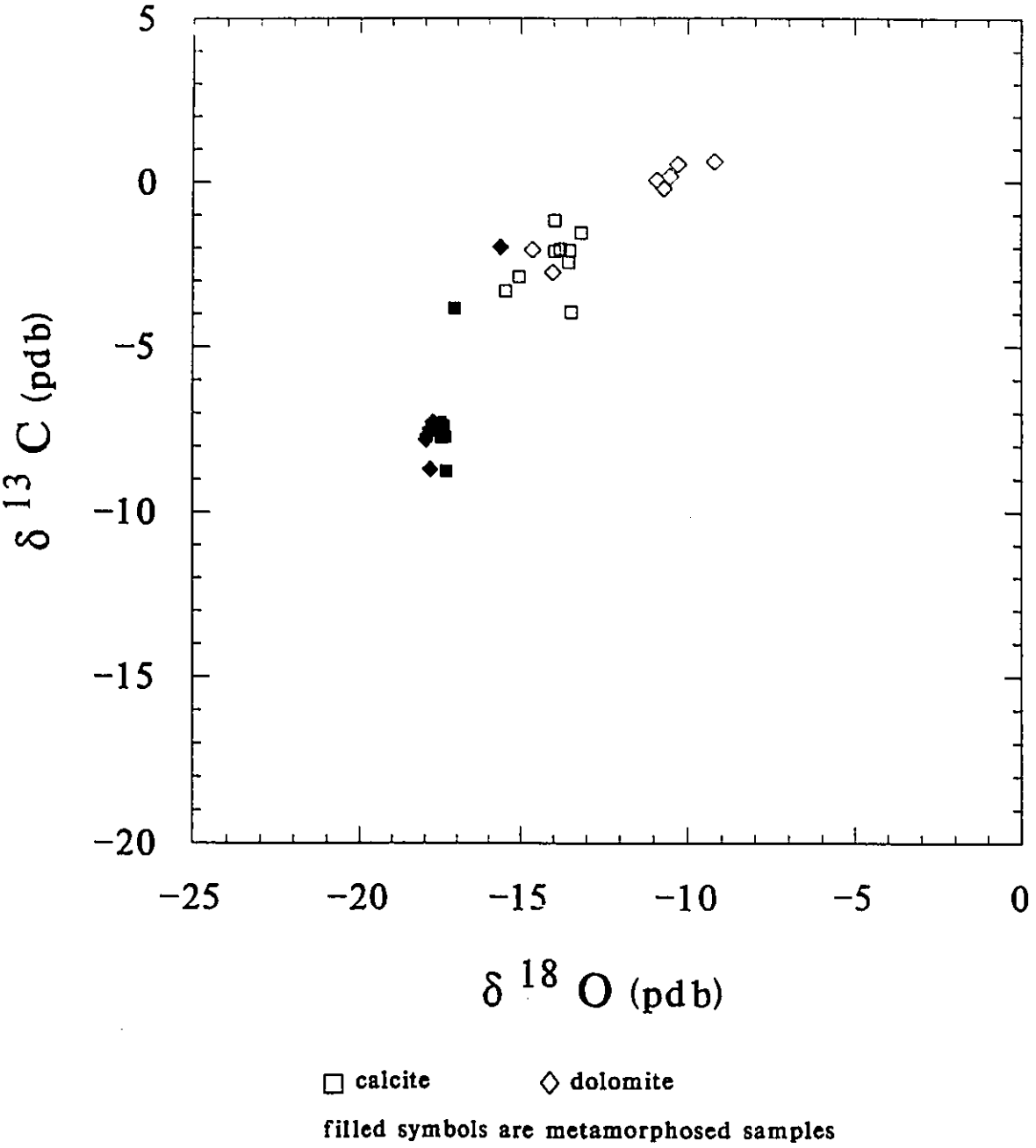

Figure 15. $\delta^{13}C$ versus $\delta^{18}O$ of calcite and dolomite from the Upper Limestone Member of the Gunflint Formation.

Calcite in unmetamorphosed rocks have a range of values between -1.2 and -7.7 ‰ (Figure 14). Within individual facies, calcite in black shale has a range of values between -2.7 and -7.7 ‰, laminated carbonate between -1.8 and -4.6 ‰, banded chert-carbonate between -1.9 and -6.8 ‰, and arenite between -1.2 and -5.5 ‰. Calcite from the Upper Limestone Member (Figure 15) varies between -1.2 and -3.9 ‰. Calcite from metamorphosed rocks have values between -5.5 and -20.0 ‰. Like ankerite, calcite also shows a progression to lighter values toward the contacts of gabbroic sills.

Differences in $\delta^{13}C$ values between coexisting carbonate phases in unmetamorphosed rocks do not show any systematic variations (Figures 16, 17, and 18). Siderite values may be enriched in ^{13}C by up to 4.0 ‰ or depleted by up to 3.5 ‰ compared to coexisting ankerite (Figure 16). Siderite values are up to 4.5 ‰ heavier and up to 3.2 ‰ lighter than coexisting calcite (Figure 17). Ankerite values can be heavier than coexisting calcite by up to 4.6 ‰ or lighter by up to 2.8 ‰ (Figure 18). Differences in isotopic ratios between coexisting carbonate phases in metamorphosed rocks are smaller and more consistent than those from unmetamorphosed rocks. Siderite is depleted in ^{13}C by 0.1 to 0.3 ‰ compared to ankerite. Ankerite may be enriched in ^{13}C by up to 3.7 ‰ compared to calcite, but differences are usually very small. No analyses of coexisting siderite and calcite were done.

Figures 19, 20 and 21 show the $\delta^{13}C$ variations with respect to stratigraphy. Siderite, ankerite (dolomite), and calcite all show variations of up to 5 ‰ over short vertical distances but the range of values are consistent throughout the section with the heaviest values close to 0 ‰ and the lightest values near -5 ‰. There are no systematic vertical variations. Analysis of metamorphosed rocks always yeilds values that are depleted in ^{13}C relative to unmetamorphosed rocks from the same stratigraphic interval.

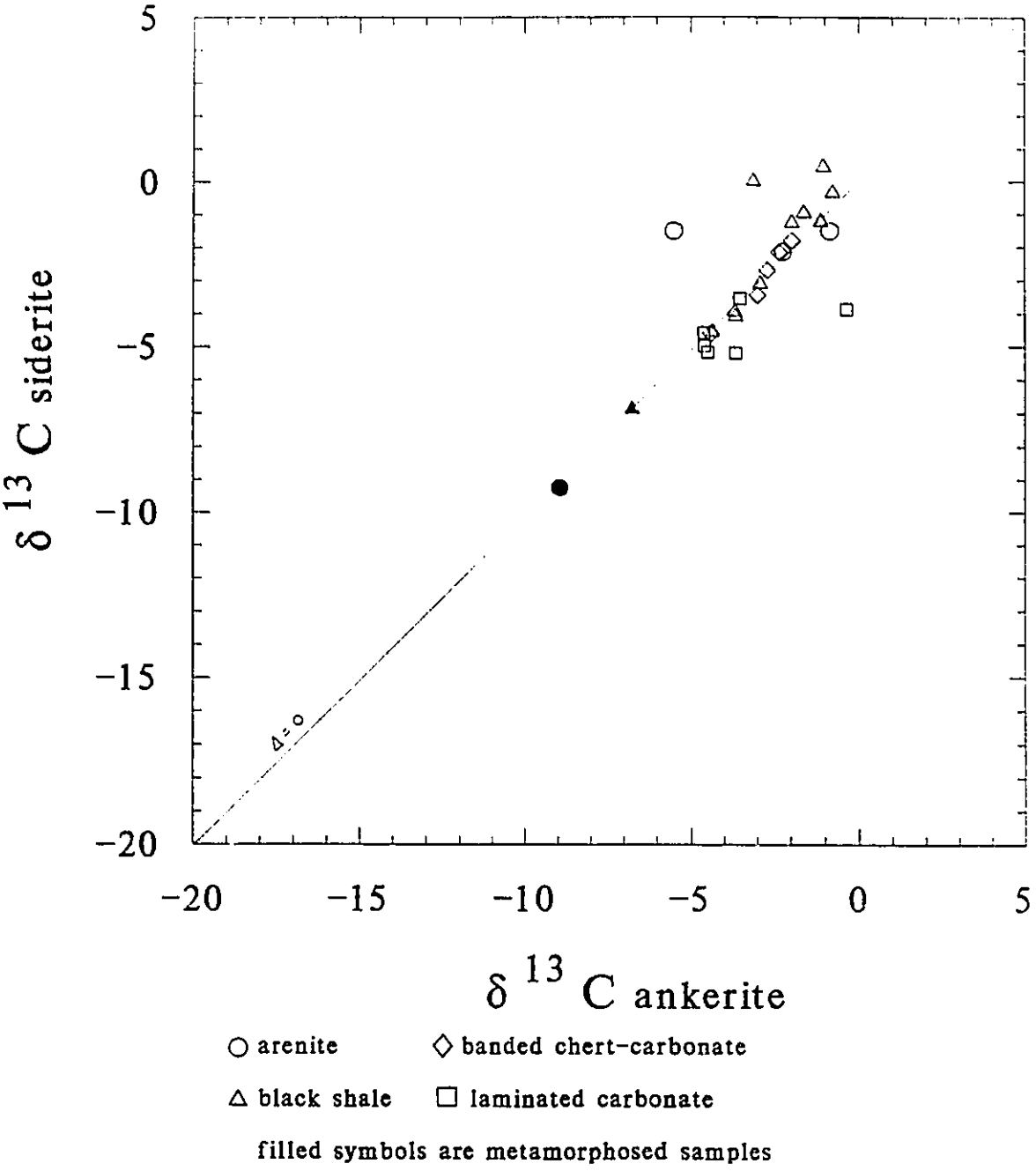

Figure 16. $\delta^{13}C$ of coexisting siderite and ankerite in the Gunflint Formation.

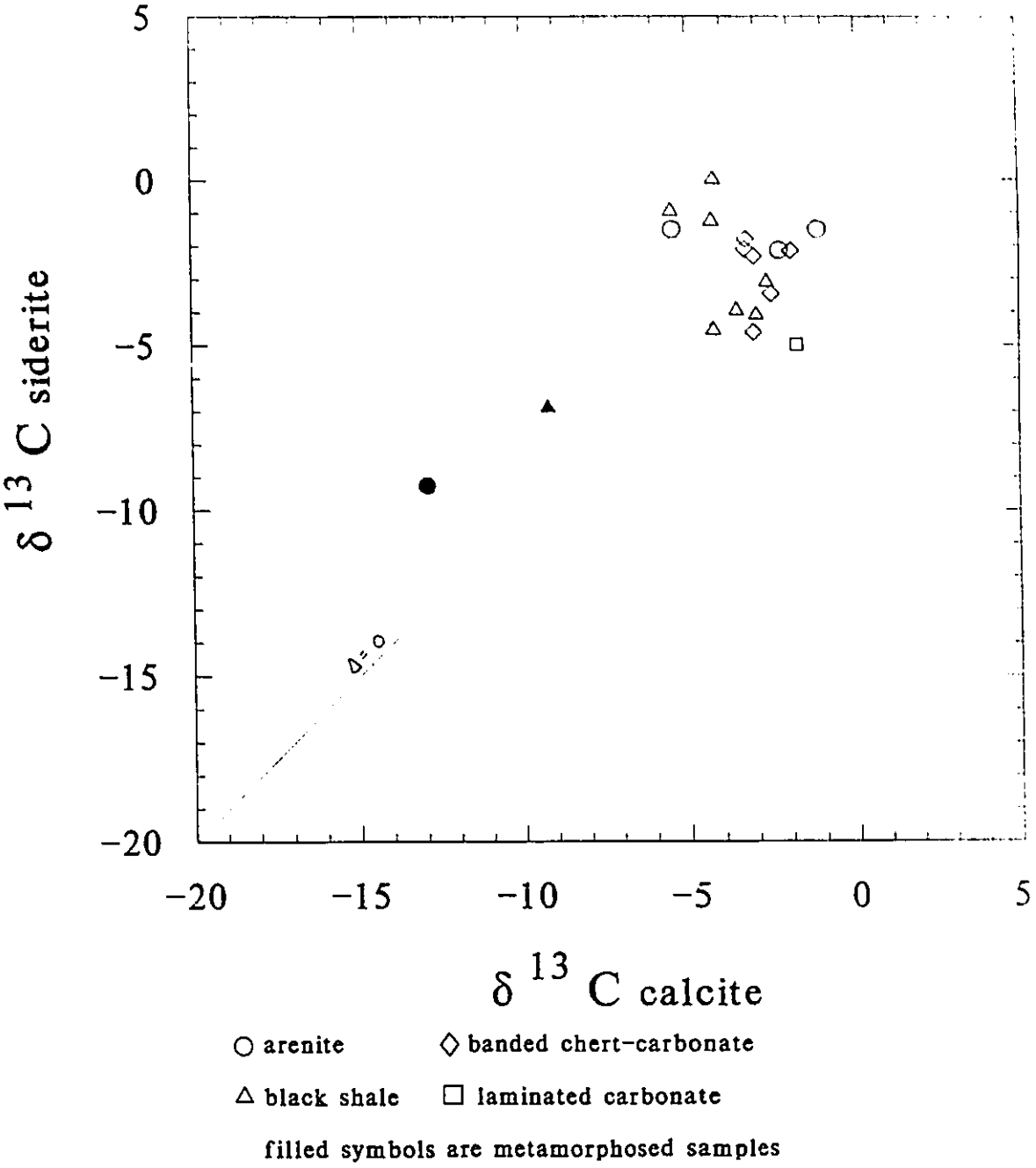

Figure 17. $\delta^{13}C$ of coexisting siderite and calcite in the Gunflint Formation.

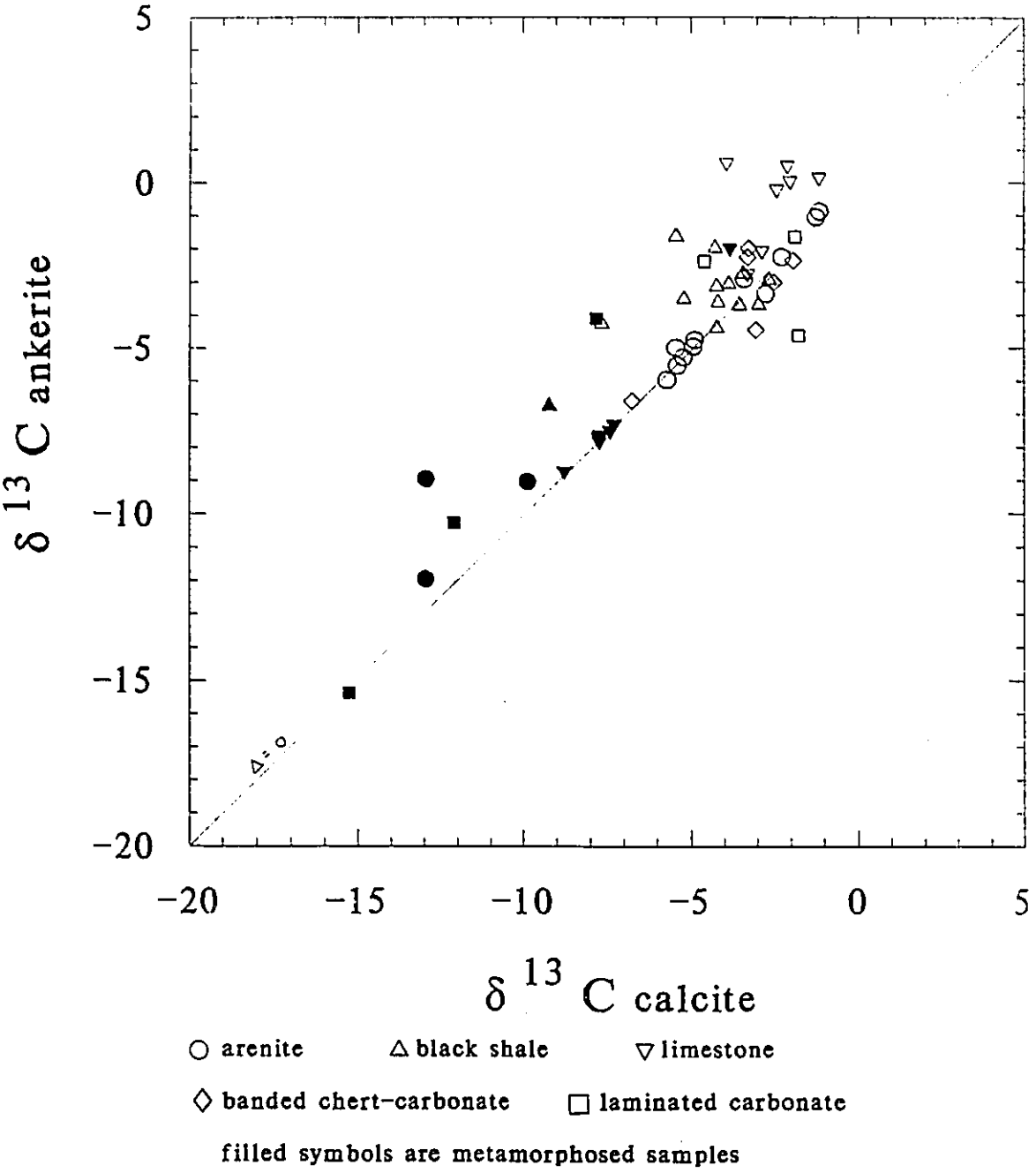

Figure 18. $\delta^{13}C$ of coexisting ankerite (or dolomite in limestone) and calcite from the Gunflint Formation.

4.2. $\delta^{18}O$ OF CARBONATE MINERALS

The $\delta^{18}O$ values from carbonate minerals vary between -5.3 and -18.0 °/oo (PDB). All $\delta^{18}O$ values will be referenced to the PDB standard rather than SMOW unless otherwise stated. $\delta^{18}O$ values from unmetamorphosed and metamorphosed rocks do not show the same clear cut distinction as the $\delta^{13}C$ values do. Unmetamorphosed rocks have values from -5.3 to -15.6 °/oo, while metamorphosed rocks have values from -9.6 to -18.0 °/oo.

Siderite in unmetamorphosed rocks has $\delta^{18}O$ values from -5.3 to -13.8 °/oo (Figure 12). Black shale has the largest range of values from between -5.3 and -13.8 °/oo, followed by banded chert-carbonate between -8.1 and -12.8 °/oo, laminated carbonate between -8.6 and -12.5 °/oo, and arenite between -11.7 and -13.7 °/oo. Siderite in metamorphosed rocks has values between -9.6 and -13.8 °/oo.

^{18}O values of ankerite in unmetamorphosed rocks vary between -6.1 and -15.0 °/oo (Figure 13). The largest range of values is found in black shale which varies between -6.1 and -14.8 °/oo and in arenite between -7.7 and -15.0 °/oo, followed by laminated carbonate between -7.7 and -13.7 °/oo and banded chert-carbonate between -7.4 and -12.8 °/oo. ^{18}O values in dolomite in the Upper Limestone Member varies between -9.2 and -14.6 °/oo. Ankerite in metamorphic rocks has values between -11.1 and -16.9 °/oo. Dolomite in metamorphosed rocks from the Upper Limestone Member fall between -15.6 and -18.0 °/oo (Figure 15). Although samples collected in proximity to gabbroic sills generally have the lightest $\delta^{18}O$ values they do not show the extreme depletion in the heavy isotope with proximity to intrusive contacts that $\delta^{13}C$ values show. They are often still in the same range or only a few per mil lighter than analyses from unmetamorphosed rocks.

Calcite in unmetamorphosed rocks has a range of values between -6.7 and -15.7 °/oo (Figure 14). Arenite has the widest range of ^{18}O values, varying between

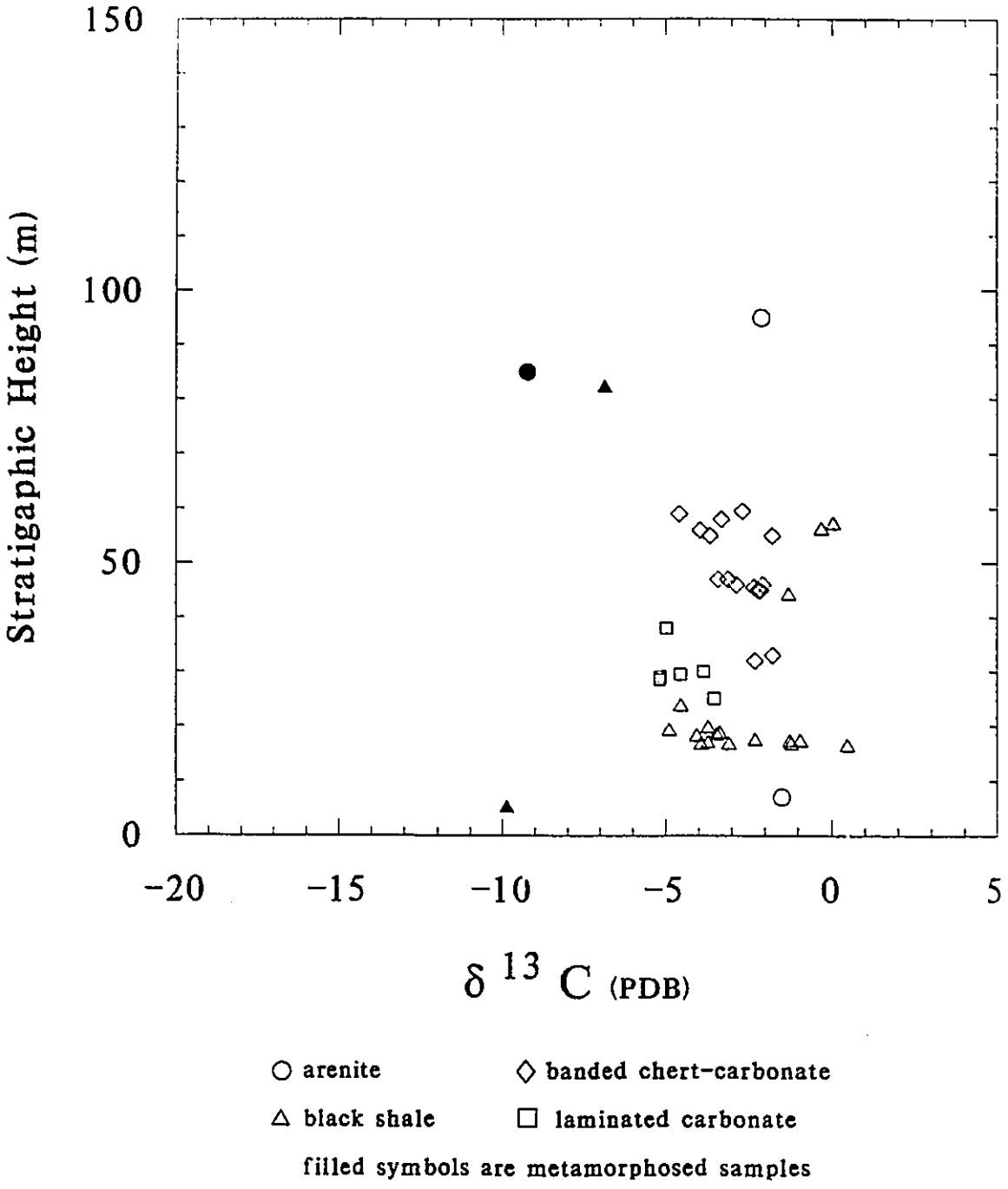

Figure 19. $\delta^{13}C$ of siderite versus stratigraphic height in the Gunflint Formation.

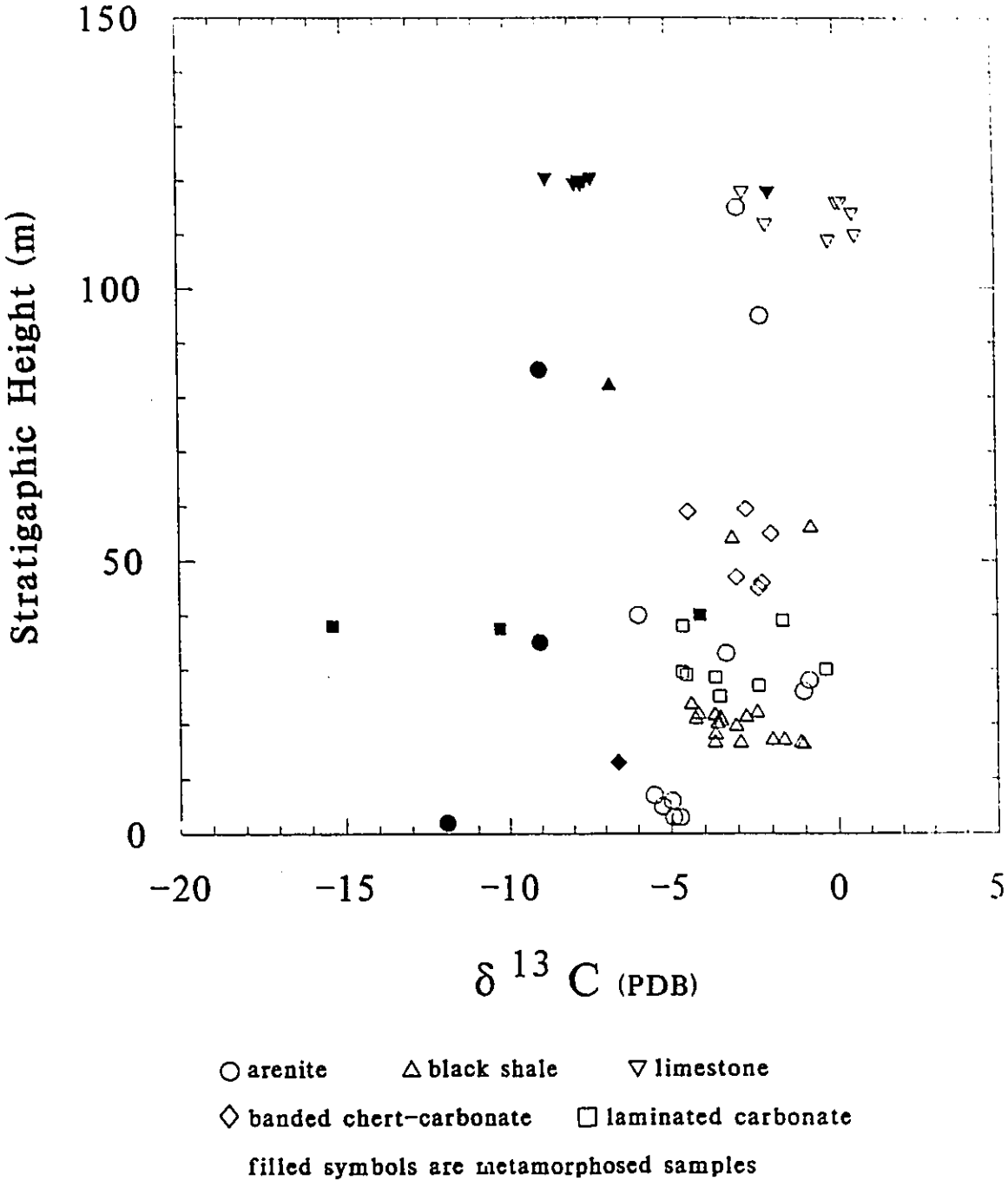

Figure 20. $\delta^{13}C$ of ankerite (or dolomite in limestone) versus stratigraphic height in the Gunflint Formation.

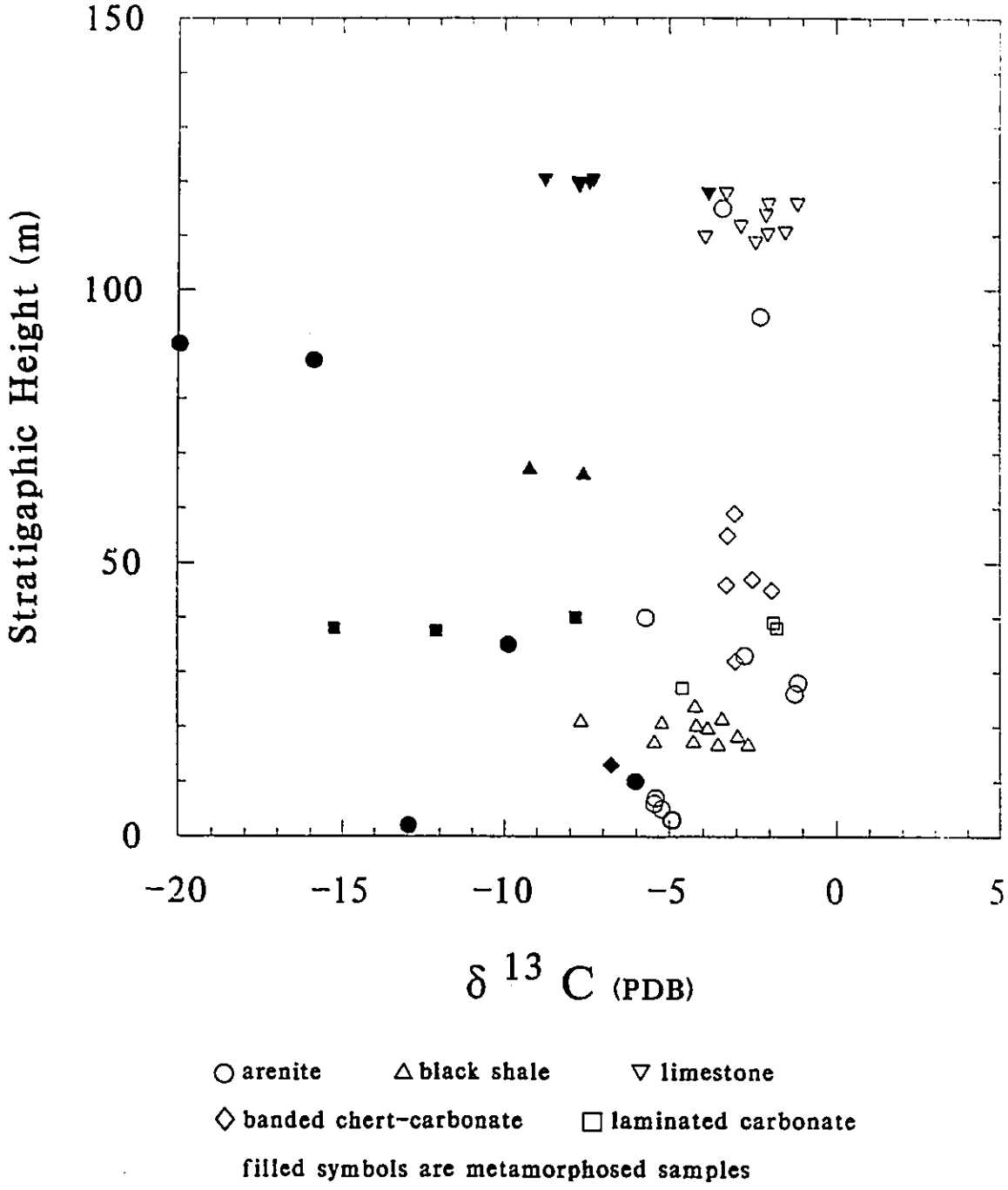

Figure 21. $\delta^{13}C$ of calcite versus stratigraphic height in the Gunflint Formation.

-6.7 and -15.7 ‰, followed by black shale between -7.4 and -15.7 ‰, banded chert-carbonate between -9.3 and -13.9 ‰, laminated carbonate between -9.4 and -13.1 ‰, and the Upper Limestone Member (Figure 15) between -13.1 and -15.5 ‰. Calcite in metamorphic rocks has $\delta^{18}O$ values between -12.0 and -17.5 ‰ and show the same distribution as ankerite.

Differences in $\delta^{18}O$ values between coexisting carbonate phases in unmetamorphosed rocks do not show any systematic variations (Figures 22, 23, and 24). Siderite values can be enriched in ^{18}O by up to 5.1 ‰ or depleted by up to 1.7 ‰ compared to coexisting ankerite (Figure 22). Siderite can also be up to 7.3 ‰ heavier or up to 4.2 ‰ lighter than coexisting calcite (Figure 23). Ankerite values can be heavier than coexisting calcite by up to 6.5 ‰ or they may be lighter by up to 4.4 ‰ (Figure 24). Differences in isotopic ratios between coexisting carbonate phases in metamorphosed rocks are smaller and more consistent than those from unmetamorphosed rocks. Siderite is enriched in ^{18}O by 1.3 to 2.2 ‰ compared to ankerite. Ankerite or dolomite is enriched in ^{18}O by up to 1.7 or depleted by up to 0.6 ‰ compared to calcite. No analyses of coexisting siderite and calcite were done.

The variations of $\delta^{18}O$ with respect to stratigraphy are a little more complex than those for carbon (Figures 25, 26 and 27). Siderite, ankerite, dolomite, and calcite all show a large range of values, up to 9 ‰, over short vertical distances although no systematic vertical trends are apparent. Analyses from metamorphosed rocks have values that overlap or are depleted in ^{18}O relative to unmetamorphosed rocks from the same stratigraphic interval.

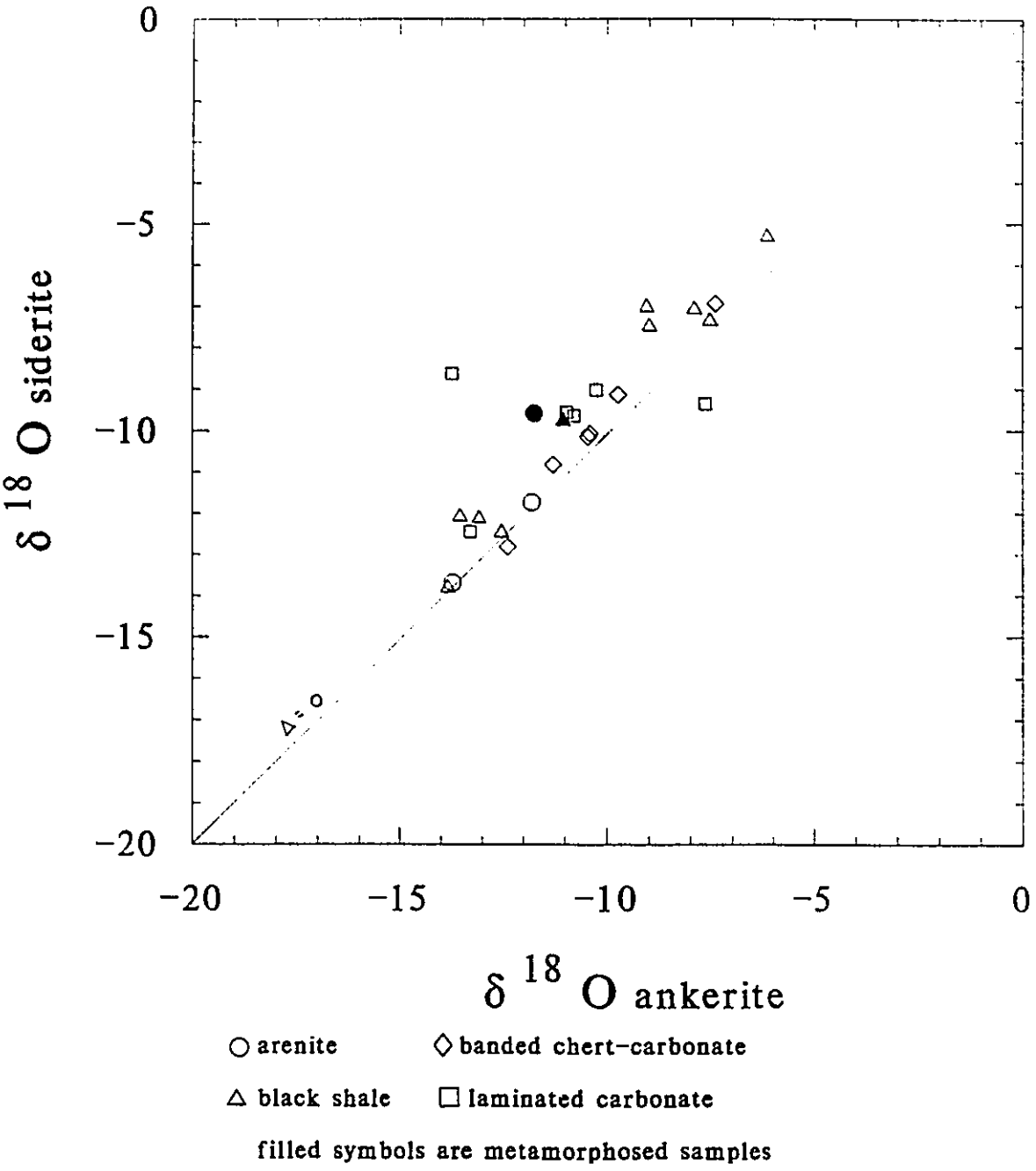

Figure 22. $\delta^{18}O$ of coexisting siderite and ankerite from the Gunflint Formation.

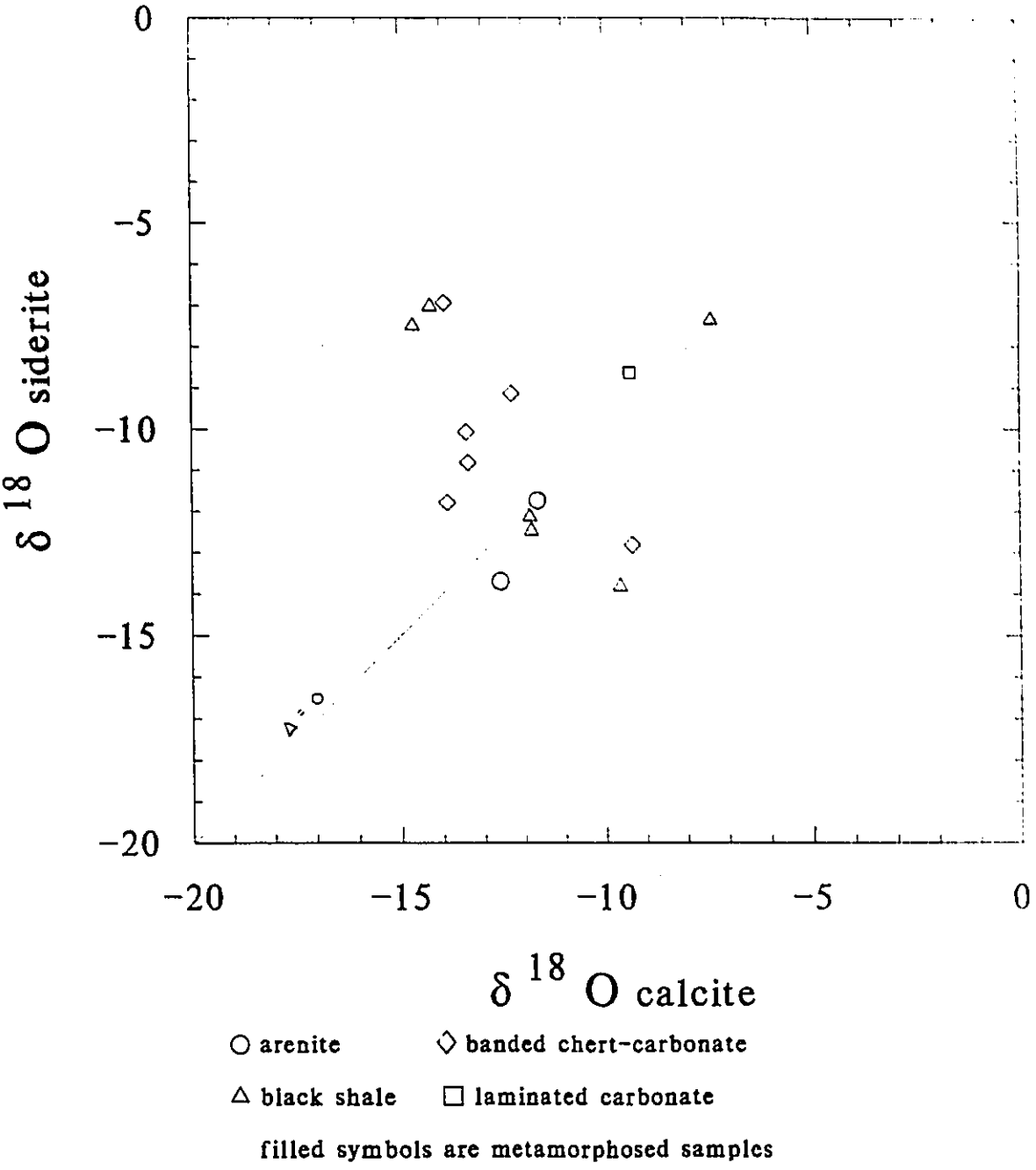

Figure 23. $\delta^{18}O$ of coexisting siderite and calcite from the Gunflint Formation.

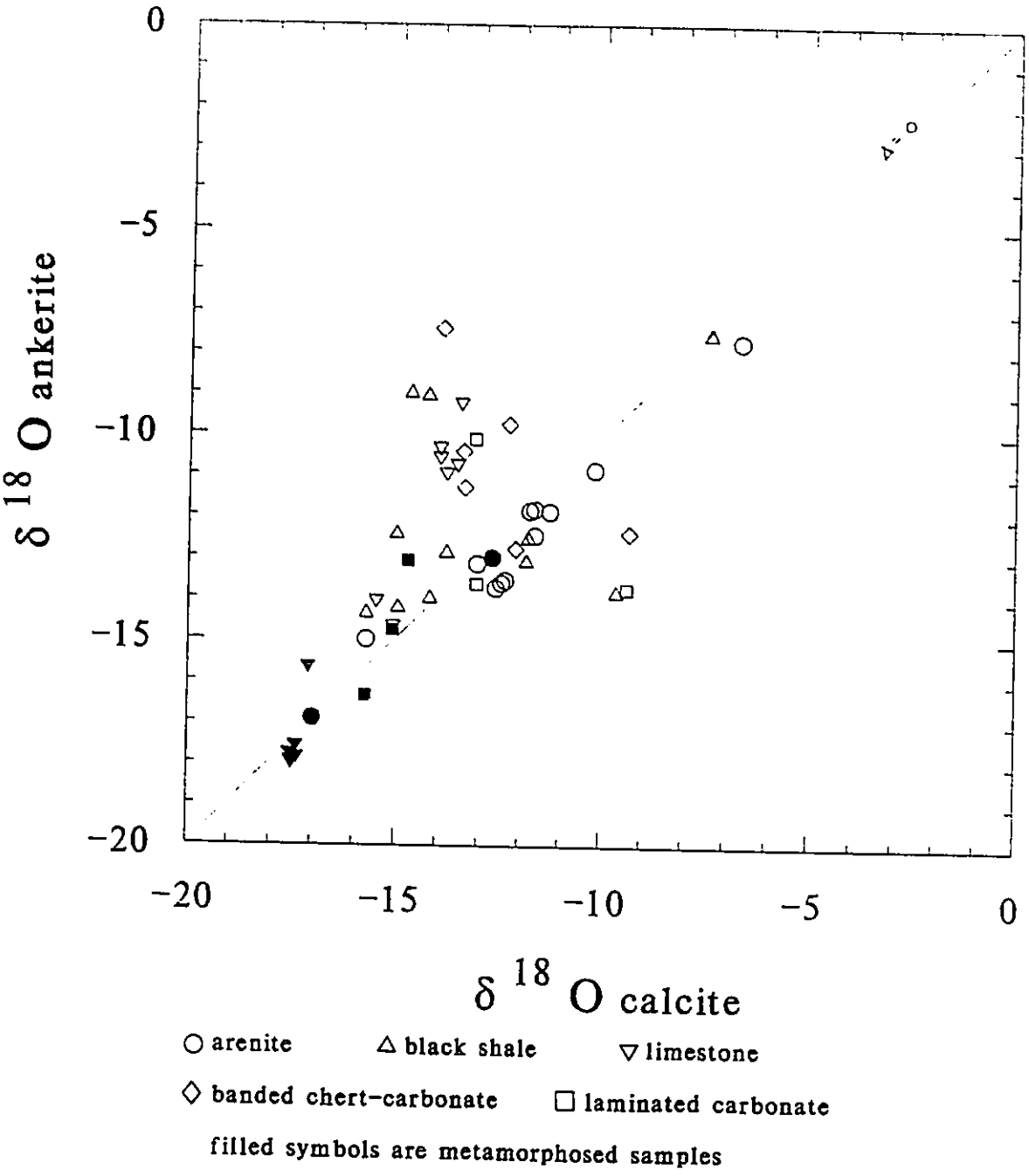

Figure 24. $\delta^{18}O$ of coexisting ankerite (or dolomite in limestone) and calcite from the Gunflint Formation.

4.3. $\delta^{34}S$ OF PYRITE

Sulfide minerals from the Gunflint Formation have a total range in $\delta^{34}S$ values of 70 ‰, with values between -32.5 to +35 ‰ (Figure 28). The $\delta^{34}S$ values do not show any systematic variations between different sedimentary facies or metamorphic grades. Instead the distribution appears to be have a geographic and stratigraphic control. The widest range of variation in $\delta^{34}S$ is restricted to the lower 20 m of the formation near Kakabeka Falls (Figure 29). Elsewhere, with only a few exceptions, sulfides have a narrow range of $\delta^{34}S$ values between about +5 and +12 ‰ (Figure 30 & 31). One analysis of coarse-grained pyrite in black chert of the basal stromatolite facies near Schrieber (location 9, Figure 8) had a value of -6.8 ‰. Two analyses from an irregular pyrite concretion (Plate 2D) were taken from the center and from the rim, yielding values of +14.5 ‰ and +21.9 ‰, respectively.

In the Kakabeka Falls area (location 3, Figure 8), coarse-grained pyrite from folded and brecciated beds of banded chert-carbonate and arenite from the lower 15 m of the formation are texturally complex and more than one generation may be present. These have $\delta^{34}S$ values between -18.2 and +22.0 ‰ (Figure 32). Black shale overlying brecciated units also have a wide range of values over a vertical distance of about 5 m (Figure 32). Three types of pyrite have been identified. The first type is very early diagenetic fine-grained pyrite, which is texturally similar to fine- grained pyrite observed throughout the rest of the formation. The second type is early diagenetic coarse-grained pyrite, which often overgrows the earlier fine-grained pyrite. The third type is early diagenetic pyrite concretions, which contain inclusions of type 2 pyrite in their cores. These are described in more detail in Chapter 3.

It was not possible to cleanly separate type 1 pyrite from these shales because

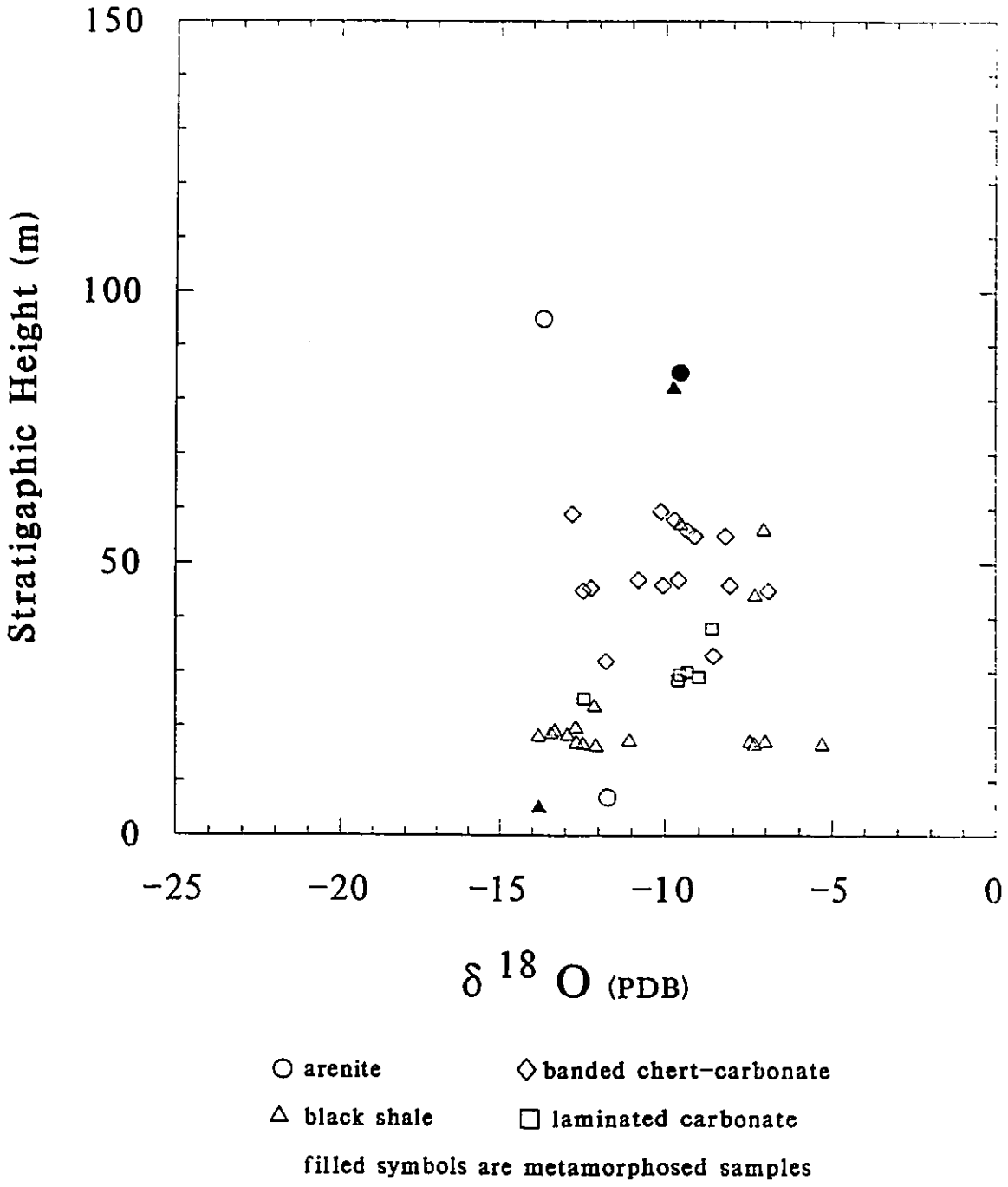

Figure 25. $\delta^{18}O$ of siderite versus stratigraphic height in the Gunflint Formation.

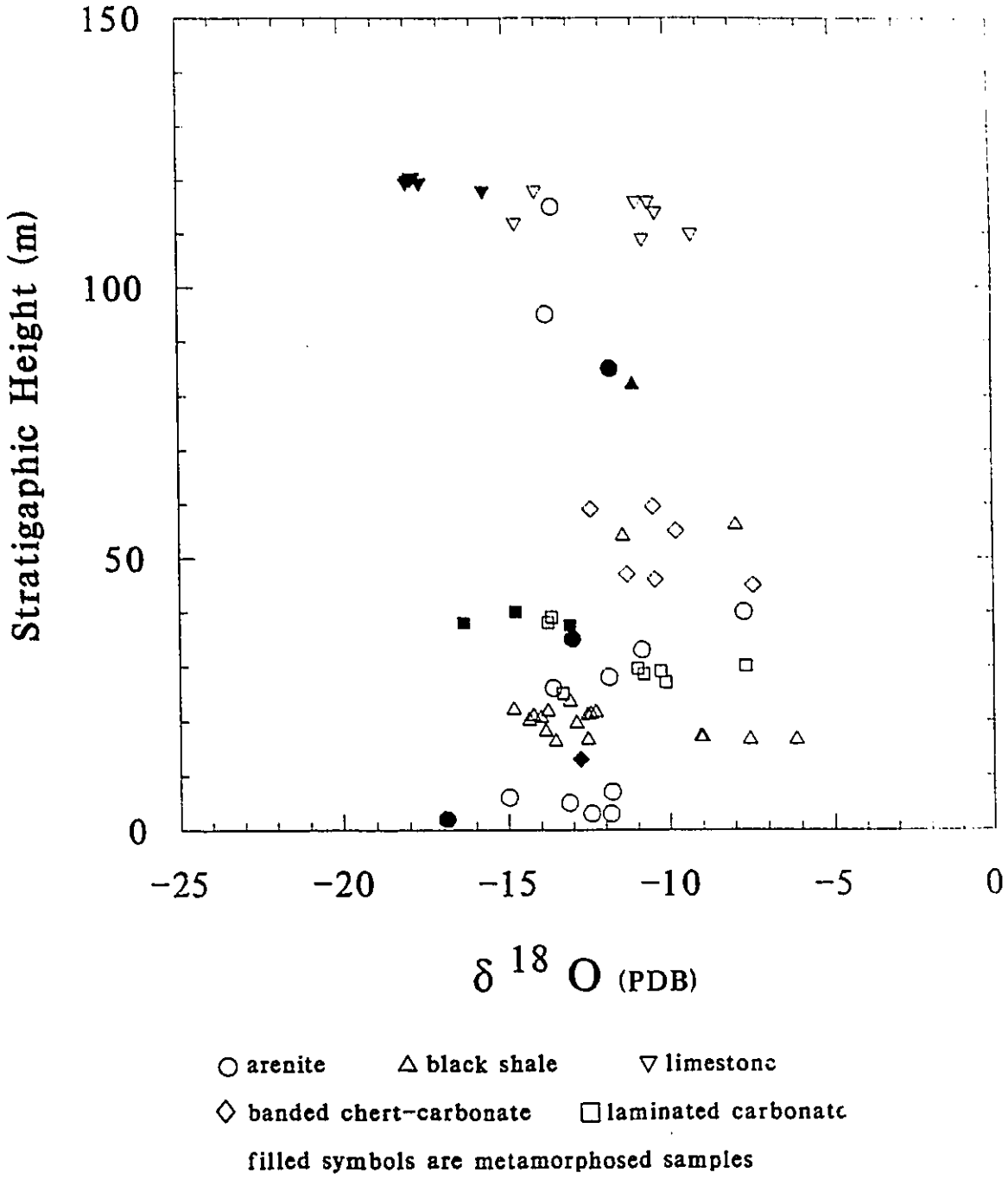

Figure 26. $\delta^{18}O$ of ankerite (or dolomite in limestone) versus stratigraphic height in the Gunflint Formation.

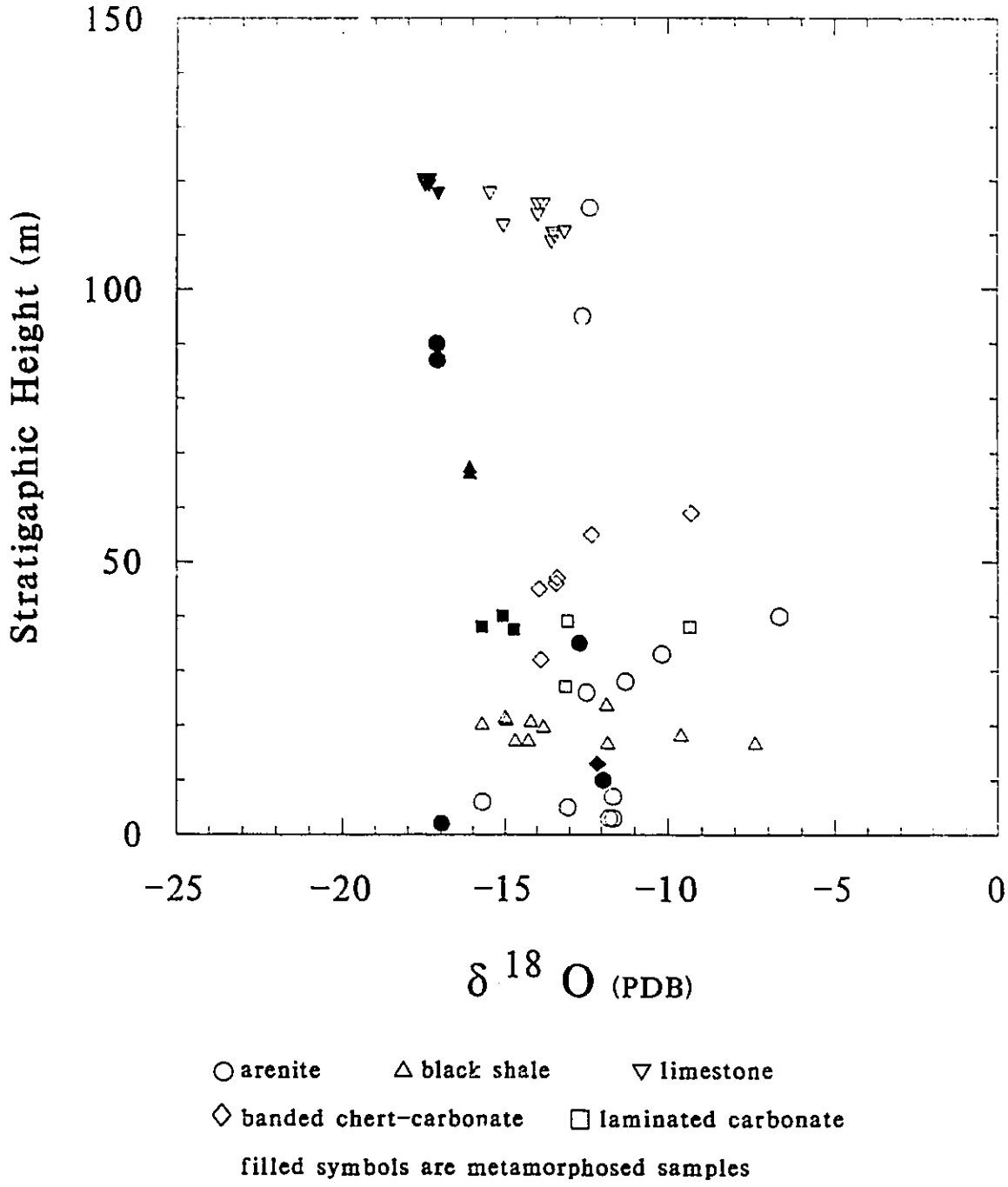

Figure 27. $\delta^{18}O$ of calcite versus stratigraphic height in the Gunflint Formation.

of their fine-grained nature and their intimate association with the slightly later formed type 2 pyrite. Therefore, analyses from these shales (with pyrite concretions removed) will reflect a variable contribution of these two types. These $\delta^{34}S$ values vary between about -2 and +35 ‰ and show a general upward trend to heavier values over a vertical distance of 5 m (Figure 32). Detailed traverses across pyrite concretions (type 3 pyrite) yield a complex distribution (Figure 33). These concretions display internal variations of between 7 to 39 ‰. In general, the heaviest values were obtained from the cores and the lightest values from the rims. These concretions also show a general upward trend to heavier values. Pyroclastic beds appear about 20 m above the base of the formation (Figure 32) after which only fine-grained pyrite (type 1) is present, which have a very narrow range of $\delta^{34}S$ values between +4 and +10 ‰, similar to the rest of the formation.

Six samples from late fractures, which cross-cut the Gunflint Formation, have a wide range of values. Two populations of $\delta^{34}S$ values may be present in these fractures: the first population has values between +1.3 and +3.1 ‰ (2 samples), whereas the second population has values between +16.6 and +28.3 ‰ (4 samples). Eight samples were analysed from the overlying Rove Formation and they have $\delta^{34}S$ values between +13 and +21 ‰ (Figure 30 & 34). These samples were taken from throughout the approximately 600 m thickness exposed in Ontario. There do not appear to be any systematic variations with stratigraphy, although the number of samples is too small to be certain.

Overall, there appears to be a distinct trend from highly variable and often ^{34}S depleted values from near the base of the Gunflint, to uniform values between +5 to +12 ‰ throughout the upper Gunflint, to uniform values between +13 to +21 throughout the Rove Formation (Figure 34).

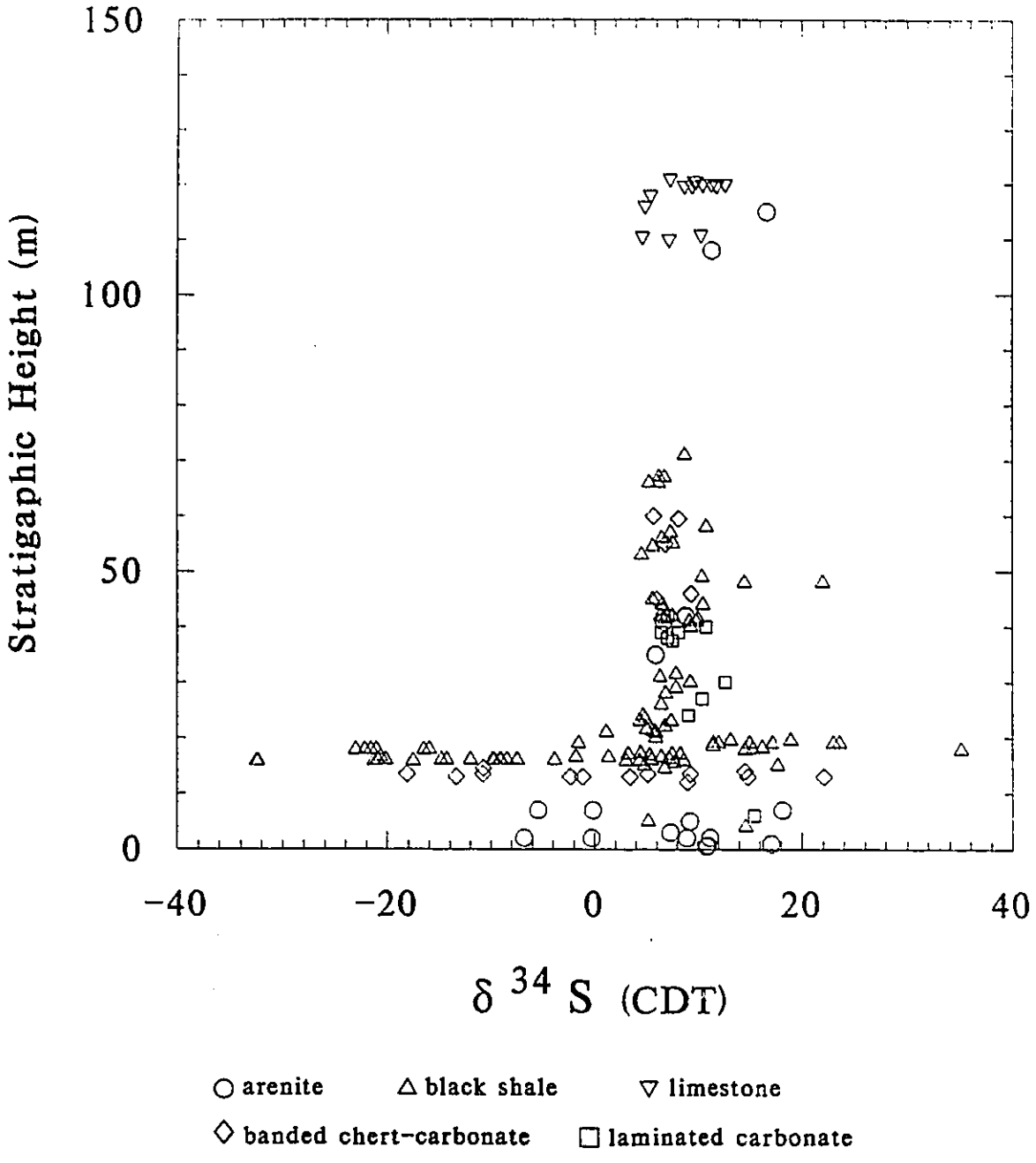

Figure 28. $\delta^{34}S$ versus stratigraphic height from all locations in the Gunflint Formation.

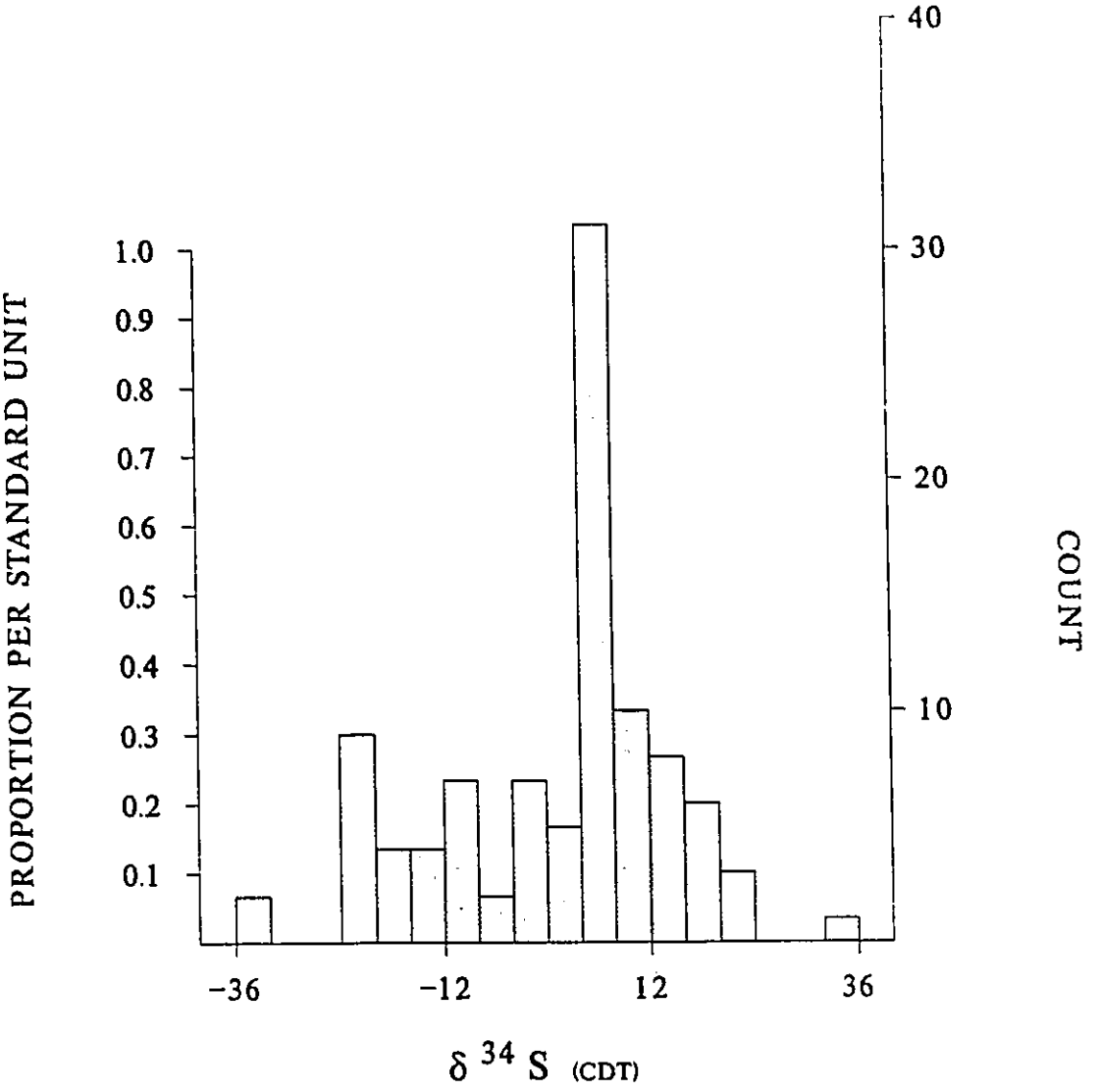

Figure 29. Histogram of $\delta^{34}S$ values from the Kakabeka Falls area in the Gunflint Formation.

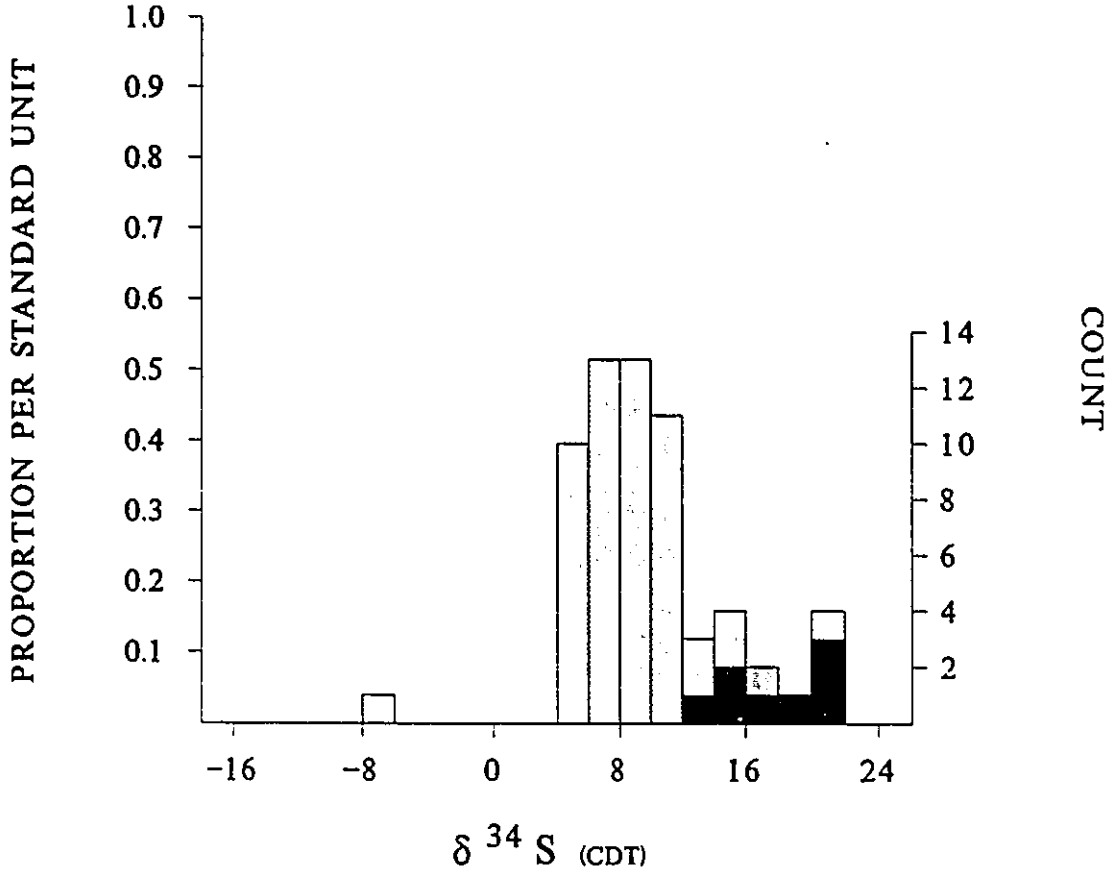

Figure 30. Histogram of $\delta^{34}S$ values from all locations, except the Kakabeka Falls area, in the Gunflint Formation (in grey) and Rove Formation (black).

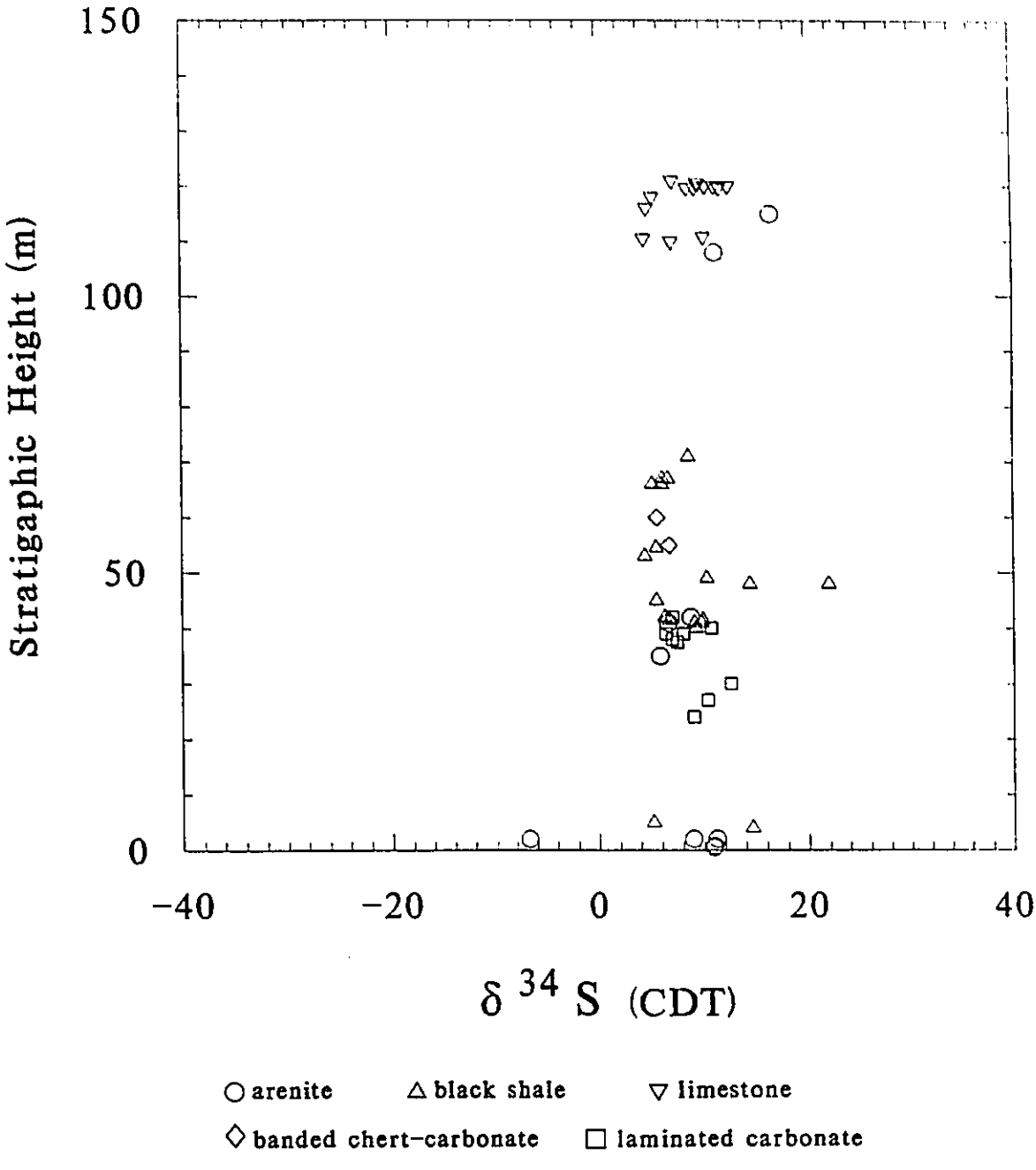

Figure 31. $\delta^{34}S$ versus stratigraphic height from all locations, except the Kakabeka Falls area, in the Gunflint Formation.

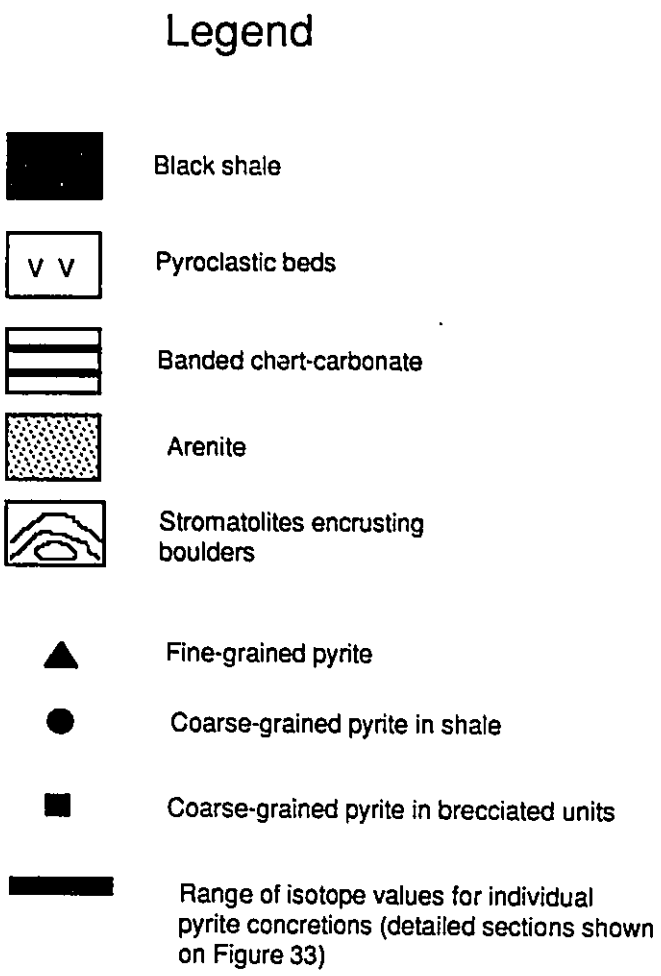

Figure 32. Sulphur isotope ratios from the Kakabeka Falls area plotted against a generalized stratigraphic section (opposite page). The range of values from four pyrite concretions are shown as horizontal bars. Detailed traverses across these concretions are shown on Figure 33. Legend for lithologic symbols and pyrite textures shown above.

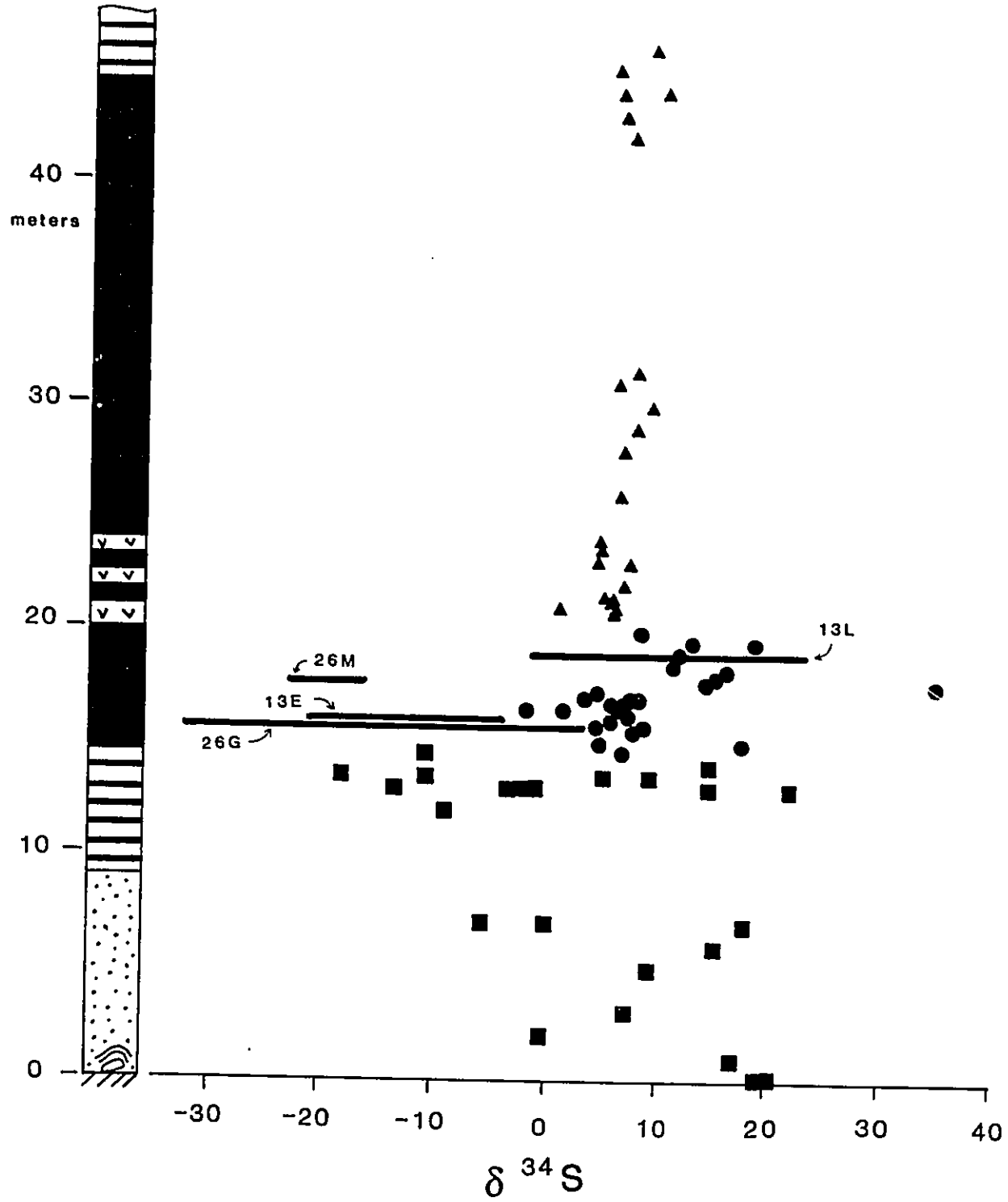
40
meters
30
20
10
0
26M
13E
26G
13L
-30
-20
-10
0
10
20
30
40
δ 34S

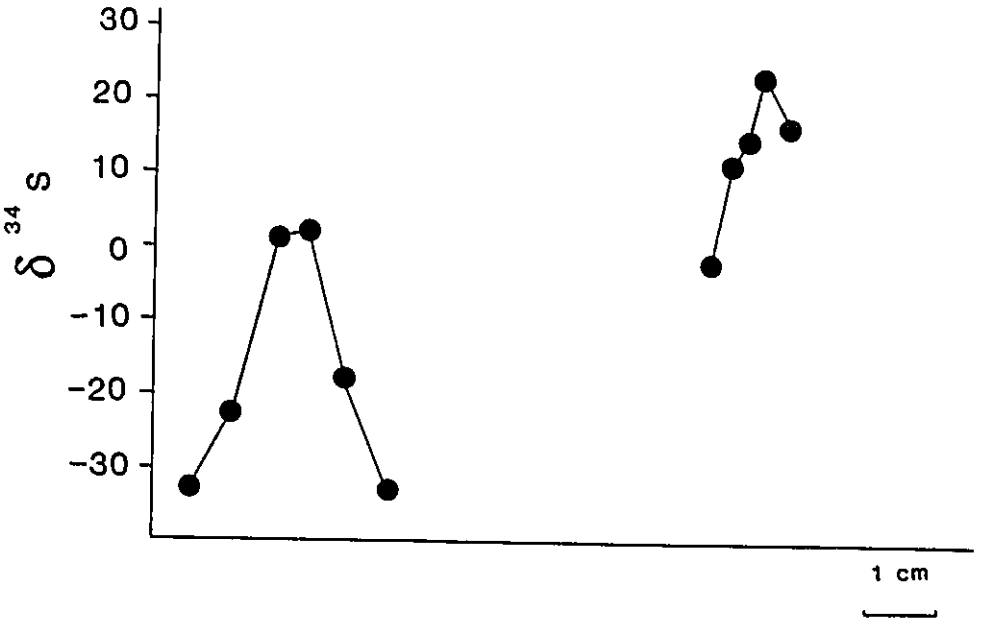

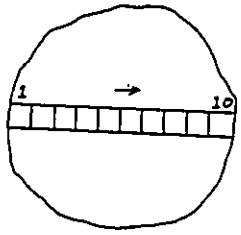

26G

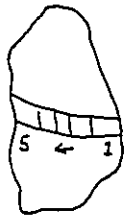

13L

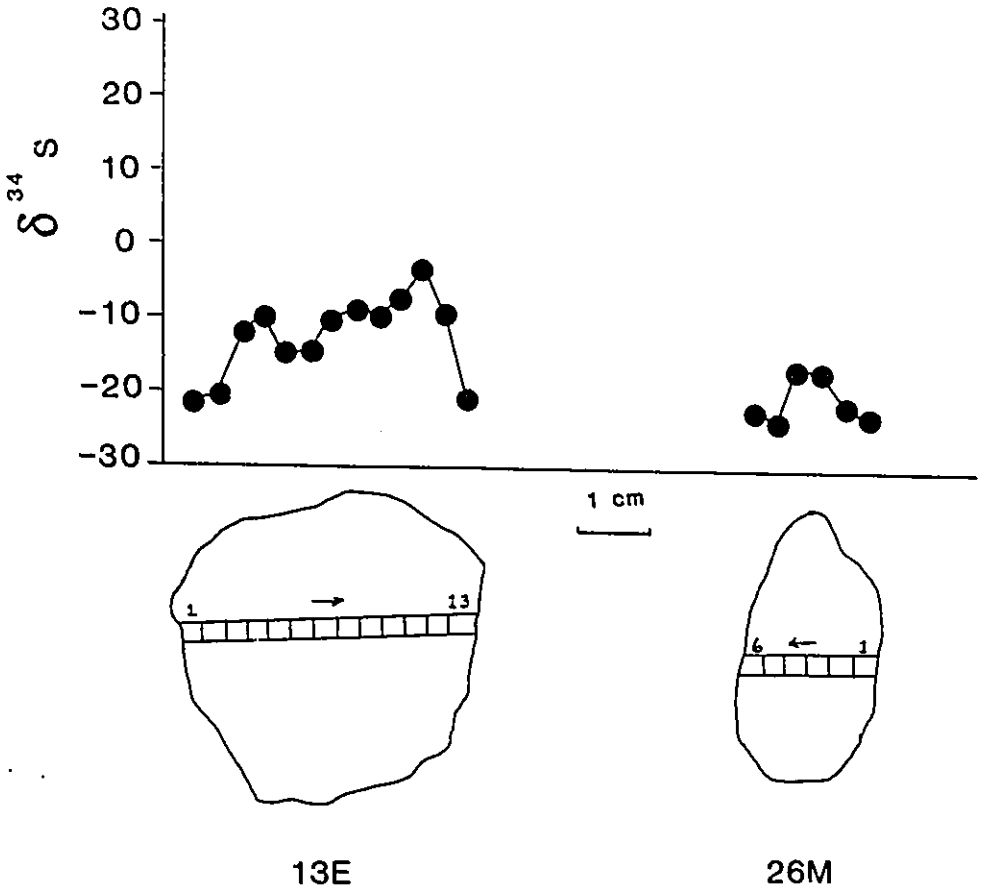

Figure 33. Isotopic profiles across individual pyrite concretions. A wafer (~2mm thick) was cut from the center of four ellipsoidal concretions (actual size shown). Subsamples (~2 mm square) were taken across these wafers, as shown by squares inside concretions, for analysis. Circles in profiles correspond to individual subsamples (numbered as shown).

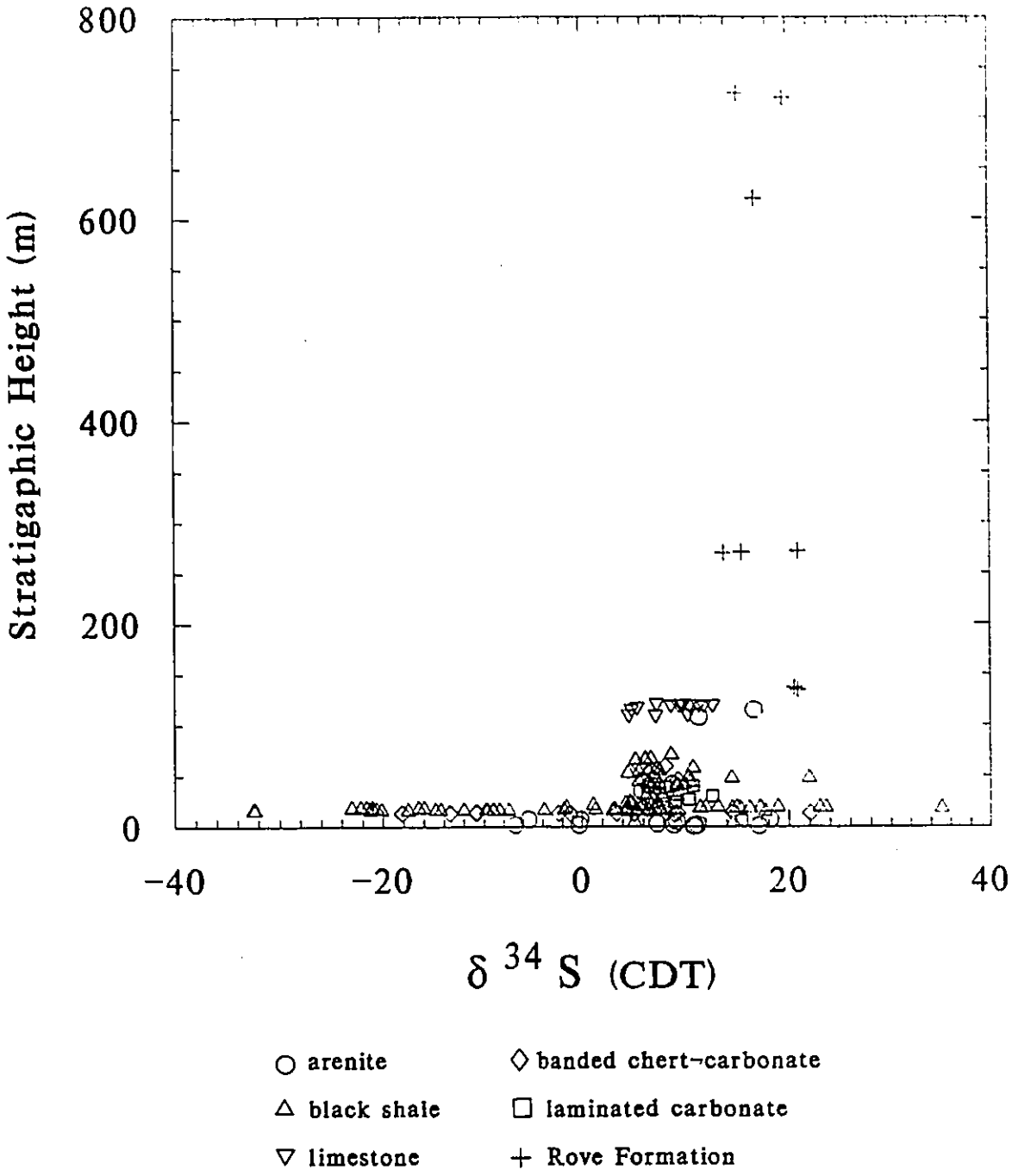

Figure 34. $\delta^{34}S$ versus stratigraphic height from all locations in the Gunflint and Rove Formations.

4.4. SULPHUR - CARBON RATIOS

Elemental abundances of sulphur and carbon were analysed from black shales of the Gunflint Formation. It was shown in the last section that the $\delta^{34}S$ values from the Kakabeka Falls area are distinct from the rest of the formation. The S/C mass ratios in black shales from the Kakabeka Falls area also show differences from the rest of the formation.

A plot of sulphur versus carbon from black shales of the Gunflint Formation, other than from the lower 20 m in the Kakabeka Falls area, are shown in Figure 35. These shales generally only contain very fine-grained, disseminated pyrite, except locally where thin laminae or layers are present. These pyrite-rich layers, which contain up to 80% pyrite, were not analysed for sulphur and carbon. Most sulphur contents are less than 1 %, although there are a few as high as 3 %, and carbon contents are variable with values as high as 7 %. Four of the highest sulphur values, between 1.7 and 3 % S, have carbon contents less than 1 % and come from the contact metamorphic zones of gabbro sills. It is probable that much of the original carbon may have been lost during metamorphism, causing an increase in their S/C ratio. Therefore these analyses may not be representative of depositional or diagenetic conditions and are not shown on Figure 35. Unlike most Phanerozoic marine shales, there is a poor correlation of S and C, the points are mostly distributed along a narrow band near the C axis, at low S concentrations.

Black shales in the lower 20 m of the Gunflint Formation in the Kakabeka Falls area have higher S/C ratios and the plot shows a great deal of scatter (Figure 36). Analyses were performed on shales that contained variable proportions of both fine and coarse-grained pyrite (Types 1 & 2), but were free of pyrite concretions. From petrographic observations, fine-grained pyrite-sulphur contents are generally less than 1 %, the scatter being due to high contents of coarse-grained pyrite. Therefore it is probable that S/C ratios for these shales are the same as the rest of

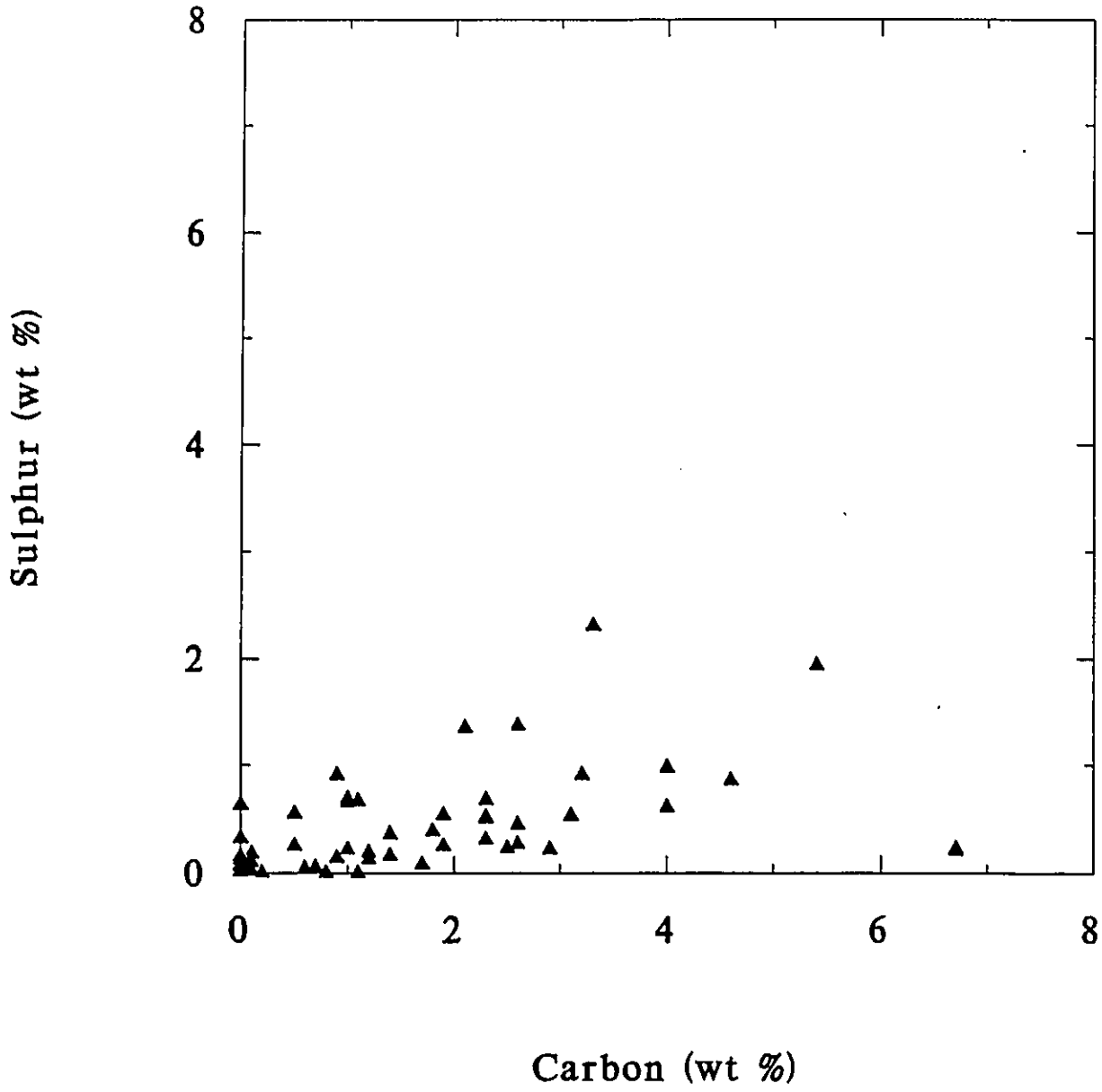

Figure 35. Plot of pyrite-sulphur versus organic carbon from all locations, except the Kakabeka Falls area (see Figure 36), in the Gunflint Formation.

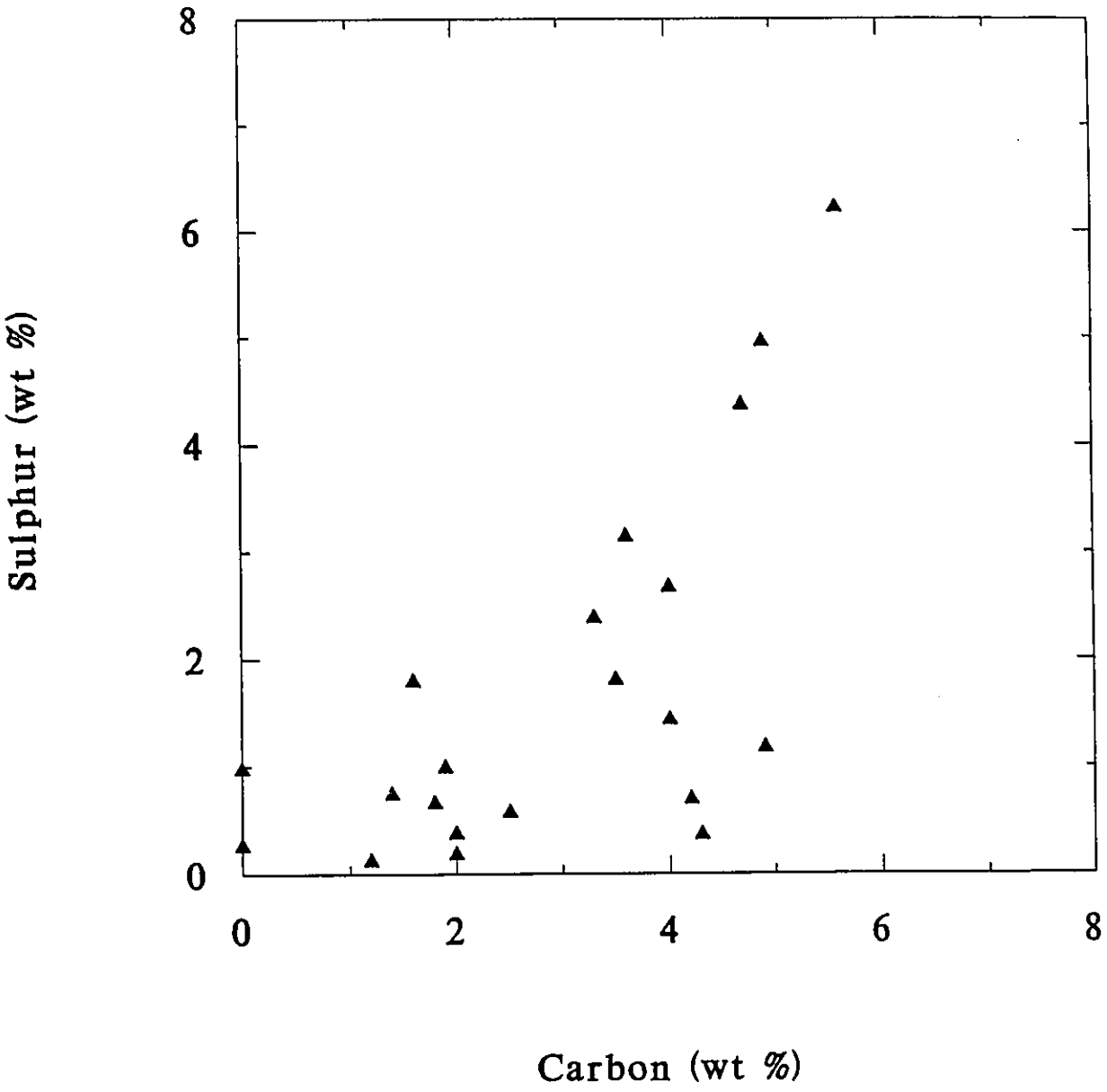

Figure 36. Plot of pyrite-sulphur versus organic carbon from the lower part of the Gunflint Formation in the Kakabeka Falls area.

the formation when coarse-grained pyrite is excluded. At the contact with underlying brecciated banded chert-carbonate, the shale contains layers of massive pyrite containing relatively small carbon contents.

5. INTERPRETATION OF ISOTOPIC RESULTS

5.1. CARBON ISOTOPES

Most marine limestones and calcareous organisms tend to reflect the $\delta^{13}C$ of total dissolved inorganic carbon (TDIC) of the water mass in which they formed. The TDIC species are carbon dioxide, carbonic acid, bicarbonate and carbonate, of which bicarbonate is the dominant species in natural waters. Under equilibrium conditions calcite is enriched in ^{13}C by 1 to 3 ‰ relative to bicarbonate (Emrich et al, 1970; Deines et al, 1974). Dolomite should have $\delta^{13}C$ values about 2 ‰ heavier than cogenetic calcites (Veizer, 1983a). However, fractionation in natural systems often does not follow theoretical equilibrium fractionation factors. Rapid rates of precipitation can cause the $\delta^{13}C$ of the carbonate to approach that of the dissolved bicarbonate (Turner, 1982). The uptake of isotopically light metabolic CO_2 into organically precipitated carbonate frequently produces small deviations from equilibrium values (Veizer, 1983a). There are no fractionation factors available for ankerite and siderite.

Present day variations of $\delta^{13}C$ for dissolved bicarbonate in the oceans are mostly within the range -1 to +3 ‰ (Veizer, 1983b). The composition of the ancient oceans, as recorded by the composition of carbonate rocks, has remained within this range since the Archean (Veizer et al, 1980; Veizer and Hoefs, 1976; Schidlowski et al, 1975, 1983). Rocks younger than late Proterozoic have superimposed second-order oscillations, of up to 4 ‰ in amplitude, at 10^7 to 10^8 year wavelengths. The isotopic record of these oscillations is not as well defined in Precambrian carbonate rocks. Veizer et al (1989,1990) have shown that the best preserved Archean and early Proterozoic marine carbonate rocks have $\delta^{13}C$ values of 0 ± 1.5 ‰, which are similar to values obtained for Phanerozoic carbonates. The

TDIC of meteoric waters does not have a unique $\delta^{13}C$ value but is generally depleted in ^{13}C relative to seawater due to the addition of organically-derived CO_2.

During diagenesis carbonate minerals may undergo isotopic exchange with the pore fluids. This takes place by a process of dissolution-reprecipitation of unstable carbonate phases (i.e. aragonite and high-Mg calcite) to form more stable phases (i.e. low-Mg calcite) (Veizer, 1983a). The $\delta^{13}C$ of the new phase will depend on: 1) the difference between the $\delta^{13}C$ of the primary phase and that of the pore fluid, 2) the deviation of the fractionation factor from unity, and 3) the proportion of solutes derived from the dissolving phase versus those contributed from the incoming water (i.e. the water/rock ratio) (Veizer, 1983a). The stabilization of carbonate rocks usually proceeds in discrete microenvironments, so that the $\delta^{13}C$ of the water in these microenvironments is buffered by the dissolving phase and primary compositions are often preserved unchanged.

Pore water chemistry can become significantly altered during diagenesis of organic-rich sediments. The oxidation of organic matter in sediments starts immediately after deposition. Six zones or stages of oxidation have been defined (Claypool and Kaplan, 1974; Hesse, 1986);(Figure 37). The top layer of sediments underlying oxic bottom waters contain freely dissolved oxygen (zone 1, Figure 37). Within the oxidation zone most of the oxygen is consumed by aerobic bacteria which oxidize organic matter producing CO_2 as a by-product of their metabolism (equation 1, Figure 38). As conditions become suboxic (zone 2, Figure 37), dysaerobic bacteria utilize nitrate, manganese, and iron rather than oxygen, as an electron acceptor during metabolism (equation 2, Figure 38). The sulphate reduction zone (zone 3, Figure 37) begins when conditions become truly anoxic, usually at depths of tens of centimeters in normal marine sediments. In euxinic basins the sulphate reduction zone may coincide or rise above the sediment/water interface. Sulphate-reducing bacteria are the dominant bacterial species responsible for the oxidation of organic matter in this

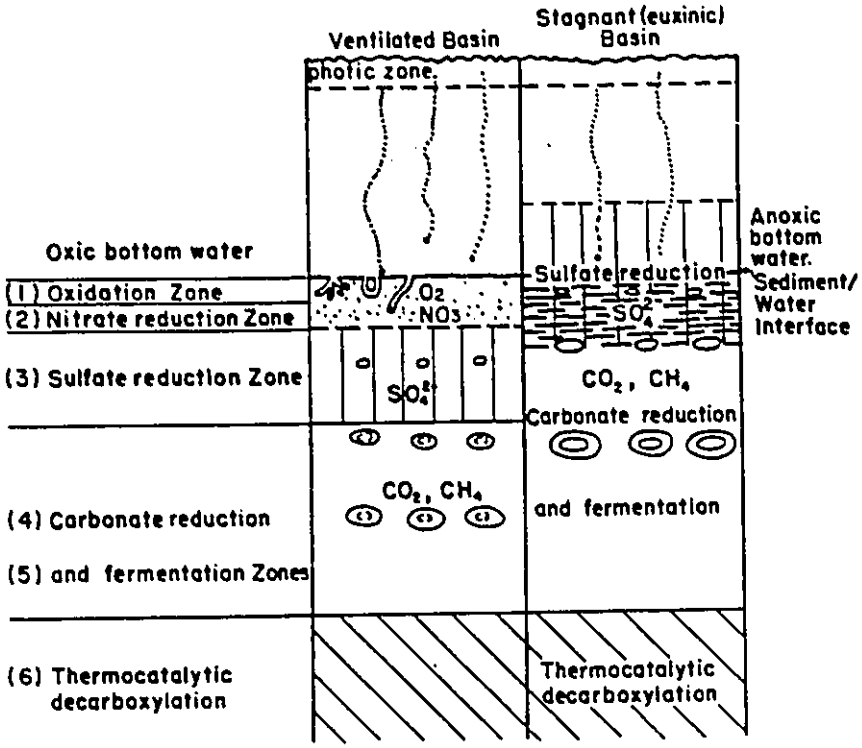

Figure 37. Stages of organic matter oxidation in anoxic sediments (modified from Claypool and Kaplan, 1974).

C : N : P = 106 : 16 : 1 = Redfield ratio for primary organic matter.
The organic matter involved in reactions (1) to (4) does not necessarily have this ratio.

	$\Delta G^{\circ\prime}$ of metabolic processes coupled with oxidation reactions (in kcal·(mol)$^{-1}$ glucose)
(1) Oxidation by freely dissolved O_2 (aerobic respiration)	
$(CH_2O)_{106}(NH_3)_{16}(H_3PO_4) + 138\ O_2 \rightarrow 106\ CO_2 + 16\ HNO_3 + 122\ H_2O$	-763
Manganese reduction	
$(CH_2O)_{106}(NH_3)_{16}(H_3PO_4) + 236\ MnO_2 + 472\ H^+ \rightarrow 236\ Mn^{2+} + 106\ CO_2 + 8\ N_2 + H_3PO_4 + 366\ H_2O$	-748 (birnessite) -698 (pyrolusite)
(2) Nitrate reduction	
$(CH_2O)_{106}(NH_3)_{16}(H_3PO_4) + 99.4\ HNO_3 \rightarrow 106\ CO_2 + 55.2\ N_2 + H_3PO_4 + 177.2\ H_2O$	-724
$(CH_2O)_{106}(NH_3)_{16}(H_3PO_4) + 84.4\ HNO_3 \rightarrow 106\ CO_2 + 42.4\ N_2 + 16\ NH_3 + H_3PO_4 + 148.4\ H_2O$	-658
Iron reduction	
$(CH_2O)_{106}(NH_3)_{16}(H_3PO_4) + 212\ Fe_2O_3$ (or 424 FeOOH) $+ 848\ H^+ \rightarrow 424\ Fe^{2+} + 106\ CO_2 + 16\ NH_3 + 530\ H_2O$ (or 742 H_2O)	-337 (hematite) -318 (limonitic goethite)
(3) Sulphate reduction	
$(CH_2O)_{106}(NH_3)_{16}(H_3PO_4) + 53\ (SO_4)^{2-} \rightarrow 106\ CO_2 + 16\ NH_3 + 53\ S^{2-} + H_3PO_4 + 106\ H_2O$	-91
(4) Carbonate reduction	
$(CH_2O)_{106}(NH_3)_{16}(H_3PO_4) \rightarrow 53\ CO_2 + 53\ CH_4 + 16\ NH_3 + H_3PO_4$	-84

Figure 38. Reactions involved in the bacterial oxidation of organic matter in sediments (modified from Froelich et al, 1979).

zone (equation 3, Figure 38).

Isotopic fractionation of carbon during oxidation is negligible and the $\delta^{13}C$ of the CO_2 formed during diagenesis will be similar to that of the parent organic matter. Eichmann and Schidlowski (1975) have shown that the $\delta^{13}C$ of organic carbon in sediments has had an average value of about -25 °/oo since about 3.5 Ga. Barghoorn et al (1977) obtained values between -15 and -35 °/oo for organic carbon extracted from the Gunflint Formation. Initially, TDIC in pore waters just below the sediment/water interface will have the same concentration (~ 2-3 mmol/l) and $\delta^{13}C$ (~ 0 °/oo) as the overlying water column (Figure 39). In organic-poor sediments no major changes will occur during early diagenesis. However, in sediments that contain abundant organic matter the concentration of bicarbonate will increase steadily with depth, as organic matter becomes oxidized, reaching a maximum at the base of the sulphate reduction zone (Figure 39). At the same time the $\delta^{13}C$ will be rapidly shifted to lighter values, reaching a minimum at the base of the sulphate reduction zone (Gautier and Claypol, 1984). In addition, extremely ^{13}C depleted methane, which is generated at lower depths, may migrate upward to become oxidized, contributing anomalously light CO_2 (Gautier and Claypool, 1984).

Once sulphate has been essentially depleted, carbonate reduction and fermentation become the most important mechanisms for bacterial oxidation of organic matter (zones 4 & 5, Figure 37). A portion of the light CO_2 produced in this and previous stages is used by methanogenic bacteria to produce methane (equation 4, Figure 38). The disproportionation of organic matter into CH_4 and CO_2 is accompanied by a strong isotope fractionation effect. The CH_4 is depleted in ^{13}C by about 70 °/oo relative to the carbon of the parent material, thus methane may have $\delta^{13}C$ values as light as -90 or -100 °/oo. As methanogenesis proceeds, the residual CO_2 will become increasingly enriched in ^{13}C. As the concentration of methane increases with depth, the concentration of bicarbonate shows a corresponding

decrease. The $\delta^{13}C$ of the residual bicarbonate, and as a result the methane, will shift towards heavier values with depth (Figure 39). The $\delta^{13}C$ of dissolved bicarbonate in this zone may become as heavy as +15 °/oo (Irwin et al, 1977) but more commonly is in the range -5 to +5 °/oo (Gautier and Claypool, 1984). This probably reflects a balance between isotopic fractionation resulting from methane generation and the continued addition of light CO_2 through fermentation reactions (Gautier and Claypool, 1984).

Above about 75 °C bacterial activity decreases substantially and oxidation of organic matter proceeds by abiogenic reactions. The $\delta^{13}C$ of CO_2 produced by thermocatalytic reactions is similar to the parent organic carbon. In summary, the $\delta^{13}C$ of bicarbonate in pore waters can show a depth zonation from a marine bicarbonate value (0 °/oo) near the sediment/water interface, to lighter values through zones 1 to 3 (0 to -25 °/oo), then a shift to heavier values through zones 4 and 5 (-25 to +15 °/oo), and finally a shift back to more negative values in zone 6 (-20 °/oo) (Irwin et al, 1977).

Authigenic carbonate precipitation requires a relatively high pH. In a carbonate-buffered system, increasing P_{CO2} will cause a drop in pH and carbonate activity, causing an increase in carbonate solubility. In anoxic environments buffering of the pH by H_2S and uptake of H^+ by Mn and Fe reduction will increase pH sufficiently to cause supersaturation with respect to carbonate. Hydrogen consumption during methanogenesis will also cause an increase in pH. Calcite is normally the first authigenic carbonate to form because dolomite formation is inhibited by the presence of substantial dissolved sulphate (Baker and Kastner, 1981). Ankerite and siderite formation is inhibited because dissolved iron in the sulphate reduction zone is preferentially incorporated in sulfides rather than carbonate. Therefore, precipitation of authigenic dolomite is favoured by any process that reduces sulphate concentration. Ankerite or siderite will form whenever excess ferrous iron becomes available.

Because the $\delta^{13}C$ and mineralogy of authigenic carbonate minerals reflect the composition of the pore water, they can be used as tracers of diagenetic processes. For example, concretions in the Gammon Shale analysed by Gautier and Claypool (1984) have a calcitic core with δ^{13} values of about -22 ‰ that is mantled by a sideritic rim in which $\delta^{13}C$ values increase outward from -10 to -4 ‰ (Figure 39). The calcitic core probably formed in the lower part of the sulphate reduction zone where $\delta^{13}C$ values were at a minimum and iron was taken up by pyrite. The siderite rim formed when dissolved iron became available below the sulphate reduction. The shift outward towards heavier $\delta^{13}C$ values (Figure 39) resulted from methanogenesis.

A typical feature of Precambrian iron-formations is the presence of carbonates that are depleted in ^{13}C relative to normal marine carbonates (Becker and Clayton, 1972; Perry and Tan, 1973; Thode and Goodwin, 1983; Baur et al, 1985; this study). Three explanations have been offered: 1) the carbonates are primary and were precipitated from ^{13}C-depleted seawater, 2) the carbonates are primary but underwent isotope exchange reactions with isotopically light CO_2, and 3) the carbonates are authigenic and formed as a result of the oxidation of organic matter. These interpretations have, in turn, been used to interpret the origin of iron-formations.

1. Becker and Clayton (1972) found that ankerite and siderite in the Dales Gorge Member of the Brockman Iron Formation from the Hammersley Group in Australia have a range of $\delta^{13}C$ values from -6.5 to -15 ‰, with most values near -10 ‰. They also noted that carbonates of the Wittenoom Dolomite and the Duck Creek Dolomite, also from the Hammersley Group, have $\delta^{13}C$ values mostly between +2 and -2 ‰, which are typical for marine carbonates. They proposed that the siderite and ankerite precipitated from isotopically light dissolved bicarbonate and, therefore, that the iron-formation formed within a basin that was separated from the open ocean reservoir of dissolved bicarbonate. Oxidation of organic matter, possibly

Figure 39. Relationship between early diagenetic mineralization reactions in carbonate concretions and depth trend of dissolved chemical species and carbon isotopes in pore waters from which concretions precipitated (from Gautier and Claypool, 1984).

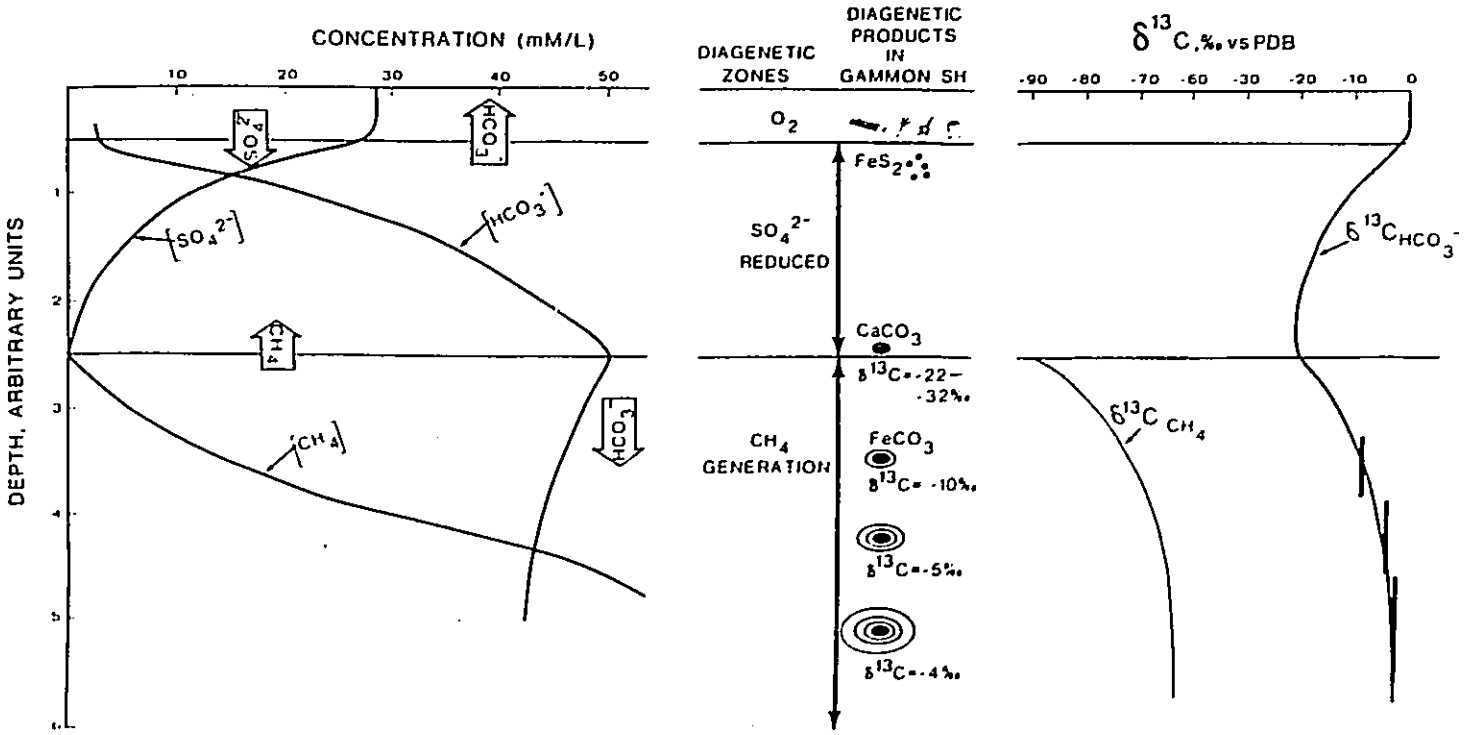
CONCENTRATION (mM/L)
10
20
30
40
50
DEPTH, ARBITRARY UNITS
1
2
3
4
5
6
SO_4
HCO_3
$[SO_4^{2-}]$
$[HCO_3^-]$
CH_4
$[CH_4]$
HCO_3
DIAGENETIC ZONES
DIAGENETIC PRODUCTS IN GAMMON SH
O_2
FeS_2
SO_4^{2-} REDUCED
$CaCO_3$
$\delta^{13}C$=-22–-32‰
CH_4 GENERATION
$FeCO_3$
$\delta^{13}C$= -10‰
$\delta^{13}C$=-5‰
$\delta^{13}C$=-4‰
$\delta^{13}C$, ‰ vs PDB
-90
-80
-70
-60
-30
-20
-10
0
$\delta^{13}C_{HCO_3^-}$
$\delta^{13}C_{CH_4}$

coupled with the reduction of ferric iron, in the water column provided the source of light bicarbonate from which siderite and ankerite formed. The normal marine composition of the dolomite units would represent periods when the basin was transgressed by the ocean.

Thode and Goodwin (1983) reported carbon isotope ratios from five Archean iron-formations within the Canadian Shield. Carbonates in the oxide, siderite, and chert facies had $\delta^{13}C$ values of +2.3 to -1.1 °/oo, whereas carbonates from the graphite-rich sulfide facies had $\delta^{13}C$ values as low as -7.6 °/oo. They agreed with Becker and Clayton (1972) that light carbonate resulted from mixing of carbonate of organic origin with marine carbonate during a period of basin emergence and isolation.

A modern, partial analogue for this may be the Black Sea, which is a marine basin closed to the open ocean. Below a depth of about 175 m the waters are anoxic and sulphate reduction occurs. The $\delta^{13}C$ of TDIC shows a progressive decrease from near 1 °/oo in surface waters to about -7 °/oo in deep waters (Deuser, 1970) due to the oxidation of organic matter. In comparison, bottom waters in the open ocean have minimum values of about -1 °/oo (Anderson & Arthur, 1983).

Holland (1984) suggests that in areas of upwelling of deep ocean waters, which because of higher contents of dissolved nutients would be areas of high biological productivity, isotopically light CO_2 would be generated by the oxidation of organic matter (i.e. sulphate reduction). These upwelled waters would have been anoxic and iron-rich. This light CO_2 would become mixed with the TDIC of upwelling waters resulting in a shift to negative $\delta^{13}C$ values for TDIC and siderite and ankerite precipitated from it. These values would represent local deviations rather than variations in the $\delta^{13}C$ value of the ocean as a whole (Holland, 1984).

Unmetamorphosed rocks from the Gunflint Formation have $\delta^{13}C$ values between +0.5 and -6 °/oo, whereas metamorphosed rocks have values lighter than -6

‰. If these values are the result of fluctuations in seawater $\delta^{13}C$ it should be reflected in a plot of $\delta^{13}C$ versus stratigraphy. From Figures 13 to 15 it is seen that, for unmetamorphosed rocks, at any given stratigraphic interval, there is a wide range of values, up to 6 ‰, with the heaviest values usually close to 0 ‰. Differences of up to 2 ‰ were found between samples only a few centimeters apart. It is unlikely that seawater $\delta^{13}C$ could have varied by as much as 6 ‰ over short periods of time. In addition, $\delta^{13}C$ values for the Upper Limestone Member are within the same range as values from iron-rich rocks, suggesting that the light values are not related to upwelling of iron-rich water. The restriction of $\delta^{13}C$ values lighter than about -6 ‰ to metamorphosed rocks indicates that the most depleted values are a product of metamorphism.

Petrographic evidence (chapter 3) indicates that the siderite formed above and/or just below the sediment/water interface and that the dolomite in the Upper Limestone Member formed during very early diagenesis (Figure 11). Because these carbonate minerals are primary, they are expected to reflect the $\delta^{13}C$ composition of the waters from which they precipitated. As discussed above, the 6 ‰ range of values do not reflect fluctuations in seawater composition. However, because the heaviest $\delta^{13}C$ values are consistently near 0 ‰ throughout the stratigraphic section, which is the expected value for marine carbonates, this is interpreted to indicate that a major component of these carbonate minerals is seawater bicarbonate having normal $\delta^{13}C$ values. Values as light as -6 ‰ were a result of either the addition of isotopically light authigenic siderite during very early diagenesis (e.g. Baur et al, 1985) or isotope exchange reactions during diagenesis or metamorphism (e.g. Perry and Tan, 1973). Ankerite and calcite formed during early to late diagenesis and during metamorphism (Figure 11), either as authigenic minerals or as replacements of pre-existing minerals. Therefore, their isotopic values would not be expected to reflect seawater $\delta^{13}C$ fluctuations. Instead they probably reflect variable components

of seawater bicarbonate and oxidized organic matter.

2. Perry and Tan (1973) and Perry et al (1973) observed that iron-carbonate rich rocks from the Biwabik Iron Formation that contain little or no magnetite have $\delta^{13}C$ values between -1.1 and -4.6 °/oo. On the other hand, magnetite rich samples vary from -6.2 to -17.5 °/oo. They proposed that iron was initially precipitated as siderite and ferric hydroxides along with variable amounts of organic material. During diagenesis or low grade metamorphism, reactions involving the reduction of ferric iron and the oxidation of organic matter produced isotopically light CO_2 and dissolved ferrous iron. This CO_2 either exchanged with primary siderite, which initially had a marine $\delta^{13}C$ near 0 °/oo, or formed authigenic siderite or ankerite. Ferrous iron also reacted with ferric hydroxide to form magnetite, resulting in the apparent correlation between isotopic depletion and magnetite content.

Isotopic exchange proceeds via a process of dissolution and reprecipitation, whereby an unstable phase is converted to a more stable phase. As discussed earlier, $\delta^{13}C$ values usually are not significantly altered during diagenetic exchange reactions. Most siderite shows well preserved primary textures suggesting that precipitation started at or above the sediment/water interface and continued during very early diagenesis. Siderite that has been moderately recrystallized has values within the same range as siderite that has retained primary textures. Therefore it is unlikely that isotopic exchange caused the shift to lighter isotopic ratios in unmetamorphosed rocks. It is more likely that siderite precipitation began in a water column which had a $\delta^{13}C$ value near 0 °/oo. Below the sediment/water interface, oxidation of organic matter ($\sim$ -25 °/oo) shifted dissolved bicarbonate $\delta^{13}C$ to lighter values (e.g. Figure 39). The continued precipitation of siderite during very early diagenesis produced the range of values between 0 and -6 °/oo. On the other hand, siderite that has been significantly recrystallized during metamorphism has values between about -6 and -10 °/oo. These are most likely a result of isotopic exchange or decarbonation reactions

during metamorphism.

The petrographic evidence indicates that ankerite and calcite formed as authigenic minerals, by the dissolution of siderite and reprecipitation as ankerite or calcite, and by the replacement of other preexisting minerals. The $\delta^{13}C$ of these carbonate minerals will depend on the relative proportion of bicarbonate derived from the oxidation of organic matter ($\sim$-25 o/oo) and the dissolution of primary carbonate minerals ($\sim$0 to -6 o/oo). The $\delta^{13}C$ values for ankerite and calcite significantly overlap those of siderite (Figures 16, 17 & 18). If ankerite and calcite were precipitated from pore fluids containing a large component of oxidized organic matter, then these minerals should have $\delta^{13}C$ values much lighter than the siderite values. Instead, it is more likely that the $\delta^{13}C$ value of pore fluids during later diagenesis was buffered by the dissolution of primary carbonate.

3. Baur et al (1985) analyzed the distribution of carbon and oxygen isotope ratios in carbonate minerals from individual laminae of microbands from iron-formations within the Hammersley Group. They found a marked alternation in both carbon and oxygen isotope ratios between individual laminae and that depletions in ^{13}C and ^{18}O appear to correlate with increased concentrations of iron. They proposed that a seasonal upsurge of photosynthesis provided enough free oxygen to the water column to precipitate iron as a hydrated oxide. A result of this process was that inputs to the sediment of organic material and ferric iron were correlated.

Baur et al (1985) consider the source of dissolved ferrous iron to be upwelling of deep, iron-rich ocean waters (e.g. Holland, 1973) and, therefore, the depositional basin must have been open to the ocean reservoir of bicarbonate. For this reason they suggest that the carbonate formed in a sediment zone that was at least partly closed to marine bicarbonate, since $\delta^{13}C$ values are too light to have been precipitated from seawater having a value near 0 o/oo. They propose that the source of the light carbonate was the bacterial oxidation of organic matter below anoxic bottom waters

(e.g. Figure 37). The reduction of ferric iron and sulphate were probably the most important redox processes. Although fermentation may also have provided light CO_2, the lack of isotopically heavy carbonate is taken as evidence that methanogenesis, which usually accompanies fermentation, did not take place (Baur et al, 1985). This interpretation is basically the same as the previous one (Perry and Tan, 1973) except for two points: 1) bacteria are responsible for the oxidation of organic matter and 2) precipitation of primary siderite from seawater was not important.

The Gunflint Formation differs from the Hammersley iron-formations in that $\delta^{13}C$ values overlap typical marine values ($\sim$ 0 o/oo), whereas $\delta^{13}C$ from the Hammersley basin has values near -10 o/oo. If iron was initially precipitated as ferric hydroxides and was subsequently reduced in the sediment during organic matter oxidation, as suggested by Baur et al (1985), then $\delta^{13}C$ values would be expected to be much lighter than those observed for the Gunflint. As discussed above, it is more likely that seawater was the most important source of bicarbonate for siderite. Bacteria were probably responsible for oxidizing organic matter during early diagenesis, as was suggested by Baur et al (1985), which contributed isotopically light bicarbonate.

It is generally accepted that iron-formations formed in anoxic waters which contained elevated concentrations (up to 20 ppm) of dissolved ferrous iron (Ewers, 1983). In such environments, the oxidation of organic matter by sulphate reduction, and also by iron reduction if ferric hydroxides were forming in the water column, begins at or just above the sediment/water interface (Figure 31). In the water column, the light CO_2 resulting from organic carbon oxidation would tend to be diluted by the oceanic reservoir of bicarbonate, although a small shift of $\delta^{13}C$ to lighter values in bottom waters would be expected. Therefore, the $\delta^{13}C$ of the water column, and also carbonate precipitated from it, should be close to 0 o/oo. In modern organic-rich sediments, calcite is the first carbonate mineral to form (Figure 39) because of the

very low concentration of dissolved Fe^{2+} in seawater. Any Fe^{2+} produced in the sulphate reduction zone would be incorporated in sulfides. Therefore, siderite normally forms below the sulphate reduction zone where it does not have to compete with H_2S for iron. However, iron-formations formed from seawater that contained elevated concentrations of dissolved Fe^{2+}, and low concentrations of dissolved sulphate (discussed in Chapter 5.4 and 5.5), which allowed siderite to form early.

Below the sediment/water interface, the $\delta^{13}C$ of dissolved bicarbonate in pore waters will be shifted to lighter values (as light as ~-25 °/oo) as organic carbon becomes oxidized, reaching a minimum at the base of the sulphate reduction zone (Figure 39). Siderite precipitated during diagenesis, i.e. as coatings on microspheres and as fine-grained rhombs, will have a similar isotopic value to that of the pore waters. Because of the fine-grained nature of these rocks, isotopic values are for whole rock analyses. Therefore the range of $\delta^{13}C$ values for siderite between 0 and -6 °/oo reflects the variable proportions of siderite precipitated from seawater and from pore waters. Siderite precipitation would eventually produce a decrease in the iron concentration of pore waters, which would result in later carbonate phases becoming less iron-rich. This is consistent with the observed paragenetic sequence.

Once the available sulphate and ferric iron have been exhausted, fermentation reactions would be the dominant process of organic matter oxidation, which is usually accompanied by methanogenesis. The $\delta^{13}C$ of carbonates in the Gunflint Formation do not have values that are enriched in ^{13}C by the amount indicated by Irwin et al (1977) to be typical of this zone (i.e. ~ +15 °/oo). However, Gautier and Claypool (1984) consider values between -5 and +5 °/oo to be more typical, due to some balance between fermentation and carbonate reduction. In this case it is probably not possible to distinguish any contribution from this process based on whole rock analyses. Thermocatalytic reactions become the dominant process of organic matter oxidation above about 75 °C. The CO_2 produced in this way is similar to the organic

matter remaining in the rock, which is usually slightly heavier than the initial value of ~ -25 °/oo. Ankerite and calcite in metamorphosed rocks, which have $\delta^{13}C$ values between -20 and -6 °/oo, probably formed this way. Hydrocarbons also become mobile at these temperatures allowing the migration into more porous zones and hence the precipitation of depleted carbonate minerals in rocks that may not have originally contained organic material. Decarbonation reactions during metamorphism also shift values of carbonates to lighter values.

In summary, siderite precipitation began in the water column and is reflected by $\delta^{13}C$ values near 0 °/oo. During early diagenesis, bacterial oxidation of organic matter contributed isotopically light bicarbonate to the pore fluids. Continued precipitation of siderite from these ^{13}C depleted pore waters produced the range of values between 0 and -6 °/oo in unmetamorphosed rocks. Dolomite in the Upper Limestone Member formed during very early diagenesis from pore waters dominated by seawater bicarbonate. Ankerite and calcite formed during early to late diagenesis either as authigenic minerals or as replacements of earlier formed minerals, including siderite. The overlap of their isotopic values with siderite indicate that the $\delta^{13}C$ composition of the pore waters during later diagenesis was buffered by dissolution of primary carbonate. During metamorphism, isotopic exchange and decarbonation reactions shifted $\delta^{13}C$ to values between -20 and -6 °/oo.

5.2. OXYGEN ISOTOPES

Oxygen isotope ratios in carbonate minerals is mainly a function of the mineral-water fractionation factor, the temperature and the $\delta^{18}O$ of the water mass from which it precipitates. Table 1 lists the various fractionation factors available for carbonate minerals. Under equilibrium conditions at 25°C, calcite is enriched in ^{18}O

by about 28 °/oo relative to seawater. Several fractionation factors, which have been determined by a variety of investigators using a variety of techniques, are available for dolomite (Table 1). Depending on the fractionation factor used, dolomite is about 3 to 6 °/oo more enriched in ^{18}O than calcite. No experimentally determined fractionation factor is available for ankerite or siderite. Dutton and Land (1985) use a fractionation factor that assumes ankerite to be about 3 °/oo heavier than calcite. A fractionation factor calculated by Becker and Clayton (1972) for siderite gives values about 1.5 °/oo heavier than calcite at 25 °C.

The oxygen isotope composition of present day ocean water is relatively uniform with $\delta\,^{18}O$ values between -1.0 and +0.5 °/oo (SMOW) with a mean value close to 0.0 °/oo (SMOW). Larger variations occur under special circumstances. At high altitudes glacial meltwater depletes near-shore ocean water in ^{18}O. Evaporation of restricted seas in arid regions, such as the Mediterranean or Red Seas, causes an enrichment of ^{18}O, whereas other restricted seas, such as the Baltic and Black Seas, are depleted in ^{18}O due to the contribution of meteoric run off (Anderson and Arthur, 1983).

Analyses of carbonates, cherts, phosphorites, and glauconites from marine sediments of different ages have revealed an apparent decrease in the mineral $\delta\,^{18}O$ with increasing geologic age. Degens and Epstein (1962) and Keith and Weber (1964) proposed that carbonate rocks and cherts had undergone progressive isotopic exchange with meteoric waters since their deposition, causing a time-dependent depletion in ^{18}O. Perry and Tan (1972), Perry et al (1978) and Veizer et al (1982) suggested that seawater has become progressively more enriched in ^{18}O towards the present, due to cycling of seawater through the mantle. Knauth and Epstein (1976), Knauth and Lowe (1978) and Karuh & Epstein (1986) propose that the lighter isotopic values indicate that the temperature of seawater was higher in the past and that the $\delta\,^{18}O$ of the oceans has remained constant. Regardless of which of the above interpretations is correct, the best preserved marine carbonates from the late Archean

Table 1. $\delta^{18}O$ isotopic fractionation factors for various carbonate minerals. Equations are in the form: $10^3 \ln\alpha_{mineral\text{-}water} = A\,(10^6 T^{-2}) + B$

Mineral	A	B	Reference
Calcite	2.78	-2.89	Freidman & O'Neil, 1977
Calcite	2.78	-3.39	O'Neil et al, 1969
Dolomite	3.20	-1.50	Northrup & Clayton, 1966
Dolomite	3.34	-3.34	O'Neil & Epstein, 1966
Dolomite	3.23	-3.29	Shepard & Schwarcz, 1970
Dolomite	2.78	+0.11	Fritz & Smith, 1970
Dolomite	3.14	-2.00	Land, 1983
Ankerite	2.78	+0.32	Dutton & Land (1985)
Siderite	2.89	-2.84	Becker & Clayton, 1972

and early Proterozoic have $\delta^{18}O$ values of about -5 °/oo (PDB) for dolomite and -7 °/oo (PDB) for calcite (Veizer et al, 1989, 1990).

Most fresh waters show a wide but systematic variation in $\delta^{18}O$ from 0 to -50 °/oo (SMOW) that displays a geographically-controlled distribution (Craig and Gordon, 1965). This is a result of evaporation and condensation cycles in which ^{18}O is concentrated in the condensed phase. Evaporation of seawater, which occurs mostly in tropical regions, concentrates ^{16}O in the vapor phase. The loss of some of this vapor as precipitation causes the residual vapor to become more depleted in the heavy isotope. Continuous condensation from atmospheric water vapor results in precipitation that becomes progressively more depleted in ^{18}O with increasing latitude.

During burial, primary carbonate minerals can undergo isotopic exchange with pore waters at higher temperatures. Assuming closed-system conditions, exchange at increasing temperatures causes a shift to lighter $\delta^{18}O$ values in carbonates and a corresponding shift to heavier values of the pore water. Diagenetic reactions, such as the alteration of volcaniclastic grains and the precipitation of ^{18}O-rich minerals (i.e. carbonate, chert and clay minerals) results in a shift of the pore water $\delta^{18}O$ to more negative values. The influx of meteoric water will also shift the pore water $\delta^{18}O$ to lighter values.

Precambrian iron-formations can potentially provide a great deal of information regarding paleotemperatures and the $\delta^{18}O$ history of the oceans. Most such studies have employed the use of quartz-magnetite pairs (i.e. Becker and Clayton, 1976; Perry et al, 1973; Perry, 1983; Gregory, 1986). The validity of these studies is dependent on the assumption that these systems have behaved as closed systems during their post-depositional history.

Becker and Clayton (1976) report analyses of siderite and ankerite from the Brockman Iron Formation that have a uniform range of $\delta^{18}O$ values between -10.6

and -9.6 °/oo for siderite and between -11.5 and -10.6 °/oo (PDB) for ankerite. They concluded that these carbonate minerals came to almost complete isotopic equilibrium with a metamorphic fluid. They estimated a temperature of metamorphism between about 270 to 310 °C using quartz-magnetite and quartz-siderite $\delta^{18}O$ pairs.

The $\delta^{18}O$ values of unmetamorphosed rocks from the Gunflint Formation are used to construct a set of curves (Figure 40) representing pore water $\delta^{18}O$ versus temperature, calculated using the minimum and maximum $\delta^{18}O$ of each carbonate phase. These curves are similar to those used by Longstaffe (1987) in studies of the fluid history of sedimentary basins. The fractionation factors used in constructing these curves are from O'Neil et al (1969) for calcite, Dutton and Land (1985) for ankerite, and Becker and Clayton (1976) for siderite.

If a $\delta^{18}O$ of 0 °/oo (SMOW) is assumed for seawater then the temperature of initial precipitation is about 45 °C, using the maximum siderite and calcite $\delta^{18}O$ value, and possibly as high as 65 °C using the maximum ankerite value (Table 2). Because siderite is a primary mineral, whereas ankerite and calcite formed during diagenesis, siderite should give a better estimate of depositional conditions (point A, Figure 40). On the other hand if it is assumed that the seawater had a temperature of 20 °C then the calculated $\delta^{18}O$ value of seawater is -5.5 °/oo (SMOW) using the maximum siderite $\delta^{18}O$ value (point A', Figure 40). The arc joining A and A' represent intermediate values of temperature and $\delta^{18}O$. A maximum burial temperature of about 115 °C has been estimated for the Gunflint Formation by Miyano (1987). If the minimum siderite $\delta^{18}O$ value represents siderite that came to complete isotopic equilibrium at this temperature, this would correspond to point B' on the curve corresponding to the minimum siderite value. Since exchange under conditions of increasing temperature would have increased the $\delta^{18}O$ value of the pore water from its initial value, this would constrain the maximum $\delta^{18}O$ of seawater

Figure 40. Plot of calculated $\delta^{18}O$ values of water versus temperature. Mineral-water fractionation curves were plotted for siderite (solid lines), ankerite (dashed lines), and calcite (dotted lines) from unmetamorphosed rocks using their maximum (upper set of curves) and minimum (lower curves) values. Point A corresponds to water temperature assuming seawater $\delta^{18}O$ = 0 ‰ (SMOW). Point A' corresponds to $\delta^{18}O$ of seawater assuming a temperature of 20 °C. Using the maximum burial temperature of 115 °C (point B') constrains the maximum seawater $\delta^{18}O$ value to -1.5 ‰ at a temperature of about 40 °C (point B), assuming closed system conditions. Arrow is one possible pathway for the evolution of the pore water $\delta^{18}O$.

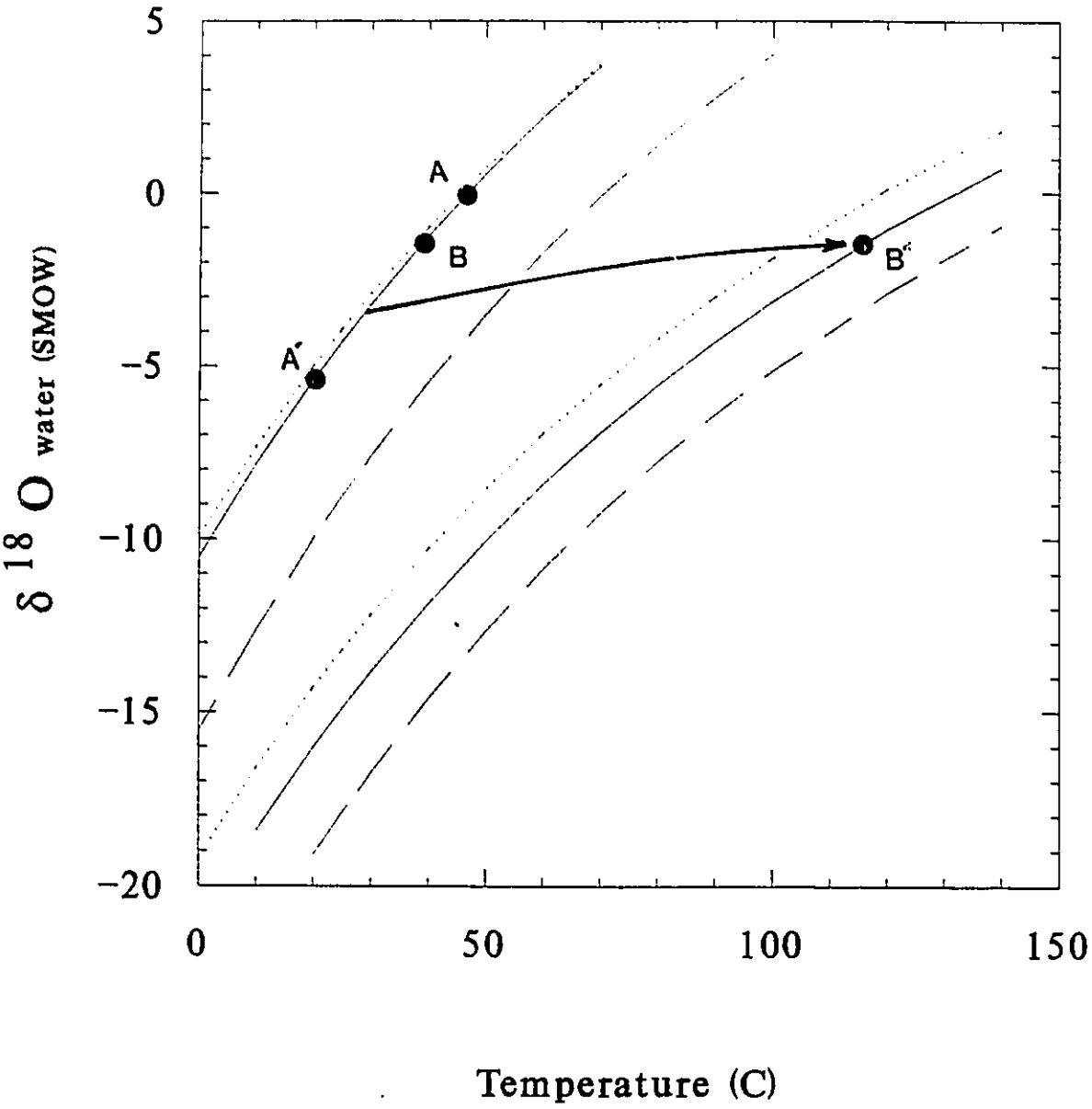
5
0
−5
−10
−15
−20
0
50
100
150
A
B
A'
B'
δ 18 O water (SMOW)
Temperature (C)

Table 2. Calculated $\delta^{18}O$ and temperature ranges for the Gunflint Formation.

1. Assuming $\delta^{18}O$ of seawater = 0 °/oo (SMOW):

	Initial T	Burial T
siderite	46 °C	132 °C
ankerite	65	155
calcite	45	119

2. Assuming a seawater temperature of 20 °C

	^{18}O water	Burial T
siderite	-5.5 °/oo (SMOW)	80 °C
ankerite	-8.0	74
calcite	-5.0	74

3. Using maximum burial T = 115 °C to calculate upper limit of seawater $\delta^{18}O$

	$\delta^{18}O$	T
siderite	-1.5 °/oo (SMOW)	38°C
ankerite	-3.5	50
calcite	-0.5	42

to some value less than -1.5 ‰ (SMOW) and a temperature less than about 38 °C (point B, Figure 40). If exchange ceased at a lower temperature, then the $\delta^{18}O$ value would be correspondingly lighter. If siderite was a primary precipitate from seawater, and closed-system conditions are assumed, then the seawater $\delta^{18}O$ value would be constrained between -5.5 and -1.5 ‰ (SMOW). A possible pathway for the evolution of pore water $\delta^{18}O$ is represented by the arrow in Figure 40.

Perry and Tan (1973) suggested that the light $\delta^{18}O$ was a result of oxidation-reduction reactions during diagenesis and metamorphism which produced shifts of oxygen from hematite, which is depleted in ^{18}O relative to seawater, to carbonate. Baur et al (1985) also noted that light $\delta^{18}O$ correlates with both $\delta^{13}C$ and with iron content. They also suggest that these values were the result of incorporation of oxygen initially bound in ferric hydroxide.

To my knowledge there is no fractionation factor for ferric hydroxide, but if it is similar to the factor for magnetite then the ferric hydroxide $\delta^{18}O$ value will be about 5 ‰ lighter than the water from which it precipitated (Becker and Clayton, 1976). Water produced by the reduction of ferric hydroxide would be at most 5 ‰ lighter than the pore waters. Because of the small difference in $\delta^{18}O$ values and the insignificant amount of H_2O produced by iron reduction relative to the pore water reservoir, it is unlikely that iron reduction could cause a significant shift in the $\delta^{18}O$ of the pore water.

Other reactions can also cause pore waters to shift to lighter values. The precipitation of significant quantities of ^{18}O-rich minerals, such as carbonates, chert and clay minerals, will cause the residual pore water to shift to lighter values. Alteration of volcanic grains (~6 to 8 ‰) to clay minerals will also cause a depletion of ^{18}O in pore waters. It is difficult to evaluate the effect of these diagenetic reactions on pore waters but shifts in $\delta^{18}O$ would probably be less than 4 ‰ (Longstaffe, 1987 and references therein) and would not account for the 13 ‰

range of $\delta^{18}O$ values in unmetamophosed rocks.

Gregory (1986) proposes that most iron-formations have suffered open-system exchange events during early diagenesis or during metamorphism. He has shown that if quartz and magnetite initially precipitated from seawater similar in temperature and isotopic composition to the present day ocean, isotopic exchange during diagenesis with meteoric water having an $\delta^{18}O$ value as light as -10 °/oo could produce the isotopic data observed in iron-formations. Carbonate minerals would have been even more susceptible to isotopic exchange.

Knauth and Epstein (1976) report a δD of -73 °/oo and a $\delta^{18}O$ of 23.6 °/oo (SMOW) for a sample of chert from the Gunflint Formation, which may indicate a component of meteoric water. The shallow water setting and proximity to a shoreline indicate that meteoric water could have had access to these sediments. If an external fluid was introduced to these sediments then no unique interpretation of surface temperature or water $\delta^{18}O$ composition is possible.

The $\delta^{18}O$ values from metamorphosed rocks are more uniform in composition and generally lighter than values from unmetamorphosed rocks. These are most likely a result of isotopic exchange reactions during metamorphism.

In summary, if closed system conditions prevailed then the isotopic value and temperature of the seawater is constrained between -5.5 and -1.5 °/o (SMOW) at 20 and 42 °C respectively. The range of $\delta^{18}O$ values of 13 °/oo represent partial to complete equilibration of isotopic values during burial. However, the large range of $\delta^{18}O$ values may have also been caused by the introduction of ^{18}O depleted meteoric water during early diagenesis. During metamorphism, $\delta^{18}O$ values probably re-equilibrated at higher temperatures.

5.3. SULPHUR/CARBON RATIOS

The abundance of organic carbon and sulfide sulphur in sediments is dependent on the timing, rate, and intensity of aerobic oxidation and sulphate reduction during early diagenesis. Because early diagenetic processes are often dependent on depositional environments, plots of sulphur and carbon (S/C) ratios can provide important environmental information.

In nature, sulphur-reducing bacteria are the principal agents that cause the reduction of sulphate at near-surface temperatures. These bacteria exist only in anoxic environments where they use sulphate as an electron acceptor during anaerobic respiration. This bacterially mediated reaction is commonly written as equation 1:

$$2R(CH_2O) + SO_4^{-2} = H_2S + 2HCO_3^- + 2R \qquad (1)$$

where RCH_2O is a simplified formula for the more complex organic compounds which are metabolized by sulphate reducing bacteria and R is the residual organic matter not metabolized but preserved in the sediment as organic carbon. The H_2S produced by sulphate reduction will either: 1) escape from the sediment into the overlying seawater, 2) become oxidized by O_2, ferric iron, or sulfide-oxidizing bacteria (i.e. to form S^o), 3) react with organic matter to form organic sulphur compounds, or 4) react with ferrous iron to form acid-soluble iron sulfides (i.e. hydrous troilite, mackinawite, greigite). Pyrite would eventually form by the reaction of S^o with acid-soluble iron sulfide (Goldhaber and Kaplan, 1974; Berner, 1970, 1984; Raiswell and Berner, 1985).

In normal marine sediments the amount of pyrite sulphur is strongly dependent on: 1) the rate of sulphate supply to the sediment, 2) the abundance of reactive iron to fix the H_2S as iron sulfide, and 3) the availability of organic matter that can be readily metabolized by sulphate-reducing bacteria (Berner, 1984). Sulphate is usually not a

limiting factor because bioturbation of the sediment allows a continuous supply of sulphate to depths of a few tens of centimeters. The degree of pyritization (DOP = wt % pyrite-iron / wt % pyrite-Fe + wt % Fe soluble in HCl) of normal marine sediments is usually much less than 1, which indicates that iron is not usually a limiting factor (Raiswell and Berner, 1985). Organic matter is usually the limiting factor in pyrite formation because only the most reactable organic carbon can be metabolized by these bacteria.

A positive correlation between pyrite-sulphur and residual organic carbon, which defines a line passing through the origin, is typical of normal marine sediments (Berner, 1970, 1984; Raiswell and Berner, 1985, 1986; Leventhal, 1983, 1987) (Figure 41A). The accumulation of much pyrite is not favoured in slowly deposited, aerobic sediments because a large fraction of the metabolizable organic matter will be lost by oxidation. Sulphate reduction rates will also be lowered, which would lead to low S/C ratios. On the other hand higher S/C ratios are predicted for rapidly deposited sediments, which contain less degraded organic matter, because sulphate reduction rates would be increased and a greater fraction of organic matter will become metabolized. The S/C ratios of normal marine sediments average about 0.36 ± 0.3 (Figure 41A).

In fresh waters, which typically contain very low sulphate concentrations, only minor amounts of sulfide can form and S/C ratios average about 0.03 (Berner, 1984) (Figure 41C). If the amount of reactive iron in sediments is low, such as in Fe-poor carbonates, S/C ratios will be low because only a small portion of the available H_2S will form pyrite. The remainder of the H_2S will either escape from the sediment or form organic sulphur compounds.

Plots of S/C ratios from euxinic sediments differ from normal marine sediments because sulphate reduction and formation of pyrite may start in the water column and because larger quantities of metabolizable organic matter will be available. As a result

Figure 41. Sulphur-carbon characteristics of sediments formed in various environments. A) The average S/C ratio for modern normal marine sediments is 0.37, but has varied from a minimum of 0.07 for Permian sediments to a maximum value of 0.73 Devonian sediments (Berner, 1985). B) S/C ratios for euxinic sediments from Raiswell and Berner (1985). Line 1, from the Lower Jurassic Posidonia shales, represents sedimentary deposition of sulfide without addition diagenetic sulfide (pyrite formation limited by availability of iron). Line 2, from the Black Sea sediments, represents the addition of C-limited diagenetic sulfide to an earlier Fe-limited syngenetic pyrite. Line 3, from the Lower Jurassic Jet Rock shales, represent the coupled deposition of iron and organic carbon. C) Fresh water sediments, which contain very low sulphate concentrations, have very low S/C ratios (Berner, 1984). D) Sediment-hosted ore deposits often contain sulfide-sulphur contents in excess of 30 %, but contain organic carbon contents of less than 1 %, indicating that sulfide deposition did not take place by simple biogenic reduction of seawater sulph e during diagenesis of the host sediments (Ohmoto et al, 1990).

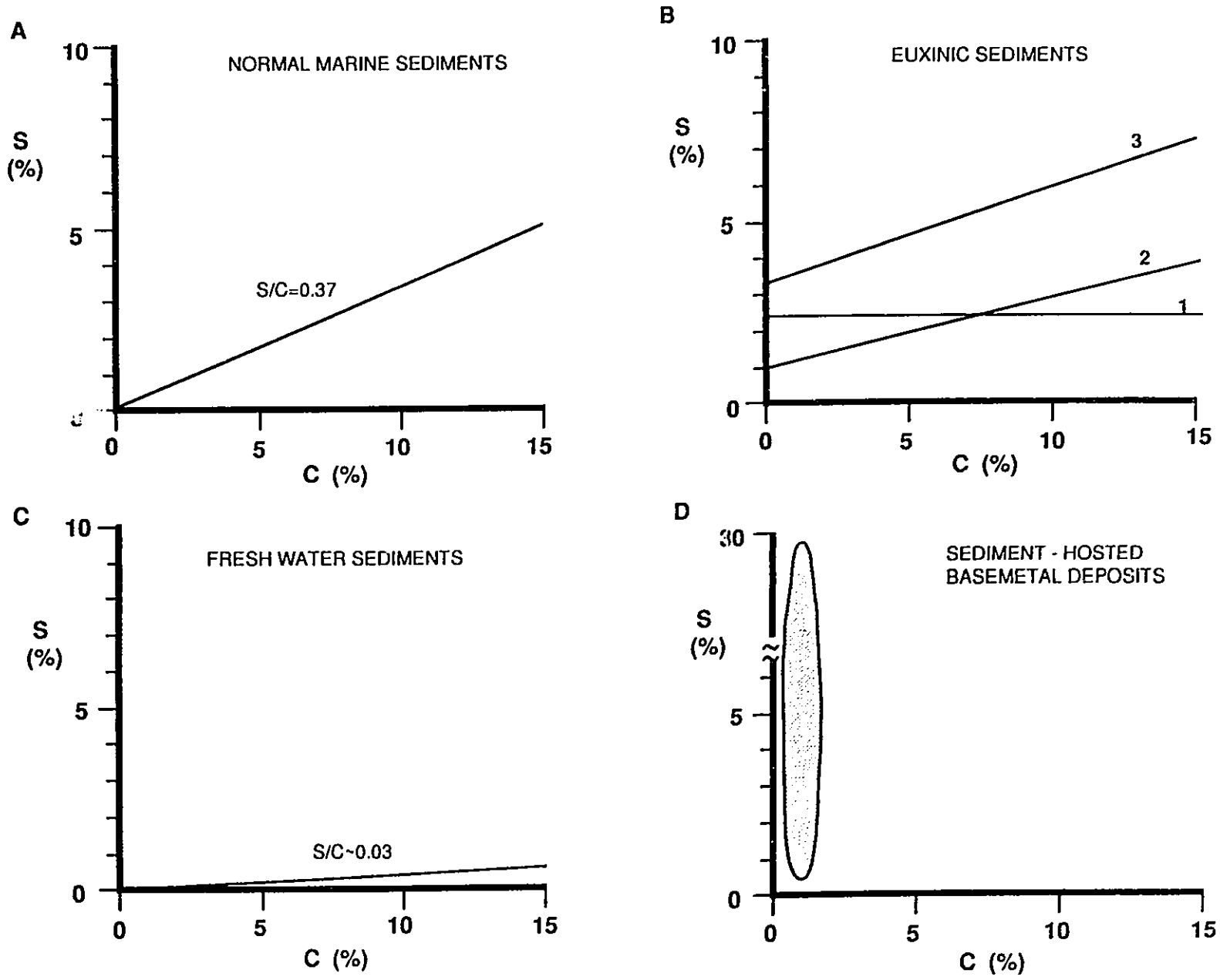
A
NORMAL MARINE SEDIMENTS
S (%)
10
5
0
S/C=0.37
0
5
10
15
C (%)
B
EUXINIC SEDIMENTS
S (%)
10
5
0
3
2
1
0
5
10
15
C (%)
C
FRESH WATER SEDIMENTS
S (%)
10
5
0
S/C~0.03
0
5
10
15
C (%)
D
SEDIMENT - HOSTED
BASEMETAL DEPOSITS
S (%)
30
5
0
0
5
10
15
C (%)

S/C ratios are usually higher and more variable (Figure 41B). Raiswell and Berner (1985) have recognized three types of S/C/Fe relationships in euxinic sediments:

1) High, relatively constant S contents with variable C contents result when all of the pyrite is syngenetic and pyrite formation is limited by the supply of iron.

2) S and C and DOP values are all positively correlated and S/C correlation line intersects the S axis at positive values. This results from the addition of C-limited diagenetic pyrite to an earlier, Fe-limited syngenetic pyrite. The amount of syngenetic pyrite is represented by the intercept with the S axis.

3) S and C contents are positively correlated but DOP values are consistently high and independent of S and C contents. The amount of pyrite in these shales was limited by Fe rather than C and the apparent positive correlations between S and C and between S and Fe content are due to coupled deposition of iron and organic carbon.

Many sediment-hosted ore deposits have an organic carbon content less than 1 % but sulfide-sulphur contents in excess of 10 % (Ohmoto et al, 1990) (Figure 41D), which suggests that the accumulation of sulfides in these deposits did not take place by simple biogenic reduction of seawater sulphate during early diagenesis of the host sediments.

The Gunflint Formation was deposited under euxinic conditions in which abundant, easily metabolizable organic matter would be predicted. This is supported by organic carbon contents that range up to about 7 % and light $\delta^{13}C$ values in carbonates. Because the only organisms existing at this time were bacteria and simple algae, virtually all of the organic matter would be easily metabolized, thus organic matter probably was not the limiting factor in pyrite formation. In Phanerozoic anoxic marine environments that are open to the oceanic reservoir of sulphate, the availability of abundant organic matter would lead to enhanced sulphate reduction. The amount of pyrite-sulphur formed under these conditions would be limited by the

availability of dissolved Fe^{2+}, or some other metal. If Fe^{2+} concentrations are high, as is proposed for iron-formations, potentially very large quantities of sulfide could be formed. However, most black shales of the Gunflint Formation have pyrite-sulphur contents less than about 1 % and low S/C ratios (Figure 35). This suggests that the limiting factor in pyrite formation was the availability of sulphate.

The rate of sulphate reduction is not limited by sulphate where concentrations are greater than about 5 mM (Berner, 1984). Modern seawater has a sulphate concentration of about 28 mM (Holland, 1978) and fresh waters may have concentrations several hundred fold less than this. Therefore, in fresh waters sulphate is the limiting factor in pyrite formation and pyrite-sulphur contents are usually less than a few tenths of a per cent. Sulphate concentrations of the Precambrian oceans are not known. During the Archean (> 2.5 Ga) sulphate concentrations are thought to have been much lower than the present (< < 1mM) such that bacterial sulphate reduction was either absent or insignificant (e.g. Lambert et al, 1978). Sulphate concentrations started to become significant either during the late Archean (e.g. Goodwin et al, 1976) or the early Proterozoic by about 2.3 Ga (e.g. Cameron, 1982). Within the ~ 1.9 Ga Gunflint Formation depositional basin, sulphate concentrations were greater than 1mM but may have been less than 5 mM.

The black shales of the Gunflint Formation show a positive correlation of sulphur and carbon (Figure 35 & 36), consistent with a biogenic origin for these sulfides. For shales other than in the lower 20 m in the Kakabeka Falls area, the intercept of the regression line with the S axis may indicate that some of the sulfide formed above the sediment/water interface. This is consistent with the presence of sulfide layers and laminae in these shales. These may have formed during periods of low sedimentation which allowed the slow accumulation of sulfide. Higher rates of sedimentation would have resulted in lower pyrite contents because there would have been less time for sulphate reduction.

Black shales from the lower 20 m of the Gunflint Formation in the Kakabeka Falls area have higher sulphur contents and S/C ratios than elsewhere in the formation (Figure 36). One sample, which contains coarse-grained pyrite that pseudomorphs siderite rhombs, has a sulphur content of 18 % with a carbon content of only 2 %. The enhanced sulphur contents reflect the presence of coarse grained pyrite. Amounts of fine grained pyrite in these shales do not differ significantly from other areas. When pyrite concretions are considered, sulphur contents of these shales may exceed 30 %, which is not consistent with simple biogenic reduction of seawater sulphate. Brecciated rocks underlying these shales contain coarse grained discordant pyrite, are associated with possible synsedimentary faults, and have a similar range of $\delta^{34}S$ values as the concretions and coarse grained pyrite in the shale. This suggests that sulphur may have been introduced to the sediments along this fault before the shales had become significantly compacted.

5.4. SULPHUR ISOTOPES

Most sulfide minerals in sedimentary rocks formed as a result of the reduction of dissolved sulphate. Sulphate can be reduced at low temperature by sulphate-reducing bacteria or at high temperature by thermochemical reactions.

The factors that control the isotopic composition of sulfide during bacterial sulphate reduction are: 1) the $\delta^{34}S$ value of seawater sulphate, which may be influenced by the open or closed nature of the basin, 2) kinetic isotope effects, and 3) the open or closed nature of the sediment system with respect to sulphate (Ohmoto et al, 1990). Dissolved sulphate in the present day ocean has a uniform isotopic composition of +20.0 ‰. The $\delta^{34}S$ value of the ancient ocean, as recorded by the isotopic composition of marine evaporites, has fluctuated between +10 and +35 ‰ during the Phanerozoic (Claypool et al, 1980). Because of the scarcity of Precambrian

sulphates, the $\delta^{34}S$ composition of the oceans before about 900 my ago are not well constrained.

Many workers consider the small spread of $\delta^{34}S$ values near 0 ‰ for Archean sedimentary sulfides and sulphates, as well as the rarity of these sulphates, to indicate either very low sulphate concentrations in Archean oceans ($<$ 1 mM compared to present value of 28 mM) or else that sulphate reducing bacteria had yet to develop (e.g. Goodwin et al, 1976; Lambert et al, 1978; Donnelly et al, 1977; Skyring and Donnelly, 1982; Cameron, 1982; Hattori et al, 1983). There is some disagreement among these workers concerning the time when isotopic fractionation became a significant sedimentary process, i.e. when sulphate concentrations began to increase in the Precambrian oceans, with ages bracketed between about 2.7 Ga (Goodwin et al, 1976; Ripley and Nicol, 1981) and 2.3 Ga (Cameron, 1982, 1983). Alternatively, it has been proposed that both appreciable levels of sulphate ($>$ 1mM) and sulphate-reducing bacteria have existed since the early Archean (Ohmoto and Felder, 1987).

The $\delta^{34}S$ of dissolved sulphur in meteoric water has no unique composition because it is acquired during oxidation of sulfides in rocks, dissolution of sulphate minerals, or solution of biogenic or abiogenic gases, all of which have widely varying compositions. Brackish waters will have essentially the same $\delta^{34}S$ value as the ocean because the fresh water component of sulphate in brackish waters is negligible relative to seawater.

During sulphate reduction, variations in the $\delta^{34}S$ of the H_2S can result from both equilibrium and kinetic isotope effects. Under equilibrium conditions at 25 °C, H_2S is depleted in ^{34}S by 75 ‰ relative to sulphate, however it would take about 10 billion years to achieve equilibrium (Ohmoto and Lasaga, 1982). Therefore kinetic isotope effects predominate at surface temperatures. The kinetic isotope effect accompanying reduction of sulphate to H_2S ranges from about -75 to 0 ‰. On the

other hand the isotope effect associated with the formation of pyrite from H_2S is usually negligible, thus the pyrite $\delta^{34}S$ closely approximates that of the H_2S.

The most common sulphate-reducing bacteria in marine and brackish environments are of the anaerobic genus Desulfovibrio. The reduction of sulphate proceeds by a series of complex reactions which can be summarized in four principal steps: 1) uptake of external sulphate by the cell, 2) sulphate activation by ATP (adenosine triphosphate) to form APS (adenylyl sulphate), 3) enzymatic reduction of APS to sulphite, and 4) reduction of sulfite to sulfide (summarized in Kaplan, 1983; Holser et al, 1988). Each of these steps imparts a kinetic isotope effect of varying magnitude. The magnitude of the total isotope effect, which is the sum of each of these steps, will vary depending on which of the steps is dominant or rate limiting. The isotope effect associated with each of these steps is not completely understood but it is generally accepted that fractionation inherent to steps 1 and 2 are on the order of a few per mill (Holser et al, 1988). Values suggested for step 3 are -25 (Rees, 1973) and -10 to -15 ^{o}/oo (Chambers & Trudinger, 1979) whereas the effect for step 4 may range anywhere between 0 and -33 ^{o}/oo (Holser et al, 1988).

Under experimental conditions with unlimited sulphate, the fractionation factor for sulphate reduction was found to be generally inversely proportional to the rate of reduction, with the largest fractionation occurring at the slowest reduction rates (Harrison and Thode, 1958; Kaplan and Rittenberg, 1964; Kemp and Thode, 1968;). The rate of reduction depends on bacterial species, types and concentrations of electron donors (i.e. nutrients for bacteria), and temperature. Harrison and Thode (1958) also found that the kinetic isotope effect decreased, as sulphate concentrations were decreased, from about -15 ^{o}/oo at concentrations greater than 10 mM, to -4 ^{o}/oo at 0.6 mM, and to +3 ^{o}/oo at 0.01 mM, at a temperature of 30 ^{o}C. This indicates that at sulphate concentrations less than about 1 mM, the small fractionation associated with step 1 becomes rate limiting. In modern marine sediments the $\delta^{34}S$ of sulfides

mostly fall within the range of -25 ± 20 °/oo (Ohmoto et al, 1990 and references cited therein). The kinetic effect of 45 ± 20 °/oo indicates that steps 3 and 4 are rate limiting in normal marine sediments.

The distribution of sulfide $\delta^{34}S$ in a particular stratigraphic unit is influenced by the open or closed nature of the system with respect to H_2S or SO_4. Systems are considered to be open to H_2S if the sediments do not have iron or other elements to fix H_2S and are open to SO_4 if the rate of sulphate supply is faster than the rate of sulphate reduction. Systems are closed to SO_4 if the rate of sulphate supply is much slower than the rate of bacterial reduction of sulphate. Sulfides formed in systems open to sulphate tend to have narrow $\delta^{34}S$ ranges, typically less than 10 °/oo, i.e. H_2S in bottom waters of the Black Sea (Figure 42). Sulfides formed in systems closed to sulphate tend to show wider δ^{34} ranges (typically between 10 and 20 °/oo) (Ohmoto et al, 1990) with a skew towards less positive $\delta^{34}S$ values, i.e. sulfides in sediments of the Black Sea (Figure 42).

In normal marine environments most of the seafloor is oxygenated. Because sulphate-reducing bacteria are anaerobic, they can only live below the sediment/water interface. Maximum sulphate reduction typically takes place a few centimeters below the surface, probably because easily metabolizable organic matter is still abundant after aerobic bacteria have consumed available oxygen. Sulphate concentrations can remain the same as the overlying seawater to depths of about 20 cm because of bioturbation (Figure 43). If reactive iron is available then H_2S will be removed as iron-sulfide, either as pyrite or more likely an iron monosulfide precursor. Approximately 50 % of the pyrite-sulphur formed in a stratigraphic column will be formed in this zone (Ohmoto et al, 1990). This fraction of pyrite formed essentially in a system open to sulphate.

Below the bioturbation zone sulphate supply is by diffusion and concentrations in pore waters decrease with depth so that sulphate reduction rates exceed rate of

Figure 42. Pyrite-sulphur content versus $\delta^{34}S$ of sediments and H_2S in waters of the Black Sea. Fields are defined by samples from sediments overlain by anoxic water and by samples from sediments overlain by oxygenated water (i.e. <200 m water depth) (modified from Ohmoto et al, 1990).

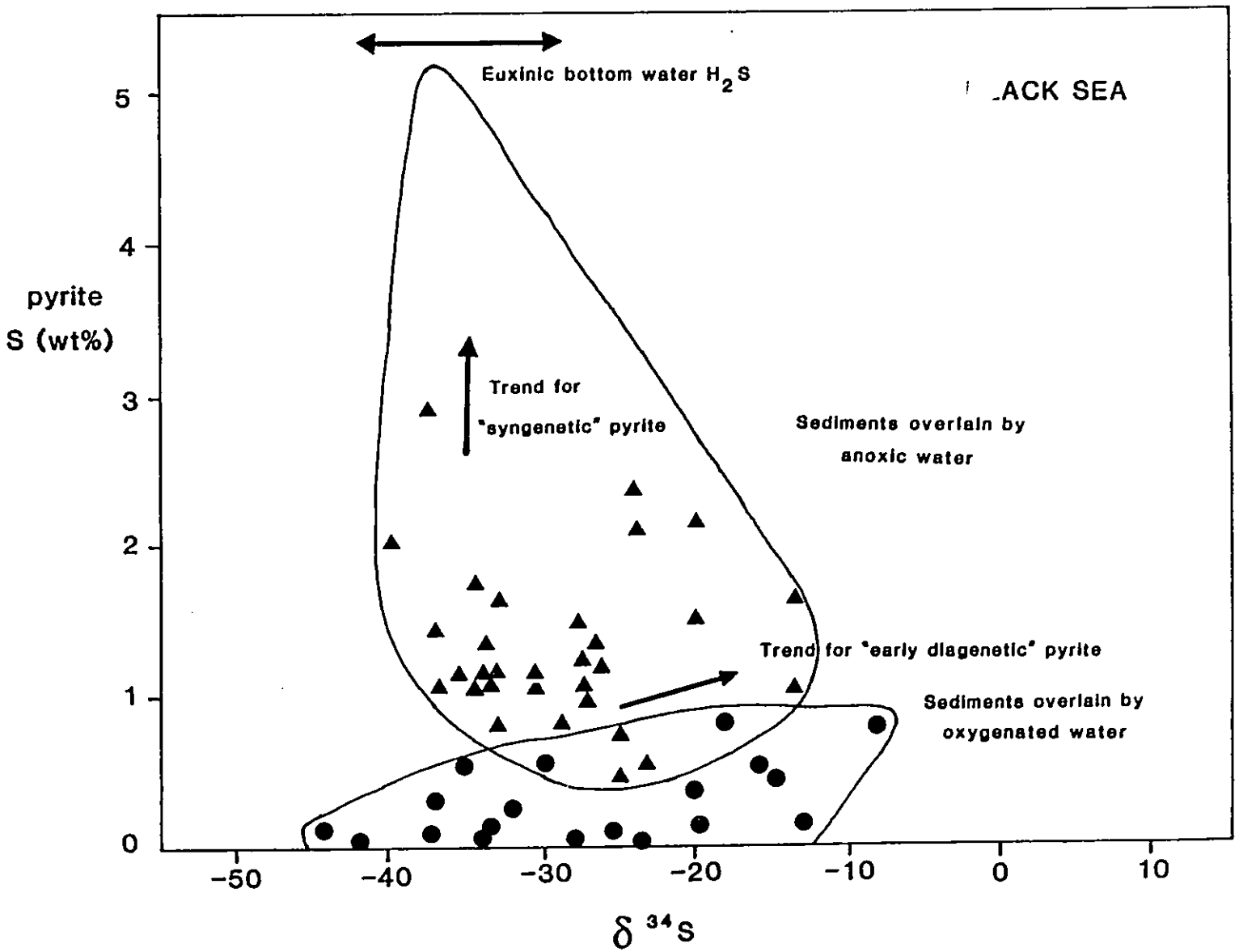
Euxinic bottom water H_2S
BLACK SEA
Trend for "syngenetic" pyrite
Sediments overlain by anoxic water
Trend for "early diagenetic" pyrite
Sediments overlain by oxygenated water
pyrite S (wt%)
0
1
2
3
4
5
-50
-40
-30
-20
-10
0
10
$\delta^{34}S$

sulphate supply (Figure 43), i.e., system becomes more closed with respect to sulphate. Continuous reduction of sulphate causes the $\delta^{34}S$ value of the residual sulphate, as well as the H_2S produced later, to increase rapidly with depth (i.e., Raleigh fractionation) often by as much as 50 °/oo. However, the increase in the $\delta^{34}S$ value of pyrite is typically only around 7 °/oo. This is because pyrite records the cumulative addition of sulfide from an open system to a progressively more closed system. About 50 % of the total amount of pyrite in a sedimentary section would have formed under open system conditions. Only a relatively small fraction of the total pyrite was formed from the heaviest H_2S, since these pore waters contained only a very small amount of sulphate.

In euxinic basins sulphate reduction may take place above the sediment/water interface. For example, in the Black Sea the concentration of H_2S increases with depth, below a water depth of about 200 m (Figure 44). The variation in $\delta^{34}S$ values of this H_2S are usually less than a few °/oo within individual sites, but overall values vary between -40 and -30 °/oo. Syngenetic pyrite will have a similar range of values. Sulphate concentrations remain relatively constant throughout the water column indicating the system is open to sulphate, at least for short time intervals. If sulphate supply to the basin is restricted then continued reduction could lead to progressively heavier $\delta^{34}S$ values of the sulphate with time. Thus over longer periods of time the basin could be considered closed with respect to sulphate.

Because bioturbation is absent in anoxic environments, the system is closed with respect to sulphate below the sediment/water interface and the $\delta^{34}S$ of the H_2S, as well as the pyrite formed from it, increases rapidly (Figure 44). Pyrite in the Black Sea sediments underlying anoxic waters have $\delta^{34}S$ values between about -40 and -15 °/oo, which represents a mixture of syngenetic and diagenetic pyrite.

Seawater sulphate may also be reduced abiologically at high temperatures either during deep burial in sedimentary basins or during the convective circulation of

Figure 43. Idealized profile of normal marine sediment, illustrating pore-water chemistry (H_2S and sulphate content and rate of sulphate reduction), pyrite content, and $\delta^{34}S$ of pyrite and pore-fluid H_2S and sulphate. Sulphate reduction begins near the base of the aerobic zone. The rate of sulphate reduction increases to a maximum in the bioturbation zone and then decreases with depth as the concentration of H_2S in pore fluids increases. The rate of sulphate supply is constant throughout the aerobic and bioturbation zones. Approximately 50 % of the total pyrite-sulphur formed in a stratigraphic column will be formed within the top 20 cm of the sediment. The $\delta^{34}S$ of this pyrite will be depleted in ^{34}S by about 50 °/oo relative to sulphate. Below the bioturbation zone, sulphate supply is by diffusion and sulphate reduction rates exceed sulphate supply, causing a decrease in the concentration of sulphate with depth. Continued reduction causes the $\delta^{34}S$ value of both the residual sulphate and the H_2S to increase with depth, often by as much as 50 °/oo. However, the $\delta^{34}S$ value of the total pyrite increases only by about 7 °/oo, because the amount of sulfide formed with depth becomes progressively smaller as sulphate concentrations diminish. Essentially no sulfide is formed below about 200 cm. (modified from Ohmoto, et al, 1989)

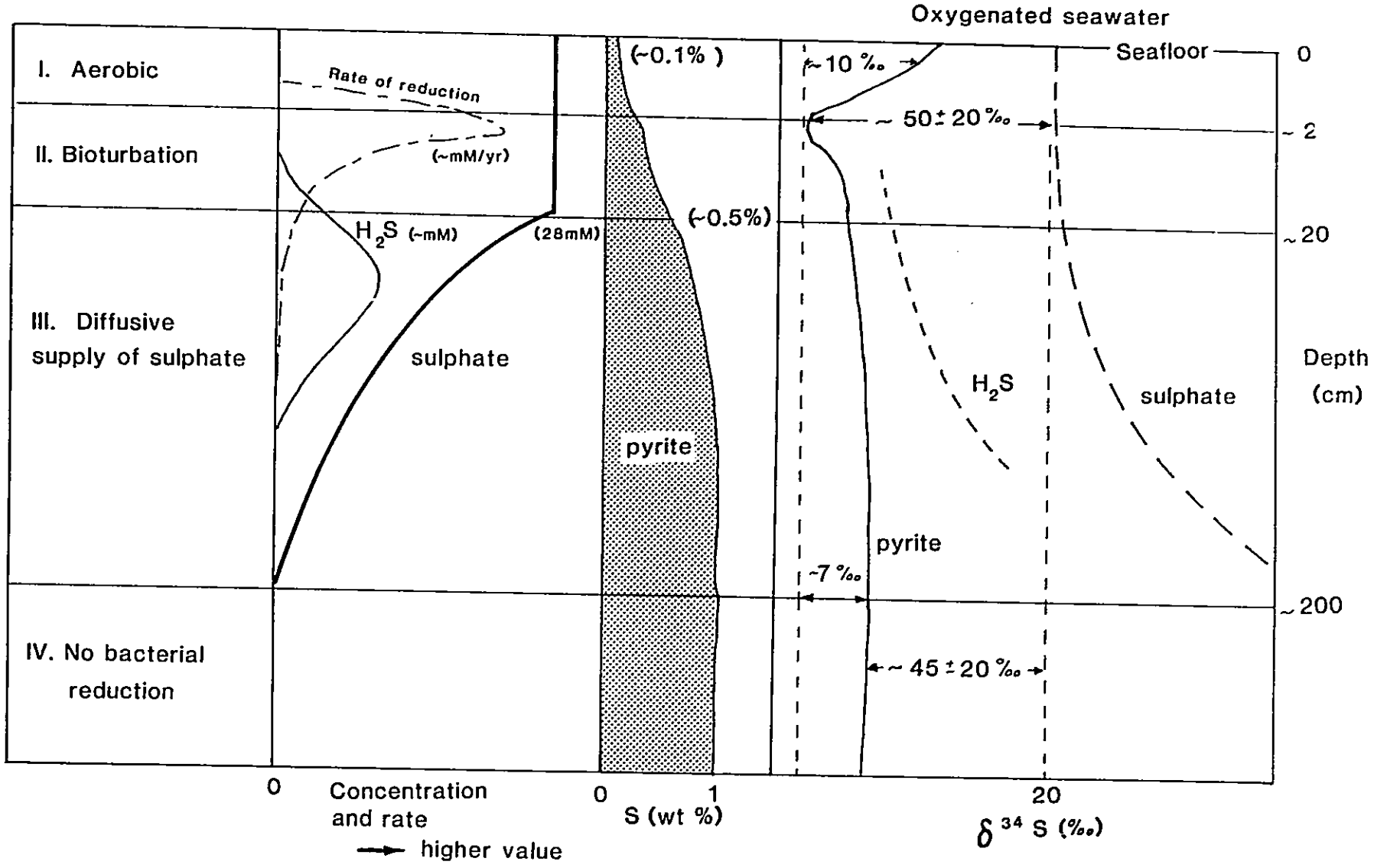
Oxygenated seawater
I. Aerobic
II. Bioturbation
III. Diffusive supply of sulphate
IV. No bacterial reduction
Rate of reduction
(~mM/yr)
H_2S (~mM)
(28mM)
sulphate
(~0.1%)
(~0.5%)
pyrite
~10 ‰
~ 50 ± 20 ‰
Seafloor
0
~ 2
~ 20
~ 200
Depth (cm)
H_2S
sulphate
pyrite
~7 ‰
~ 45 ± 20 ‰
0
Concentration and rate
higher value
0
1
S (wt %)
20
δ^{34} S (‰)

Figure 44. Idealized profile of euxinic water-column and underlying marine sediment, illustrating water chemistry (H_2S and sulphate content) and $\delta^{34}S$ composition of pyrite and pore fluid H_2S and sulphate (based on the Black Sea). H_2S concentrations in the water column increase with depth below about 200 m (the 2 curves represent two separate locations), whereas sulphate concentrations remain relatively constant. The $\delta^{34}S$ value of the H_2S is relatively constant and is depleted in ^{34}S by 50 to 60 °/oo, relative to sulphate. Below the sediment/water interface, the supply of sulphate is restricted and sulphate concentrations decrease rapidly. The $\delta^{34}S$ of the H_2S and residual sulphate increase rapidly with depth. The $\delta^{34}S$ of the total pyrite formed in these sediments varies between -40 and -15 °/oo, and represents a mixture of syngenetic and diagenetic pyrite.

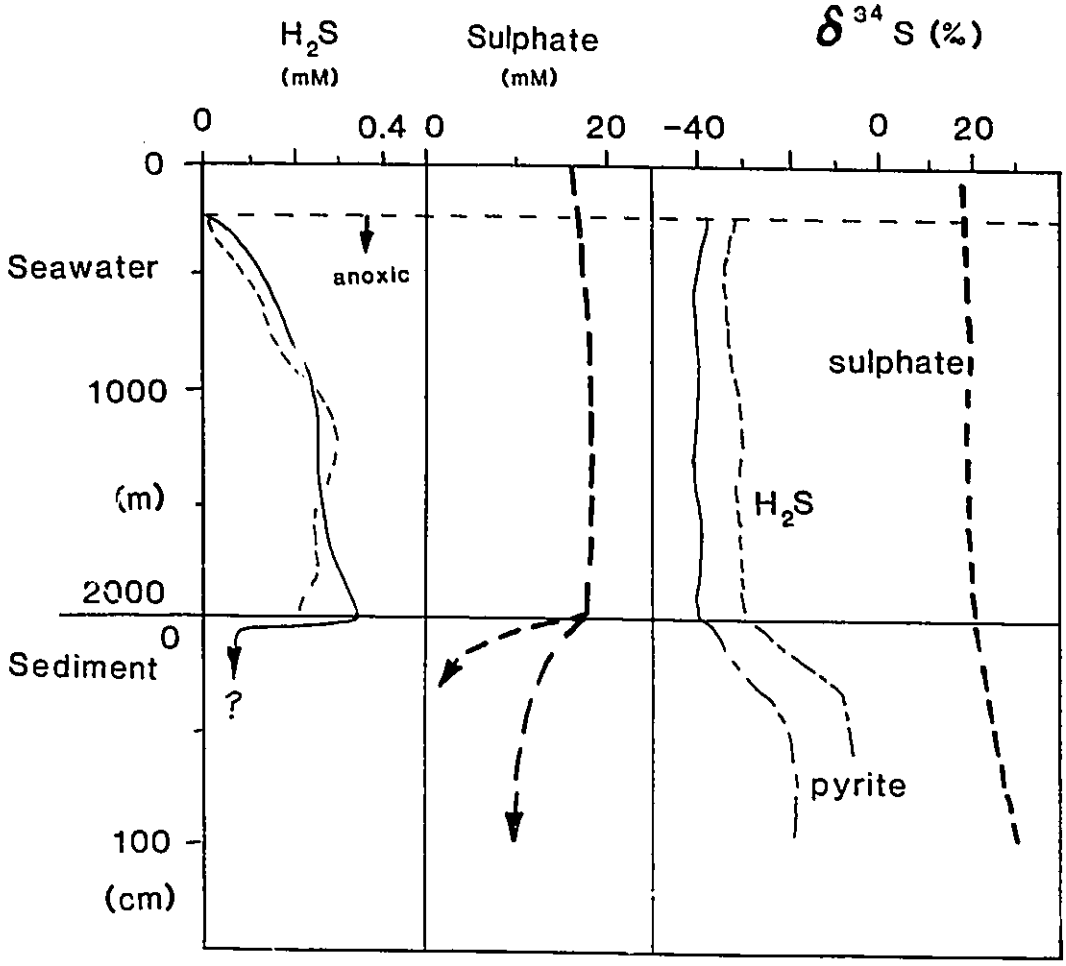
H2S
(mM)
Sulphate
(mM)
δ 34 S (‰)
0
0.4
0
20
-40
0
20
0
Seawater
anoxic
1000
(m)
2000
sulphate
H2S
0
Sediment
?
pyrite
100
(cm)

seawater through fracture systems in ocean floor basalts. Hydrothermal fluids may transport dissolved H_2S and metals from their source regions to the seafloor where they can form massive sulfide deposits.

Seawater sulphate is commonly retained in sediments as gypsum or anhydrite. Part of this sulphate may be converted to H_2S during burial by reaction with ferrous iron, organic carbon, or H_2 at high temperatures. The isotopic composition of the H_2S will be the same as the original sulphate. Hydrolysis of sedimentary pyrite at elevated temperatures will also produce H_2S, which will retain the isotopic signature of the pyrite. Some workers suggest that the H_2S in these hydrothermal fluids is the source of sulphur for sediment-hosted massive sulfide deposits (i.e., Ohmoto et al, 1990). Others (i.e., Goodfellow and Jonasson, 1984) suggest that the H_2S was derived from sulphate-reduction in anoxic bottom waters. These sulfide deposits have a wide range of $\delta^{34}S$ values (Gustafson and Williams, 1981; Ohmoto et al, 1990), which probably indicates a variety of sulphur sources for these deposits.

The sulphur in volcanogenic massive sulfide deposits of Proterozoic age and younger, typically have a narrow range of $\delta^{34}S$ values between igneous sulfide values ($\sim$0 $^{o}/_{oo}$) and coeval seawater values (Franklin et al, 1981). This has been taken to indicate that a major portion of the sulfide was derived from the high temperature reduction of seawater sulphate (Kajiwara, 1971; Kajiwara and Date, 1971). In seawater-basalt experiments (Mottl et al, 1979; Shanks et al, 1981; Sakai et al, 1980) sulphate was readily reduced by ferrous iron minerals at temperatures greater than about 350 ^{o}C. The reduction mechanism appears complex, involving mineral-dissolution and rock-sulfidation reactions. From these experiments it is inferred that the reduced sulphur in the hydrothermal fluids was in part reduced seawater sulphate and in part sulfide extracted from the host rock. Volcanogenic massive sulfide deposits of Archean age have $\delta^{34}S$ values close to 0 $^{o}/_{oo}$ (Franklin et al, 1981). This has been taken as evidence that the hydrothermal fluids contain only a

minor component of reduced sulphate and that the oceans contained low concentrations of sulphate (Cameron & Hattori, 1987).

Archean iron-formations are usually associated with volcanic sequences and are considered by many to be genetically related (i.e. James, 1966; Gross, 1965, 1983). Many have a narrow range of $\delta^{34}S$ values near 0 ‰, which has been taken as evidence for a mantle origin of sulphur, either by dissolution of pyrite from volcanic rocks by hydrothermal solutions or from juvenile magmatic fluids (Monster et al, 1979; Fripp et al, 1979). On the other hand the relatively wide range of $\delta^{34}S$ values for late Archean iron-formations in the southern Canadian Shield has been interpreted to indicate that at least some of the sulfide was derived by the bacterial reduction of seawater sulphate (Thode and Goodwin, 1983; Goodwin et al, 1976, 1985; Crocket et al, 1983; Lavigne and Crocket, 1982) implying significant concentrations of sulphate in the ocean at this time. A minor component of biogenic sulfides has been identified in Phanerozoic volcanogenic massive sulfide deposits (Rye et al, 1984; Eastoe et al, 1986). Alternatively, the sulfides having a wide range of $\delta^{34}S$ values were formed by hydrothermal fluids undergoing changing redox conditions (Skyring & Donnelly, 1982; Cameron & Hattori, 1987).

Relatively few sulphur isotope studies of Proterozoic iron-formations have been carried out. There is a difference of opinion as to whether the source of sulphur in Proterozoic iron-formations is biogenic or hydrothermal. Cameron (1983) analyzed sulfides from seven early Proterozoic iron-formations (including the Gunflint Formation), ranging in age from about 2.5 to 1.9 Ga. He reported that the means of the $\delta^{34}S$ values from each iron-formation ranged between -4.9 and +6.6 ‰ and that the sample variance is low within each unit. Cameron (1983) considers these isotope ratios to be more typical of hydrothermal-exhalative mineral deposits than normal, sedimentary sulfides of biogenic origin. He also indicates that these hydrothermal fluids also supplied the iron for these deposits.

However, because of the very low solubility of iron sulfide, only vanishingly small amounts of H_2S would be present in the oceans if they contained the amount of iron required to form iron-formations (Holland, 1973, 1984; Drever, 1974; Skyring and Donnelly, 1982; Walker and Brimblecombe, 1985). Cameron (1983) points out that in stratified basins, such as the Black Sea (Brewer and Spencer, 1974) and Saanich Inlet (Jacobs and Emerson, 1982), iron is most soluble in the weakly sulfidic waters just below the oxygen zero boundary. He proposes that iron could be transported within this zone to oxygenated shelves where it would be precipitated as oxide facies iron-formation. Sulfide facies would be precipitated in the deeper anoxic portion of the basin.

The simplified stratigraphy predicted by this model is contradicted by the geological evidence. The iron-formations in the Lake Superior region have been deposited in a wide range of environments from deep basinal settings associated with volcanic rocks to the intertidal zone of a shallow shelf. Sulfide-rich rocks are interlayered with other rock types in all of these iron-formations, indicating that the simple depth related facies model of James (1954), i.e. the transition from sulfide facies to oxide facies, is not generally valid.

In the Black Sea concentrations of dissolved iron in the transition zone are as high as 0.05 ppm (50 μg/kg), whereas concentrations above and below this zone are held to below 0.01 ppm by the low solubility of iron oxides and iron sulfides respectively. The concentration of iron required to precipitate iron-formations is uncertain and estimates range from 1.0 ppm (Holland, 1984, page 397), to 20 ppm (Ewers, 1983), and even as high as 100-400 ppm (Mel'nik, 1982). The concentration of iron at saturation with respect to siderite and calcite, assuming Ca concentrations similar to modern values, is about 3 ppm (Holland, 1984, page 388). Even using the conservative estimates, the concentration of iron in the transition zone of the Black Sea would have to be increased 20 to 400 times to supply the amount required to form

iron-formations. Iron concentrations could be increased substantially if H_2S was removed from the water column by precipitation as metal sulfides near the hydrothermal vents i.e. as massive sulfide deposits. However, this would eliminate hydrothermal activity as a source of sulphur for iron-formations. Thus hydrothermal activity may have been the source of either iron or sulphur for Lake Superior type iron-formations, but not both.

In Chapter 4 it was shown that, with the exception of the lower 20 m in the Kakabeka Falls area, $\delta^{34}S$ values of sulfides in the Gunflint Formation have a narrow range between +5 and +12 °/oo (Figure 30). This is a similar range to the "synsedimentary sulfides" of Shegelski (1985), which he interpreted to have formed from bacterial reduction of seawater sulphate from an open reservoir. It was shown in the previous section that the S/C ratios from black shales are consistent with a biogenic origin for pyrite. Mixing of biogenically-produced H_2S in an anoxic water column can lead to relatively uniform sulfide $\delta^{34}S$ values. However, in a system open to sulphate the fractionation effect will be large. For example H_2S in the water column of the Black Sea have $\delta^{34}S$ values between -40 and -30 °/oo (Figure 42). Pyrite formed from this H_2S will have similar isotope ratios. Thus open system sulphate reduction in the water column is not consistent with the observed values for the Gunflint Formation unless unrealistically heavy sulphate $\delta^{34}S$ values are invoked (i.e. ~ +50 to +60 °/oo).

Within anoxic sediments, diagenetic sulphate reduction becomes closed to sulphate and $\delta^{34}S$ values of H_2S increase rapidly with continued reduction (Figure 44). The Black Sea sediments contain a large component of synsedimentary pyrite and a smaller component of diagenetic sulfide resulting in highly variable $\delta^{34}S$ values (-40 to -15 °/oo, Figure 42) for total sedimentary pyrite. Thus the Black Sea is probably a poor analogue for the Gunflint Formation. In Saanich Inlet, the water column undergoes intermittent stagnation leading to the production of free H_2S in bottom

waters for only a few months of the year (Nissenbaum et al, 1972). Therefore, synsedimentary sulfide would only be a minor component of total sedimentary pyrite. Sedimentation rates here are very high, thus this system would be expected to approximate closed system sulphate reduction. Within the sediment, sulphate concentrations are rapidly depleted, due to biogenic sulphate reduction, and the H_2S has $\delta^{34}S$ values between +4 and +18 °/oo. Sulphate in the overlying water column has a concentration and $\delta^{34}S$ value similar to normal marine values (28 mM and +20 °/oo respectively). No analyses of iron sulfides were available but if the fraction of synsedimentary sulfide is minor, the $\delta^{34}S$ of total sedimentary pyrite will be similar to the values for the H_2S. If sulphate is quantitatively reduced the final value will be similar to the original sulphate. Thus biogenic sulfides formed in a closed system can have a narrow range of positive values similar to that expected for hydrothermal sulfides.

Based on the above examples the narrow range of $\delta^{34}S$ values around +8 °/oo for sulfides in the Gunflint Formation are better explained by closed system rather than open system biogenic-reduction of seawater sulphate. If sulphate concentrations were comparable to modern values (~28 mM), the water column would have to be dysaerobic, rather than anaerobic, otherwise open system sulphate reduction would take place in the water column. Because burrowing organisms did not exist at this time, supply of sulphate to the sediment would be by diffusion. If the rate of reduction was greater than the supply of sulphate, the fraction of sulphate reduced would be large and the $\delta^{34}S$ value of the total pyrite would approach that of the sulphate. However, because sedimentation rates were probably very low, the sulphate reduction zone would begin at the sediment/water interface, which is consistent with observed laminae and layers of sulfide, and so sulphate in the upper layers of sediment would have had time to exchange with sulphate in the water column. Therefore the system would still be at least partially open to sulphate and some variation in $\delta^{34}S$ values

would be expected.

If the concentration of dissolved sulphate were significantly lower than modern values, the kinetic isotope effect would be smaller (Harrison and Thode, 1958). The $\delta^{34}S$ value of seawater during Gunflint time is not known and so the magnitude of the isotope effect can not be determined. If the seawater value was the same as the present (20 ‰) then the isotope effect would be about 12 ‰, based on the average pyrite value of 8 ‰. This would be consistent with a sulphate concentration less than about 10 mM (~ 1/3 of the present day value) based on Harrison and Thode's (1958) experimental data. At very low sulphate concentrations, sulphate reduction would exceed sulphate supply, which would approximate closed system reduction and lead to pyrite $\delta^{34}S$ values approaching that of sulphate. During periods of very slow sedimentation, sulfide laminae and layers could accumulate. Higher rates of sedimentation would lead to low contents of disseminated pyrite. This is consistent with the elemental concentrations of pyrite-sulphur and organic carbon, discussed in the last section, which indicate that sulphate was the limiting factor in sulphate reduction.

In summary, there are three possible origins for the fine-grained pyrite: 1) hydrothermal sulfide, 2) biogenic pyrite formed under dysaerobic conditions in a closed or nearly closed system within the sediment, and 3) biogenic sulfide formed under anaerobic conditions in which sulphate concentrations were significantly lower than the present. The first option is not consistent with the high concentrations of dissolved iron required to form iron-formation. Option 3 is favoured over option 2 by the elemental ratios of pyrite-sulphur and organic carbon and also by the $\delta^{34}S$ values in the overlying Rove Formation.

Disseminated pyrite in the Rove Formation has $\delta^{34}S$ values between +13 to +21 ‰. It was indicated in Chapter 2 that the Gunflint Formation may have been deposited in a foredeep, which had restricted communication with the open ocean and

hence was partially closed to the oceanic supply of sulphate over long intervals of time. Goodfellow and Jonasson (1984) have suggested that secular trends of the $\delta^{34}S$ in pyrite and barite from the Selwyn Basin was a result of the oscillation from open to closed conditions. Periods of restriction and stratification of the water column led to heavier $\delta^{34}S$ values, which persisted until opening of the basin reestablished normal marine conditions. The gradual increase in the $\delta^{34}S$ of the Animikie Basin, in which the Gunflint and Rove Formations were deposited, are consistent with a closed system in which the $\delta^{34}S$ of the dissolved sulphate increased with time.

Pyrite textures and isotopic ratios from the lower 20 m of the Gunflint Formation in the Kakabeka Falls area are complex (Figure 32). Coarse-grained, discordant pyrite in brecciated arenite and banded chert-carbonate have $\delta^{34}S$ values between -18 and +22 ‰. The wide range of values indicates that they were formed by biogenic sulphate reduction. However, textural evidence indicates they were formed later than the fine-grained disseminated pyrite found throughout the formation. If these were formed by the reduction of residual sulphate in pore waters it would be expected that amounts would be smaller and isotope ratios heavier compared to fine-grained pyrite. An external source of sulphur is more likely. The coarse-grained pyrite is found in brecciated rocks associated with a possible synsedimentary fault. The most likely source of this sulphur is from fluids moving upward along this fault. The origin of this fluid is speculative. It may be related to tectonic activity associated with volcanic activity in the area or may be related to dewatering of shales during compaction in the deeper part of the basin.

The black shales overlying the brecciated rocks contain fine-grained and coarse-grained pyrite as well as elliptical pyrite concretions. The coarse-grained pyrite in the black shale overgrow fine-grained pyrite and displays textures indicating it formed during early diagenesis. Shale containing both fine and coarse-grained pyrite have $\delta^{34}S$ values between -2 and +35 ‰ that show an upward trend to heavier

values (Figure 32). These are consistent with biogenic reduction of sulphate in a system that became more closed with time. However, because these two types of pyrite could not be separated it is not certain whether they both formed from continued reduction from seawater sulphate in porewater or each formed from different sources of sulphur.

Pyrite concretions also formed during early diagenesis, but contain inclusions of earlier formed coarse-grained pyrite in their interiors. An unusual feature of these concretions is that the rims have lighter $\delta^{34}S$ values than the earlier formed interiors (Figure 33). In addition, the concretions show an upward trend to lighter values parallel to that observed for the coarse-grained pyrite. These concretions occur in shale directly overlying the brecciated rocks and have a similar range of values, which suggests that they probably had a common source of sulphur. It was suggested above that sulphate was introduced along the fault where it was reduced in the brecciated rocks to form discordant pyrite. Sulphate may have diffused upward through the black shale, which was probably still uncompacted, where it was reduced to sulfide. As the residual sulphate diffused upward it would become progressively heavier as reduction proceeded. An external source of sulphur is consistent with S/C ratios, discussed in the last section.

6. DISCUSSION

Dozens of theories have been advanced to explain the origin of iron-formations, or characteristics of them. Any model for the origin of these deposits, especially the very large Lake Superior-type, must explain: 1) the source of the iron, as well as other constituents such as silica, 2) their transport to the depositional basin, and 3) the mechanism by which the minerals were precipitated. Any model must also take into account the oxidation state of the atmosphere-ocean system at this time.

6.1. OXIDATION STATE OF THE OCEAN-ATMOSPHERE SYSTEM

The concentration of free O_2 in the atmosphere and oceans during the early history of the Earth is a controversial topic. Many researchers (e.g. Cloud, 1972) have maintained that the atmosphere and oceans were essentially anoxic before about 1.9 Ga. This hypothesis is based largely on the apparent need to maintain an anoxic atmosphere in order to transfer large quantities of iron in solution to form the Superior-type iron-formations. The decline in iron-formation abundance after about 2.0 Ga represents a rise in O_2 levels in the atmosphere. At the other extreme, some researchers have proposed that there were no major differences between Archean and modern atmospheric or hydrospheric conditions (e.g. Dimroth and Kimberley, 1976). More recently it has been demonstrated that the atmosphere and surface ocean layers were at least mildly oxidizing prior to 1.9 Ga as a result of oxygen-producing photosynthesis (Walker et al, 1983; Cloud, 1980). The timing of this rise in oxygen levels is placed at about 2.4 Ga by Kasting (1987), although others propose that photosynthesis has been occurring since the early Archean (Holland, 1984; Clemmey and Badham, 1982). Before the development of photosynthesis, the

atmosphere-ocean system would have been anaerobic (Walker et al, 1983; Walker and Drever, 1988; Kasting, 1987).

Walker et al (1983) and Kasting (1987) propose models in which pO_2 increased to progressively higher levels as the rate of supply of reduced substrates to the atmosphere-ocean system declined. Stage I (Figure 45) corresponds to the interval before oxygen-producing photosynthesis had evolved. A small amount of molecular oxygen was produced by photochemical reactions, but was consumed in the atmosphere by a larger source of reduced gases released during volcanism. The composition and oxidation state of the ocean was strongly influenced by hydrothermal circulation with the ocean crust (Fryer et al, 1979; Cameron, 1982; Veizer et al, 1982). The pO_2 of the atmosphere during Stage I was maintained below 10^{-13} atm (5×10^{-12} present atmospheric level) and both the surface and deep ocean were anoxic (Kasting, 1987).

Stage II (Figure 45) began after oxygen-producing photosynthesis had evolved and began producing O_2 at a rate greater than the rate of supply of reduced substrates to the atmosphere (Kasting, 1987; Walker et al, 1983). The atmosphere and surface layer of the ocean became relatively oxidizing; but the deep oceans remained anoxic either because of higher hydrothermal circulation rates through ocean crust, relative to the present ocean (Fryer et al, 1979; Cameron, 1982; Veizer et al, 1982; Veizer, 1983c), or because of a lower primary productivity in the surface ocean (Holland, 1984). As long as the deep ocean remained anoxic, O_2 levels in the atmosphere would have been significantly lower than the modern Earth. The upper limit of pO_2 in stage II is set at 0.03 PAL (present atmospheric level) by Kasting (1987) (Figure 46).

There is some disagreement concerning the time of the transition from stage I to stage II. A minimum age of about 2.4 Ga is based on several lines of evidence: the decreased occurrence of detrital uraninite and the increased occurrence of redbeds

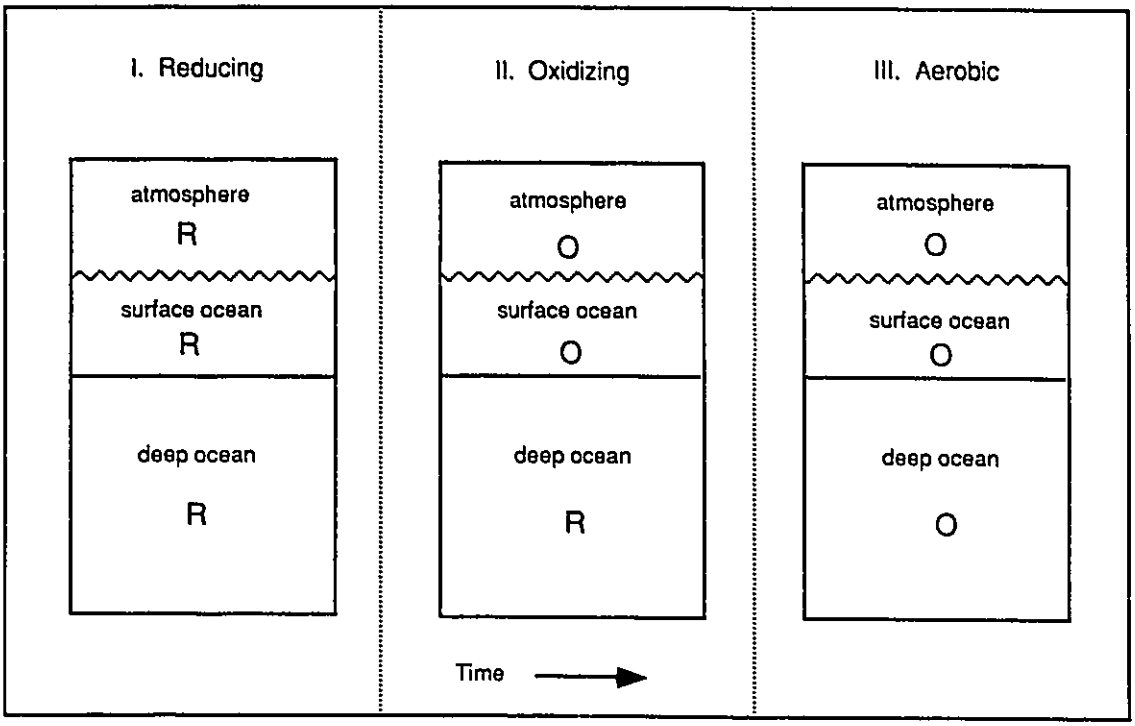

FIGURE 45. Schematic diagram showing the three expected stages in the evolution of atmospheric oxygen. "O" indicates oxidizing conditions; "R" indicates reducing conditions. (modified from Kasting, 1987)

at this time (Kasting 1987); an increase in isotopic fractionation of sedimentary sulfides (Cameron, 1982) implies an increase in sulphate concentrations and hence increased oxygen levels at about this time; and increased oxidation of sulfides in terrestrial detritus also indicate an increase in atmospheric oxygen at this time (Hattori et al, 1983). Holland (1984) argues that survival of uraninite is kinetically possible under O_2 partial pressures of up to $\sim 4 \times 10^{-3}$ bar (0.02 PAL) and that paleosol data show no obvious change in oxidation state between 1.5 and 3.0 Ga ago. He therefore proposes that the atmosphere and surface ocean were mildly oxidizing as far back as the middle Archean.

Stage III (Figure 45) would have developed when the supply of reduced substrates to the deep ocean declined. The pO_2 would then become high enough to support aerobic respiration and O_2 would pervade the entire atmosphere-ocean system (Kasting, 1987; Walker et al, 1983). The transition from stage II to stage III is considered by Kasting (1987) to have coincided with the decline in abundance of iron-formations at about 1.7 Ga. On the other hand, Holland and Beukes (1989) propose a dramatic increase in pO_2, between about 2.2 and 1.9 Ga, based on paleosol data from the Kuruman Iron-formation in South Africa. They indicate that the pO_2 of the atmosphere, during weathering of this iron-formation at about 1.9 Ga, was in excess of 0.05 atm (25 % PAL) compared to a value of 3.3×10^{-5} atm at about 2.2 Ga (Holland and Zbinden, 1988). The $\sim$1.8 Ga Flin Flon paleosol also shows a highly oxidized nature (Holland et al, 1989).

The pCO_2 of the atmosphere is thought to have been much higher during the early history of the Earth than it is today and has declined as pO_2 increased (Walker et al, 1983; Holland, 1984; Kasting, 1987). Because of lower solar luminosity, the Earth's surface temperature would have been below freezing, unless CO_2 concentrations in the Archean were 100 to 1000 times their present level. Figure 46 shows the estimated changes in pCO_2 and pO_2 over geologic time.

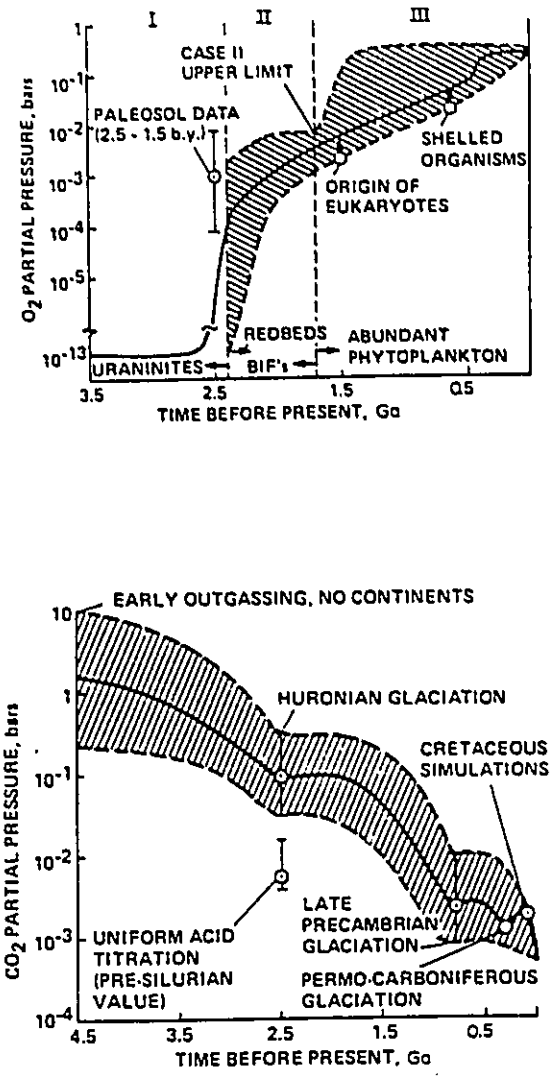

Figure 46. A) Estimated change in pO_2 over geologic time. B) Estimated change in pCO_2 over geologic time. The solid curve is the best guess and the shaded area represents the range of uncertainty (from Kasting, 1987).

In conclusion, at the time of deposition of the Gunflint Formation (~ 1.9 Ga), the atmosphere and surface ocean were oxidizing and atmospheric pO_2 may have been as high as 0.25 PAL. The pCO_2 of the atmosphere at this time is less certain but it was probably significantly higher than modern levels.

6.2. SOURCE OF IRON:

The chemistry of Archean (>2.5 Ga) and Proterozoic (~ 1.8 to 2.5 Ga) iron-formations are similar, although significant variations occur both within and between different formations (Gole and Klein, 1981, Davy, 1983). The major components of iron-formation are silica and iron, having a Fe/Si mole ratio averaging about 0.7 (Garrels, 1987). Carbonate can be a significant component in all facies but is a major component of the carbonate facies (Davy, 1983). Sulfide can be a major component of the sulfide-facies, particularly in Archean iron-formations, but it is normally only a minor constituent. Other elements, notably Al, K, and Na, have low concentrations (James, 1966; Gole and Klein, 1981; Davy, 1983). The composition of these rocks requires that their constituents must have been separated in solution from any geological source (Ewers, 1983).

Iron-formations span a period of time from the earliest known rocks (~ 3.8 Ga) up to about 1.8 Ga. Gole and Klein (1981) have shown that the similarities between Proterozoic and Archean iron-formations are probably more significant than their differences, implying a common source of iron. The great lateral extent of the Proterozoic deposits implies a relatively unrestricted access to a large and constantly replenished reservoir of soluble iron, rather than a local source (Ewers and Morris, 1981). The mean rate of iron precipitation between 2.0 and 2.5 Ga is estimated to be greater than 0.4×10^{12} gm Fe/year (Holland, 1984). However, it is more likely that iron-formations were being formed at different locations and at

different times rather than being continuously precipitated throughout the entire ocean. Therefore, individual iron-formations would have required a greater rate of supply of iron. For example, it is estimated that the Hammersley Basin required a supply of about 2 x 10^{13} gm Fe/year (Holland, 1973, 1984). Estimates of the concentration of dissolved iron required to form iron-formation vary between 1 ppm (Holland, 1984), 20 ppm (Ewers, 1983), 40 ppm (Garrels, 1987), to as high as 100 to 400 ppm (Mel'nik, 1982). The concentration of iron in anoxic seawater saturated with respect to siderite and calcite is about 3 ppm at pH = 7.0 and 30 ppm at pH = 8.0 (Holland, 1973).

Weathering of the continental landmass has been proposed as the principal source of iron (Garrels et al, 1973; Garrels, 1987; Lepp and Goldich, 1964). In this model, iron is liberated by lateritic weathering under an anoxic atmosphere and then transported in surface waters to the depositional basin as dissolved ferrous iron. Holland (1973) estimated that if rivers contained about 7 ppm Fe^{2+} then a flow rate equivalent to about half that of the Amazon River would be required to supply the Hammersley Basin. It is unlikely that sediments that are devoid of terrigenous detritus could have been deposited near the mouth of such a large river. It was concluded early in this chapter that the atmosphere was mildly oxidizing since at least 2.4 Ga. Therefore, significant quantities of iron could only be transported as part of the sediment load not as dissolved iron, making a continental source of iron even more unattractive.

Many iron-formation basins contain iron-poor marine carbonates that occur stratigraphically above and/or below the iron-rich units (Gole and Klein, 1981; Trendall and Morris, 1983). If rivers were supplying dissolved iron to these basins then drastic changes in either their drainage patterns or in the oxidation state of the atmosphere would have to be invoked to explain the alternations between iron-rich and iron-poor chemical sediments. In the Gunflint Formation, the basal stromatolite

facies, which formed on the Archean basement or on a thin conglomerate developed on basement rocks, is generally iron-poor. If surface waters or ground waters were iron-rich then these shallow water sediments would be expected to be iron-rich. Instead, iron becomes significant above this facies in rocks deposited in deeper water. These observations are consistent with a submarine rather than a continental source of iron.

Volcanic activity and hydrothermal solutions have been proposed as a source of iron, particularly for the Archean deposits (Van Hise and Leith, 1911; Goodwin, 1954; Gross, 1980; Cameron, 1983; Simonson, 1985). The Ebeko volcano in the Kurile Islands, an unusually productive volcano, annually releases about 1.8×10^{10} gm of iron (Holland, 1973; Maynard, 1983). About 1000 such volcanos would be required to supply the estimated 2×10^{13} gm Fe/year for the Hammersley Basin. However, there is no indication in the geological record for contemporaneous volcanic activity of this magnitude within this basin. Other iron-formation basins would require fewer volcanos but the number would still be very large.

The circulation of seawater through basalt at mid-ocean ridges can supply significant quantities of dissolved iron to the oceans. Holland (1984), assuming a rate of seawater cycling similar to the modern ocean, calculated that about 2×10^{12} gm Fe/year could have been added this way. However, hydrothermal circulation rates and temperatures would have been higher in the Precambrian (Veizer, 1983c). Derry and Jacobsen (1988) assumed a 10 % increase in temperature and twice the modern hydrothermal water mass flux to calculate an iron flux of 5.4×10^{13} gm Fe/year. This value is more than twice that needed to supply the Hammersley Basin. However, the iron flux will be supplied to the entire Earth's oceans, not just to the Hammersley Basin, so that higher iron concentrations are required or else a mechanism to confine deposition to a restricted area (Morris and Horwitz, 1983). They suggest that iron was derived from concentrated hot spot activity rather than the dispersed ridge

systems of today, and was possibly supplemented by normal continental drainage (e.g. Holland, 1973).

At present the total input of iron to the oceans as part of the sediment load of rivers is estimated to be about 1 x 10^{15} gm Fe/year (Holland, 1984). If weathering rates were faster, because of higher pCO_2 (e.g. Kasting, 1987), or continents smaller (e.g. Veizer, 1983c) this rate would be higher or lower respectively, but this estimate is probably a good approximation. If the ocean below the surface mixed layer was anoxic or dysaerobic then the reduction of a small portion (~2 %) of the ferric iron contained in sediments of the deep ocean could supply the required amount of iron for deposition of iron-formations (Holland, 1973; 1984; Drever, 1974).

Under anoxic conditions, dissolved sulphate would be reduced to sulfide, which would prevent the accumulation of dissolved iron because of the very low solubility of iron sulfide. Holland (1984) proposes that conditions were dysaerobic rather than anoxic. Ferric iron is reduced to ferrous iron during the oxidation of organic matter by dysaerobic bacteria and also by reaction with H_2S formed during sulphate reduction (Froelich et al, 1979). If the oxidation of organic matter did not proceed to the sulphate reduction stage then ferrous iron could migrate upward and accumulate in the overlying water column. Dysaerobic conditions could only be maintained if the supply of organic matter was sufficient to keep O_2 concentrations very low, but not sufficient to reach the sulphate reduction stage. Holland (1984) indicates that biological productivity would have to be about 1 % of the present day rate to maintain these conditions. However, Schidlowski (1982) interprets the carbon isotope record of organic carbon and carbonate rocks to indicate a steady state biomass since at least 3.5 Ga. This is also supported by the distribution of organic carbon and the correlation between sulfide-sulphur and organic-carbon in Archean and early Proterozoic shales, including shales in iron-formations, which are similar to recent shales (this study; Dimroth & Kimberly, 1976; Cameron & Garrels, 1980;

Schidlowski, 1982; Holland, 1984). It was concluded in Chapter 5.5 that pyrite in the Gunflint Formation was a result of bacterial sulphate reduction. Therefore, conditions would have been anoxic rather than dysaerobic.

Drever (1974) proposes that the supply of iron was greater than the supply of sulphate, so that sulfide would be quantitatively removed from the water column, allowing dissolved iron to accumulate to concentrations of several ppm. Dissolved iron would be transported to shallow platforms by upwelling ocean currents. Assuming the present day rate of input of sulphur into the ocean, the steady state concentration of dissolved sulphate in the mixed surface layer would have been about 0.2 mmoles/l (15 ppm), compared to 28 mmoles/l in the modern ocean (Drever, 1974).

From the previous discussion it is apparent that both the circulation of seawater through ocean crust and the reduction of ferric iron in sediments could have contributed significant quantities of iron to the ocean. Today the dissolved constituents of the ocean are largely supplied by continental runoff with a lesser contribution from seafloor hydrothermal systems. Because the mantle surface heat flow was higher during the early history of the Earth and because the area of continents was smaller, it has been proposed that seafloor hydrothermal systems buffered the chemistry of Archean oceans (Fryer et al, 1979; Cameron, 1982; Veizer et al, 1982). Veizer et al (1982) and Veizer (1989) show that the $^{87}Sr/^{86}Sr$ ratio of Archean seawater was buffered by the mantle. An increase in ^{87}Sr at about 2.5 Ga indicates a crossover point between two coupled phenomena: the exponentially decreasing heat flux from the mantle and the concomitant growth of continents (Veizer, 1989). According to Veizer, the circulation of seawater through ocean crust regulated the oxidation state of the ocean-atmosphere system and was the dominant source of iron for iron-formations.

Additional evidence for a mantle buffered ocean come from rare earth

elements and Nd isotopes. The ϵ_{Nd} ratios of iron-formations have positive values (i.e. a mantle dominated source) during the Archean and then a transition towards more negative values (i.e. a significant increase in continental input) at about 2.5 Ga (Jacobsen and Pimentel-Klose, 1988a, b; Derry and Jacobsen, 1988). Like Veizer et al (1982), they propose a higher hydrothermal water to river water flux during the Archean and early Proterozoic. Archean iron-formations are often characterized by positive Eu anomalies, although normal and even depleted abundances have been observed, (Fryer, 1983; Barrett et al, 1988; Dymek and Klein, 1988), whereas early Proterozoic iron-formations have slight positive to slight negative Eu anomalies (Fryer, 1983). The Eu anomalies are considered by these authors to reflect a major contribution of strongly reducing hydrothermal fluids to the seawater.

As indicated earlier, iron-formations and iron-poor carbonate units were often deposited within the same sedimentary basins (Gole and Klein, 1981; Trendall and Morris, 1983). Many of these iron-formations contain sedimentary structures indicating they were formed in relatively shallow water, similar to the iron-poor carbonate units. However, unlike iron-formations, the carbonates are considered to have formed under oxic conditions (Veizer, 1983c). This implies alternating expansion and contraction of the redox zones (e.g. the O_2 minimum layer) within a stratified basin, which was most likely caused by variations in the intensity of hydrothermal activity at ocean ridges. During periods of increased hydrothermal activity, the supply of reduced substrates, such as ferrous iron, to the ocean would lead to consumption of oxidized species, such as dissolved oxygen and sulphate, and to the expansion of the redox zone to shallower water. This would enhance the the transport of dissolved ferrous iron to the shallow shelf.

In summary, the available evidence favours the circulation of seawater through ocean crust (Figure 47) as the dominant control on the oxidation state of the ocean and as the primary source of iron for both Archean and early Proterozoic

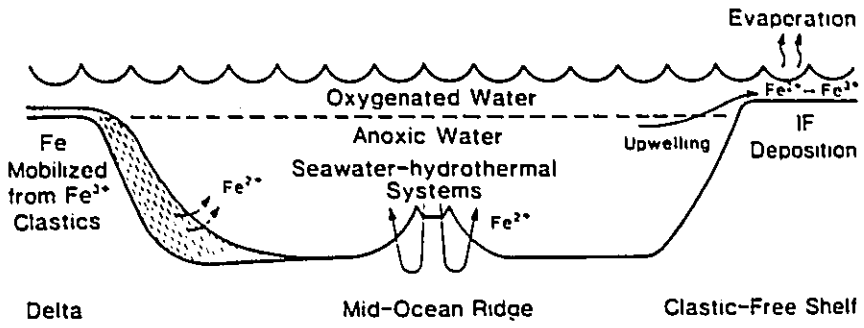

Figure 47. Source of iron for Lake Superior type iron-formation. Deeper water, enriched in Fe^{2+} from hydrothermal systems and mobilized from clastic sediments, is upwelled onto a shallow shelf. More intense hydrothermal activity during this time would have kept concentrations of oxidized species, such as O_2 and sulphate, to low levels and so the deep oceans would have remained anoxic.

iron-formations. The reduction of ferric iron during the oxidation of organic carbon could have complemented the supply of dissolved iron. Variations in the intensity of hydrothermal activity caused variations in the supply of iron and in the oxidation state of the ocean.

6.3. SOURCE OF SULPHUR

In Chapter 5.5, three options were outlined for the source of sulfide in the Gunflint Formation: 1) hydrothermal sulfide, 2) bacterial sulphate reduction in the sediment under near closed system conditions, below a dysaerobic water column, and 3) bacterial sulphate reduction beneath an anoxic water column in which sulphate concentrations were significantly lower than the present day. Option 1 is not favoured because of the difficulty in transporting dissolved sulfide, from seafloor hydrothermal vents to laterally extensive shallow water environments, in the presence of ppm quantities of dissolved ferrous iron. Option 3 is favoured over option 2 because elemental ratios of pyrite-sulphur and organic carbon indicate that sulphate was the limiting factor in sulphate reduction.

Sulphate concentrations had increased to levels above the very low values, characteristic of the reduced atmosphere of the early Earth, by at least 2.3 Ga (Cameron, 1982; Hattori et al, 1983) or possibly as early as 2.7 Ga (Goodwin et al, 1976; Ripley and Nicol, 1981). This conclusion is based on the observation of isotopically variable and ^{34}S depleted sulfides in sediments of this age. A high sulphate concentration allows the preferential partitioning of ^{32}S into sedimentary sulfides and ^{34}S into dissolved sulphate during bacterial sulphate reduction. Increased sulphate concentrations also allows isotopic fractionation in hydrothermal systems during the partial reduction of sulphate to sulfide, resulting in the preferential partitioning of ^{34}S into the residual sulphate (Walker and

Brimblecombe, 1985).

However, many early Proterozoic sedimentary sulfides younger than 2.3 Ga, including those examined in this study, have isotopically heavy ratios (Cameron and Garrels, 1980; Walker and Brimblecombe, 1985; Lambert and Donnelly, 1990). Lambert and Donnelly (1990) propose that the apparent dominance of heavy sulfides are partly a result of biased sampling in mineralized areas in which the $\delta^{34}S$ values reflect hydrothermal sulphate reduction or bacterial sulphate reduction in restricted basins. Most sampling has been from the cratons and not from sediments of the open ocean, which presumably are the reservoir of ^{34}S depleted sulfides. Walker and Brimblecombe (1985) propose that the distribution of $\delta^{34}S$ values of sedimentary sulfides during the early Proterozoic are a result of biological sulphate reduction under conditions of occasional sulphate limitation.

It was proposed in chapter 5.5 that the increase in $\delta^{34}S$ values from the Gunflint Formation to the overlying Rove Formation is consistent with sulphate reduction in a restricted basin. The cause of basin restriction was the convergence of a complex volcanic arc with the continental margin and the transformation of this margin into a foreland basin (Hoffman, 1987; Southwick et al, 1988; Barovich et al, 1989). Magmatism is indicated within this basin by the Emperor Volcanic Complex, which is interlayered with iron-formation in northwestern Michigan. If circulation with the open ocean was partially restricted, such that supply of oceanic sulphate to the basin was less than the amount of sulphate being reduced, then sulphate concentrations could be held to low values resulting in a smaller kinetic isotope effect (i.e. Harrison and Thode, 1958). In addition, the $\delta^{34}S$ of dissolved sulphate would gradually increase with time as ^{32}S is preferentially incorporated into sulfides. Hydrothermal activity would also provide a source of dissolved iron for these iron-formations.

6.4. SOURCE OF SILICA

The concentration of silica in the modern ocean is kept to very low values (1 to 10 mg/l) by silica-secreting organisms. However, these organisms are not considered to have existed before about 1.3 Ga (Cloud, 1973; Drever, 1974; Ewers, 1983). In the absence of such organisms the early oceans would have been saturated or supersaturated with respect to amorphous silica, magadiite and/or sepiolite. The solubility of amorphous silica is about 120 mg/l at 25 ^{o}C and 200 mg/l at 50 ^{o}C between a pH of 4 and 9 (Drever, 1974). The solubility of silica is held to lower concentrations by magadiite and sepiolite, which are the stable phases above a pH of 5.2 and 7.7 respectively. Mel'nik (1982) reports that sols of colloidal silica could attain concentrations of about 1000 mg/l. Ewers (1983) indicates that a saturated solution of amorphous silica at 120 mg/l would be ample to supply the silica content of iron-formations. Silica would be supplied to the ocean by continental weathering and by hydrothermal activity (Heinen and Oehler, 1979).

6.5. SOURCE OF OTHER CONSTITUENTS

Carbon exists in iron-formations as carbonate minerals and as organic matter. The organic matter is the residue of microorganisms that inhabited the water column and the sediments during deposition of these iron-formations. It was shown in Chapter 5 that dissolved seawater bicarbonate was the source of most of the carbonate and that a lesser amount of carbonate was contributed by oxidation of organic carbon during diagenesis and metamorphism.

Other constituents are usually present only in minor quantities. Magnesium, calcium, sodium and potassium are all normal constituents of seawater. Manganese,

like iron, is soluble in its reduced state but insoluble when it is oxidized. Therefore, it was most likely introduced with dissolved iron. Aluminum and titanium, which are very insoluble, were most likely introduced in solid phases such as suspended clays and volcanic ash. Phosphorous, which is an essential nutrient for living organisms, is released during the degradation of organic matter in the deep ocean and is transported to shallow shelves by upwelling currents.

6.6. PRECIPITATION OF Fe-MINERALS AND SILICA:

The present mineralogy of iron-formations is a consequence of its depositional environment and of subsequent diagenetic and metamorphic modifications. For these reasons, observed mineral assemblages are rarely the original primary precipitate. Of the carbonate minerals, siderite and possibly some ankerite are considered to be primary minerals (Floran and Papike, 1975; Klein and Bricker, 1977; Klein and Fink, 1976; this study). However, a significant portion of carbonate, notably ankerite and calcite, formed during diagenesis or metamorphism. Greenalite may be a primary or very early diagenetic mineral, but other iron-silicates, such as stilpnomelane and minnesotaite, are either late diagenetic or metamorphic. A hydrous ferric oxide or ferric hydroxide is presumed to be the precursor phase to hematite, which crystalized during diagenesis. Magnetite crystallized from a hydromagnetite precursor (Klein and Bricker, 1977) or as a replacement of hematite (LaBerge, 1964; LaBerge et al, 1987). Pyrite precipitated from a metastable iron monosulfide such as mackinawite (Berner, 1970).

A mineral stability diagram for the primary mineral phases in iron-formations has been constructed by Ewers (1983) (Figure 48), based on free energies of formation at 298 ^{o}K, an fCO_2 of $10^{-3.5}$, and using the following activities for dissolved species: 10^{-4} M ($\sim$20 ppm) for Fe^{2+}, $10^{-2.7}$ M for H_4SiO_4 (saturated

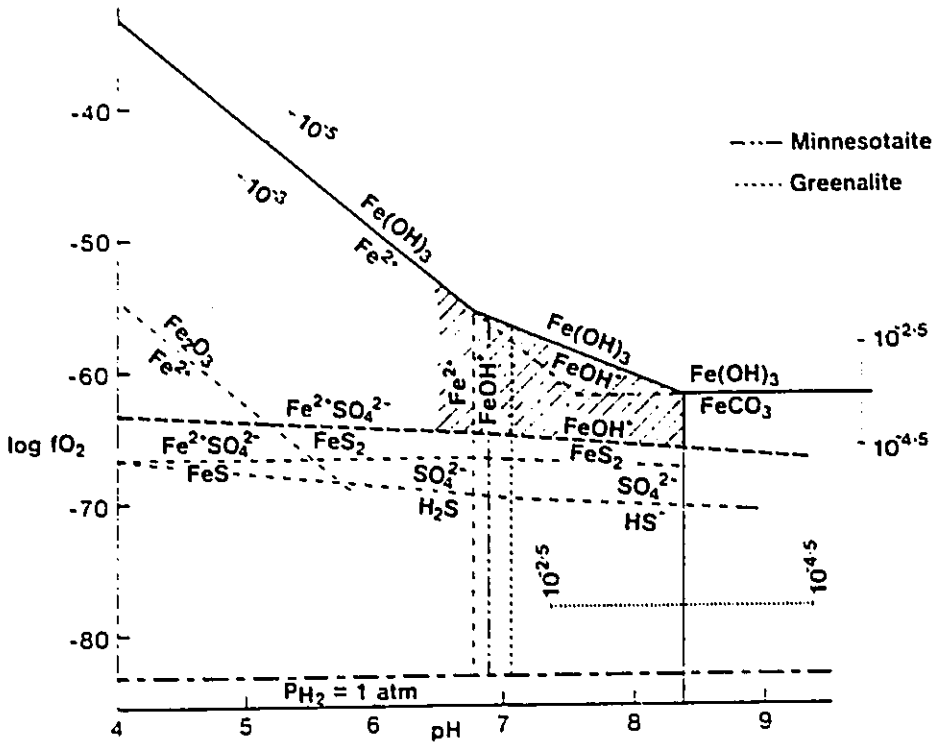

Figure 48. pH - fO_2 diagram defining the limits for Fe^{2+} to exist at an activity greater than 10^{-4} M at 25°C, assuming $aSO_4^{-2} = 10^{-2.76}$ M, $fCO_2 = 10^{-3.5}$ atm. The bar across the boundary Fe^{2+}, $Fe(OH)_3$ indicates shifts when aFe^{2+} is set at 10^{-3} and 10^{-5} M. Bars on boundaries of $FeCO_3$ field show shifts when fCO_2 is set at $10^{-2.5}$ and $10^{-4.5}$ atm. (from Ewers, 1983)

with respect to amorphous silica), and $10^{-2.76}$ for SO_4^{-2} ($\sim$6 % of present concentration). The hatched area represents conditions of fO_2 and pH in which the activity of Fe^{2+} or $FeOH^+$ might be expected to be equal to or greater than 10^{-4} M. The solid lines represent equilibria between the dissolved species and the solid phases $Fe(OH)_3$ and $FeCO_3$, whereas the dotted lines represent equilibria with greenalite and minnesotaite. Ewers (1983) notes that depending on the free energy data used, the species $FeOH^+$ may be eliminated and the equilibrium between Fe^{2+} and $FeCO_3$ would be shifted to a pH of 7.55. Precipitation of iron hydroxide would occur by increasing fO_2, siderite would precipitate by increasing pH and/or fCO_2, and greenalite could form by increasing pH or decreasing fCO_2.

In the absence of free oxygen, the photochemical oxidation of ferrous iron has been suggested as a mechanism to precipitate significant quantities of ferric oxides (Cairns-Smith, 1978; Francois, 1986). Although this may be a viable mechanism for the early Archean iron-formations, the atmosphere and surface waters during the early Proterozoic are considered to have been oxidizing (Kasting, 1987), therefore oxygen and ozone levels may have been high enough to screen light at this wavelength. Many authors (i.e. Lepp and Goldich, 1964; Cloud, 1973,1983; Garrels et al, 1973) have proposed that ferrous iron was oxidized in the photic zone by oxygen producing but oxygen-intolerant photosynthetic, procaryotic microorganisms. The banding of iron-formations resulted from either seasonal microbial blooms or else intermittent availability of iron. LaBerge et al (1987) and Robbins et al (1987) appeal to iron-stripping bacteria as a means of precipitating iron. These mechanisms were proposed for an atmosphere that was anoxic before about 2.0 Ga. Holland (1973) and Drever (1974) propose that mildly oxidizing surface waters reacted with ferrous iron, which was upwelled from the deep, anoxic ocean onto a shallow shelf. This would require a stratified ocean, as proposed by Degens and Stoffers (1976), to allow a significant proportion of the deep ocean to remain anoxic in the presence of

an oxidizing atmosphere.

Some researchers (i.e. Drever, 1974; LaBerge et al, 1987) propose that all of the iron in iron-formations was initially precipitated as some form of hydrous ferric oxide, which was deposited along with silica and organic matter. During diagenesis, oxidation of organic matter resulted in the reduction of ferric iron and the formation of magnetite, greenalite or siderite. The resulting mineral facies would depend on the amount of organic matter deposited in the sediments. Hematite would be preserved in shallow, well oxygenated sediments that contained little or no organic matter. Magnetite would have been the stable iron-mineral in sediments that contained organic carbon if ferric iron was in excess relative to carbon. With increasing amounts of organic matter, greenalite then siderite would become the stable phases.

Alternatively, iron-minerals other than ferric hydroxide may also have been primary precipitates. In this study, textural evidence (Chapter 3) and isotopic evidence (Chapter 5) indicate that most of the siderite, and possibly some of the ankerite, in the Gunflint Formation is primary. The origin of greenalite is less certain, but it is considered by many to be either a primary mineral or else formed from an amorphous greenalite precursor (Floran and Papike, 1975; Klein andBricker, 1977; Ewers, 1983; Maynard, 1983). Magnetite is almost always coarse grained and often occurs as overgrowths around hematite (LaBerge, 1964), implying a diagenetic origin. In the Gunflint Formation, magnetite is most commonly found in the contact metamorphic zones adjacent to gabbroic sills or within the contact metamorphic aureole of the Duluth Complex, indicating a metamorphic origin.

If the deep ocean was saturated with respect to siderite, upwelling would cause a decrease in pressure and increase in temperature, causing a decrease in the solubility of carbonate and hence the precipitation of siderite. However, the

formation of carbonate by reaction (2) constitutes a release of acid to the system, as does the oxidation of ferrous iron (3) and the precipitation of iron silicates (4).

$$Fe^{2+} + HCO_3^- = FeCO_3 + H^+ \quad (2)$$

$$Fe^{2+} + .25\,O_2 + 2.5\,H_2O = Fe(OH)_3 + 2H^+ \quad (3)$$

$$Fe^{2+} + 2/3H_4SiO_4 + 1/3H_2O = 1/3Fe_3Si_2O_5(OH)_4 + 2H^+ \quad (4)$$

For precipitation to continue the acid has to be neutralized. Ewers and Morris (1981) propose that reaction with volcanic ash, or other silicates, was responsible for maintaining the required pH. Pyroclastic detritus is widespread throughout the Gunflint Formation and most of it is significantly altered. However, siderite is most abundant in the banded chert-carbonate facies, which does not contain significant quantities of pyroclastic material. The photosynthetic withdrawal of CO_2 can cause an increase in pH and decrease in carbonate solubility. However, if oxygen is produced during photosynthesis then precipitation of iron oxides would be favoured. Evaporation has been proposed by a number of workers (Garrels et al, 1973; Garrels, 1987; Eugster and Chou, 1973; Ewers, 1983) as a mechanism to precipitate siderite as well as silicates. If CO_2 were lost to the atmosphere during evaporation then siderite would form by reaction (5) and greenalite by reaction (6).

$$Fe^{2+} + 2\,HCO_3^- = FeCO_3 + CO_2 + H_2O \quad (5)$$

$$Fe^{2+} + 2/3\,H_4SiO_4 + 1/3\,H_2O + 2HCO_3 =$$

$$1/3\,Fe_3Si_2O_5(OH)_4 + 2CO_2 + 2H_2O \quad (6)$$

It has been suggested that the presence of silica microspheres in chert are the fossilized remains of siliceous microorganisms (LaBerge, 1973; LaBerge et al, 1987; Klemm, 1979). However, it has been shown that microspheres can form during the initial crystallization of inorganically precipitated siliceous colloids (Oehler, 1976). In the absence of silica secreting organisms the oceans would have been saturated with respect to amorphous silica or magadiite. Inorganic precipitation of siliceous sediments would have occurred in areas where the influx of dissolved silica was high

or where evaporation produced supersaturated conditions (Heinen and Oehler, 1979; Drever, 1974; Garrels, 1987).

Below the redox boundary, bacterial sulphate reduction may have taken place in the water column, either in deeper water or in shallow water where the influx of organic matter was sufficient to establish anoxic conditions. Sulphate reduction would also take place in the sediment wherever organic matter was deposited in sufficient quantity. The low sulphate concentration (~2 mmoles/l) assumed by Ewers (1983) is consistent with the minor amount of isotopic fractionation observed in fine grained pyrite found throughout the Gunflint Formation.

6.7. IMPLICATIONS OF ISOTOPIC DATA

Carbon isotope ratios for siderite from the Gunflint Formation indicate that most of the siderite precipitated from seawater, which had a $\delta^{13}C$ value near 0 ‰ and contained ppm concentrations of dissolved ferrous iron. The $\delta^{13}C$ value near 0 ‰ is typical of marine carbonates throughout geologic time. The range of values from 0 to -6 ‰ indicates that a small component of siderite was formed during early diagenesis from CO_2 released by the bacterial oxidation of organic carbon. The range of isotopic values in the Upper Limestone Member are similar to the iron-rich rocks, which implies a common source of bicarbonate. The iron-poor nature of the limestone indicates an abrupt decline in the supply of dissolved ferrous iron. A common source of marine bicarbonate favours a marine source of iron rather than a continental source during a period of basin emergence.

The heaviest $\delta^{18}O$ values (-5 to -7 ‰) of carbonate minerals from the Gunflint Formation are similar to values reported for calcite and dolomite from early Proterozoic marine carbonates (Veizer et al, 1990). These values are interpreted to represent original values and hence reflect seawater conditions. This

indicates that the $\delta^{18}O$ of seawater in the Gunflint basin was similar to other Precambrian carbonate basins. However, it cannot be resolved whether these values, which are depleted in ^{18}O relative to the modern ocean, indicate that the oceans were depleted in ^{18}O or were warmer during the Precambrian. The range of $\delta^{18}O$ values between -5 and -16 ‰ (PDB) probably is the result of the introduction of ^{18}O-depleted meteoric water during early diagenesis.

The source of sulphur for sulfides in the Gunflint Formation was dissolved sulphate in seawater, which was reduced to sulfide by sulphate-reducing bacteria. Positive $\delta^{34}S$ values and low S/C ratios suggest that the concentration of sulphate was the limiting factor that controlled the amount of sulfide formed and the magnitude of the kinetic isotope effect. Decreased sulphate concentrations and high iron concentrations were probably the result of increased hydrothermal circulation of seawater through ocean crust at spreading centers. The trend to heavier $\delta^{34}S$ values in the overlying Rove Formation indicates that the basin was partially closed to the supply of sulphate over long intervals of time. This is consistent with the interpretation that the Animikie Group was deposited in a tectonic foredeep. Active volcanism or rifting within this basin would have kept concentrations of dissolved sulphate and oxygen to low levels and also would have provided a source of iron. Sulphate concentrations may have been higher in the open ocean.

6.8. DEPOSITIONAL MODEL FOR THE GUNFLINT FORMATION

The evidence is consistent with the deposition of the Gunflint Formation in a foreland basin in which volcanism was active (Hoffman, 1987) or else a backarc basin (Southwick et al, 1988). Hydrothermal activity associated with spreading centers or volcanism within the basin was the dominant source of dissolved iron and may have provided a significant quantity of silica. Sulphate was held to low

concentrations by reduction during hydrothermal circulation of seawater through the ocean crust. This sulfide would have precipitated on the seafloor near hydrothermal vents and may have formed massive sulfides, analogous to those present in the Wisconsin magmatic terranes. Upwelling of deep basin water onto the shallow shelf provided the supply of iron. Because the pCO_2 during the early Proterozoic was probably higher than modern levels, the ocean may have been saturated with respect to siderite.

The sediments of the Gunflint Formation can be divided into clastic textured (arenite and stromatolite facies) and laminated (banded chert-carbonate, laminated carbonate and black shale) rocks. Unmetamorphosed laminated rocks contain mostly chert and siderite with variable amounts of pyroclastic detritus, organic carbon and pyrite. The lack of ferric iron minerals and the presence of pyrite and organic carbon indicates that these sediments were deposited under low fO_2 conditions. Lamination also indicates that they were either deposited below wave base or in a shallow, protected environment, which contained sufficient organic matter to keep fO_2 low. Upwelling of iron-rich water into these environments, in the absence of clastic detritus, would favour the precipitation of banded chert-carbonate, probably as a result of evaporation. Chert, which is also present in carbonate layers, was probably being continually precipitated, whereas siderite bands may indicate a variable input of iron. The black shale facies formed when there was an abundant input of pyroclastic detritus. The laminated carbonate facies represents a transitional facies. Bacterial sulphate reduction proceeded wherever anoxic conditions prevailed.

Unmetamorphosed clastic textured rocks are composed mostly of chert, greenalite and hematite and minor amounts of carbonate. These sediments contain primary structures indicating they were deposited in a shallow, energetic environment. Banded oxide-facies iron-formation, similar to that observed in

Archean deposits and in the Hammersley deposits, is not observed in the Gunflint Formation. If ferric iron was precipitated as laminated sediments, it was subsequently reworked as intraclasts and redeposited as cross-laminated beds. Alternatively, intraclasts were derived from laminated siderite beds and were reworked in shallow oxidizing water and, depending on fO_2, was oxidized to greenalite or hematite before being redeposited. Thin layers and rip-up clasts of siderite are present in arenite facies, which is consistent with this interpretation. Silica was mostly precipitated as early diagenetic cements.

The Upper Limestone Member contains iron-poor carbonate (dolomite and calcite), chert and variable quantities of pyroclastic detritus. These rocks represent the termination of iron into the basin, possibly because of reduced hydrothermal activity.

7. CONCLUSIONS

1. The Gunflint Formation is divided into seven lithofacies. The conglomerate facies is located at the base of the formation and represents a transgressive lag deposit. The main part of the formation is composed of iron-rich, complexly interlayered arenitic (arenite and stromatolite facies) and lutitic (banded chert-carbonate, laminated carbonate, and black shale facies) lithologies. Greenalite and hematite are the dominant iron-minerals in arenitic beds, whereas only reduced iron-minerals are contained in lutitic beds (i.e. siderite, ankerite, greenalite, and pyrite). The top of the Gunflint Formation is an iron-poor limestone facies.

2. The sediments of the Gunflint Formation were deposited on a shallow shelf, similar to modern shelf carbonate environments. The transitions between the different lithofacies represent variations in the physical and/or chemical environment, caused by minor changes in sea level or depositional topography and the position of the O_2-minimum layer. Lutitic lithologies were precipitated under reducing conditions in a low energy environment, for example in deeper water, in depressions on the shelf, or in lagoons protected by sand shoals. Arenitic lithologies were either deposited or reworked under more oxidizing conditions in a higher energy environment.

3. In all facies of the Gunflint Formation, except the Upper Limestone Member, siderite was the earliest formed carbonate mineral. Precipitation initiated either within the water column or else at the sediment/water interface. Ankerite and calcite formed during early to late diagenesis, as authigenic minerals or as replacements of earlier formed minerals, and during

metamorphism by the breakdown of siderite. In the Upper Limestone Member dolomite was the earliest formed carbonate mineral. It formed during very early diagenesis and is cemented by early diagenetic chert. Calcite formed either contemporaneous with chert or, at least locally, by replacement of chert. Disseminated, very fine-grained pyrite formed during very early diagenesis. Locally, in the Kakabeka Falls area, coarse-grained pyrite and pyrite concretions post-date fine-grained pyrite but still formed during early diagenesis.

4. The $\delta^{13}C$ values mostly near 0 °/oo indicate that the source of carbon for the carbonate minerals was marine bicarbonate. The shift to lighter values was the result of the incorporation of oxidized organic matter during diagenesis (0 to -6 °/oo) and metamorphism (< -6 °/oo).

5. The heaviest $\delta^{18}O$ values for unmetamorphosed carbonate minerals, -5.3 °/oo (PDB) for siderite, -6.1 °/oo for ankerite, and -6.7 °/oo for calcite, is similar to $\delta^{18}O$ values reported for least altered calcite and dolomite in Precambrian marine carbonate formations, that are considered to represent original marine values. The shift to lighter values represents isotopic exchange reactions with pore fluids at higher temperatures and/or isotopic exchange with ^{18}O-depleted meteoric water.

6. Pyrite-sulphur content shows a poor correlation with organic carbon content in black shales of the Gunflint Formation, except for the lower 15 m of the formation in the Kakabeka Falls area. The average S/C ratio of the shales is much less than typical Phanerozoic shales. Because of the high iron contents of these shales, the low S/C ratios indicate that dissolved sulphate was the limiting

factor in bacterial sulphate reduction, suggesting that sulphate concentrations in the Gunflint basin were significantly lower that modern levels. Elevated sulphur contents in shales in the Kakabeka Falls area with relatively low organic carbon contents suggests that pyrite here did not form by simple biogenic reduction of seawater sulphate. Much of this sulphur was probably introduced along syndepositional faults.

7. The disseminated, fine-grained pyrite found throughout the Gunflint Formation has relatively uniform $\delta^{34}S$ values between +5 and +12 °/oo. There are three possible origins for the fine-grained pyrite: 1) hydrothermal sulfide, 2) biogenic pyrite formed in sediments beneath a dysaerobic water column within a closed or nearly closed system, and 3) biogenic sulfide formed within an anoxic basin, which contained sulphate concentrations significantly lower that the present. The first option is not favoured because of the difficulty in transporting H_2S to a shallow shelf in water containing the high concentrations of dissolved iron required to form iron-formation. Option 3 is favoured over option 2 by S/C ratios, which indicate low sulphate concentrations.

8. The overlying Rove Formation has $\delta^{34}S$ values between +13 and +21 °/oo, which indicates that the basin was partially closed to the open ocean supply of sulphate over long intervals of time. This is consistent with the interpretation that the Animikie Group was deposited in a basin with restricted communication with the open ocean such as a foredeep or backarc basin.

9. Coarse-grained pyrite and pyrite concretions in the Kakabeka Falls area has $\delta^{34}S$ values between -33 and +35 °/oo. The wide range of values suggests a

biogenic origin, but from a different sulphate reservoir than the fine-grained pyrite, as is suggested by the elevated S/C ratios.

10. The distribution of $\delta^{13}C$ and $\delta^{18}O$ values for both the iron-rich rocks and the iron-poor Upper Limestone Member indicate they were formed from the same marine source of bicarbonate. The trend to heavier $\delta^{34}S$ values in the overlying Rove Formation, which suggests that the basin remained closed to the ocean reservoir of sulphate, indicates that the transition from iron-formation to the iron-poor limestone member does not represent deposition of iron-formation during a period of basin isolation (e.g. Becker and Clayton, 1972) followed by an incursion of the open ocean. Instead a stratified ocean in which iron existed in solution below a redox boundary in favoured. Expansion of the redox boundary to shallow water would allow the transport of dissolved ferrous iron to the shallow shelf. The transition to iron-poor conditions would be related to the contraction of the redox boundary.

11. The wide-spread evidence of penecontemporaneous volcanism suggests a hydrothermal origin for the iron, although reduction of detrital ferric iron below the redox boundary may also have contributed significant amounts of dissolved ferrous iron. Expansion and contraction of the redox boundary may have been related to cycles of tectonic activity.

12. During deposition of iron-formation, siderite precipitation would be favoured on deeper or sheltered parts of the shelf where conditions were reducing and seawater was saturated with respect to siderite. A limited amount of pyrite may have formed above the sediment/water interface in anoxic water, but most

pyrite probably formed within the sediment by bacterial sulphate reduction during very early diagenesis. In shallower or more energetic environments, oxidizing conditions would favour the precipitation iron as a ferric hydroxide. Greenalite, or some amorphous precursor, would precipitate in transitional environments. Evapouration of seawater, which was saturated with respect to silica, would promote the continuous precipitation of silica in all environments.

REFERENCES

Al-Aasm, I.S., Taylor, B.E., and South, B., 1990, Stable isotope analysis of multiple carbonate samples using selective acid extraction., Chem. Geol. (Isotope Geoscience Sect.), 80, p. 119-125.

Anderson, T.F. and Arthur, M.A., 1983, Stable isotopes of oxygen and carbon and their application to sedimentologic and paleoenvironmental problems., in Stable Isotopes in Sedimentary Geology, SEPM Short Course No. 10, p. 1.1-1.151.

Ashendorf, D., 1980, Are sulfur isotope ratios sufficient to determine the antiquity of sulphate reduction., Origins Life, 10, p. 325-333.

Baker, P.A. and Kastner, M., 1981, Constraints on the formation of sedimentary dolomite., Science, 213, p. 214-216.

Banks, P.O. and Van Schmus, W.R., 1972, Chronology of Precambrian rocks of Iron and Dickinson Counties, Michigan., Proceedings, Institute on Lake Superior Geology, p. 18.

Barghoorn, E.S., Knoll, A.H., Dembicki, H., and Meinschein, W.G., 1977, Variations in stable carbon isotopes in organic matter from the Gunflint Formation., Geochim. Cosmochim. Acta, 41, p. 425-430.

Barghoorn, E.S. and Tyler, S.A., 1965, Microorganisms from the Gunflint chert., Science, 147, p. 563-577.

Barovich, K.M., Patchett, P.J., Peterman, Z.E., and Sims, P.K., 1989, Nd isotopes and the origin of 1.9-1.7 Ga Penokean continental crust of the Lake Superior region., Geol. Soc. Am. Bull., 101, p. 333-338.

Barrett, T.J., Fralick, P.W. and Jarvis, I., 1988, Rare-earth-element geochemistry of some Archean iron formations north of Lake Superior, Ontario., Can. Jour. Earth Sci., 25, p. 570 - 580.

Baur, M.E., Hayes, J.M., Studley, S.A., and Walter, M.R., 1985, Millimeter-scale variations of stable isotope abundances in carbonates from banded iron-formations in the Hammersley Group of western Australia., Econ. Geol., 80, p. 270-282.

Beck, W. and Murthy, V.R., 1982, Rb-Sr and Sm-Nd isotopic studies of Proterozoic mafic dikes in northeastern Minnesota., Proceedings, Institute on Lake Superior Geology, 28, p. 5.

Becker, R.H. and Clayton, R.N., 1972, Carbon isotopic evidence for the origin of a banded iron-formation in western Australia., Geochim. Cosmochim. Acta, 36, p. 577-595.

Becker, R.H. and Clayton, R.N., 1976, Oxygen isotope study of a Precambrian banded iron-formation, Hammersley Range, western Australia., Geochim. Cosmochim. Acta, 40, p. 1153-1165.

Berner, R.A., 1970, Sedimentary pyrite formation., Am. Jour. Sci., 268, p. 1-23.

Berner, R.A., 1984, Sedimentary pyrite formation: an update., Geochim. Cosmochim. Acta, 48, p. 605-615.

Berner, R.A., 1985, Sulphate reduction, organic matter decomposition and pyrite formation., Royal Society of London, Phil. Trans., London, A 315, p. 251-273.

Bourgeois, J., 1980, A transgressive shelf sequence exhibiting hummocky stratification: the Cape Sebastion Sandstone (Upper Cretaceous), southwestern Oregon., Jour. Sed. Pet., 50, p. 681-702.

Brewer, P.G. and Spencer, D.W., 1974, Distribution of some trace elements in Black Sea and their flux between dissolved and particulate phases., in Degens, E.T. and Ross, D.A. eds., The Black Sea - Geology, Chemistry, and Biology., A.A.P.G. Memoir 20, p. 137-143.

Cairns-Smith, A.G., 1978, Precambrian solution photochemistry, inverse segregation, and banded iron formations., Nature, 276, p. 807-808.

Cambray, F.W., 1978, Plate tectonics as a model for the environment of deposition and deformation of early Proterozoic (Precambrian X) of northern Michigan., Geol. Soc. Am. Abst. Programs, 10, p. 376.

Cameron, E.M., 1982, Sulphate and sulphate reduction in early Precambrian oceans., Nature, 296, p. 145-148.

Cameron, E.M., 1983, Genesis of Proterozoic iron-formations: sulphur isotope evidence., Geochim. Cosmochim. Acta, 47, p. 1069-1074.

Cameron, E.M. and Garrels, R.M., 1980, Geochemical compositions of some Precambrian shales from the Canadian Shield., Chem. Geol., 28, p. 181-197.

Cameron, E.M. and Hattori, K., 1987, Archean sulphur cycle: evidence from sulphate minerals and isotopically fractionated sulfides in Superior Province, Canada., Chem. Geol. (Isotope Geoscience Section), 65, p. 341-358.

Card, K.D. and Ciesielski, A., 1986, Subdivisions of the Superior of the Canadian Shield., Geoscience Canada, 13, p. 5-13.

Chambers, L.A., Trudinger, P.A., Smith, J.W., Burns, M.S., 1979, Fractionation of sulphur isotopes by continuous cultures of Desulfovibrio desulfuricans., Can. Jour. Microbiol., 21, p. 1602-1607.

Claypool, G.E., Hosler, W.T., Kaplan, I.R., Sakai, H. and Zak, I., 1980, The age curves of sulphur and oxygen isotopes in marine sulphate and their mutual interpretations., Chem. Geol., 28, p. 199-260.

Claypool, G.E. and Kaplan, I.R., 1974, The origin and distribution of methane in marine sediments., in Kaplan, I.R. ed., Natural Gases in Marine Sediments., Marine Science, 3, p. 99-140.

Clemmey, H. and Badham, N., 1982, Oxygen in the Precambrian atmosphere: an evaluation of the geological evidence., Geology, 10, p. 141-146.

Cloud, P.E., 1972, A working model for the primitive earth., Am. Jour. Sci., 272, p. 537-548.

Cloud, P.E., 1973, Paleoecological significance of the banded iron-formation., Econ. Geol., 68, p. 1135-1143.

Cloud, P.E., 1980, Early biogeochemical systems., in Trudinger, P.A. ed., Biogeochemistry of Ancient and Modern Environments, Australian Acad., Springer Verlag, p. 7-27.

Cloud, P.E., 1983, Banded iron-formation - a gradualist's dilemma., in Trendall, A.F. and Morris, R.C. eds., Iron-Formation: Facts and Problems, Elsevier, Amsterdam, p. 401-418.

Craig, H. and Gordon, L.I., 1965, Deuterium and oxygen-18 variations in the ocean and the marine atmosphere., in Tongiorgi, E. ed., Stable Isotopes in Oceanographic Studies and Paleotemperatures., Consiglio Nazionale delle Richerche, Laboratorio di Geologia Nucleare, Pisa, p. 9-130.

Crocket, J.H., McNutt, R.H., Schwarcz, H.P., Rees, C.E., Blum, N., Hurley, T., Bowins, R., and Kabir, A., 1983, Isotopic and geochemical characterization of Archean iron formations and associated volcanic rocks - some preliminary results from the Temagami and Boston Iron Formations., Ont. Geol. Sur., Misc. Paper 113, p. 29-40.

Davy, R., 1983, A contribution on the chemical composition of Precambrian iron-formations., in Trendall, A.F. & Morris, R.C. eds., Iron-Formation: Facts and Problems., Elsevier, Amsterdam, p. 325-343.

Degens, E.T. and Epstein, S., 1962, Relationship between $^{18}O/^{16}O$ ratios in coexisting carbonates, cherts and diatomites., A.A.P.G. Bull., 46, p. 534-542.

Degens, E.T. and Stoffers, P., 1976, Stratified waters as a key to the past., Nature, 263, p. 22-27.

Deines, P., Langmuir, D. and Harmon, R.S., 1974, Stable carbon isotope ratios and the existence of a gas phase in the evolution od carbonate groundwaters., Geochim. Cosmochim. Acta, 39, p. 1147-1154.

Derry, L.A. and Jacobsen, S.B., 1988, The Nd and Sr isotopic evolution of Proterozoic seawater., Geophysical Research Letters, 15, p. 397-400.

Deuser, W.G., 1970, Carbon-13 in Black Sea waters and implications for the origin of hydrogen sulfide., Science, 268, p. 1575-1577.

Dimroth, E., 1976, Aspects of the sedimentary petrology of cherty iron-formations., in Wolf, K.H. ed., Handbook of Strata-bound and Stratiform Ore Deposits, Elsevier, Amsterdam, 7, p. 203-254.

Dimroth, E. and Chauvel, J.-J., 1973, Petrography of Sokoman Iron Formation in part of the central Labrador trough, Quebec, Canada., Geol. Soc. Am. Bull., 84, p. 111-134.

Dimroth, E. and Kimberley, M.M., 1976, Precambrian atmospheric oxygen: Evidence in the sedimentary distributions of carbon, sulfur, uranium and iron., Can. Jour. Earth Sci., 13, p. 1161-1185.

Donnelly, T.H., Lambert, I.B., Oehler, O.Z., Hallberg, J.A., Hudson, D.R., Smith, J.W., Bavinton, O.A., and Golding, L., 1977, A reconnaisance study of stable isotope ratios in Archean rocks from the Yilgarn Block, Western Australia., Jour. Geol. Soc. Australia, 24, p. 409-420.

Drever, J.I., 1974, Geochemical model for the origin of Precambrian banded iron-formations., Geol. Soc. Am. Bull., 85, p. 1099-1106.

Dutton, S.P. and Land, L.S., 1985, Meteoric burial diagenesis of Pennsylvanian arkosic sandstones, southwestern Anadarko Basin, Texas., A.A.P.G. Bull., 69, p. 22-38.

Dymek, R.F. and Klein, C., 1988, Chemistry, petrology and origin of banded iron-formation lithologies from the 3800 Ma Isua Supracrustal Belt, West Greenland., Precambrian Res., 39, p. 247-302.

Eastoe, C.J., Solomon, M., and Garcia Palomero, S., 1986, Sulphur isotope study of massive and stockwork pyrite deposits at Rio Tinto, Spain., Trans. Inst. Mineral. Metall., Sect. B, p. 201-207.

Eichmann, R. and Schidlowski, M., 1975, Isotope fractionation between coexisting organic carbon-carbonate pairs in Precambrian sediments., Geochim. Cosmochim. Acta, 39, p. 585-595.

Emrich, K., Erhalt, D.H. and Vogel, J.C., 1970, Carbon isotope fractionation during the precipitation of calcium carbonate., Earth Planet. Sci. Lett., 8, p. 363-371.

Epstein, S., Graf, D.L., and Degens, E.T., 1964, Oxygen isotope studies on the origin of dolomites., in Craig et al., eds., Isotopic and Cosmic Chemistry, North Holland Publ. Co., Amsterdam, p. 169-180.

Eugster, H.P. and Chou, I.M., 1973, The depositional environment of Precambrian banded iron formations., Econ. Geol., 68, p. 1144-1168.

Ewers, W.E., 1983, Chemical factors in the deposition and diagenesis of banded iron-formation., in Trendall, A.F. and Morris, R.C. eds., Iron-Formation: Facts and Problems, Elsevier, Amsterdam, p. 491-512.

Ewers, W.E. and Morris, R.C., 1981, Studies of the Dales Gorge Member of the Brockman Iron Formation, Western Australia., Econ. Geol., 76, p. 1929-1953.

Floran, R.J. and Papike, J.J., 1975, Petrology of the low grade rocks of the Gunflint Iron-Formation, Ontario-Minnesota., Geol. Soc. Am. Bull., 86, p. 1169-1190.

Floran, R.J. and Papike, J.J., 1978, Mineralogy and petrology of the Gunflint Iron Formation, Minnesota-Ontario: Correlation of compositional and assemblage variations at low to moderate grade., Jour. Petrology, 19, p. 215-288.

Fralick, P., 1989, Microbial bioherms, lower Proterozoic Gunflint Formation, Thunder Bay, Ontario., in Geldstzer, H.H.J., James, N.P., and Tebbutt, G.E.

eds., Reefs, Canada and Adjacent Area., C.S.P.G. Memoir 13, p. 24-29.

Francois, L.M., 1986, Extensive deposition of banded iron formation was possible without photosynthesis., Nature, 320, p. 352-354.

Franklin, J.M., Lydon, J.W. and Sangster, D.F., 1981, Volcanic-associated massive sulfide deposits., Econ. Geol. 75th Anniv. Vol., p. 485-627.

Freidman, I. and O'Neil, J.R., 1977, Compilation of stable isotope fractionation factors of geochemical interest., U.S. Geol. Surv. Prof. Paper, 440-KK, p. 1-12.

Fripp, R.E.P., Donnelly, T.H., and Lambert, I.B., 1979, Sulphur isotope results for the Archean banded iron formation, Rhodesia., Spec. Publ. Geol. Soc. S. Africa 5, p. 205-298.

Fritz, P. and Smith, D.C.W., 1970, The isotopic composition of secondary dolomites., Geochim. Cosmochim. Acta., 34, p. 1161-1173.

Froelich, P.N., Klinkhammer, G.P., Bender, M.L., Luedtke, N.A., Heath, G.R., Cullen, D., Dauphin, P., Hammond, D., Hartman, B., and Maynard, V., 1979, Early oxidation of organic matter in pelagic sediments of the eastern equitorial Atlantic: suboxic diagenesis., Geochim. Cosmochim. Acta, 43, p. 1075-1090.

Fryer, B.J., 1983, Rare earth elements in iron-formations., in Trendall, A.F. and Morris, R.C. eds., Iron-Formation: Facts and Problems, Elsevier, Amsterdam, p. 345-358.

Fryer, B.J., Fyfe, W.S., and Kerrich, R., 1979, Archaean volcanogenic oceans., Chem. Geol., 24, p. 25-33.

Garrels, R.M., 1987, A model for the deposition of the microbanded Precambrian iron formations., Am. Jour. Sci., 287, p. 81-106.

Garrels, R.M., Perry, E.A. Jr., and Mackenzie, F.T., 1973, Genesis of Precambrian iron-formation and the development of atmospheric oxygen., Econ. Geol., 68, p. 1173-179.

Gautier, D.L. and Claypool, G.E., 1984, Interpretation of methanic diagenesis in ancient sediments by analogy with processes in modern diagenetic environments., in McDonald, D.A. and Surdam, R.C. eds., Clastic Diagenesis., A.A.P.G. Mem. 37, p. 111-123.

Goldhaber, M.B. and Kaplan, I.R., 1975, Controls and consequences of sulphate reduction rates in recent marine sediments., Soil Science, 119, p. 42-55.

Gole, M.J. and Klein, C., 1981, Banded iron-formation through much of Precambrian time., Jour. Geol., 89, p. 169-183.

Goodfellow, W.D. and Jonasson, I.R., 1984, Ocean stagnation and ventilation defined by $\delta^{34}S$ secular trends in pyrite and barite, Selwyn Basin, Yukon., Geology, 12, p. 583-586.

Goodwin, A.M., 1956, Facies relations in the Gunflint Iron Formation., Econ. Geol., 51, p. 565-595

Goodwin, A.M., 1960, Gunflint Iron Formation of the Whitefish Lake Area., Ontario Dept. Mines, 69, part 7, p. 41-63.

Goodwin, A.M., Monster, J., and Thode, H.G., 1976, Carbon and sulphur isotope abundances in Archean iron-formations and early Precambrian life., Econ. Geol., 71, p. 870-891.

Goodwin, A.M., Thode, H.G., Chou, C.L., and Karkhansis, S.N., 1985, Chemostratigraphy and origin of the late Archean siderite-pyrite rich Helen Iron Formation, Michipicoten belt, Canada., Can. Jour. Earth Sci., 22, p. 72-84.

Greenberg, J.K. and Brown, B.A., 1983, Lower Proterozoic volcanic rocks and their setting in the southern Lake Superior district., Geol. Soc. Am. Mem. 160, p. 67-84.

Gregory, R.T., 1986, Oxygen isotope systematics of quartz-magnetite pairs from Precambrian iron-formations: evidence for fluid-rock interaction during diagenesis and metamorphism., in Walther J.V. and Wood B.J. eds., Fluid-Rock Interactions During Metamorphism, Springer, New York, p. 132-153.

Gross, G.A., 1965, Geology of iron deposits in Canada; Volume 1, General geology and evaluation of iron deposits., G.S.C., Econ. Geol. Rep. No. 22.

Gross, G.A., 1972, Primary features in cherty iron-formations., Sed. Geology, 7, p. 241-261

Gross, G.A., 1980, A classification of iron-formation based on depositional environments., Can. Mineral., 18, p. 223-229.

Gross, G.A., 1983, Tectonic systems and the deposition of iron-formation., Precambrian Res., 20, p. 171-187.

Gustafson, L.B. and Williams, N., 1981, Sediment-hosted stratiform deposits of copper, lead, and zinc., Econ. Geol. 75th Anniv. Vol., p. 139-178.

Harrison, A.G. and Thode, H.G., 1958, Mechanisms of the bacterial reduction of sulphate from isotope fractionation studies., Trans. Faraday Soc., 54, p. 84-92.

Hassler, S.W. and Simonson, B.M., 1989, Deposition and alteration of volcaniclastic strata in two large, early Proterozoic iron-formations in Canada., Can. Jour. Earth Sci., 26, p. 1574-1585.

Hattori, K., Krouse, H.R., and Campbell, F.A., 1983, The start of sulphur oxidation in continental environments: about 2.2×10^9 years ago., Science, 221, p. 549-551.

Hayes, J.M., Kaplan, I.R., and Wedeking, K.W., 1983, Precambrian organic geochemistry, preservation of the record., in Schopf, J.W. ed., Earth's Earliest Biosphere: Its Origin and Evolution, Princeton Univ. Press, New Jersey, p. 93-134.

Heinen, W. and Oehler, J.H., 1979, Evolutionary aspects of biological involvement in the cycling of silica., in Trudinger, P.A. and Swaine, D.J. eds., Biogeochemical Cycling of Mineral-Forming Elements., Elsevier, Amsterdam., p. 431-443.

Hesse, R., 1986, Early diagenetic pore water/sediment interaction: Modern offshore basins., Geoscience Canada, 13, p. 165-196.

Hoffman, P.F., 1987, Early Proterozoic foredeeps, foredeep magmatism, and Superior-type iron-formations of the Canadian Shield, in Kroner, A. ed., Proterozoic Lithospheric Evolution, Am. Geophys. Union Geodynamics Series, 17, p. 85-98.

Hofmann, H.J., 1969, Stromatolites from the Proterozoic Animikie and Sibley Groups, Ontario., Geol. Surv. Canada, Paper 68-69, 77pp.

Hofmann, H.J. and Schopf, J.W., 1983, Early Proterozoic microfossils., in Schopf, J.W. ed., Earth's Earliest Biosphere: Its Origin and Evolution, Princeton Univ. Press, New Jersey, p. 321-360.

Holland, H.D., 1973, The oceans: a possible source of iron in iron-formations., Econ. Geol., 68, p. 1169-1172.

Holland, H.D., 1978, The chemistry of the atmosphere and oceans, John Wiley & Sons, New York, 351 pp.

Holland, H.D., 1984, The Chemical Evolution of the Atmosphere and Oceans, Princeton University Press, Princeton, N.J., 582pp.

Holland, H.D. and Beukes, N.J., 1989, Evidence for a dramatic rise in atmospheric oxygen between 2.2 and 1.8 BYBP., Geol. Soc. America, Abstracts with Programs, 21, No.6, p. A24.

Holland, H.D., Feakes, C.R., and Zbinden, E.A., 1989, The Flin Flon paleosol and the composition of the atmosphere at 1.8 BYBP., Am. Jour. Sci., 289, p. 362-389.

Holland, H.D. and Zbinden, E.A., 1988, Paleosols and the evolution of the atmosphere, part I., in Lerman, A. and Meybeck, M. eds., Physical and Chemical Weathering in Geochemical Cycles., Reidel, Dordrecht, p. 61-82.

Holser, W.T., Schidlowski, M., Mackenzie, F.T., and Maynard, J.B., 1988, Biochemical cycles of carbon and sulfur., in Gregor, C.B., Garrels, R.M., Mackenzie, F.T. and Maynard, J.B. eds., Chemical Cycles in the Evolution of the Earth., John Wiley & Sons, New York, p. 105-173.

Irwin, H., Curtis, C.D., and Coleman, M.L., 1977, Isotopic evidence for the source of diagenetic carbonates formed during the burial of organic-rich sediments., Nature, 269, p. 209-213.

Jacobs, L. and Emerson, S., 1982, Trace metal solubility in an anoxic fjord., Earth Planet. Sci. Lett., 60, p. 237-252.

Jacobsen, S.B. and Pimentel-Klose, M.R., 1988, A Nd isotopic study of the Hamersley and Michipicoten banded iron-formations: the source of REE and Fe in Archean oceans., Earth Planet. Sci. Lett., 87, 29-44.

James, H.L., 1954, Sedimentary facies of iron-formation., Econ. Geol., 49, p. 235-293.

James, H.L., 1958, Stratigraphy of pre-Keweenawan rocks in parts of northern Michigan., U.S. Geol. Surv. Prof. Paper 314-C, p. 27-44.

James, H.L., 1966, Chemistry of iron-rich sedimentary rocks., U. S. Geol. Surv. Prof. Paper 440-W.

James, H.L., 1983, Distribution of banded iron-formation in space and time., in Trendall, A.F. and Morris R.C. eds., Iron-Formation: Facts and Problems, Elsevier, Amsterdam, p. 471-490.

James, H.L. and Clayton, R.N., 1962, Oxygen isotope fractionation in metamorphosed iron formations in the Lake Superior region and in other iron-rich rocks., in H.L. James, A.E.G. Engel and B.F. Leonard eds., Petrologic Studies, volume to honor A.F. Buddington, Geol. Soc. Am., Denver, p. 217-239.

James, H.L., Dutton, C.E., Pettijohn, F.J., and Wier, K.L., 1968, Geology and ore deposits of the Iron-River Crystal Falls district, Iron County, Michigan., U.S. Geol. Surv. Prof. Paper, 570, 134p.

James, N.P., 1984, Shallowing-upward sequences in carbonates., in Walker R.G. ed., Facies Models, 2nd. edition, Geoscience Canada Reprint Series 1, p. 213-228.

Kajiwara, Y., 1971, Sulphur isotope study of the Kuroko-ores of the Shakanai No. 1 deposits , Akita Perfecture, Japan., Gechem. Jour., 4, p. 157-181.

Kajiwara, Y. and Date, J., 1971, Sulphur isotope study of Kuroko-type strata-bound massive sulfide deposits in Japan., Geochem. Jour., 5, p. 133-150.

Kaplan, I.R., 1983, Stable isotopes of sulfur, nitrogen and deuterium in recent marine environments., in Stable Isotopes in Sedimentary Geology, S.E.P.M. Short Course No. 10, 2.1-2.108.

Kaplan, I.R. and Rittenberg, S.C., 1964, Microbiological fractionation of sulfur isotopes., Jour. Gen. Microbiol., 34, 195-212.

Karhu, J. and Epstein, S., 1986, The implication of the oxygen isotope records in coexisting cherts and phosphates., Geochim. Cosmochim. Acta, 50, p. 1745-1756.

Kasting, J.F., 1987, Theoretical constraints on oxygen and carbon dioxide concentrations in the Precambrian atmosphere., Precambrian Res., 34, p. 205-229.

Kazmierczak, J., 1979, The eukaryotic nature of Eosphaera-like ferriferous structures for the Precambrian Gunflint iron formation, Canada: A comparative study., Precambrian Research, 9, p. 1-22.

Kemp, A.L.W. and Thode, H.G., 1968, The mechanism of the bacterial reduction of sulphate and of sulphite from isotope fractionation studies., Geochim. Cosmochim. Acta, 32, p. 71-91.

Keith, M.L. and Weber, J,N., 1964, Carbon and oxygen isotopic composition of selected limestones and fossils., Geochim. Cosmochim. Acta, 28, p. 1787-1816.

Klasner, J.S., Cannon, W.F., and Ojakangas, R.W., 1989, Geology of the Marquette Range Supergroup and the Penokean fold belt in northern Michigan., in Early Proterozoic Rocks of the Great Lakes Region, 28th International Geological Congress, Field trip guidebook T145, p. 19-31.

Klein, C. and Bricker, O.P., 1977, Some aspects of the sedimentary and diagenetic environment of Proterozoic banded iron-formation., Econ. Geol., 72, p. 1457-1470.

Klein, C. and Fink, R.P., 1976, Petrology of the Sokoman Iron Formation in the Howells River area, at the western edge of the Labrador Trough., Econ. Geol., 71, p. 453-487.

Klemm, D.D., 1979, A biological model of the formation of the banded iron formation in the Transvaal Supergroup, South Africa., Mineral. Deposita, 14, p. 381-385.

Knauth, L.P. and Epstein, S., 1976, Hydrogen and oxygen isotope ratios in nodular and bedded cherts., Geochim. Cosmochim. Acta, 40, p. 1095-1108.

Knauth, L.P. and Lowe, D.R., 1979, Oxygen isotope geochemistry of cherts from the Onverwacht Group (3.4 billion years), Transvaal, South Africa, with implications for secular variations in the isotopic composition of cherts., Earth and Planet. Sci. Lett., 41, p. 209-222.

LaBerge, G.L., 1964, Development of magnetite in iron-formations of the Lake Superior region., Econ. Geol., 59, p. 1313-1342.

LaBerge, G.L., 1973, Possible biological origin of Precambrian iron-formations., Econ. Geol., 68, p. 1098-1109.

LaBerge, G.L., Robbins, E.I. and Han, T.-M., 1987, A model for the biological precipitation of Precambrian iron-formations - A: geological evidence., in Appel P.W.U. and LaBerge G.L. eds., Precambrian Iron-formations, Theophrastus, Athens, p. 69-96.

Lambert, I.B. and Donnelly, T.H., 1990, The paleoenvironmental significance of trends in sulphur isotope compositions in the Precambrian. A critical review., in Herbert, H.K. ed., Stable Isotopes and Fluid Processes in Mineralisation., Univ. Western Australia Geol. Publ., 23 (in press).

Lambert, I.B., Dunlop, J.S.R. and Groves, D.I., 1978, Stable isotope compositions of early Archean sulphate deposits of probable evaporitic and volcanogenic origins., Nature, 276, p. 806-810.

Land, L.S., 1983, The application of stable isotopes to the studies of the origin of dolomite and to problems of diagenesis of clastic sediments., in Stable Isotopes in Sedimentary Geology, S.E.P.M. Short Course No. 10, p. 4.1-4.22.

Larue, D.K., 1981, The early Proterozoic pre-iron-formation Menominee Group siliciclastic sediments of the Lake Superior region: evidence for sedimentation in platform and basinal settings., Jour. Sed. Pet., 51, p. 397-414.

Larue, D.K., 1983, Early Proterozoic tectonics of the Lake Superior region: tectonostratigraphic terranes near the purported collision zone., Geol. Soc. Am. Memoir, 160, p. 33-47.

Larue, D.K. and Sloss, L.L., 1980, Early Proterozoic sedimentary basins of the Lake Superior region., Geol. Soc. Am. Bull., 91, p. 450-452.

Larue, D.K. and Ueng, W.L., 1985 , Florence-Niagara terrane: an early Proterozoic accretionary complex, Lake Superior region, U.S.A., Geol. Soc. Am. Bull., 96, p. 1169-1187.

Lavigne, M.J. and Crocket, J.H., 1982, A comparative study of sulphur isotope distribution of sulfide facies banded iron formations and the East South C ore zone, Dickenson Gold Mine, Red Lake District: a preliminary report., Geol. Surv. Canada, Paper 82-1A, p. 265-274.

Lepp, H. and Goldich, S.S., 1964, Origin of Precambrian iron formations, Econ. Geol., 59, p. 1025-1060.

Leventhal, J.S., 1983, An interpretation of carbon and sulphur relationships in the Black Sea sediments as indicators of environments of deposition., Geochim. Cosmochim. Acta, 47, p. 133-137.

Leventhal, J.S., 1987, Carbon and sulfur relationships in Devonian shales from the Appalachian basin as an indicator of environment of deposition., Am. Journ. Sci., 287, p. 33-49.

Longstaffe, F.J., 1987, Stable isotope studies of diagenetic processes., in Kyser, T.K. ed., MAC Short Course in Stable Isotope Geochemistry of Low Temperature Fluids, vol. 13, p. 187-257.

Lougheed, M.S., 1983, Origin of Precambrian iron-formations in the Lake Superior region., Geol. Soc. Am. Bull., 94, p. 325-340.

Markun, C.D. and Randazzo, A.F., 1980, Sedimentary structures in the Gunflint Iron Formation, Schreiber Beach, Ontario., Precambrian Res., 12, p. 287-310.

Maynard, J.B., 1983, Geochemistry of Sedimentary Ore Deposits., Springer-Verlag, New York, 305 pp.

Mel'nik, Y.P., 1982, Precambrian Banded Iron-Formations, Physicochemical Conditions of Formation., Elsevier, Amsterdam, 310 pp.

Mengel, J.T., 1973, Physical sedimentation in Precambrian cherty iron formations of the Lake Superior type., in Amstutz G.C. and Bernard A.J. eds., Ores in Sediments, Springer-Verlag Berlin, Heidelberg and New York, p. 179-193.

Miyano, T., 1987, Diagenetic to low-grade metamorphic conditions of Precambrian iron-formations., in Appel P.W.U. and Laberge G.L. eds., Precambrian Iron-formations., Theophrastus, Athens, p. 155-186.

Monster, J., Appel, P.W.U., Thode, H.G., Schidlowski, M., Carmichael, C.M., and Bridgewater, D., 1979, Sulphur isotope studies in early Archean sediments from Isua, West Greenland: inplications for the antiquity of bacterial sulphate

reduction., Geochim. Cosmochim. Acta, 43, p. 405-413.

Moorhouse, W.W., 1960, Gunflint iron range in the vicinity of Port Arthur, Ontario Dept. Mines, 69, part 7, p. 1-40.

Morey, G.B., 1967, Stratigraphy and sedimentology of the middle Precambrian Rove Formation in north-eastern Minnesota., Jour. Sed. Pet., 37, p. 1154-1162.

Morey, G.B., 1973, Mesabi, Gunflint and Cuyuna ranges, Minnesota., in Genesis of Precambrian Iron and Manganese Deposits., Proceedings Kiev Symposium, 1970, Paris, UNESCO, p. 193-208.

Morey, G.B., 1978, Lower and middle Precambrian stratigraphic nomenclature for east-central Minnesota., Minnesaota Geol. Surv. Rept. Invest., 21, 52pp.

Morey, G.B., 1983a, Animikie basin, Lake Superior region, U.S.A., in Trendall A.F. and Morris R.C. eds., Iron-formation: Facts and Problems, Amsterdam, Elsevier, p. 13-68.

Morey, G.B., 1983b, Lower Proterozoic stratified rocks and the Penokean Orogeny in east-central Minnesota., in Medaris Jr., L.G. ed., Early Proterozoic Geology of the Great Lakes Region, G.S.A. Mem. 160, p. 97-112.

Morey, G.B., Sims, P.K., Cannon, W.F., Mudrey, Jr., M.G., and Southwick, D.L., 1982, Geologic Map of the Lake Superior Region., (1:1,000,000 scale), Minnesota Geol. Surv., State Map S-13.

Morey, G.B. and Van Schmus, W.R., 1988, Correlation of Precambrian rocks of the Lake Superior region, United States., U. S. Geol. Surv. Prof. Paper, 1241-F, 31 pp.

Morris, R.C. and Horwitz, R.C., 1983, The origin of the iron-formation-rich Hammersley Group of Western Australia - deposition on a platform., Precambrian Res., 21, p. 273-297.

Mottl, M.J., Holland, H.D., and Corr, R.F., 1979, Chemical exchange during hydrothermal alteration of basalt by seawater - II. Experimental results for Fe, Mn, and sulphur species., Geochim. Cosmochim Acta, 43, p. 869-884.

Nissenbaum, A., Presley, B.J., and Kaplan, I.R., 1972, Early diagenesis in a reducing fjord, Saanich Inlet, British Columbia - I. Chemical and isotopic changes in major components of interstitial waters., Geochim. Cosmochim. Acta, 36, p. 1007-1027.

Northrop, D.A. and Clayton, R.N., 1966, Oxygen-isotope fractionation in systems containing dolomite., Jour. Geology, 74, p. 174-196.

O'Neil, J.R. and Epstein, S., 1966, Oxygen isotope fractionationin the system dolomite-calcite-carbon dioxide., Science, 152, p. 198-201.

O'Neil, J.R., Clayton, R.N. and Mayeda, T.K., 1969, Oxygen isotope fractionation in divalent metal carbonates., Jour. Chem. Phys., 51, p. 5547-5548.

Oehler, J.H., 1976, Hydrothermal crystallization of silica gel., Geol. Soc. Am. Bull., 87, p. 1143-1152.

Ohmoto, H. and Felder, R.P., 1987, Bacterial activity in the warmer, sulphate-bearing, Archaean oceans., Nature, 328, p. 244-246.

Ohmoto, H. and Lasaga, A.C., 1982, Kinetics of reactions between aqueous sulphates and sulfides in hydrothermal systems., Geochim. Cosmochim. Acta, 46, p. 1727-1745.

Ohmoto, H., Kaiser, C.J., and Geer, K.A., 1990, Systematics of sulphur isotopes in recent marine sediments and ancient sediment-hosted basemetal deposits., in Herbert, H.M. ed., Stable Isotopes and Fluid Processes in Mineralisation., Univ. Western Australia Geol. Publ., 23, (in press).

Perry, E.C., 1983, Oxygen isotope geochemistry of iron-formations., in Trendall A.F. and Morris R.C. eds., Iron-Formation: Facts and Problems, Elsevier, Amsterdam, p. 359-372.

Perry, E.C. and Ahmad, S.N., 1980, Oxygen isotope study of Transvaal System iron formation from the vicinity of Kuruman, Cape Province, South Africa., Geol. Soc. Am., Abstr. Programs, 12, p. 497.

Perry, E.C. and Ahmad, S.N., 1981, Oxygen and carbon isotope geochemistry of the Krivoy Rog iron formation, Ukrainian SSR., Lithos, 14, p. 83-92.

Perry, E.C. and Tan, F.C., 1973, Significance of carbon isotope variations in carbonates from the Biwabik Iron Formation, Minnesota., in Genesis of Precambrian Iron and Manganese Deposits: Proc. Kiev Symposium, 1970, Paris, UNESCO, p. 299-305.

Perry, E.C., Ahmad, S.N., and Swulius, T.M., 1978, The oxygen isotope composition of 3,800 m.y. old metamorphosed chert and iron formation from Isukasia, Western Greenland., J. Geol., 86, p. 223-239.

Perry, E.C., Jr., Tan, F.C., and Morey, G.B., 1973, Geology and stable isotope geochemistry of the Biwabik Iron Formation. Northern Minnesota., Econ. Geol., 68, p. 1110-1125.

Peterman, Z.E., Zartman, R.E., and Sims, P.K., 1980, Tonalitic gneiss of early Archean age from northern Michigan., in Selected studies of Archean gneisses and lower Proterozoic rocks, southern Canadian Shield., Morey, G.B. and Hanson, G.N. eds., Geol. Soc. Am. Special Paper, 182, p. 124-134.

Prinz, W.C., 1976, Correlative iron-formations and volcanic rocks of Precambrian X age, northern Michigan., Proceedings, Inst. Lake Superior Geology, 22, p. 50.

Raiswell, R. and Berner, R.A., 1985, Pyrite formation in euxinic and semi-euxinic sediments., Am. Jour. Sci., 285, p. 710-724.

Raiswell, R. and Berner, R.A., 1986, Pyrite and organic matter in Phanerozoic normal marine shales., Geochim. Cosmochim. Acta, 50, p. 1967-1976.

Ripley, E.M. and Nicol, D.L., 1981, Sulphur isotope studies of Archean slate and greywacke from northern Minnesota: evidence for the existence of sulphate reducing-bacteria., Geochim. Cosmochim. Acta, 45, p. 839-846.

Robbins, E.I., LaBerge, G.L., and Schmidt, R.G., 1987, A model for the biological precipitation of Precambrian iron-formations - B: morphological evidence and modern analogs., in Appel, P.W.U. and LaBerge, G.L. eds., Precambrian Iron-formations, Theophrastus, Athens, p. 97-138.

Rosenbaum, J. and Sheppard, S.M.F., 1986, An isotopic study of siderites, dolomites and ankerites at high temperatures., Geochim. Cosmochim. Acta, 50, p. 1147-1150.

Rye, R.O., Roberts, R.J., Snyder, W.S., Lahusen, G.L., and Motica, J.E., 1984, Textural and stable isotope studies of the Big Mike cupriferrous volcanogenic massive sulfide deposit, Pershing County, Nevada., Econ. Geol., 79, p. 124-140.

Sakai, H., Takenaka, T., and Kishima, N., 1980, Experimental study of the rate and isotope effect in sulphate reduction by ferrous iron oxides and silicates under hydrothermal conditions., in Proceedings, Third International Symposium on Water-Rock Interaction, Edmonton, Alberta, p. 75-76.

Sasaki, A., Arikawa, Y., and Folinsbee, R., 1979, Kiba reagent method of sulphur extraction applied to isotopic work., Bull. Geol. Surv. Japan, 30, p. 241-245.

Schidlowski, M., 1982, Content and isotopic composition of reduced carbon in sediments., in Holland, H.D. and Schidlowski, M. eds., Mineral Deposits and the Evolution of the Biosphere, Springer-Verlag, New York, p. 103-122.

Schidlowski, M., Appel, P.W.U., Uichmann, R., and Junge, C.E., 1979, Carbon isotope geochemistry of the 3.7 x 10^9 yr. old Isua sediments, West Greenland: Implications for the Archaean carbon and oxygen cycles., Geochim. Cosmochim. Acta, 43, p. 189-199.

Schidlowski, M., Eichmann, R., and Junge, C.E., 1975, Precambrian sedimentary carbonates: Carbon and oxygen isotope geochemistry and implications for the terrestrial oxygen budget., Precambrian Res., 2, p. 1-69.

Schidlowski, M., Hayes, J.M., and Kaplan, I.R., 1983, Isotopic inferences of ancient biochemistries: Carbon, sulfur, hydrogen, and nitrogen., in Schopf, J.W. ed., The Earth's Earliest Biosphere: Its Origin and Evolution. Princeton University Press, p. 361-384.

Schulz, K.J., 1987, An Early Proterozoic ophiolite in the Penokean Orogen., G.A.C. Programs with Abstracts, 12, p. 87.

Shanks, W.C., Bischoff, J.L. and Rosenbauer, R.J., 1981, Seawater sulphate reduction and sulphur isotope fractionation in basaltic systems: Interaction of seawater with fayalite and magnetite at 200-350oC., Geochim. Cosmochim. Acta, 45, p. 1977-1995.

Shegelski, R.J., 1982, The Gunflint Formation in the Thunder Bay area, in Proterozoic Geology of the Northern Lake Superior Area., Franklin, J.M. ed., GAC/MAC Field Trip Guidebook, Trip 4, p. 14-31.

Shegelski, R.J., 1985, Sulfur isotope study of the Aphebian Gunflint Formation, Ontario., GAC/MAC Programs with abstracts, p. A56.

Sheppard, S.M.F. and Schwarcz, H.P., 1970, Fractionation of carbon and oxygen isotopes and magnesium between metamorphic calcite and dolomite., Contrib. Mineral. Petrol., 26, p. 161-198.

Simonson, B.M., 1987, Early silica cementation and subsequent diagenesis in arenites from four Proterozoic iron formations of North America., Jour. Sed. Pet., 57, p. 494-511.

Simonson, B.M., 1985, Sedimentological constraints on the origins of Precambrian iron-formations., G.S.A. Bull., 96, p. 244-252.

Simonson, B.M. and Lanier, W.P., 1987, Early silica cementation and microfossil preservation in cavities in iron-formation stromatolites, early Proterozoic of Canada., in Appel P.W.U. and LaBerge G.L. eds., Precambrian Iron-formations, Theophrastus Athens, p. 187-213.

Sims, P.K., Card, K.D., Morey, G.B. and Peterman, Z.E., 1980, The Great Lakes tectonic zone - a major crustal structure in central North America., G.S.A. Bull., 91, p. 690-698.

Sims, P.K., Van Schmus, W.R., Schulz, K.J., and Peterman, Z.E., 1989, Tectonostratigraphic evolution of the early Proterozoic Wisconsin magmatic terrane of the Penokean orogen., Can. Jour. Earth Sci., 26, p. 2145-2158.

Skyring, G.W. and Donnelly, T.H., 1982, Precambrian sulphur isotopes and a possible role for sulfite in the evolution of biological sulphate reduction., Precambrian Res., 17, p. 41-61.

Southwick, D.L., Morey, G.B., and McSwiggen, P.L., 1988, Geologic map (scale 1:250,000) of the Penokean orogen, central and eastern Minnesota, and accompanying text., Minnesota Geol. Surv. Rept. Invest., 37, 25 pp.

Thode, H.G. and Goodwin, A.M., 1983, Further sulfur and carbon isotope studies of late Archean iron-formations of the Canadian Shield and the rise of sulphate reducing bacteria., Precambrian Res., 20, p. 337-356.

Trendall, A.F., 1983, Introduction., in Trendall, A.F. and Morris, R.C. eds., Iron Formation: Facts and Problems, Elsevier, Amsterdam, p. 1-12.

Trendall, A.F. and Blockley, J.C., 1970, The iron formations of the Precambrian Hammersley Group, Western Australia., West. Australia Geol. Surv. Bull., 119, 366 pp.

Trendall, A.F. and Morris, R.C., 1983, Iron-Formation: Facts and Problems., Elsevier, Amsterdam, 558 pp.

Turner, J.V., 1982, Kinetic fractionation of carbon-13 during calcium carbonate precipitation., Geochim. Cosmochim. Acta, 46, p. 1183-1192.

Ueng, W.C., Fox, T.P., Larue, D.K. and Wilband, J.T., 1988, Geochemistry and petrogenesis of the early Proterozoic Hemlock volcanic rocks and the Kiernan sills, southern Lake Superior region., Can. Jour. Earth Sci., 25, p. 528-546.

Van Hise, C.R. and Leith, C.K., 1911, The geology of the Lake Superior region., U.S. Geol. Surv. Mon., 52, 641 pp.

Van Schmus, W.R., 1980, Chronology of igneous rocks associated with the Penokean orogeny in Wisconsin, in Selected studies of Archean gneisses and lower Proterozoic rocks, southern Canadian Shield., in Morey, G.B. and Hanson, G.N. eds., Geol. Soc. Am. Special Paper, 182, p. 159-168.

Van Schmus, W.R., Medaris, L.G., and Banks, P.O., 1975, Geology and age of the Wolf River batholith, Wisconsin., Geol. Soc. Am. Bull., 86, p. 907-914.

Veizer, J, 1983a, Trace elements and isotopes in sedimentary carbonates., in Reeder R.J. ed., Carbonates: Mineralogy and Chemistry., Min. Soc. Am. Reviews in Mineralogy, Vol. 11, p. 265-299.

Veizer, J., 1983b, Chemical diagenesis of carbonates: theory and application of trace element technique., in Stable Isotopes in Sedimentary Geology, SEPM Short Course No. 10, p. 3.1-3.100.

Veizer, J., 1983c, Geological evolution of the Archean-Early Proterozoic Earth., in Schopf, J.W. ed., The Earth's Earliest Biosphere: Its Origin and Evolution, Princeton Univ. Press, p. 240-259.

Veizer, J., 1989, Strontium isotopes in seawater through time., Ann. Rev. Earth Planet. Sci., 17, p. 141-167.

Veizer, J., Clayton, R.N., and Hinton, R.W., 1990, Geochemistry of Precambrian carbonates: IV Early Proterozoic (2.25 ± 0.25 Ga) seawater., Geochim. Cosmochim. Acta, (in press).

Veizer, J., Compston, W., Hoefs, J., and Nielsen, H., 1982, Mantle buffering of the early oceans., Naturwissenschaften, 69, p. 173-180.

Veizer, J. and Hoefs, J., 1976, The nature of O18/O16 and C13/C12 secular trends in sedimentary carbonate rocks., Geochim. Cosmochim. Acta, 40, p. 1387-1395.

Veizer, J., Hoefs, J., Lowe, D.R., and Thurston, P.C., 1989, Geochemistry of Precambrian carbonates: II. Archean greenstone belts and Archean sea water., Geochim. Cosmochim. Acta, 53, p. 859-871.

Veizer, J., Holser, W.T. and Wilgus, C.K., 1980, Correlation of 13C/12C and 34S/32S secular variations., Geochim. Cosmochim. Acta, 44, p. 579-587.

Walker, J.C.G. and Brimblecombe, P., 1985, Iron and sulfur in the pre-biologic ocean, Precambrian Res., 28, p. 205-222.

Walker, J.C.G. and Drever, J.I., 1988, Geochemical cycles of atmospheric gases., in Gregor, C.B., Garrels, R.M., Mackenzie, F.T., and Maynard, J.B. eds., Chemical Cycles in the Evolution of the Earth., John Wiley & Sons, New York, p. 55-76.

Walker, J.C.G., Klein, C., Schidlowski, M., Stevenson, D.J., and Walter, M.R., 1983, Environmental evolution of the Archean-Early Proterozoic Earth., in Schopf, J.W. ed., The Earth's Earliest Biosphere: Its Origin and Evolution, Princeton University Press, p. 260-290.

White, D.A., 1954, Stratigraphy and structure of the Mesabi range, Minnesota., Minnesota Geol. Surv. Bull., 38, 92 pp.

Wilson, J.E. and Jordan, C., 1983, Middle Shelf., in Scholle, P.A., Bebout, D.G., and Moore, C.H. eds., Carbonate Depositional Environments., A.A.P.G. Mem., 33, p. 297-343.

Wolff, J.F., 1917, Recent geologic developments on the Mesabi range, Minnesota., Trans. Am. Inst. Min. Metall. Eng., 56, p. 142-169.

APPENDIX A. ANALYTICAL METHODS

STABLE ISOTOPES

Most of the samples in this study contained variable proportions of siderite, ankerite, dolomite, and/or calcite. Because of the fine-grained nature of these carbonate minerals, physical separation of individual phases was not possible. A chemical separation technique was utilized, based on the differential reaction rates of various carbonate minerals with phosphoric acid at different temperatures. Mixtures of calcite and dolomite were separated using the technique of Epstein et al (1964) and mixtures of siderite, ankerite and calcite were separated by the method of Al-Aasm et al (1990).

CO_2 was produced by reacting 10 to 20 mg (depending on carbonate content) of powdered rock (<200 mesh), which contained variable mixtures of carbonate minerals, with 100% H_3PO_4. For calcite extraction, samples were reacted at 25 ^oC for 4 hours after which the CO_2 was extracted, purified of water vapour and liquid nitrogen non-condensible gases on a vacuum line, and then transferred to a glass break seal for storage. The reaction of calcite with acid at 25 ^oC is essentially complete after 4 hours (Al-Aasm et al, 1990), however the other carbonate minerals react very slowly at this temperature. Therefore, contamination of calcite CO_2 will be minimal.

The unreacted portion of the sample was then allowed to continue reacting at 50^oC for an additional 16-20 hours. Dolomite reaction is virtually complete after about 24 hours at 50 ^oC (Al-Aasm et al, 1990). However, reaction times for ankerite are unknown and is dependent on iron content. For this study it is assumed that ankerite reaction was similar to dolomite. Siderite reaction at this temperature is much slower; complete reaction takes up to 11 days. Therefore, the CO_2 extracted at

this time is considered to represent dolomite, for samples from the limestone facies, and ankerite for remaining samples.

For samples that contained siderite, the unreacted portion was reacted at 50 ^{o}C for an additional 4 days, after which CO_2 was collected. Although siderite reaction is not complete after 4 days, Al-Aasm et al (1990) have shown that the isotopic composiiton of the CO_2 extracted after this time does not change.

The isotopic ratios of carbon and oxygen were determined on the CO_2 using a VG Isogas SIRA 12 mass spectrometer at the University of Ottawa. The precision and accuracy of this technique is 0.1 ^{o}/oo for both isotopes. Oxygen isotope fractionation factors for acid released CO_2 used in this study are 1.01025 for calcite at 25^{o}C (Friedman and O'Neil, 1977), 1.01065 for dolomite and ankerite at 50^{o}C (Rosenbaum and Sheppard, 1986), and 1.010453 for siderite at 50 ^{o}C (Rosenbaum and Sheppard, 1986).

Pyrite was physically separated from samples whenever possible. For very fine-grained samples, pyrite sulphur was extracted chemically using the KIBA method (Sasaki et al, 1979), which produces sulphur as Ag_2S. Pyrite and Ag_2S was burnt directly, with Cu_2O, in an electric furnace at 1100 ^{o}C to produce SO_2, which was purified in a vacuum line and collected in glass break seals. The isotopic ratios were analysed on a Micromass 602E mass spectrometer at the University of Ottawa. The precision and accuracy for this procedure is 0.2 ^{o}/oo.

Stable isotope ratios are expressed in convential δ (^{o}/oo) notation relative to the Pee Dee Belemnite (PDB) carbonate standard for $\delta\,^{13}C$ and $\delta\,^{18}O$. The Canyon Diablo troilite (CDT) is the standard for $\delta\,^{34}S$ results.

ELEMENTAL ANALYSES

Whole rock analyses of organic carbon, carbonate-carbon and total sulphur were analysed at the Geological Survey of Canada. Total carbon (CO_2t) and sulphur was analysed by LECO induction furnace. Carbonate-carbon (CO_2) was analysed by acid evolution and organic carbon was calculated as $C_{org} = (CO_2t - CO_2) \times .273$.

Energy dispersive analyses of carbonate minerals were done at the Geological Survey of Canada using a Material Analysis Company (MAC) microprobe equipped with a Kevex Corporation detector. The data reduction is by means of software (system EDDI) developed in house. The instrument is operated at 20 kV accelerating voltage, 10 nanoamperes sample current, 10 ev/ch spectrometer range, and a 50 second acquisition time. Precision is generally ± 2 % of the amount present for concentrations greater than 5 %.

APPENDIX B.

Isotopic Ratios of Carbon and Oxygen in Carbonate Minerals

	Calcite		Ankerite		Siderite	
Sample	$\delta^{13}C$	$\delta^{18}O$	$\delta^{13}C$	$\delta^{18}O$	$\delta^{13}C$	$\delta^{18}O$
Laminated Carbonate						
6f	-12.11	-14.73	-10.28	-13.07		
6h	-15.26	-15.73	-15.38	-16.35		
6j	-7.83	-15.09	-4.10	-14.75		
15a	-1.88	-13.07	-1.65	-13.64		
16a			-0.39	-7.67	-3.86	-9.36
16b			-4.63	-10.98	-4.57	-9.56
16c			-4.51	-10.27	-5.16	-9.02
16d			-3.66	-10.80	-5.19	-9.64
16f	-4.62	-13.13	-2.38	-10.11		
16g			-3.54	-13.31	-3.54	-12.45
16j	-1.78	-9.37	-4.61	-13.74	-4.98	-8.63
Banded Chert-carbonate						
5b	-1.94	-13.95	-2.35	-7.42	-2.14	-6.93
5c					-2.87	-8.11
5d					-3.12	-9.63
25q	-3.04	-13.89			-2.30	-11.78
25r					-1.78	-8.59
28a	-2.52	-13.38	-3.01	-11.30	-3.43	-10.81
28d					-2.34	-12.24
28e					-2.21	-12.47
31d	-6.75	-12.13	-6.60	-12.77		
32e	-3.30	-13.42	-2.25	-10.41	-2.08	-10.08
35b	-3.28	-12.32	-1.98	-9.76	-1.79	-9.13
35l			-2.70	-10.45	-2.69	-10.14
39c					-3.67	-8.24
39d					-3.98	-9.36
39h					-3.32	-9.74
39j	-3.05	-9.33	-4.43	-12.39	-4.60	-12.81
Arenite						
3a	-4.91	-11.78	-4.74	-11.85		
3c	-4.95	-11.66	-4.94	-12.45		
6a	-1.25	-12.47	-1.04	-13.61		
6d	-2.76	-10.19	-3.34	-10.85		
6e	-9.88	-12.69	-9.04	-12.99		
9g	-3.42	-12.37	-2.90	-13.54		
10j	-15.90	-17.12				
10m	-19.96	-17.13				
29e	-6.03	-11.97				
30d	-12.96	-16.99	-11.96	-16.91		
32c	-5.46	-15.72	-4.98	-14.99		
32d	-5.42	-11.67	-5.52	-11.81	-1.49	-11.73
32f	-5.24	-13.06	-5.27	-13.14		
40c	-5.72	-6.67	-5.96	-7.71		
43b	-1.15	-11.29	-0.87	-11.87		
44g			-8.96	-11.75	-9.25	-9.58
45a	-2.28	-12.61	-2.24	-13.73	-2.12	-13.69

Sample	Calcite $\delta^{13}C$	Calcite $\delta^{18}O$	Ankerite $\delta^{13}C$	Ankerite $\delta^{18}O$	Siderite $\delta^{13}C$	Siderite $\delta^{18}O$
Black shale						
5a					-1.29	-7.34
13f-b	-3.56	-11.82	-3.69	-12.54	-3.94	-12.47
13gi	-5.45	-14.69	-1.62	-9.01	-0.94	-7.49
13giii	-4.29	-14.28	-1.97	-9.07	-1.24	-7.02
13k	-2.98	-9.63	-3.67	-13.85	-4.08	-13.82
13n	-3.87	-13.81	-3.05	-12.89		
13p	-4.20	-15.72	-3.61	-14.36		
13q	-7.68	-14.96	-4.25	-14.23		
13r	-3.44	-15.01	-2.75	-12.44		
26h			-1.05	-13.55	0.46	-12.09
26jii	-2.66	-7.40	-2.93	-7.55	-3.09	-7.36
26jv			-2.93	-7.55	-1.21	-5.32
26k					-3.73	-12.67
26l					-2.30	-11.07
26n					-3.46	-12.95
26p					-3.38	-13.43
26q					-4.91	-13.32
26r					-3.72	-12.68
27a	-5.23	-14.20	-3.50	-13.99		
27b			-3.53	-12.54		
27d			-3.69	-12.30		
27e			-4.18	-13.77		
27f			-2.43	-14.83		
27h	-4.24	-11.86	-4.38	-13.09	-4.55	-12.13
35d			-0.79	-7.92	-0.33	-7.08
35f					0.02	-9.56
39a			-3.12	-11.40		
42a	-7.59	-16.11				
42b	-9.23	-16.11				
44c			-6.76	-11.06	-6.88	-9.76
46e					-9.88	-13.81
Upper Limestone Member						
8a	-3.31	-15.49	-2.74	-14.03		
8b	-2.03	-13.82	0.05	-10.93		
8c	-2.10	-13.98	0.53	-10.31		
8d	-2.87	-15.07	-2.06	-14.65		
8e	-3.94	-13.48	0.61	-9.22		
8f	-2.42	-13.57	-0.20	-10.72		
9a	-1.16	-13.98	0.16	-10.54		
9b	-3.84	-17.10	-1.97	-15.64		
9ci	-7.76	-17.52	-7.69	-17.92		
9cii	-7.42	-17.43	-7.50	-17.84		
9dii	-7.31	-17.52	-7.31	-17.76		
9div	-8.78	-17.35	-8.72	-17.84		
9fi	-7.72	-17.38	-7.62	-17.57		
9fii	-7.74	-17.49	-7.82	-17.98		
41b	-2.06	-13.53				
41c	-1.52	-13.18				

APPENDIX C.

Isotopic ratios of sulfide minerals

Sample	$\delta^{34}S$
Arenite	
1a	10.82
3c	7.33
6e	5.88
8g	11.36
24iv	-6.82
30c	11.17
30d	8.92
30e	10.94
32a	-5.45
32b	18.13
32d	-0.20
32f	9.23
40a	6.69
40b	8.82
87-GF- 8	17.04
87-GF- 9	-0.32
Banded Chert-carbonate	
4a	9.00
5b	6.02
13a	-2.38
13b	5.12
13bc	-10.78
13bm	-18.16
26a	-13.40
26b	9.26
26c	14.55
26d	-10.76
31a	22.04
31b	-1.20
31c	14.80
31d	3.38
32e	9.34
35l	8.13
39c	6.83
87-GF-11	5.70
Black Shale	
5a	6.56
6m	9.33
6n	9.84
6p	9.18
6q	6.80
6s	9.98
6t	6.38
13c	6.74
13d	17.66
13e	5.47

Sample	$\delta^{34}S$
13e- 1	-21.00
13e- 2	-20.19
13e- 3	-12.02
13e- 4	-9.85
13e- 5	-14.87
13e- 6	-14.34
13e- 7	-9.68
13e- 8	-8.46
13e- 9	-9.16
13e-10	-7.49
13e-11	-3.86
13e-12	-9.03
13e-13	-20.95
13f-a	-20.65
13f-b	6.41
13g	7.48
13gi	8.27
13giii	3.22
13k	15.31
13l-1	17.21
13l-2	23.54
13l-3	14.99
13l-4	11.50
13l-5	-1.59
13l-a	22.96
13l-b	12.00
13m	18.90
13p	5.89
13q	5.89
13r	5.57
20a	5.58
20c	10.40
25c	6.43
25g	6.87
25j	7.89
25l	9.27
25n	6.30
25p	7.86
26e	4.79
26f	7.74
26g	8.60
26g- 1	-32.51
26g- 3	-21.32
26g- 5	3.02
26g- 6	4.29
26g- 8	-17.56
26g-10	-32.37
26h	7.18
26jii	1.31
26jv	-1.85
26k	5.32
26l	4.43

Sample	$\delta^{34}S$
26mi	14.54
26mii	35.09
26m-1	-22.19
26m-2	-21.11
26m-3	-16.55
26m-4	-16.03
26m-5	-23.06
26m-6	-21.64
26n	16.18
26p	11.44
26r	13.17
27b	1.10
27c	5.84
27d	5.01
27f	6.80
27gi	7.40
27gii	4.32
27h	4.81
27j	4.66
28g	10.49
28j	6.64
28l	7.53
35a	7.58
35d	6.51
35f	7.34
35h	10.80
39b	5.60
39e	4.53
42a	5.25
42b	6.20
42f	8.74
46b	14.60
46e	5.15
87-GF- 1	6.15
87-GF- 2	6.75
87-GF- 4C	14.50
87-GF- 4R	21.94
Laminated Carbonate	
6f	7.51
6h	7.07
6j	10.77
6k	7.08
6l	6.46
15a	8.13
16a	12.64
16f	10.39
16h	9.05
87-GF- 3	15.44
Upper Limestone Member	
8e	7.22

Sample	$\delta^{34}S$
9a	4.87
9b	5.42
9c	11.35
9ci	10.50
9cii	12.69
9d	9.67
9dii	9.87
9e	7.34
9f	8.74
9fi	11.80
9fii	9.49
41b	4.62
41c	10.30
Rove Formation	
7a	20.88
7b	20.54
17a	13.77
17b	15.49
17c	20.92
18a	19.68
18c	15.21
38a	16.85
Pyrite in Fractures	
6b	28.33
9g	16.64
34a	20.28
34b	19.67
43a	3.13
47a	1.25